Shedding light on the ‘invisible’ water crisis

Modelling past and future global surface water quality

Edward R. Jones

297 UTRECHT STUDIES IN EARTH SCIENCES

Shedding light on the 'invisible' water crisis

Modelling past and future global surface water quality

Nieuw licht op de 'onzichtbare' watercrisis

Wereldwijde modellering van recente en toekomstige oppervlaktewaterkwaliteit

(met een samenvatting in het Nederlands)

PROEFSCHRIFT

ter verkrijging van de graad van doctor aan de Universiteit Utrecht
op gezag van de rector magnificus, prof. dr. H. R. B. M. Kummeling,
ingevolge het besluit van het college voor promoties in het openbaar te verdedigen
op 01 december 2023 des morgens te 10.15 uur

door

Edward Russell Jones

geboren op 2 April 1995 te Londen, Verenigd Koninkrijk

Promotor:
Prof. dr. ir. M. F. P. Bierkens

Copromotor:
Dr. M. T. H. van Vliet

Utrecht Studies in Earth Sciences 297

Shedding light on the 'invisible' water crisis

Modelling past and future global surface water quality

Edward R. Jones

Utrecht 2023

Faculty of Geosciences, Utrecht University

Examination committee:

Prof. dr. M. Flörke, Ruhr-Universität Bochum

Dr. R. Kumar, Helmholtz Centre for Environmental Research GmbH – UFZ

Prof. dr. A. van Griensven, Vrije Universiteit Brussel

Prof. dr. ir. A. P. van Weezel, Universiteit van Amsterdam

Prof. dr. ir. A. F. Bouwman, Utrecht University

ISBN: 978-90-6266-669-0

DOI: 10.33540/2030

Published by: Faculty of Geosciences, Universiteit Utrecht, The Netherlands, in: Utrecht Studies in Earth Sciences (USES), ISSN 2211–4335

Typeset using: XeLaTeX

Cover image: XStudio3D
Cover binding: Prof. Ed Hawkins, https://showyourstripes.info/
Cover design: Margot Stoete

Chapter covers: Andrés Riestra

Printed by: Ipskamp, The Netherlands

Correspondence to: edward.russell.jones@gmail.com

Contents

Preface

While I have long been dismissive of the seemingly obligatory tradition to include a clever epigraph at the start of your PhD thesis, I eventually caved. The quote below, originally a Haitian proverb but also included in the lyrics of the song that unquestionably became the soundtrack of my thesis writing (*Sprawl II* by Arcade Fire), particularly resonated with me during the final phases of my PhD and as I began to reflect on the previous four years of my life:

Beyond mountains there are mountains

On the surface, it might seem an overly pessimistic worldview – along the lines of 'the challenges are endless', or 'as you solve one problem, another one will present itself'. A more optimistic reading could be 'life is a continuous journey of growth', or 'overcoming challenges leads to new opportunities'. In my opinion, both interpretations are valid.

Doing a PhD is somewhat unique in that you have a lot of flexibility to choose what you want to research, who you want to engage with, and which skills you want to develop. I found that this freedom, combined with the four-year duration of a PhD, allowed for a lot of personal and professional growth. The sense of achievement I gained from the more tangible high points of my PhD – such as publishing papers, receiving positive reactions at conferences, and engaging with the media – definitely helped to renew my enthusiasm for tackling the next challenge.

In the context of undertaking research, and as I think many of my colleagues would agree, the pessimistic interpretation can often feel more appropriate. Topic wise, the 'wickedness' of environmental problems, such as the ones discussed in this thesis, can be extremely daunting – especially against the backdrop of anthropogenic climate change. Completing a PhD is also fraught with personal challenges. The culture of critique in academia, while essential for maintaining the integrity of science, is also one that permeated into my private life and made detachment from work difficult. Conducting multi-year research, mostly independently, can also be a lonely endeavour, which in my case was exacerbated by a global pandemic. Overcoming, or at least better navigating, these challenges requires having the right people around you. In that respect, I have been extremely fortunate and I take the opportunity here to show my gratitude to those people.

To begin, I would like to thank my supervisory team at Utrecht University. I very much appreciate the faith you have placed in me since the beginning of my PhD, and for allowing me the opportunity to largely shape the project myself. Your guidance and feedback over the last four years has not only been invaluable for the research showcased in this thesis, but also for my personal development in becoming a more confident and independent researcher. I extend my thanks to the other collaborators from DFG, who, while having no official supervisory obligations, would always spare me some of their time, expertise, or advice whenever I came knocking. To my other colleagues at Utrecht University, and especially the PhD cohort, it has been a pleasure to share in experiences, celebrate milestones and vent frustrations together over the last four years.

Outside of the academic world, I would like to pay special thanks to three groups of people. While your contribution to this thesis from a scientific perspective has undoubtedly been detrimental (read: debaucherous late nights), you have kept me sane enough to ensure its completion.

Firstly, to my (rugby club) Wageningen friends: thank you for welcoming me to the Netherlands with open arms back in 2016. Despite the speed and eagerness with which you designated me as a Brexit refugee, I immediately felt at home. It has been a privilege to meet people from all different walks of life: students and non-students, young and old, Dutch and internationals. The fact you remain the core of my social life here in the Netherlands is a testament to the depth of the camaraderie built through exchanging blood, sweat and beers on a rugby pitch. I cannot overstate the importance of your friendships to me, especially during the dog-days of COVID.

Secondly, to my British friends: thanks for sticking by me over all these years. While the time we spend together has dramatically decreased since leaving school, and even more so since I moved abroad, it is fantastic to maintain such strong friendships with you all. Our many weekend reunions – Ameland, Lille and Gent, to name a few – have been an enormous source of fun and stress relief. I hope we can continue to blow the lid off unsuspecting places for many years to come.

Finally, to my family: thank you for your unwavering love. Lonneke, thank you for standing with me day-by-day, through the good, the great and the bad, and for adding a new and exciting dimension to my life. Mum and Dad, thank you for giving me the best possible start in life, and for your continued support for everything I do. This includes, of course, my decision to move overseas to pursue higher education – despite your (self-confessed) obliviousness to what it is I *actually* do. Perhaps this book will finally help to make this clearer, but I suspect that it is more likely to be squirreled away in the muck box.

Edward Jones
November 2023

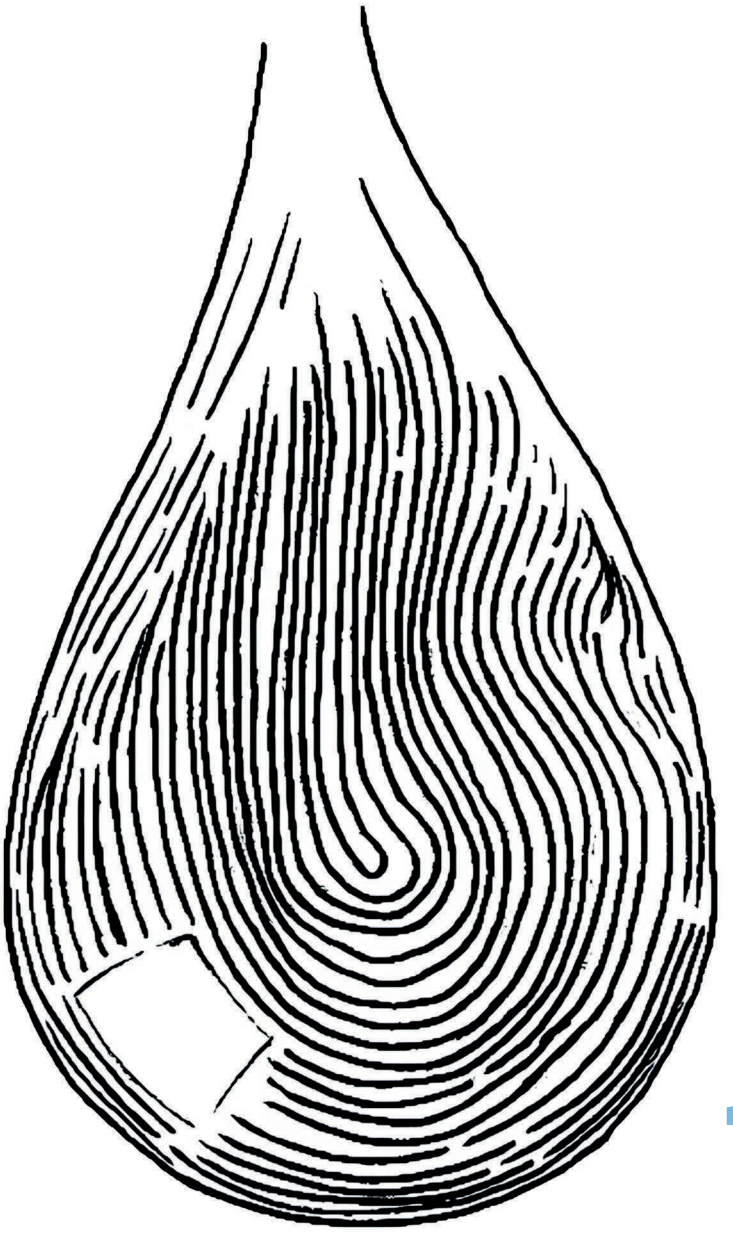

1

Chapter 1 | Introduction

1.1 The 'invisible' water crisis

Safeguarding the quality of our surface waters is a global challenge. Water pollution can pose direct risks to human and environmental health, while also impacting the usability of water for a diverse range of purposes (UNEP, 2016; Damania et al., 2019; van Vliet et al., 2021). For example, water temperature is critical for the cooling of thermoelectric power plants (van Vliet et al., 2012b), salinity for determining the suitability of water for irrigation (Rietz and Haynes, 2003; Thorslund et al., 2022), while the presence of heavy metals and pathogens can impact the safety of drinking water (Ashbolt, 2004; Chowdhury et al., 2016). Excessive nutrient (particularly nitrogen and phosphorus) delivery to aquatic environments enhances eutrophication, which can induce conditions of hypoxia and harm biodiversity (Binzer et al., 2016; Wurtsbaugh et al., 2019). More recently, emerging contaminants such as pharmaceuticals, pesticides and (micro-)plastics have gained significant attention in the scientific community (Geissen et al., 2015; Rice and Westerhoff, 2017; van Wijnen et al., 2019).

While humans are susceptible to the impacts of poor water quality, somewhat paradoxically, anthropogenic activities are key drivers of water quality deterioration. Water that is extracted to fulfil sectoral demands, but that is not consumed in the process, is often discharged back to the environment (termed 'return flows' or 'wastewater'). The composition of these return flows is altered by water use. For example, domestic wastewater will contain elevated concentrations of organic and fecal matter from human waste (WWAP, 2017), while discharges of cooling water from thermoelectric powerplants contain additional heat energy relative to the ambient surface waters (van Vliet et al., 2012b; Raptis et al., 2016). Environmental discharge of these flows, commonly to surface waters, represent a significant source of pollution. The existence of and degree to which treatment practices reduce contaminant levels (Mateo-Sagasta et al., 2015) and the proportion of (treated) wastewater relative to streamflow (Macedo et al., 2022) are crucial determinants of the impact of these return flows on the quality of receiving surface waters.

Despite widespread recognition of its importance, our knowledge of global surface water quality is severely impaired by a lack of information. This lack of information, combined with the imperceptibility of water quality issues, has led the World Bank to label water quality issues as an 'invisible crisis' (Damania et al., 2019). However, global surface water quality data is required to assess the critical regions (hotspots) where pollution poses risks to safe water use, and therefore for devising a combination of technological solutions and effective governance measures to protect surface water quality (UNEP, 2016). The need to improve surface water quality is also recognised as an integral part of the Sustainable Development Agenda, with wider implications for almost all Sustainable Development Goals (SDGs) (UNEP, 2016). Furthermore, there is a growing recognition of the importance of including water quality in water scarcity assessments (van Vliet et al., 2017; Vanham et al., 2018; van Vliet et al., 2021). A pre-requisite for these assessments, and ultimately for improving surface water quality, is to understand the current quality status of surface waters, the main drivers of pollution and how these may change in the future.

The huge range of water quality constituents, their complex interactions and their implications for different sectoral users are so numerous they defy full comprehension (Rode et al., 2010; UNEP, 2016). Focus has therefore been placed on investigating critical water quality constituents and

determining maximum concentrations (i.e. 'safe' thresholds) at which the water is acceptable for specific purposes (van Vliet et al., 2017). In this thesis, surface water quality is assessed with respect to water temperature (Tw) and concentrations of total dissolved solids (TDS), biological oxygen demand (BOD) and fecal coliform (FC). These water quality constituents were selected due to their key role in constraining different sector water uses and environmental health (van Vliet et al., 2021), in addition to acting as proxies for other pollutants. Furthermore, SDG 6.3.2 ('Proportion of bodies of water with good ambient water quality') includes both salinity (TDS) and organic (BOD) pollution as indicators of the quality status of surface waters (UN, 2015), while FC has commonly been used as an overarching indicator of bacterial or pathogenic pollution (Reder et al., 2015).

This thesis focuses on understanding the past, present and future status of surface water quality globally, as indicated by these constituents. To this end, a new high-resolution process-based model was developed, evaluated and applied to identify the major spatio-temporal patterns in surface water quality. To better represent the abatement of pollutant loadings due to management practices, novel spatially explicit datasets on the distribution and pollutant removal efficiencies of wastewater treatment plants were generated and included in model simulations. In line with the key purposes of large-scale water quality models, our evaluation of global water quality focuses on: 1) hot- and bright-spot identification; 2) assessing trends over time; and 3) estimating the potential exposure of populations to poor surface water quality.

1.2 Global surface water quality assessment

Our quantitative understanding of historical surface water quality is mostly predicated on the analysis of in situ observations made at water quality monitoring stations. While the value of ground-truthed measurements is irrefutable, in-stream water quality sampling and analysis can be both time-consuming and expensive. Observations from water quality monitoring stations are therefore unevenly distributed across space (Fig. 1.1a) and highly fragmented across time (Fig. 1.1b) (Damania et al., 2019).

North America is the most data-rich world region, with 45%, 76%, 62% and 92% of all monitoring stations for Tw, TDS, BOD and FC located in this region, respectively, accounting for 39%, 32%, 50% and 83% of the total number of observations, respectively. Observations made across Western Europe account for 28%, 14% and 4% of global Tw, BOD and FC measurements, respectively, but just 3% of the TDS observations. Australia is data-rich for TDS measurements, yet the number of observations from across the rest of the East Asia and Pacific region is relatively low. Recent efforts to improve monitoring of Tw and BOD in Latin America are notable, but measurements before 2010 are lacking. Data is extremely scarce across the other world regions. While there are some localised pockets of high data availability in different regions (e.g. TDS measurements in South Africa), publicly accessible observational data records are virtually non-existent across Africa, the Middle East and most of Asia. Therefore, it is not possible to rely solely on measured data to assess the global status of surface water quality. Techniques that can further improve our understanding of global water quality dynamics with less reliance on in situ measurements are rapidly emerging.

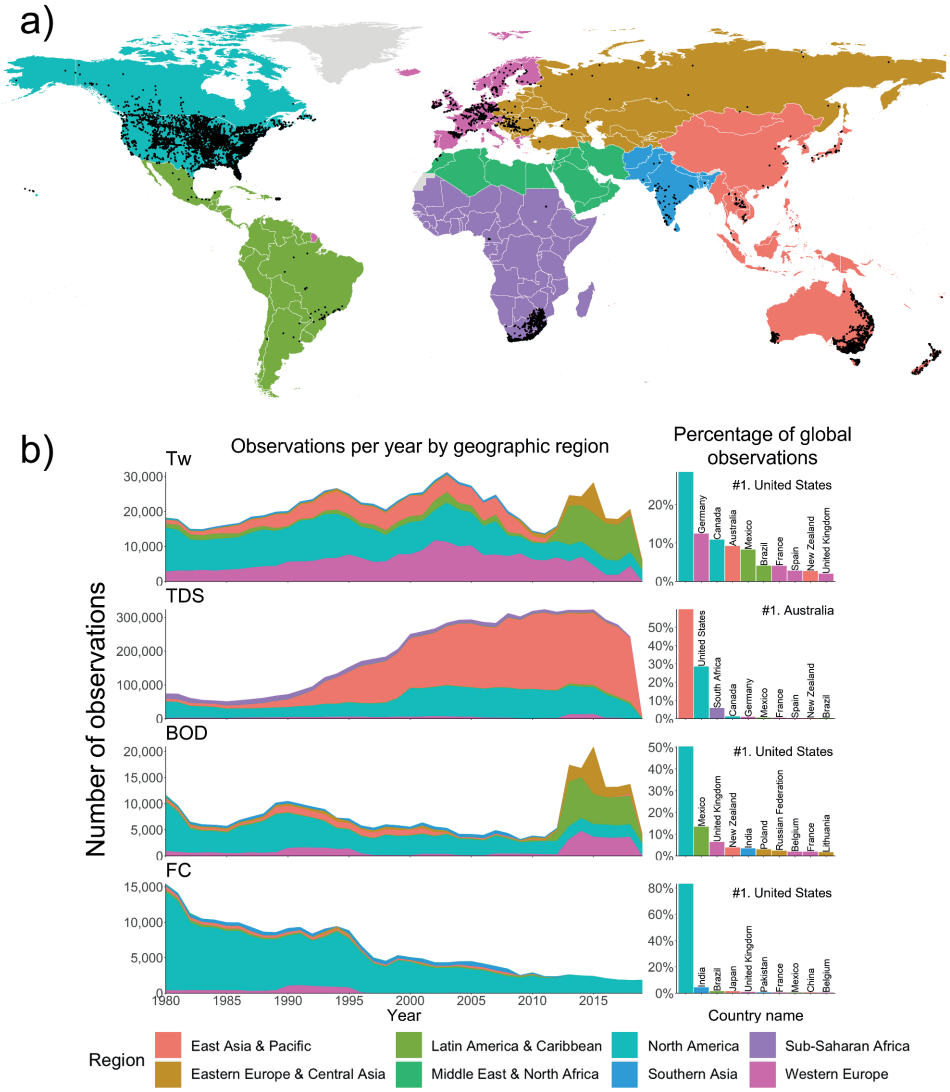

Figure 1.1 a) Locations of water quality monitoring stations with >90 observations from 1980–2019 of any of the following water quality constituents: water temperature (Tw), total dissolved solids (TDS), biological oxygen demand (BOD) or fecal coliform (FC). Line plots in panel b) display the number of observations per year, aggregated per geographic region, while bar plots show the ten countries with the most observations per water quality constituent.

Remote sensing techniques can be applied to assess surface water quality with a wide spatio-temporal coverage, while the use of historical images can facilitate the reconstruction of past conditions (Gholizadeh et al., 2016). Further improvements to the radiometric, spatial and spectral resolution of remote sensing techniques, in combination with the increasing availability of images over space and time, will continue to increase the potential for large-scale monitoring of optically-active water quality constituents (e.g. turbidity, chlorophyll-a, dissolved oxygen) (Gholizadeh et al., 2016). However, remote sensing applications are limited to constituents with distinguishable spectral features and are constrained by the spatio-temporal resolution of the available imagery (Damania et al., 2019).

With the limitations associated with in situ observations and the analysis of remote sensing images, modelling approaches have been developed to assess surface water quality. Global water quality modelling is an emerging field (Kroeze et al., 2016; Tang et al., 2019), particularly compared to global hydrological modelling (Bierkens, 2015; Sood and Smakhtin, 2015). The field incorporates a range of modelling approaches, from machine-learning algorithms that predict water quality based on anthropogenic and environmental data (Desbureaux et al., 2022), to more mechanistic and process-based approaches (Beusen et al., 2015; UNEP, 2016; Vermeulen et al., 2019; van Vliet et al., 2021). Process-based surface water quality models offer opportunities to overcome shortcomings related to deficiencies in the observational records by simulating the emission and transport of pollutant loadings along the river network directly, based on climatic, hydrological and socioeconomic forcings. In addition to state assessment, these models can be used to elucidate the drivers of pollution or to assess the impact of management interventions (Tang et al., 2019). Furthermore, process-based modelling approaches offer unique opportunities to project future surface water quality under different climate change and socioeconomic development scenarios.

While the field of large-scale surface water quality modelling is still in its relative infancy, there are increasing efforts to simulate a diverse range of water quality constituents. This has included physical parameters (e.g. water temperature, salinity), indicators of organic pollution (e.g. biological oxygen demand), microorganisms (e.g. fecal coliform, cryptosporidium), nutrients (e.g. nitrogen, phosphorus) and emerging contaminants (e.g. microplastics, triclosan) (Table. 1.1). In addition to the variety in water quality constituents, there is high diversity in the existing large-scale water quality models with respect to aspects including: 1) spatial extent (e.g. distributed vs. lumped); 2) temporal resolution (e.g. daily to decadal); and 3) reporting form (e.g. pollutant loads vs. concentrations).

As with in situ monitoring and remote sensing approaches, large-scale surface water quality modelling approaches have significant limitations. The availability of high quality and easily accessible global datasets, both for model inputs and evaluation, presents the biggest challenge (Tang et al., 2019). Aiming for consistency across large scales, globally available datasets of socioeconomic drivers (e.g. population, urbanisation, GDP) are typically used to represent drivers of pollution. However, it should be noted that large uncertainties exist in the translation of these drivers into pollutant loadings (UNEP, 2016; Moreno-Rodenas et al., 2019).

Table 1.1 A selection of existing global surface water quality models and their key characteristics (adapted from WWQA, 2021).

Global surface water models	Water quality constituent(s)		Hydrology	Spatial resolution[2]	Temporal resolution[3]	Key reference
	Parameter group	Parameters[1]				
GREMiS	Other	Microplastics	WBM	Basin	Annual	van Wijnen *et al.,* (2019)
MARINA-Global	Nutrients Microorganisms Other	DIN, DON, DIP, DOP Cryptosporidium Microplastics, Triclosan	VIC	Sub-basin	Annual	Strokal et al., (2019)
IMAGE-GNM	Nutrients	TN, TP, Si	PCR-GLOBWB2	Gridded (0.5 degree)	Annual	Beusen *et al.,* (2015)
GloWPa	Microorganisms	Cryptosporidium, Rotavirus	VIC	Gridded (0.5 degree)	Monthly	Vermeulen *et al.,* (2019)
QUAL	Physical Organic	Tw, TDS BOD	VIC	Gridded (5 arc-minutes)	Monthly	van Vliet *et al.,* (2021)
WORLDQUAL	Physical Organic Nutrients Microorganisms	Tw, TDS BOD TN, TP FC	WaterGap	Gridded (5 arc-minutes)	Monthly	UNEP (2016)
DynQual	Physical Organic Microorganisms	Tw, TDS BOD FC	PCR-GLOBWB2	Gridded (5 arc-minutes)	Monthly	Jones *et al.,* (2023)

[1]DIN: dissolved inorganic nitrogen; DON: dissolved organic nitrogen; DIP: dissolved inorganic phosphorus; DOP: dissolved organic phosphorus; TN: total nitrogen; TP: total phosphorus; Si: Silicia; Tw: water temperature; TDS: total dissolved solids; BOD: biological oxygen demand; FC: fecal coliform.

[2]Typical spatial resolution of output data.

[3]Typical temporal resolution of output data. Note that the simulation resolution may be finer, and subsquently aggregated.

Uncertainties in pollutant loading calculations and the high variability of biogeochemical processes, combined with the propagation of prediction errors from climate and hydrological models, translate into relatively large uncertainties in the output of global water quality models (van Griensven and Meixner, 2006). Given these uncertainties, parsimonious approaches should be the basis of future developments in the field of global water quality modelling (UNEP, 2016). Coupled hydrological and pollutant transport modelling is beneficial for water quality simulations, as interactions between these components (e.g. dilution, flow velocities) are important determinations of in-stream concentrations. With many pollutants sharing common sources (e.g. wastewater treatment plants, agriculture), represented in water quality models using similar input datasets, multi-pollutant approaches can be computationally efficient while facilitating a more holistic understanding of the surface water quality status. Multi-pollutant modelling approaches can also facilitate the representation of biological, physical and chemical interactions between pollutants (Kroeze et al., 2016). For example, decay rates of many pollutants are strongly water temperature dependent, while plastics can bind hydrophobic chemicals and pesticides (Kroeze et al., 2016).

Therefore, this thesis advocates for models that provide consistent descriptions of water, energy and (multiple) pollutant fluxes. This is particularly important for realising two of the key aims of large-scale water quality modelling: 1) to simulate water quality in ungauged catchments; and 2) to project water quality under (uncertain) future change. However, given the necessary model approximations, uncertainties in input data and the overall complexity in the drivers of pollutant loadings, understanding and communicating the purpose(s) of global water quality models is paramount (UNEP, 2016).

In this thesis, a new global surface water quality model (the **Dyn**amical Surface Water **Qual**ity model), henceforth *DynQual*, is introduced. *DynQual* is a high-spatio-temporal resolution surface water quality model that can be used to simulate water temperature (Tw) and concentrations of total dissolved solids (TDS), biological oxygen demand (BOD) and fecal coliform (FC) at 5 arc-min spatial resolution (~10x10km at the equator) with a daily timestep. *DynQual* extends the current representation of human-water interactions in the hydrological model *PCR-GLOBWB2* (Sutanudjaja et al., 2018), in which dynamic human water demands, withdrawals and return flows per sector are fully integrated, to also consider these sectors as sources of surface water pollution (Fig. 1.2). The development of *DynQual* is rooted in past large-scale water temperature and pollutant concentration modelling, most notably *DynWat* (van Beek et al., 2012; Wanders et al., 2019), *VIC-RBM* (van Vliet et al., 2012a), *QUAL* (van Vliet et al., 2021) and *WorldQual* (UNEP, 2016).

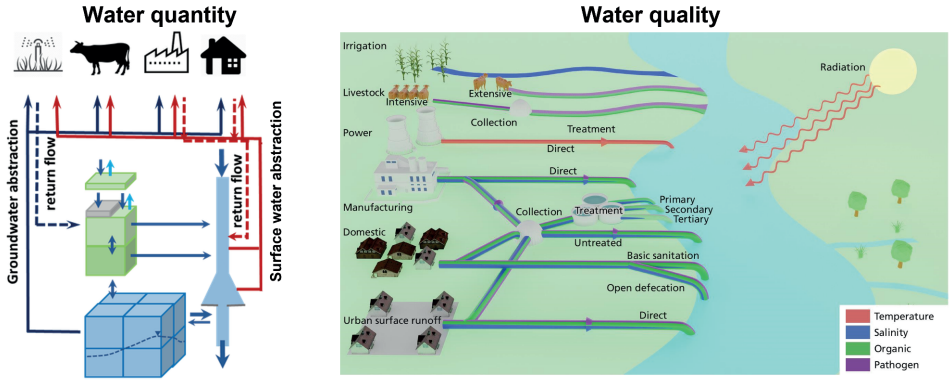

Figure 1.2 Human interactions with the water system included in the *DynQual* modelling framework, from both water quantity and water quality perspectives.

The key strengths of *DynQual* both supplement and extend the possibilities of existing large-scale water quality models. The high spatial resolution at which *DynQual* is implemented is advantageous as simulations of both hydrological variables and water temperature are improved at finer spatial extents (Sutanudjaja et al., 2018; Wanders et al., 2019). High fidelity simulations of discharge and water temperature are important due to the impact of dilution and in-stream decay processes, respectively, on in-stream pollutant concentrations. Unlike static models, the dynamic nature of *DynQual* enables analysis of intra- and inter- annual trends in surface water quality. Pollutant loadings are estimated and tracked from different water user sectors (i.e. irrigation, livestock, domestic, manufacturing, thermoelectric power) separately, which can facilitate increased understanding on the main drivers of pollution in different rivers via (dynamic) sectoral attribution.

Furthermore, the accessibility and flexibility of *DynQual* is a key strength over existing surface water quality models. The source code, standard parameterisation and input datasets for *DynQual* are openly accessible (https://github.com/UU-Hydro/DYNQUAL). The model can be run in multiple configurations depending on user preference. For example, the routing can be run as a stand-alone routine, facilitating the use of hydrological input from any land surface or hydrological model. Similarly, there is flexibility in the quantification of pollutant loadings, which can be estimated within *DynQual* simulations or forced to the model directly. The second option enables users to quantify pollutant loadings via their preferred methodology, and subsequently route these through the global stream network, account for in-stream decay processes and compute in-stream pollutant using the *DynQual* model framework.

Of course, *DynQual* is not immune to the many challenges that complicate large-scale water quality modelling efforts. Nevertheless, *DynQual*, together with the existing suite of large-scale models (Table. 1.1), represent valuable tools that facilitate first-order assessments of global water quality dynamics which are consistent across space and time. This is especially advantageous for investigating surface water quality in ungauged catchments, facilitating meaningful comparisons across different world regions and for projecting surface water quality under (uncertain) future change.

1.3 Global change scenarios and surface water quality

Climate change and socioeconomic developments will impact both the availability and quality of global surface waters in the future, with implications for human water uses and freshwater ecosystem health (Arnell, 1999; Haddeland et al., 2014). While the impacts of global change on water availability have been studied extensively (Schewe et al., 2014), quantitative projections of future surface water quality are sparse, particularly at the global scale (Caretta et al., 2022). However, changes in water quantity and water quality aspects are intrinsically linked, with a combination of alterations to hydrological regimes (Trenberth et al., 2014; Konapala et al., 2020; Kraaijenbrink et al., 2021), water withdrawals (Wada et al., 2016) and pollutant loadings under (uncertain) climate change and socioeconomic developments driving changes in future surface water quality.

Given fundamental uncertainties, exploring different possible futures are an essential part of global change assessments (Riahi et al., 2017). The current framework adopted by the climate research community, and as featured in the Intergovernmental Panel Report on Climate Change Sixth Assessment Report (IPCC AR6) (IPCC, 2022), combines Shared Socioeconomic Pathways (SSPs) and Representative Concentration Pathways (RCPs) in scenario matrix architecture (van Vuuren et al., 2014; O'Neill et al., 2016). SSPs and RCPs describe future plausible developments in socioeconomic and climatic conditions, respectively, to provide integrated scenarios for exploring uncertain future change in a consistent framework. RCPs describe alternative trajectories of atmospheric greenhouse gas concentrations and other radiative forcings. On the other hand, SSPs describe plausible alternate

pathways of future societal development (narratives) with respect to factors such as population, technological and economic growth.

Narratives and quantitative projections for the SSPs are further used for the development of integrated scenarios, which elaborate the SSPs in terms of factors such as energy systems (Bauer et al., 2017), land use (Popp et al., 2017), sectoral water demands (Wada et al., 2016) and greenhouse gas emissions (Riahi et al., 2017; Meinshausen et al., 2020) using a range of Integrated Assessment Models (IAMs). While many SSP-RCP combinations are plausible, priority scenarios have been identified as part of Phase 6 of the Coupled Model Intercomparison Project (CMIP6). These 'Tier 1' scenarios (i.e. SSP1-RCP2.6; SSP2-RCP4.5; SSP3-RCP7.0 and SSP5-RCP8.5) are selected to span a wide range of uncertainty in future conditions (O'Neill et al., 2016) and are displayed in Fig. 1.3.

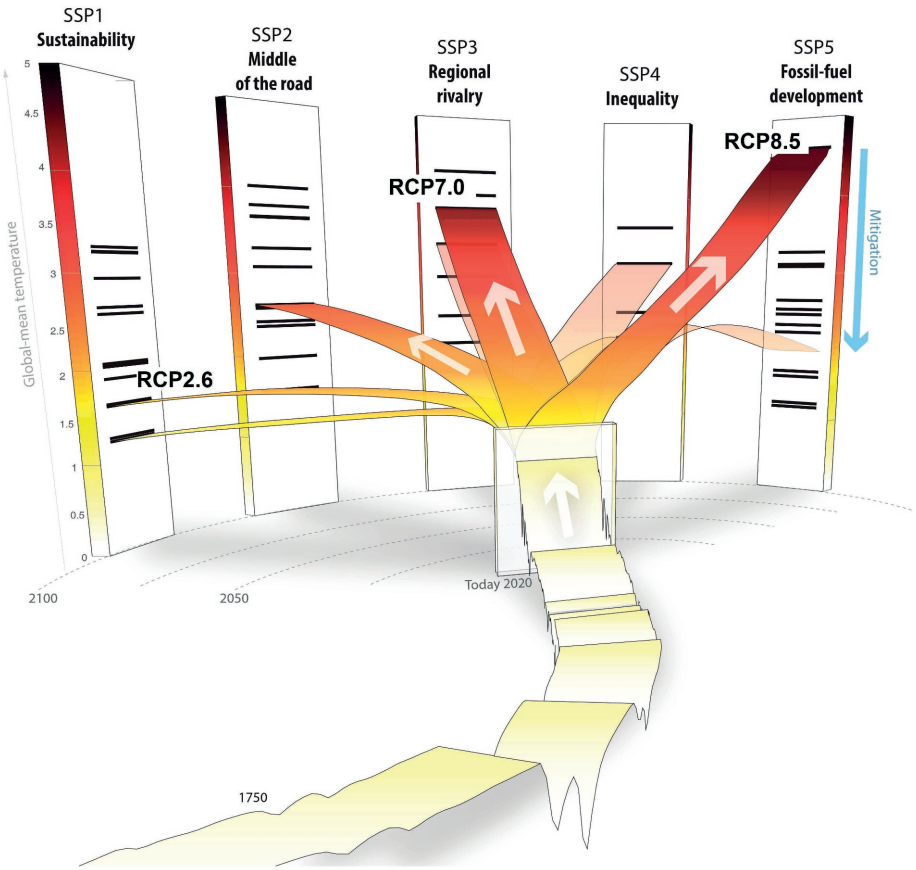

Figure 1.3 The RCP scenarios with their corresponding (feasible) SSP pathways (adapted from: Meinshausen *et al.*, 2020)

For modelling future global water quality, projections of changes to both climate and socioeconomic forcings under different scenarios is required. To produce projections of future climate, global climate models (GCMs) are forced with these emissions scenarios. Output from GCMs, such as precipitation, air temperature and solar radiation, is commonly bias-corrected for use in hydrological models. On the other hand, changes in sectoral water demands and anthropogenic pollution are quantified based on socioeconomic variables, such as population, economic development and urbanisation, commonly

derived from IAMs. In this thesis, future surface water quality is simulated using bias-corrected daily CMIP6 climate output from the five primary GCMs (GFDL-ESM4; IPSL-CM6A-LR; MPI-ESM1-2-hr; MRI-ESM2-0 and UKESM1-0-LL) of the Inter-Sectoral Impact Model Intercomparison Project (ISIMIP3b) (Lange and Buchner, 2021) for three SSP-RCP scenarios (SSP1-RCP2.6; SSP3-RCP7.0 and SSP5-RCP8.5). These scenarios capture a large range of plausible future developments in societal and climatic conditions, while using output from five GCMs better accounts for uncertainties inherent in the climatological projections.

1.4 Research objectives and questions

Human activities, including crop and livestock production, the manufacturing of goods, power generation and domestic activities rely upon the availability of water in both adequate quantities and of acceptable quality for an intended use. Water uses that are not fully consumptive generate return flows, the composition of which will be reflective of the water use activity. These return flows, if managed inadequately or ineffectively (e.g. insufficient wastewater treatment capacities or efficiencies), can degrade the quality of the receiving waters. This can both threaten ecosystem health and impact our ability to safely use surface water resources further downstream.

Inability to meet our clean water demands, both now and in the future, is considered one of the major risks to humankind both in terms of likelihood and potential impacts. While many studies have addressed this topic from a water quantity perspective, limited knowledge exists regarding the current quality status of global surface waters. Even less is known about how climate and socioeconomic change will impact surface water quality in the future.

To address these knowledge gaps, the following research objective was defined:

To assess the past and current status of surface water quality globally, and to evaluate the impact of (uncertain) global change on future surface water quality.

This objective was addressed in three sequential steps, each associated with a specific research question:

1. What is the current global status of wastewater management (i.e. production, collection, treatment and reuse)? (Chapters 2 and 3)
2. What is the past and current status of global surface water quality, as indicated by water temperature (Tw) and indicators of salinity (total dissolved solids), organic (biological oxygen demand) and pathogen (fecal coliform) pollution? (Chapters 3 and 4)
3. How does global surface water quality change in the future under near-term sustainability targets (Chapter 4) and long-term scenarios of climate and socioeconomic change (Chapter 5)?

1.5 Research approach and thesis outline

The objective and research questions are addressed in four scientific papers, which are presented in Chapters 2 to 5. An overview of all Chapters, including their interconnections and dependencies, is presented in Fig. 1.4.

To address the first research question, the global status of wastewater production, collection, treatment and reuse was assessed using a data-driven approach (Chapter 2). Country-level wastewater data was collated from various databases, with multiple linear regression used to predict missing values. Subsequently, these data were downscaled to 5 arc-min resolution (Chapter 2) and wastewater treatment was further disaggregated by treatment level (Chapter 3). The country-level database serves as a reference for understanding the global status of wastewater, while spatially explicit results are suited to more detailed hydrological, water quality and water resource assessments.

To answer the second research question, the **Dyn**amical Surface Water **Qual**ity model (*DynQual*) model was developed, evaluated and applied for the time period 1980–2019 (Chapters 3 and 4). Notable features of *DynQual* include the high spatial (5 arc-min) and temporal (daily) resolution, full coupling with the global hydrological model *PCR-GLOBWB2* (Sutanudjaja et al., 2018) and the inclusion of the high-resolution wastewater data (i.e. Chapters 2 and 3). Presentation of results in Chapter 3 focuses on hot- and bright- spot identification, trends in surface water quality dynamics (seasonal and long-term) and the relative contribution of different water sectors to in-stream pollutant concentrations.

Conversely, the results presented in Chapter 4 focus on linking simulated in-stream concentrations to critical water quality thresholds for different water use sectors and environmental health. Furthermore, *DynQual* was applied to investigate the benefit of achieving SDG 6.3 (i.e. to halve the proportion of untreated wastewater entering the environment by 2030) on global surface water quality especially considering exceedances of these critical thresholds.

In Chapter 5, the first assessment of the impact of (uncertain) climate change and socioeconomic development on long-term water quality is provided. To this end, *DynQual* was forced with an ensemble of bias-correct GCM output, together with socioeconomic scenarios for estimating pollutant loadings and developments in wastewater treatment, under multiple scenarios to simulate surface water quality until the end of the century. To elucidate the implications of changing surface water quality in the future, the number of people exposed to in-stream concentrations that exceed safe water quality thresholds was estimated.

Chapter 6 combines the main findings of the previous Chapters to fulfil the research objective of this thesis. Here, the scientific contribution and outlook for future research is also discussed. Incorporating novel findings from all preceding Chapters, this thesis presents the first (preliminary) analysis of future water scarcity including water quality aspects. This also provides an example of how the water quality simulations presented in this thesis can inform large-scale water resource assessments.

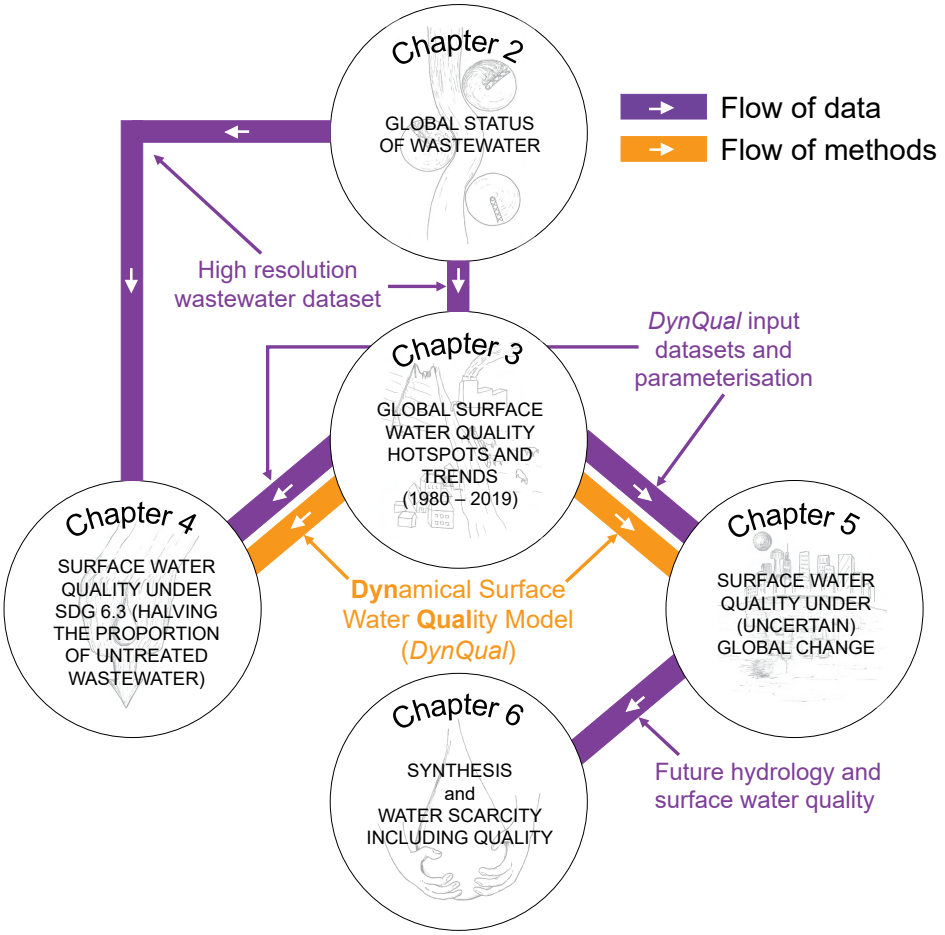

Figure 1.4 Overview of the Chapters presented in this thesis, including their interconnections and dependencies.

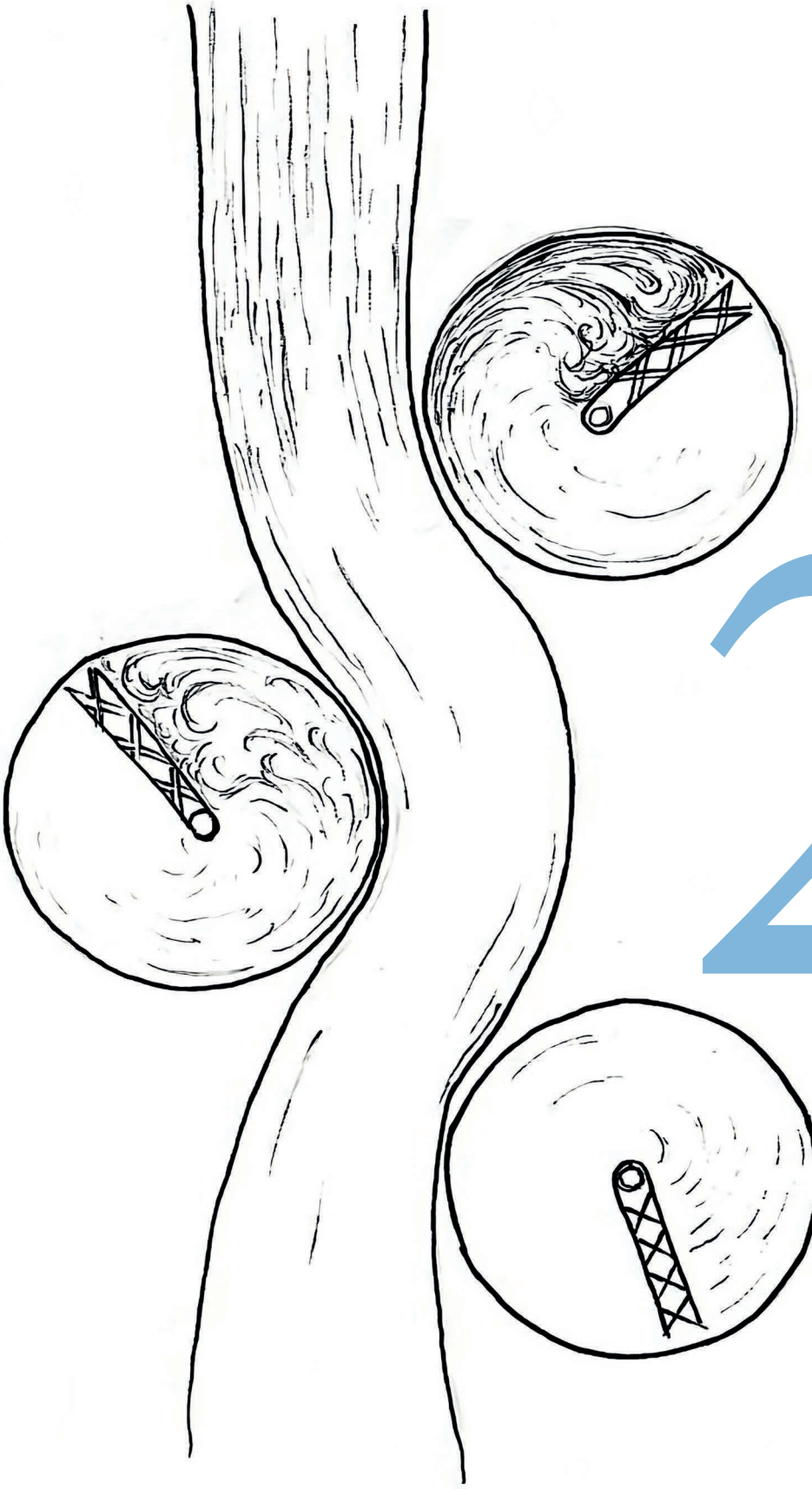

2

Chapter 2 | Country-level and gridded estimates of wastewater production, collection, treatment and reuse

Abstract

Continually improving and affordable wastewater management provides opportunities for both pollution reduction and clean water supply augmentation, while simultaneously promoting sustainable development and supporting the transition to a circular economy. This study aims to provide the first comprehensive and consistent global outlook on the state of domestic and manufacturing wastewater production, collection, treatment and reuse. We use a data-driven approach, collating, cross-examining and standardising country-level wastewater data from online data resources. Where unavailable, data are estimated using multiple linear regression. Country-level wastewater data are subsequently downscaled and validated at 5 arc-min (∼10 km) resolution. This study estimates global wastewater production at 359.4 billion m^3 yr^{-1}, of which 63% (225.6 billion m^3 yr^{-1}) is collected and 52% (188.1 billion m^3 yr^{-1}) is treated. By extension, we estimate that 48% of global wastewater production is released to the environment untreated, which is substantially lower than previous estimates of ∼80%. An estimated 40.7 billion m^3 yr^{-1} of treated wastewater is intentionally reused. Substantial differences in per capita wastewater production, collection and treatment are observed across different geographic regions and by level of economic development. For example, just over 16% of the global population in 'high income' countries produce 41% of global wastewater. Treated wastewater reuse is particularly substantial in the Middle East and North Africa (15%) and Western Europe (16%), while comprising just 5.8% and 5.7% of the global population, respectively. Our database serves as a reference for understanding the global wastewater status and for identifying hotspots where untreated wastewater is released to the environment, which are found particularly in south and southeast Asia. Importantly, our results also serve as a baseline for evaluating progress towards many policy goals that are both directly and indirectly connected to wastewater management. Our spatially-explicit results available at 5 arc-min resolution are well suited for supporting more detailed hydrological analyses such as water quality modelling and large-scale water resource assessments, and can be accessed at: https://dx.doi.org/10.1594/PANGAEA.918731.

Published: Jones, E.R., van Vliet, M.T.H., Qadir, M., and Bierkens, M.F.P. (2021). Country-level and gridded estimates of wastewater production, collection, treatment and reuse. *Earth System Science Data, 13(2)*, pp. 237–254, DOI:10.5194/essd-13-237-2021

2.1 Introduction

Clean water is essential for supporting human livelihoods, achieving sustainable development and maintaining ecosystem health. All major human activities, such as crop and livestock production, manufacturing of goods, power generation and domestic activities rely upon the availability of water in both adequate quantities and of acceptable quality at the point of intended use (Ercin and Hoekstra, 2014; van Vliet et al., 2017). It is increasingly recognised that conventional water resources such as rainfall, snow-melt and runoff captured in lakes, rivers and aquifers are insufficient to meet human demands in water scarce areas (Hanasaki et al., 2013; Kummu et al., 2016; Jones et al., 2019). While increases in water use efficiencies can somewhat reduce the water demand-supply gap, these approaches must be combined with supply and quality enhancement strategies (Gude, 2017). Conventional supply enhancement strategies, such as reservoir construction, surface water diversion and pipeline construction are contingent on geographic and climate factors, can face strong public opposition and often lack water quality considerations.

A growing set of viable but unconventional water resources offer enormous potential for narrowing the water demand-supply gap towards a water-secure future. Unconventional water resources encapsulate a range of strategies across different scales, from localised fog-water and rainwater harvesting, to mega-scale desalination plants and wastewater treatment and reuse facilities (Jones et al., 2019; Morote et al., 2019; Qadir et al., 2020). The use of unconventional water resources has grown rapidly in the last few decades, often out of necessity, and their importance across various geographic scales is already irrefutable (Qadir et al., 2018; Jones et al., 2019). Furthermore, continually improving unconventional water resources technologies have permitted more efficient and economical 'tapping' of water resources which were previously unusable due to access constraints or the added costs related to unsuitable water quality (e.g. seawater desalination, wastewater treatment).

Wastewater is broadly defined as 'used' water that has been contaminated as a result of human activities (Mateo-Sagasta et al., 2015). While agricultural runoff is rarely collected or treated (WWAP, 2017), return flows from domestic and manufacturing sources (henceforth 'wastewater') can be collected in infrastructure including piped systems (sewerage) or on-site sanitation systems (e.g. septic tanks, pit latrines). Wastewater is increasingly recognised as a reliable and cost-effective source of freshwater, particularly for agricultural applications (Jiménez and Asano, 2008; Mateo-Sagasta et al., 2015). Nevertheless, wastewater remains an 'untapped' and 'undervalued' resource (Mateo-Sagasta et al., 2015). Wastewater treatment aims to improve the quality of 'used' water sources to reduce contaminant levels below sectoral quality thresholds for intentional reuse or to minimise the environmental impacts of wastewater return flows. Treated wastewater flows can also provide a substantial source of (clean) freshwater flows for maintenance of river flows, especially during drought (Luthy et al., 2015). Where treated wastewater discharges form a substantial part of the river flow, de-facto wastewater reuse, defined as the incidental presence of treated wastewater in a water supply, can be high (Rice et al., 2013; Beard et al., 2019). Treated wastewater can also be used for groundwater recharge, helping to preserve the viability of freshwater extraction from groundwater into the future (Qadir et al., 2015), in addition to applications in agroforestry systems (Moussaoui et al., 2019) and aquaculture (Khalil and Hussein, 2008). In summary, wastewater treatment can improve river water quality and ecosystem health, while providing an alternative source of freshwater for human use and subsequently reducing competition for conventional water supplies.

Historically, wastewater (both treated and untreated) has predominantly been used for non-potable purposes, particularly agriculture and landscape irrigation (Qadir et al., 2007; WWAP, 2017; Zhang and Shen, 2019). Agricultural activities are expected to increasingly rely on alternative water resources, as this sector has the largest water demands globally (Wada et al., 2013). Furthermore, the agricultural sector faces reductions in conventional water resources allocation (Sato et al., 2013). The

reliable supply of water, reduced need for additional fertilizer and potential for growing high value vegetables promote wastewater irrigation in water-scarce developing countries (Sato et al., 2013). However, much of the wastewater currently reused is inadequately treated or even untreated (Qadir et al., 2010). Demands for wastewater are increasing at a faster pace than treatment solutions and institutions that ensure the safe distribution and management of wastewater (Sato et al., 2013). The primary challenge in promoting reuse is ensuring safety – both for human and ecosystem health – and therefore ensuring that wastewater is adequately treated prior to use or environmental discharge (Scott et al., 2010; WWAP, 2017). This is needed to achieve the required paradigm shift in water resources management, whereby wastewater is viewed as a resource (for energy, nutrients and water) rather than as 'waste' (WWAP, 2017; Qadir et al., 2020).

To understand the current state and explore the future potential of wastewater as a resource, a comprehensive and consistent global assessment of wastewater production, collection, treatment and reuse is required. This information is essential for assessing progress towards Sustainable Development Goal (SDG) 6, such as SDG 6.3 that specifically focuses on achieving water quality improvements through halving the proportion of untreated wastewater and promoting safe reuse globally. Furthermore, this information is important for identifying hotspots where improvements in wastewater management are highly necessary and as input data for a range of scientific assessments (e.g. stream water quality dynamics, water scarcity assessments). However, the availability of wastewater data at the continental and global scales is sparse, and often outdated or from inconsistent reporting years (Sato et al., 2013). Previous studies remain limited in their approach and estimates, relying on a few data sources covering less than half of the countries across the world (Sato et al., 2013; Mateo-Sagasta et al., 2015). A recent study explored the global and regional 'potential' of wastewater as a water, nutrient and energy source, but did not address the collection, treatment and reuse aspects of wastewater (Qadir et al., 2020). This paper presents the first global assessment of spatially-explicit wastewater production, collection, treatment and reuse, consistently combing different data sources. Country-level quantifications are downscaled to a grid level of 5 arc-min for inclusion in large-scale water resource assessments and water quality models.

2.2 Methods

2.2.1 Wastewater data sources

The fate of domestic and manufacturing wastewater after production can follow a number of paths (Fig. 2.1). Wastewater from these activities can be collected, typically in sewers, septic tanks or pit latrines, or uncollected and discharged directly to the environment (e.g. open defecation). Collected wastewater can undergo treatment, ranging from basic primary treatment (e.g. removing suspended solids) to specialised tertiary or triple barrier treatment (e.g. nutrient removal, toxic compound removal), or can be discharged to the environment untreated (Mateo-Sagasta et al., 2015). When treated, wastewater can be released to the environment or intentionally reused as a 'fit-for-purpose' water source. Untreated wastewater can similarly be discharged to the environment or intentionally used as a source of freshwater. Furthermore, both treated and untreated wastewater can be used unintentionally where wastewater is incidentally present in a water supply ('de-facto reuse').

Country-level wastewater data was collated from four online databases (Table. 2.1): Global Water Intelligence; Food and Agricultural Organisation of the United Nations, Eurostat and United Nations Statistics Division. For consistency, the year 2015 was selected for all wastewater data. Where wastewater data from the online sources was reported in a different year (up to a maximum of 10 years, i.e. 2006 onwards), all wastewater data was standardised to 2015 based on data from the most recent reporting year (see Table 2.1 for the standardisation method).

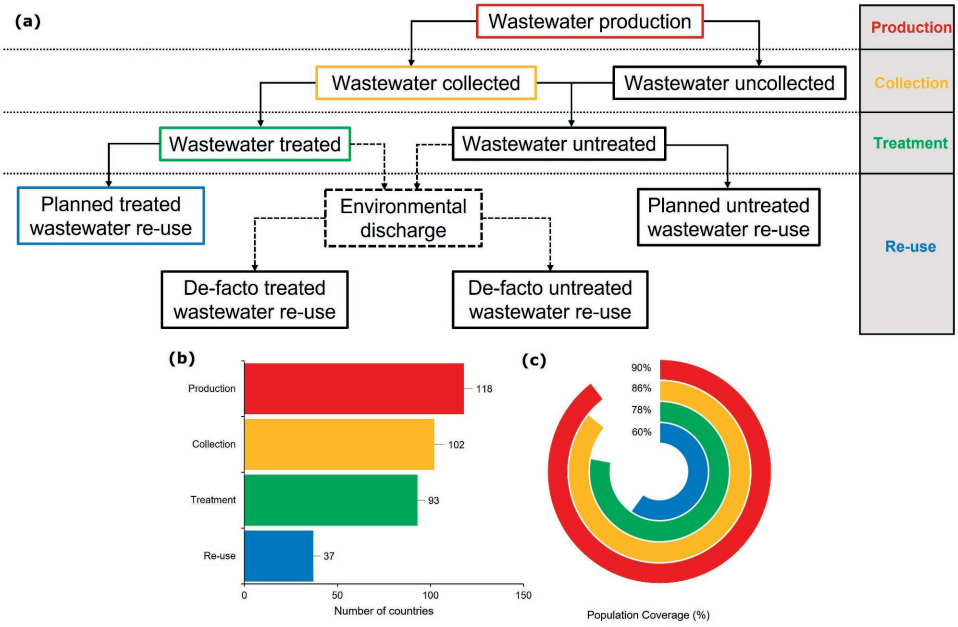

Figure 2.1 a) Fate of wastewater: including b) the number of countries for which wastewater data is available; and c) the percentage of population coverage (i.e. the proportion of the global population for which wastewater data is available).

Data from different sources was cross examined to check for consistency and to remove implausible data. Where large discrepancies (exceeding one order of magnitude) existed between different data sources for a country, data points were excluded. For example, GWI report Kazakhstan to produce 6,205 million m^3 yr^{-1}, whereas FAO report just 411 million m^3 yr^{-1}. Similarly, FAO report Moldova to produce 46.7 million m^3 yr^{-1} compared to 672.1 million m^3 yr^{-1} by UNSD. In total, reported data for 11 countries were excluded for wastewater production. For wastewater collection and treatment, percentage data was cross referenced with reported connection rates (i.e. percentage population connected to wastewater infrastructure). Six and seven countries were excluded for collection and treatment, respectively. For example, GWI report a 95.2% collection rate for Azerbaijan, while UNSD report that only 32.4% of people are connected to wastewater collection systems. Similarly, GWI report a 17% treatment rate in Hong Kong, whereas UNSD report that 93.5% of people are connected to wastewater treatment plants. No data points were excluded for wastewater reuse. In a small number of cases where percentage values obtained were marginally illogical (i.e. wastewater collection < wastewater treatment, wastewater treatment < wastewater reuse), percentage values were set to the proceeding level in the wastewater chain (Fig. 2.1).

Table 2.1 displays the data sources and the associated number of countries with wastewater data for production, collection, treatment and reuse. The procedure for standardising data to the year 2015, when required, is presented. Wastewater production is assumed to be dependent upon both population size and per capita production (related to per capita wealth). Hence, we standardise wastewater production linearly with GDP, a combined metric of population size and wealth. Conversely, wastewater collection and treatment are assumed to be more dependent on economics, hence we linearly apply GDP per capita for standardisation. The methods used to compile wastewater production, collection, treatment and reuse data from multiple sources to provide a single quantification per country is also displayed. Lastly, the population coverage in percentage terms and

by the number of unique countries is displayed both per geographic region and by economic classification. The number of unique countries and the population coverage of data at each stage of the wastewater chain is also displayed in Fig. 2.1. Reported wastewater data was available for the majority of the world's most populous countries. This results in a high percentage population coverage relative to the number of countries. Both the number of countries and population coverage reduces through the wastewater chain, with available wastewater data decreasing from 118 to 37 countries (90% to 60% population coverage) from wastewater production to wastewater reuse data.

Table 2.1 Wastewater data sources and population coverage by regional and economic aspects, including the number of unique countries (in square brackets). Method for standardisation of wastewater data to 2015 and the method for compiling wastewater data from multiple sources into a single quantification per country.

	Data sources[1]	Standardisation to 2015	Data compiling method	Regional aspects		Economic aspects	
				Region	Population coverage[2]	Income	Population coverage[3]
Production	GWI [94] FAO [98] UNSD [23] Eurostat [20]	Divide by GDP ($) in reporting year, multiply with GDP ($) in 2015.	Average of all available sources.	North America Latin America & Caribbean Western Europe Middle East & North Africa Sub-Saharan Africa Southern Asia Eastern Europe & Central Asia East Asia & Pacific	100% [2] 93.9%) [19] 99.8% [19] 98.8% [19] 49.6% [17] 96.4% [4] 89.4% [23] 95.3% [15]	High Upper middle Lower middle Low	99.4% [48] 98.0% [34] 94.6% [31] 13.3% [5]
Collection	GWI [95] FAO [55]	Divide by GDP per capita ($ per capita) in reporting year, multiple with GDP per capita ($ per capita) in 2015.	GWI data prioritised. FAO data if unavailable.	North America Latin America & Caribbean Western Europe Middle East & North Africa Sub-Saharan Africa Southern Asia Eastern Europe & Central Asia East Asia & Pacific	100% [2] 96.7% [20] 99.8% [18] 88.3% [17] 61.1% [13] 96.4% [4] 69.9% [16] 83.6% [12]	High Upper middle Lower middle Low	99.4% [47] 97.7% [29] 81.0% [21] 34.9% [5]
Treatment	GWI [76] FAO [78] UNSD [21]	Divide by GDP per capita ($ per capita) in reporting year, multiple with GDP per capita ($ per capita) in 2015.	GWI data prioritised. FAO or UNSD where unavailable (most recent reporting year prioritised)	North America Latin America & Caribbean Western Europe Middle East & North Africa Sub-Saharan Africa Southern Asia Eastern Europe & Central Asia East Asia & Pacific	100% [2] 90.0% [17] 99.8% [19] 65.9% [13] 25.7% [8] 95.2% [3] 73.4% [21] 80.2% [10]	High Upper middle Lower middle Low	98.4% [46] 91.2% [27] 69.4% [15] 27.1% [5]
Re-use	GWI [20] FAO [32]	Wastewater production normalised to reporting year of wastewater re-use based on GDP ($), percentage re-use calculated, applied to 2015 production data.	GWI data prioritised. FAO data if unavailable.	North America Latin America & Caribbean Western Europe Middle East & North Africa Sub-Saharan Africa Southern Asia Eastern Europe & Central Asia East Asia & Pacific	90.0% [1] 67.2% [5] 42.5% [3] 83.0% [13] 21.5% [6] 74.9% [1] 0.6% [2] 70.2% [6]	High Upper middle Lower middle Low	68.7% [19] 77.7% [10] 48.7% [4] 24.8% [4]

[1]Abbreviations for the data sources are as follows: Global Water Intelligence (GWI), Food and Agricultural Organisation of the United Nations (FAO), United Nations Statistics Department (UNSD), European Union Statistics Office (Eurostat).

[2]Data availability per region expressed as a percentage of the total population. Total number of countries per geographic region are: East Asia and Pacific [38], Eastern Europe and Central Asia [30], Latin America and Caribbean [41], Middle East and North Africa [21], North America [3], Southern Asia [8], Sub-Saharan Africa [48] and Western Europe [26].

[3]Data availability per economic classification expressed as a percentage of the total population. Total number of countries per economic classification are: High [76], Upper middle [56], Lower middle [52], and Low [31] income.

2.2.2 Regression for country-level predictions

Datasets of predictor variables for regression analyses were downloaded from multiple sources (see overview Table 2.2). Datasets spanned a wide range of predictor variables covering social (e.g. total and urban population), economic (e.g. GDP, HDI), hydrological (e.g. irrigation water scarcity) and geographic (e.g. land area, agricultural land) dimensions. The selected predictor variables were expected to have a physical basis for correlation with wastewater production, collection, treatment or reuse. Where appropriate, datasets from these sources were combined to produce comparable metrics for countries of different population and geographic sizes (e.g. GDP per capita [$ per capita]; desalination capacity per capita [$m^3\ yr^{-1}$ per capita]). Values were taken for the year 2015, where available, or from the closest reporting year when unavailable. Irrigation water scarcity and desalination capacity were taken from 2019 and 2018, respectively. Data was transformed, either using a log or square root transformation, to reduce the skew in the independent variables and to ensure normality.

Table 2.2 Data sources of predictor variables for wastewater production, collection, treatment and reuse regression analysis.

Data Source	Predictor Variable	Year	Link
World Bank	Land area (km^2)	2015	data.worldbank.org/indicator/AG.LND.TOTL.K2
	Total population (millions)	2015	data.worldbank.org/indicator/sp.pop.totl
	Urban population (%)	2015	data.worldbank.org/indicator/SP.URB.TOTL
	GDP (billion USD)	2015	data.worldbank.org/indicator/NY.GDP.MKTP.CD
	Access to basic sanitation (%)	2015	data.worldbank.org/indicator/SH.STA.BASS.ZS
	Mortality rate attributed to unsafe WASH	2015	data.worldbank.org/indicator/SH.STA.WASH.P5
	Access to internet (%)	2015	data.worldbank.org/indicator/it.net.user.zs
	Access to electricity (%)	2015	data.worldbank.org/indicator/EG.ELC.ACCS.ZS
	People practicing open defecation (%)	2015	data.worldbank.org/indicator/SH.STA.ODFC.ZS
	Agricultural land (%)	2015	data.worldbank.org/indicator/AG.LND.AGRI.ZS
	Fertilizer consumption (kg ha^{-1} arable land)	2015	data.worldbank.org/indicator/ag.con.fert.zs
	Renewable internal water resources ($10^9\ m^3$)	2015	data.worldbank.org/indicator/ER.H2O.INTR.K3
United Nations Development Programme (UNDP)	Human Development Index (-)	2015	dasl.datadescription.com/datafile/hdi-2015/
World Resources Institute (WRI)	Baseline Irrigation Water Scarcity (-)	2019	www.wri.org/resources/data-sets/aqueduct-30-country-rankings
Global Water Intelligence (GWI)	Desalination capacity ($10^6\ m^3\ yr^{-1}$)	2018	www.desaldata.com/ as synthesised in Jones et al. (2019)

Multiple linear regression was used to predict country-level wastewater variables (i.e. production, collection, treatment and reuse) for countries without reported data. Stepwise elimination was used for feature selection to remove redundant predictor variables and reduce overfitting. Wastewater production was predicted in volumetric flow rate units (million $m^3\ yr^{-1}$). Conversely, wastewater collection, treatment and reuse were predicted as a percentage of wastewater production. Predicted values of percentages were bounded to the 0–100% range (i.e. <0 = 0; >100 = 100). Predicted percentages were subsequently applied to reported or predicted values of wastewater production to obtain wastewater collection, treatment and reuse in volumetric flow rate units. Bootstrap regression was used to quantify the uncertainty in the predictions (by geographic region, economic classification and at the global scale) at the 95th confidence level. In total, 1,000 regressions with random sampling and replacement were fit to provide predictions at countries lacking data. Wastewater observations were combined with these 1,000 bootstrapped predictions, with the 2.5th and 97.5th confidence intervals taken as lower and upper confidence limits, respectively.

Wastewater data (reported and predicted) are at the national level, for the 215 countries as listed by the World Bank (https://data.worldbank.org/country). Wastewater data are also aggregated to eight geographic regions based on the World Bank regional classifications: 1) East Asia and Pacific; 2) Eastern Europe and Central Asia; 3) Latin America and Caribbean; 4) Middle East and North Africa;

5) North America; 6) Southern Asia; 7) Sub-Saharan Africa; and 8) Western Europe. Furthermore, data are also aggregated to four economic classifications based on the World Bank Atlas Method: 1) 'high income' (>$12,056 GNI per capita); 2) 'upper-middle income' ($3896 to $12,055); 3) 'lower-middle income' ($966 to $3895); and 4) 'low income' (<$995). Predicted wastewater data was used to supplement reported data, where unavailable, to develop a comprehensive global outlook of wastewater production, collection, treatment and reuse.

2.2.3 Downscaling and validation

Country-level wastewater production, collection, treatment and reuse data was downscaled to 5 arc-min resolution (~10km at the equator) based on the sum of averaged annual domestic and industrial return flow data (henceforth 'return flow'). Return flows represent the water extracted for a specific sectoral purpose, but which is not consumed, and hence it returns to and dynamically interacts with surface and ground water hydrology (Graaf et al., 2014; Sutanudjaja et al., 2018). Return flows used for downscaling are calculated as gross minus net water demands from the Water Futures and Solutions (WFaS) initiative for the years 2000–2010 (Wada et al., 2016). The WFaS water demand dataset follows the approach developed for *PCR-GLOBWB2* (Wada et al., 2014). Domestic return flows only occur where the urban and rural population have access to water, whereas industrial return flow occur from all areas where water is withdrawn. Both domestic and industrial return flows are dependent on country-specific recycling ratios based on GDP and the level of economic development (Wada et al., 2011; Wada et al., 2014).

Gridded return flows were divided by the countries total return flow to obtain the fraction per gridcell. Wastewater production was downscaled directly proportionally to return flows by multiplying the gridcell return flow fraction per gridcell with wastewater production at the country-level. Wastewater collection is assigned sequentially to gridcells with the largest downscaled produced wastewater flows. Therefore, collected wastewater is preferentially allocated to gridcells with the highest levels of municipal activities, where centralised wastewater collection (and treatment) is assumed to be most economically feasible. Wastewater treatment is assigned to gridcells only where wastewater collection exists, at an average treatment rate calculated at the country-level. The treatment rate is calculated as the proportion of collected wastewater that undergoes treatment, and hence can differ from the country-level wastewater treatment percentage (which is calculated as the proportion of produced wastewater that is treated). For the downscaling of wastewater reuse an additional criterion was introduced to represent water scarcity, a key driver of wastewater reuse. The ratio of water demand to water availability was calculated. Gridcells within a country with a treated wastewater allocation are then ordered based off this ratio and treated wastewater reuse was assigned sequentially to these gridcells.

The location and design capacity of individual wastewater treatment plants were used to validate the downscaled wastewater treatment data. Reported data for 25,901 wastewater treatment plants located across Europe were obtained from the European Environmental Agency (EEA, 2019). Data for a further 4,283 wastewater treatment plants was obtained for the contiguous United States from the US Environmental Protection Agency (US-EPA, 2020). An additional 478 wastewater treatment plants, distributed globally (excluding Europe and the US), were extracted from the GWI wastewater database (GWI, 2015). For EEA and GWI wastewater treatment plants, treatment capacity reported only in Population Equivalent (PE) was approximated in volume flow rate units based on the linear regression obtained for wastewater treatment plants reporting capacity in both population equivalent and volume flow rate (EEA: $R^2 = 0.80$, $p < 0.001$; GWI: $R^2 = 0.81$, $p < 0.001$). Wastewater treatment plants were assigned to their nearest gridcell and treatment capacities were aggregated per cell. In total, wastewater treatment data was available for 22,133 unique gridcells. For validating downscaled wastewater reuse, only plants (with treatment capacity > 1 million $m^3\ yr^{-1}$) using tertiary or higher wastewater treatment technologies were considered. In total, 572 wastewater treatment plants in the

EEA database met this criterion. A further 78 wastewater treatment plants, which are specifically designated as wastewater reuse facilities, were sourced from the GWI database. In total, wastewater reuse data was available for 601 gridcells. Downscaled wastewater treatment and reuse were compared to wastewater design capacities.

To account for the large variation in the treatment capacities of wastewater treatment plants considered, in addition to the geographical mismatch between where wastewater is produced and treated (i.e. wastewater treatment plants are typically located on the outskirts of urban areas), validation occurred at differing geographical scales. Wastewater treatment plant capacity was divided by wastewater production per capita to approximate the number of people that the wastewater treatment plant serves. If the population served by a wastewater plant exceeds the gridcell population, the validation extent was expanded to the directly neighbouring cells. This is allowed to occur until the population served by the treatment plant is reached, but up to a maximum of 3 iterations, reflecting a radius of ∼30km around the wastewater treatment plant. The total downscaled wastewater treated over the extended area was then compared to that of the treatment plant.

To quantify the performance of the downscaling approaches, the root-mean-square error (RMSE) and mean bias (BIAS) were calculated. Normalised values of RMSE and BIAS were calculated (nRMSE and nBIAS) by dividing by the standard deviation of the wastewater treatment plant capacity. Pearson's (r) coefficients were calculated to quantify the linear dependence, with R^2 values based on both the linear and log-log relationship between downscaled and observed values also calculated.

2.3 Results

2.3.1 Regression and country-level predictions

The results of the regression analysis for wastewater production, collection, treatment and reuse are summarised in Table 2.3. All regression models were significant at the $p < 0.001$ level with adjusted R^2 values ranging between 0.61 and 0.89. Country-level observed versus simulated wastewater production (log million m^3 yr^{-1}), collection (%), treatment (%) and reuse (%) data are displayed in Fig. 2.2. The regression equations were applied for 97, 113, 122 and 178 countries with no or excluded data representing 10%, 14%, 22% and 40% of the global population for wastewater production, collection, treatment and reuse, respectively.

Wastewater production was best predicted based on total population, GDP per capita and access to basic sanitation. A significant regression equation was found ($p<0.001$) with an adjusted R^2 value of 0.89, with all predictor variables also significant at the $p<0.001$ level. While the number of people within a country was found to have the strongest influence on total wastewater production ($\beta = 0.96$), the average economic output per inhabitant ($\beta = 0.31$) and the level of access to wastewater services ($\beta = 0.19$), such as flushing toilets to piped sewers are important for determining the amount of wastewater produced per capita. These three factors therefore account for the combined effect of population size and variations in wastewater production per capita linked to economic and development factors in determining total wastewater production in a country. Comparing observed with predicted total wastewater production data demonstrates the overriding importance of a country's population, with wastewater production spread across multiple orders of magnitude for countries irrespective of geographical region or economic classification (Fig. 2.2a).

Table 2.3 Wastewater production, collection, treatment and reuse multiple linear regression results.

Regression model	Explanatory Variables (units)	*B* (SE *B*)	β	P	Adjusted R^2
Production (log)	Intercept (-)	-1.68 (0.45)		**	0.89**
	GDP (log $ yr^{-1} per capita)	0.45 (0.06)	0.31	**	
	Population (log millions)	1.02 (0.03)	0.96	**	
	Access to basic sanitation (%)	0.02 (0.00)	0.19	**	
Collection	Intercept (-)	-80.73 (11.06)		**	0.69**
	Human Development Index (-)	120.82 (26.94)	0.5	**	
	Urban population (%)	0.22 (0.13)	0.14	.	
	Wastewater production (log m^3 yr^{-1} per capita)	8.01 (2.97)	0.25	*	
Treatment	Intercept (-)	-61.32 (14.06)		*	0.80**
	Wastewater collection (%)	0.72 (0.08)	0.66	*	
	GDP (log $ yr^{-1} per capita)	7.2 (1.88)	0.28	*	
Re-use (primary)	Intercept (-)	-5.29 (4.59)		0.26	0.70**
	Desalination capacity (sqrt m^3 yr^{-1} per capita)	1.50 (0.78)	0.29	.	
	Treated wastewater for irrigation water scarcity alleviation (-)	13.66 (3.50)	0.6	*	
Re-use (alternate)	Intercept (-)	-4.11 (6.10)		0.5	0.61**
	Desalination capacity (sqrt m^3 yr^{-1} per capita)	3.22 (0.63)	0.63	*	
	Treated wastewater (%)	0.23 (0.12)	0.24	.	

B indicates unstandardised regression weights, SE *B* indicates the standard error of *B*, β indicates standardised regression weights.
Significance level represent by: '**' (p<0.001), '*' (p<0.01), '.' (p<0.1), or as stated numerically.

Wastewater collection was predicted (adjusted R^2 = 0.69; p <0.001) based on the Human Development Index (HDI), urban population and wastewater production per capita. HDI, an overarching proxy for level of development, was found to be the strongest influence over wastewater collection (β = 0.50; p<0.001). Urban population (β = 0.14; p<0.01) and wastewater production per capita (β = 0.25; p<0.01) were also significant but less important predictor variables of wastewater collection. For urban population, a greater proportion of a population living in urban areas resulted in higher collection rates for the country, while higher levels of wastewater production per capita corresponded to larger collection rates. The observed versus predicted wastewater collection rates are depicted in Fig. 2.2b, which displays the trend across different geographic zones and economic classifications.

Wastewater treatment was predicted (adjusted R^2 = 0.80; p <0.001) based on GDP per capita (β = 0.28; p < 0.01) and wastewater collection (β = 0.66; p < 0.01). Countries with larger economic outputs per capita likely have more resources for wastewater treatment, resulting in higher overall treatment rates. As wastewater treatment is dependent upon wastewater collection, countries with higher wastewater collection rates typically also treat a greater proportion of their wastewater. Observed versus predicted wastewater treatment rates are displayed in Fig. 2.2c.

The amount of wastewater treated will determine the maximum potential for treated wastewater reuse within a country. Water scarcity, particularly when driven by high irrigation water demands, is also a primary driver of wastewater reuse (Garcia and Pargament, 2015). To account for this relationship, the fraction of wastewater undergoing treatment processes and irrigation water scarcity was multiplied to give an integrated metric indicating the 'availability of treated wastewater for

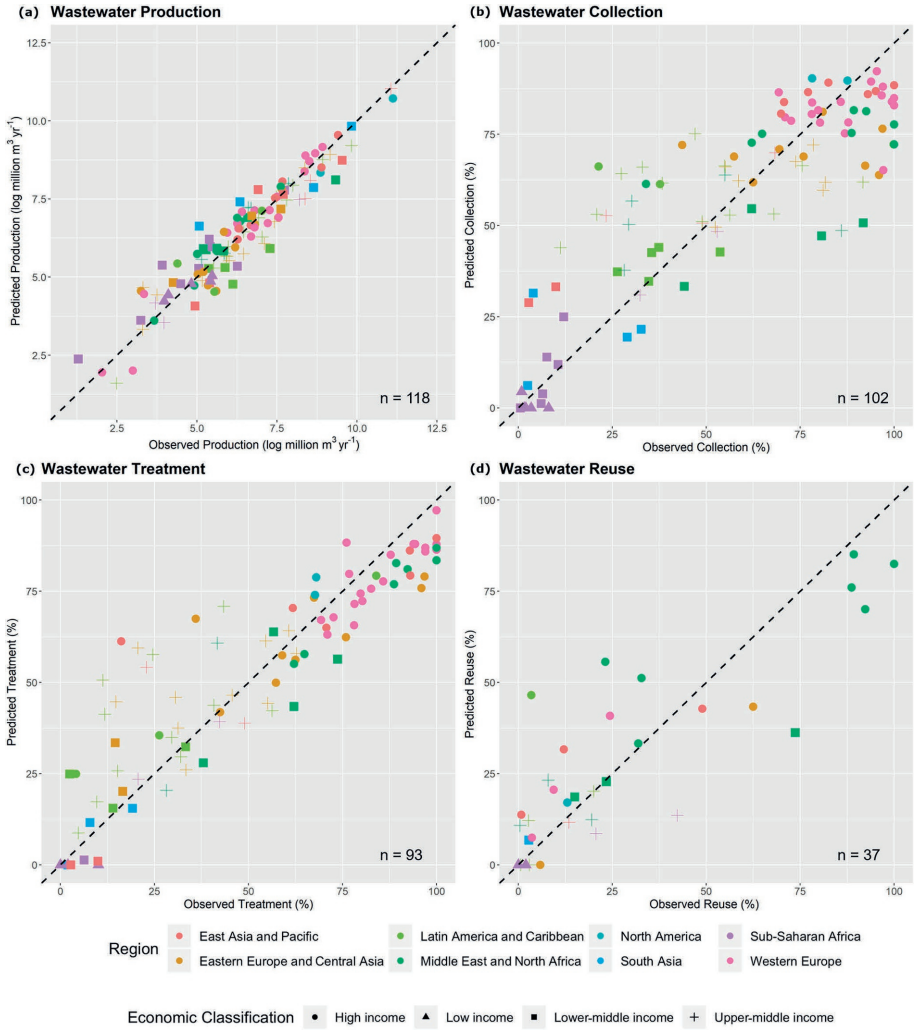

Figure 2.2 Observed versus predicted wastewater a) production; b) collection; c) treatment; and d) reuse, from regression analysis.

irrigation water scarcity alleviation'. Wastewater reuse was predicted (adjusted R^2 = 0.70; p <0.001) from this metric (β = 0.60; p < 0.01) in combination with the desalination capacity per capita (β = 0.29; p < 0.1), as an indicator of the prevalence of unconventional water resources in a country. The observed versus predicted wastewater reuse rates from this regression are displayed in Fig. 2.2d. Irrigation water scarcity data was unavailable for 53 countries, mostly small island nations. Here an alternate regression model was constructed based on desalination capacity per capita (β = 0.63; p < 0.01) and wastewater treatment (β = 0.24; p < 0.1) only, resulting in a slightly lower explained variance (R^2 = 0.61). While these countries represent <1% of the global population, this alternate regression was necessary to account for wastewater reuse occurring particularly in water-scarce small island nations. These islands typically lack renewable water resources and hence unconventional water resources such as desalinated water and treated wastewater represent a substantial proportion of the water availability (Jones et al., 2019).

2.3.2 Global production, collection, treatment and reuse

Globally, this study estimates annual wastewater production at 359.4 (358.0–361.4) billion m^3 yr^{-1}, with a global average of 49.0 (48.8–49.2) m^3 yr^{-1} per capita. Global wastewater collection and treatment is estimated at 225.6 (224.4–226.9) and 188.1 (186.6–189.3) billion m^3 yr^{-1}, respectively. These values indicate that approximately 63% and 52% of globally produced wastewater is collected and treated, respectively, with approximately 84% of collected wastewater undergoing a treatment process. Wastewater reuse is estimated at 40.7 (37.2–47.0) billion m^3 yr^{-1}, representing approximately 11% of the total volume of wastewater produced. This estimate also indicates that approximately 22% of treated wastewater undergoes intentional reuse, with the remaining 78% (totalling 147.4 billion m^3 yr^{-1}) discharged to the environment. This compares to the estimated 171.3 billion m^3 yr^{-1} of wastewater discharged directly to the environment without undergoing any form of treatment. It is worth highlighting that the vast majority of wastewater data are from reported sources, with just 2.4%, 4.8% and 5.2% of global wastewater production, collection and treatment being from predicted values using regression. This occurs both due to the high population coverage and due to the missing data primarily being from developing countries, where wastewater production per capita and percentage collection and treatment rates are lower. The global quantification of wastewater reuse relies more heavily on predicted values, constituting 23.4% of reuse volume globally. This occurs primarily due to poor data availability, particularly in countries with large populations in Eastern Europe and Central Asia (e.g. Russia, Turkey and Poland) and Western European countries where wastewater treatment rates are generally high but the proportion of wastewater reused relies on simulations (e.g. Germany, Italy and Greece).

Table 2.4 displays wastewater production per capita (m^3 yr^{-1} per capita) and wastewater production, collection, treatment and reuse (billion m^3 yr^{-1}), aggregated from the country data (reported plus simulated) at the global scale and by region and level of economic development. Fig 2.3 displays wastewater data plotted at the country scale in proportional terms (m^3 yr^{-1} per capita for production; percentage of produced wastewater for collection, treatment and reuse), facilitating direct comparisons between countries.

Substantial differences in wastewater production, collection, treatment and reuse occur across different geographic regions and by the level of economic development. Wastewater production per capita is notably highest in North America at 209.5 m^3 yr^{-1} per capita, over double that of Western Europe (91.7 m^3 yr^{-1} per capita), the next highest producing region per capita. When considering individual countries in these regions, the USA (211 m^3 yr^{-1} per capita) and Canada (198 m^3 yr^{-1} per capita), in addition to small, prosperous European countries (e.g. Andorra: 257 m^3 yr^{-1} per capita; Austria: 220 m^3 yr^{-1} per capita; Monaco: 203 m^3 yr^{-1} per capita) are the highest producers per capita. Comparatively, the larger Western European countries have lower wastewater production per capita, with Germany, the U.K. and France at 92, 92 and 66 m^3 yr^{-1} per capita, respectively. Conversely, most Sub-Saharan African countries produce less than 10 m^3 yr^{-1} per capita. Wastewater production values are comparable to the World Health Organisation's absolute minimum water requirements for survival of 2.7 m^3 yr^{-1} per capita (WHO, 2011) in countries such as Niger (2.7 m^3 yr^{-1} per capita), Burkina Faso (3.4 m^3 yr^{-1}) and Ethiopia (4.2 m^3 yr^{-1} per capita). Aggregated for the region, Sub-Saharan Africa produces approximately 20 times less wastewater than North America per capita, at 11.0 m^3 yr^{-1} per capita.

In volumetric flow rate terms, East Asia and Pacific produces the most wastewater (117.6 billion m^3 yr^{-1}), coinciding with the largest population share (31%). Conversely, Southern Asia produces just 7% of global wastewater despite a population share of 24%, whereas the 5% of people living in North America account for 20% of global wastewater production. Wastewater production also varies greatly with level of economic development. The prominent discrepancies between economic classifications indicate a strong relationship between wealth and wastewater production regardless of geographic

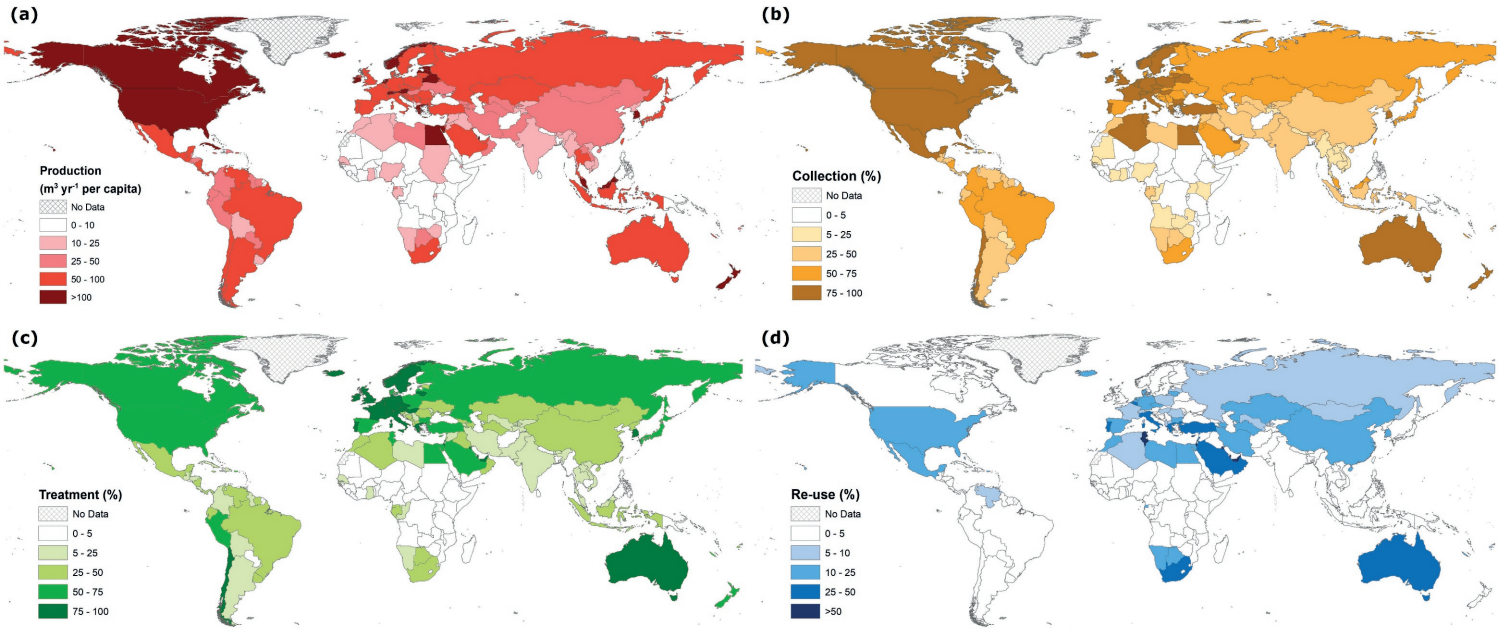

Figure 2.3 Country scale wastewater a) production (m^3 yr^{-1} per capita); b) collection (%); c) treatment (%); and d) reuse (%).

Table 2.4 Wastewater production, collection, treatment and reuse (billion m^3 yr^{-1}) by region and level of economic development. The numbers in parentheses display the prediction uncertainty (2.5th and 97.5th confidence limits, in m^3 yr^{-1}) on the totals based on the results of 1,000 bootstrap regressions with random sampling and replacement.

	Global Population (%)	Production (m^3 yr^{-1} per capita)	Production (billion m^3 yr^{-1})	Collection (billion m^3 yr^{-1})	Treatment (billion m^3 yr^{-1})	Re-use (billion m^3 yr^{-1})
Global	100	49.0 (48.8 – 49.2)	359.4 (358.0 – 361.4)	225.6 (224.4 – 226.9)	188.1 (186.6 – 189.3)	40.7 (37.2 – 47.0)
Geographic Region						
North America	4.9	209.5 (209.5 - 209.5)	74.7 (74.7 – 74.7)	59.1 (59.1 – 59.1)	50.6 (50.6 – 50.6)	9.1 (8.8 – 9.5)
Latin America & Caribbean	8.5	67.6 (67.3 – 67.9)	42.1 (41.9 – 42.3)	25.2 (25.2 – 25.2)	15.4 (15.2 – 15.5)	2.1 (2.0 – 2.5)
Western Europe	5.7	91.7 (91.7 – 91.8)	38.5 (38.4 – 38.5)	33.7 (33.7 – 33.7)	33.0 (33.0 – 33.0)	6.7 (4.1 – 9.5)
Middle East & North Africa	5.8	51.4 (51.3 – 51.5)	21.9 (21.8 – 21.9)	16.1 (16.1 – 16.2)	11.4 (11.2 – 11.5)	6.1 (6.0 – 6.2)
Sub-Saharan Africa	13.6	11.0 (10.1 – 12.4)	11.0 (10.1 – 12.4)	2.5 (2.5 – 2.6)	1.8 (1.7 – 1.9)	1.6 (1.6 – 1.8)
Southern Asia	23.8	14.6 (14.5 – 14.7)	25.6 (25.4 – 25.7)	7.8 (7.8 – 7.8)	4.0 (4.0 – 4.1)	0.5 (0.5 – 0.8)
Eastern Europe & Central Asia	6.6	57.9 (57.2 – 58.8)	28.2 (27.8 – 28.6)	18.4 (18.2 – 18.7)	14.9 (14.7 – 15.1)	2.6 (1.3 – 4.4)
East Asia & Pacific	31.1	51.5 (51.5 – 51.7)	117.6 (117.3 – 117.9)	62.8 (61.9 – 63.8)	57.0 (56.1 – 57.8)	11.9 (11.7 – 13.5)
Income Level						
High	16.1	126.0 (125.9 – 126.2)	149.1 (149.0 – 149.3)	121.7 (121.6 – 121.7)	110.4 (110.4 – 110.5)	21.2 (19.1 – 24.9)
Upper middle	34.8	54.7 (54.5 – 54.8)	139.5 (139.1 – 139.9)	74.8 (74.6 – 74.9)	60.2 (59.7 – 60.6)	15.1 (13.9 – 16.9)
Lower middle	40.5	22.5 (22.3 – 22.6)	66.8 (66.4 – 67.4)	28.8 (27.7 – 29.9)	17.3 (16.2 – 18.2)	4.4 (3.6 – 5.7)
Low	8.6	6.4 (5.0 – 8.5)	4.0 (3.2 – 5.3)	0.4 (0.3 – 0.4)	0.2 (0.1 – 0.2)	0.0 (0.0 – 0.1)

location. Wastewater production per capita more than doubles at each income classification level from 'low income' (6.4 m^3 yr^{-1} per capita) to 'high income' (126.0 m^3 yr^{-1} per capita). With respect to population size, people living in 'high income' countries (16% global population) produce 42% of global wastewater, compared to 'low income' and 'lower-middle income' countries (~50% global population) producing 20% of global wastewater.

Wastewater collection and treatment rates are highest in Western Europe (88% and 86%, respectively) and lowest in Southern Asia (31% and 16%, respectively) and Sub-Saharan Africa (23% and 16%, respectively). Wastewater collection is notably low in the East Asia and Pacific region, where total wastewater production is high. Conversely, wastewater collection in the Middle East and North Africa region is relatively high at 74%, likely resulting from the lack of renewable water supplies. Wastewater treatment percentages follow similar regional patterns. Notably, wastewater treatment is substantially lower than wastewater collection in the Latin America and Caribbean and Southern Asia regions, potentially indicative of high rates of untreated wastewater reuse in these regions. Wastewater collection and treatment percentages follow similar patterns as wastewater production with respect to income level, with 'high income' countries collecting and treating the majority of their wastewater (82% and 74%, respectively) down to 'low income' countries with small collection and treatment rates (9% and 4%, respectively). The proportion of collected wastewater being treated also decreases with income level, at 91%, 73%, 60% and 47% for 'high', 'upper-middle', 'lower-middle' and 'low' income classifications, respectively. The fact that 40% and 53% of collected wastewater is untreated in the 'lower-middle' and 'low' income classifications, respectively, may also

be indicative of the higher prevalence of intentional untreated wastewater reuse (whereby collected wastewater is reused without undergoing treatment).

High utilisation of treated wastewater reuse occurs predominantly in the Middle East and North Africa, with the United Arab Emirates, Kuwait and Qatar reusing more than 80% of their produced wastewater. Water scarce small island developed countries, including the Cayman Islands, US Virgin Islands and Malta also have high rates of intentional treated wastewater reuse of 78%, 75% and 67%, respectively. Treated wastewater reuse is prohibitively low in areas with low wastewater treatment rates, such as Sub-Saharan Africa and Southern Asia. In addition, treated wastewater reuse is also low in areas with sufficient availability of conventional water resources such as across Scandinavia (where reuse is <5%).

In volumetric flow rate terms, intentional treated wastewater reuse is estimated to be largest in East Asia and Pacific (11.9 billion m^3 yr^{-1}) and North America (9.1 billion m^3 yr^{-1}) and lowest in Southern Asia (0.5 billion m^3 yr^{-1}) and Sub-Saharan Africa (1.6 billion m^3 yr^{-1}). Conversely the Middle East and North Africa (27.8%) and Western Europe (17.5%) dominate in percentage terms. In volumetric flow rate units, the Middle East and North Africa (15%) and Western Europe (16%) account for almost a third of treated wastewater reuse globally, despite only accounting for 5.8% and 5.7% of the global population, respectively. Approximately half (52%) of intentional treated wastewater reuse occurs in 'high income' countries, with 37% from 'upper-middle' income countries. Intentional treated wastewater reuse is contingent upon the availability of treated wastewater resources, which is typically more prevalent in 'high income' countries (who both produce more wastewater per capita and treat a higher percentage of the resource). However, the proportion of treated wastewater intentionally reused is higher in the 'upper-middle' (25%) and 'lower-middle' (25%) income groups than in the 'high income' group (19%).

2.3.3 Gridded production, collection, treatment and reuse

Fig. 2.4 displays gridded wastewater production, collection, treatment and reuse, allowing for the identification of hotspot regions and zones at 5 arc-min resolution. Wastewater production occurs across the globe, with hotspots coinciding with the largest metropolitan areas (e.g. Tokyo and Mumbai) where the largest concentration of domestic and industrial activities occurs (Fig. 2.4a). In contrast, wastewater production is close to zero in world regions with low concentrations of people and industrial activities, such as the Sahara desert, inland Australia and the high latitude climate zones (e.g. Northern Canada and Russia). In countries where municipal activities are heavily concentrated in a small number of cities, such as in the Middle East and Australia, small clusters of gridcells with very high wastewater production (>5 million m^3 yr^{-1}) occur. Wastewater collection (Fig. 2.4b) and treatment (Fig. 2.4c) are typically more concentrated in urban areas within individual countries. This is particularly prominent in Latin America and Sub-Saharan Africa. Conversely, downscaled wastewater collection and treatment reflect wastewater production in regions where wastewater collection and treatment rates are very high, such as Western Europe and Scandinavia. Wastewater reuse is constrained to the lowest area (number of gridcells), being concentrated in regions with where treated wastewater resources are available and where water scarcity issues are of particular concern.

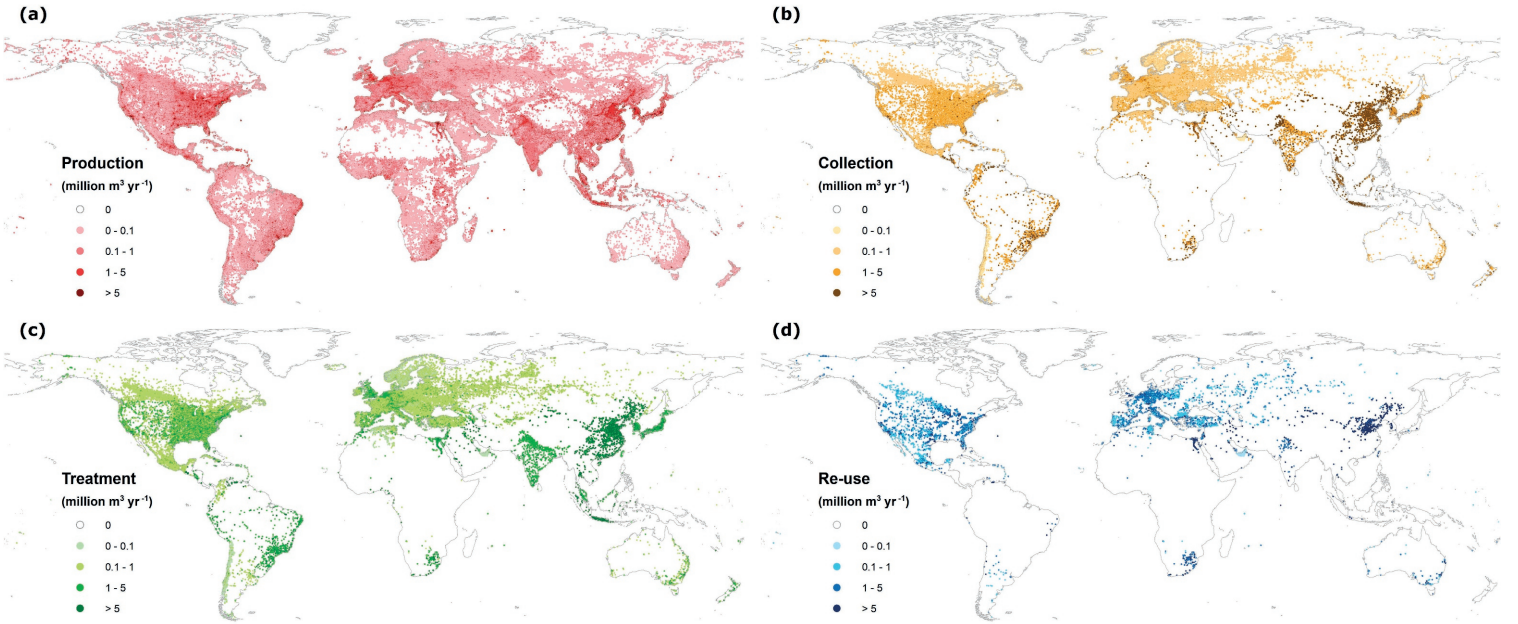

Figure 2.4 Wastewater a) production; b) collection; c) treatment; and d) reuse, at 5 arc-min spatial resolution (million ^{3} yr^{-1}).

Fig. 2.5a displays the global distribution of the wastewater treatment plants and designated wastewater reuse sites considered in this study. Plant capacities were compared to downscaled quantifications for validation of wastewater treatment (Fig. 2.5b) and wastewater reuse (Fig. 2.5c). Overall, a reasonable performance is obtained at most wastewater treatment and reuse plants with linear R^2 values of 0.57 ($p < 0.001$) and 0.50 ($p < 0.001$), respectively. The observed negative normalised biases suggest that downscaled wastewater treatment (-0.32) and reuse (-0.51) was underestimated with respect to the observed treatment capacities. This may occur due to discrepancies between the design (i.e. maximum) capacity of wastewater treatment plants, which is commonly the capacity that is reported, versus the actual treated wastewater volumes. Factors such as the construction year of wastewater treatment plant are important, as plants are constructed to be larger than current requirements in anticipation of future increases in wastewater flows. Furthermore, uncertainties in the data used as basis for downscaling wastewater production (i.e. *PCR-GLOBWB2* return flows) directly impacts the downscaled results of wastewater treatment. For example, the underprediction of return flows in urban areas and overprediction in rural areas could lead to the overprediction of wastewater treatment in areas without treatment plants and underprediction of wastewater treatment for gridcells with large treatment capacities.

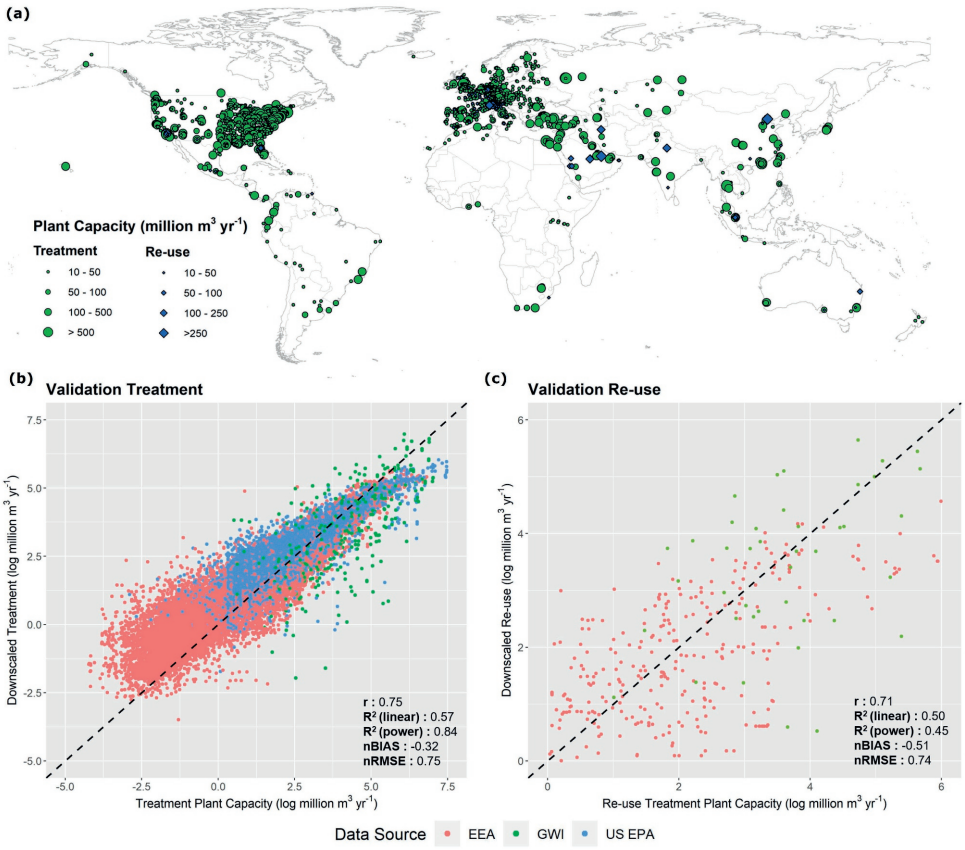

Figure 2.5 a) Global distribution of wastewater treatment plants and designated wastewater reuse sites; and validation of downscaling approach for b) wastewater treatment; and c) and wastewater reuse (c).

2.4 Discussion and conclusions

This study aimed to develop a consistent and comprehensive spatially-explicit assessment of global domestic and manufacturing wastewater production, collection, treatment and reuse for the reference year of 2015. Multiple linear regression models using a diverse set of social, economic, geographic and hydrological datasets were fit for country-level wastewater data collated for a variety of sources. These relationships were applied for predictions of wastewater production, collection, treatment and reuse for countries where data was unavailable. Bootstrapping with random sampling and replacement was employed to quantify prediction uncertainty. It should be noted that bootstrapping only accounts for uncertainty in the regression terms, not for uncertainties in the underpinning source data. Uncertainties associated with wastewater observations are not accounted for in this study, despite likely being substantial. Nevertheless, this study represents the first attempt to simultaneously analyse wastewater production, collection, treatment and reuse for all countries across the globe. While agricultural runoff is also a substantial source of pollution, this is outside the scope of this study. Country-level data on agricultural runoff is sparse, necessitating modelling approaches to quantify irrigation return flow by calculating net demand (e.g. based on crop composition and irrigated area per gridcell), gross irrigation demand (to account for irrigation efficiency and losses) and water withdrawals (Sutanudjaja et al., 2018). Agricultural runoff is also rarely collected or treated (WWAP, 2017), hence is less applicable for inclusion in this study.

Our global quantification of wastewater production of 359.4 (358.0–361.4) billion m^3 yr^{-1} is broadly in accordance with previous quantifications, such as 380 billion m^3 yr^{-1} quantified based on reported data and urban population (Qadir et al., 2020), and 450 billion m^3 yr^{-1} quantified by modelling of return flows in WaterGAP3 (Flörke et al., 2013). Few studies were found analysing the global state of wastewater collection, treatment and reuse. Our quantification of wastewater collection, which is estimated at 225.6 (224.4–226.9) billion m^3 yr^{-1}, can give an important indication of the amount of collected wastewater that goes untreated. At the global scale, this study estimates that wastewater treatment is 188.1 (186.6–189.3) billion m^3 yr^{-1}, or 52% of the produced wastewater. By extension, 48% of produced wastewater is released to the environment without treatment (either directly, or following collection). This is substantially lower than the commonly cited statistic that ∼80% of global wastewater is released to the environment without treatment (WWAP, 2017). Our quantifications of wastewater treatment must be treated with caution however – particularly in the developing world – as wastewater treatment plants typically operate at capacities below the installed (and usually reported) capacities (Murray and Drechsel, 2011; Mateo-Sagasta et al., 2015) that are used for country-level estimates. Similarly, wastewater plants may be entirely non-functional (mothballed) due to lack of funding and maintenance, or have unsuitable treatment processes for the incoming wastewater, yet the associated wastewater volumes are still reported as treated (Qadir et al., 2010). Therefore, it is possible that the actual treated volume of wastewater is somewhat below our estimated 52% and the proportion of collected wastewater which is not treated could far exceed 16%. 'Wastewater treatment' is also a generic term that may refer to any form of wastewater treatment regardless of level (e.g. primary, secondary or tertiary), which this study does not attempt to distinguish between. This is due to different data sources reporting different levels of treatment, for instance with GWI only reporting secondary treatment or above while FAO-AQUASTAT also includes primary treatment.

In percentage terms, wastewater treatment by economic classification is broadly in line with previous work (Sato et al., 2013), who estimate wastewater treatment to be 70%, 38%, 28% and 8% for 'high', 'upper-middle', 'lower-middle' and 'low' income countries, respectively, compared to our quantifications of 74%, 43%, 26% and 4.2%. While similar, these estimations could potentially indicate that percentage collection and treatment have increased in the developed world, but have decreased in the developing world. This could be caused by wastewater production, particularly in the

developing world, rising at a faster pace than the development of collection infrastructure and treatment facilities (Sato et al., 2013). It should be noted that while the aim of wastewater collection and treatment is to reduce pollutant loadings to minimise risks to human health and the environment, these facilities can also act as point sources of pollution. Wastewater collection concentrates pollutants, which can pose serious water quality issues if discharged with insufficient treatment. Furthermore, a range of emerging pollutants (e.g. pharmaceuticals, pesticides and industrial chemicals) are concentrated in wastewater collection networks (Geissen et al., 2015). These pollutants are of particular concern as they are not typically monitored for or sufficiently removed in wastewater treatment processes, with ambiguous risks posed to human and environmental health even in low concentrations (Deblonde et al., 2011; Geissen et al., 2015). The solution is not however to collect less wastewater, but to increase treatment in terms of percentage of collected wastewater, treatment level and the number of pollutants (UNEP, 2016).

The drivers behind wastewater reuse are a complex mixture of social, economic, geographic and hydrological factors, and data are highly limited globally. Nevertheless, this study represents the first attempt to quantify intentionally treated wastewater reuse at the country scale. It should be noted that this study does not aim to quantify either de-facto (unintentional) treated wastewater reuse or any form (intentional or unintentional) of untreated wastewater reuse. The total volume of wastewater reused for human purposes is therefore likely much greater than the 40.7 billion $m^3\ yr^{-1}$ of intentional treated wastewater reuse estimated in this study. For example, previous research has indicated that the magnitude of intentional untreated wastewater reuse may be approximately ten times greater than intentional treated wastewater reuse (Scott et al., 2010).

This study sought to downscale country-level wastewater estimates to spatially-explicit (grid-based) quantifications for purposes such as large-scale water resource assessments and water quality modelling. Wastewater production has previously been quantified based only on simulated return flows in hydrological models (Flörke et al., 2013). We instead used the proportions of simulated return flows to downscale country-based volumes of wastewater production. Our results also represent the first efforts to quantify global wastewater collection, treatment and reuse at the sub-national level. Our validation results suggest that our downscaled estimates of wastewater treatment and reuse are, in general, realistic. However, a number of uncertainties should also be considered. Firstly, our downscaling for wastewater production inherently relies on the ability to accurately simulate domestic and industrial return flows, and hence on the methodology for calculating gross and net water demand (Wada et al., 2014). As we downscale using the return flows proportionally, accurate spatial disaggregation of return flows is more important than the absolute simulated flow volumes. The accuracy of downscaled wastewater collection relies on the assumption that this preferentially occurs in areas where wastewater production is highest. Due to the high capital costs of wastewater treatment plants, combined with economies of scale, we deem this a logical assumption (Hernandez-Sancho et al., 2011; Hernández-Chover et al., 2018). Lacking more detailed information on the spatial variance in wastewater collection compared to treatment, we assume an equal wastewater treatment rate across all cells that have a collected wastewater allocation. Wastewater reuse is downscaled with the only additional criteria being an indicator of water scarcity. While water scarcity is an important driver of wastewater reuse, site-specific social, economic and political factors will also have a large influence on the viability of wastewater reuse on a case-by-case basis (WWAP, 2017). Accounting for these factors is outside the scope of this study. Furthermore, uncertainties in the validation datasets, both in terms of treatment capacity and geographical location, must also be recognised. Overall, due to the global scale of this work and the available data for validation, we purposely opt for more simple and parsimonious approaches where possible.

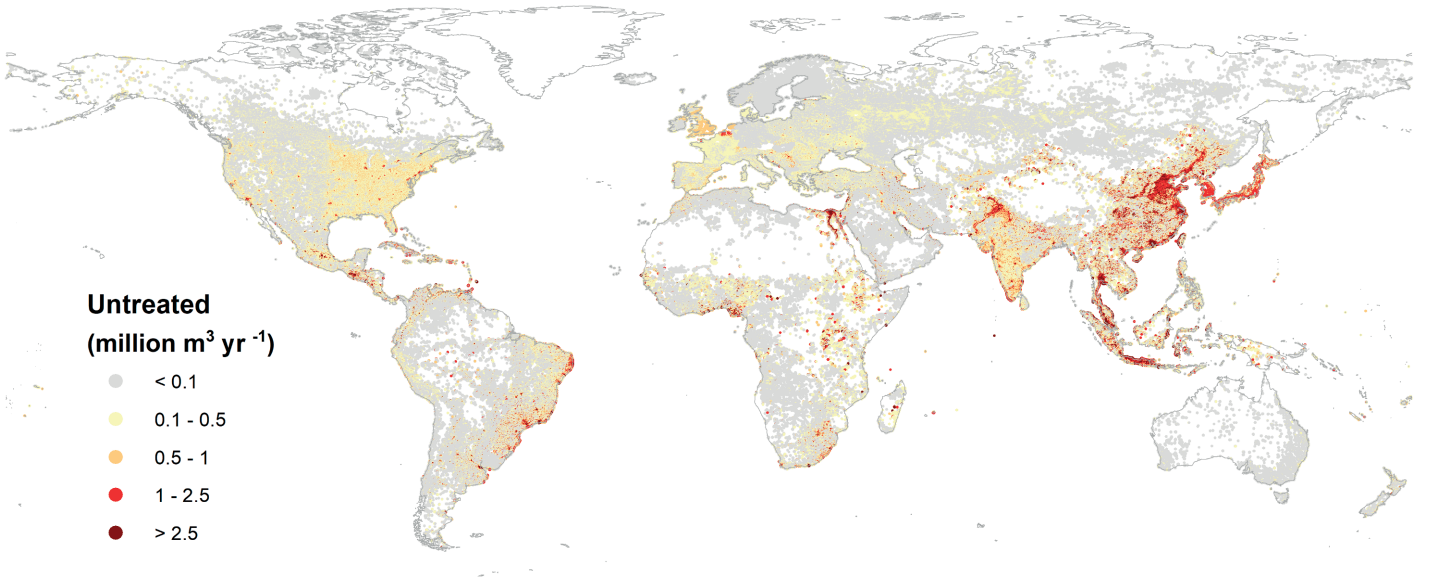

Figure 2.6 Gridded untreated wastewater flows to the environment (million $m^3\ yr^{-1}$) at 5 arc-min spatial resolution.

This study did not target acreage in its considerations of wastewater reuse, which has been a common method in previous work. For example, estimates made a decade ago suggest that up to 200 million farmers practice wastewater irrigation over an area of 4.5–20.0 million ha worldwide (Jiménez and Asano, 2008; Raschid-Sally and Jayakody, 2008). More recently, a global, spatially explicit assessment of irrigated croplands influenced by municipal wastewater flows estimated the area under direct and indirect wastewater irrigation at 36 million ha, of which 29 million ha are likely exposed to untreated wastewater flows (Thebo et al., 2017). These estimates were based on modelling studies and considered wastewater in both diluted and undiluted forms with a cropping intensity of 1.48 (Thebo et al., 2014). Considering the same cropping intensity and recent estimates of wastewater production (380 billion $m^3\ yr^{-1}$), the irrigation potential of undiluted wastewater was estimated at 42 million ha (Qadir et al., 2020).

Our results have a range of important applications including as input data for water resource assessments and as a baseline for informing and evaluating economic and management policies related to wastewater. For example, our data can be used to assess progress towards SDG 6.3 aimed at halving the proportion of untreated wastewater discharged into water bodies. As our data is standardised for 2015 and provides full geographic coverage, problems of discrepancies in data reporting years and missing data are reduced. Similarly, our data allows for identification of hotspot regions whereby the proportion of wastewater collected and treated are low, and of areas where large volumes of wastewater are entering the environment untreated (see Fig. 2.6). Volumetrically, substantial untreated wastewater flows to the environment are found across south and southeast Asia, particularly in the populous regions of Pakistan, Malaysia, Indonesia, India and China. Information on untreated wastewater flows have a diverse range of important implications for global water quality modelling and human health assessments.

Our results also highlight the vast potential of treated wastewater as an unconventional water resource for augmenting water resources and alleviating water scarcity, particularly in water scarce regions. To put wastewater as a potential resource into perspective, the estimated global volume of $\sim$360 $km^3\ yr^{-1}$ is comparable to the global consumptive use of non-renewable groundwater of 150–400 $km^3\ yr^{-1}$ over the years 2000–2010 (Bierkens and Wada, 2019). As wastewater production continues to rise with population and economic growth, wastewater management and reuse practices will become more important in the future (WWAP, 2017). Expansion in reuse of wastewater must be accompanied by strong legislation and regulations to ensure its safety (Voulvoulis, 2018; Smol et al., 2020). However, in response to concerns related to groundwater contamination, disruption to industrial processes and impacts for human health, tightening regulation can also be a barrier to expansion in treated wastewater reuse (Voulvoulis, 2018). It should also be recognised that wastewater reuse is not viable in all regions due to economic, technical and social considerations (Voulvoulis, 2018). Particularly in water-scarce developing countries with economic constraints, the application of untreated wastewater (diluted or undiluted) will likely remain the dominant form of wastewater reuse (Qadir et al., 2010). This is especially true in dry areas, despite official restrictions and regardless of potential health implications, where untreated wastewater reuse is triggered because: 1) wastewater is a reliable or often the only guaranteed water source available throughout the year; 2) the need to apply fertilisers decreases as wastewater is a source of nutrients; 3) wastewater reuse can be cheaper and less energy intensive than other water sources, such as if the alternative clean water source is deep groundwater; and 4) additional economic benefits including higher income generation from the cultivation and marketing of high-value crops, which can create year-round employment opportunities.

Continued failure to address wastewater as a major social and environmental challenge prohibits progress towards the 2030 Agenda for Sustainable Development (WWAP, 2017). Ultimately, the cost of action must also be weighed against the cost of inaction (Hernandez-Sancho et al., 2011). A paradigm shift in wastewater management is required from viewing wastewater as solely an environmental problem associated with pollution control and regulations, to recognise the economic opportunities of wastewater, which can provide a means of financing management and treatment (Drechsel et al., 2015; WWAP, 2017). In addition to revenue from selling treated wastewater for reuse, these opportunities include 'fit-for-purpose' treatment (Chhipi-Shrestha et al., 2017), recovery of energy and nutrients (Qadir et al., 2020) and cascading reuse of water from high to lower quality (Hansen et al., 2016). Creative exploitation of these opportunities offers potential to support the transition to a circular economy (Voulvoulis, 2018; Smol et al., 2020) and make progress towards many interconnected SDGs such as achieving a water-secure future for all (WWAP, 2017).

Data availability

The country-level and spatially-explicit (5 arc-min) wastewater production, collection, treatment and reuse datasets can be accessed at: https://dx.doi.org/10.1594/PANGAEA.918731.

Acknowledgements

The authors are grateful to dr. Edwin Sutanudjaja, dr. Rens van Beek and prof. dr. Yoshihide Wada for providing data from *PCR-GLOBWB2* and WFaS to support this work. MQ appreciates support of the Government of Canada for UNU-INWEH through Global Affairs Canada.

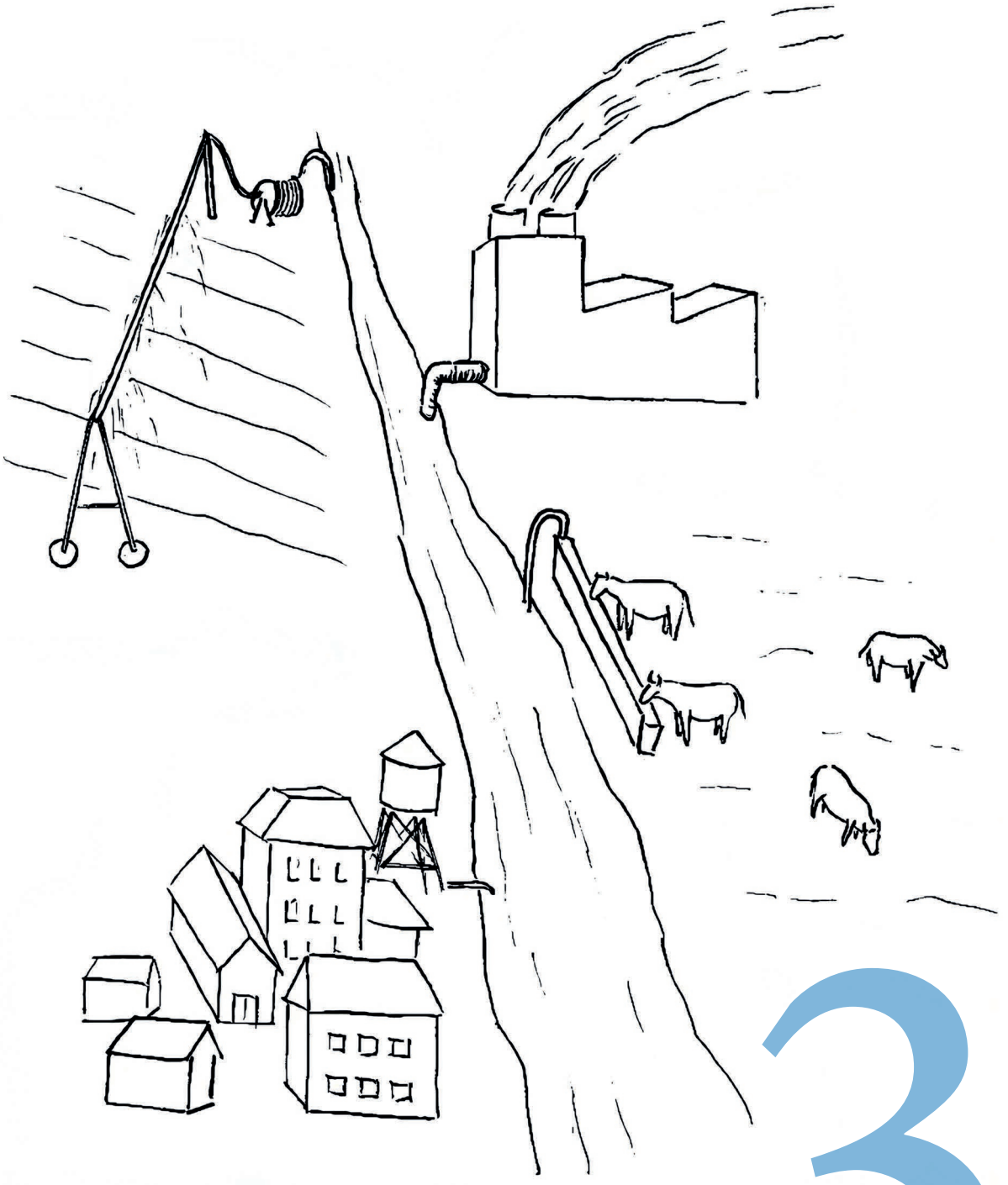

3

Chapter 3 | DynQual v1.0: a high-resolution global surface water quality model

Abstract

Maintaining good surface water quality is crucial to protect ecosystem health and for safeguarding human water use activities. However, our quantitative understanding of surface water quality is mostly predicated upon observations at monitoring stations that are highly limited in space and fragmented across time. Process-based models, based upon pollutant emissions and subsequent routing through the hydrological network, provide opportunities to overcome these shortcomings. To this end, we have developed the dynamical surface water quality model (*DynQual*) for simulating water temperature (Tw) and concentrations of total dissolved solids (TDS), biological oxygen demand (BOD) and fecal coliform (FC) with a daily timestep and at 5 arc-min (∼10km) spatial resolution. Here, we describe the main components of this new global surface water quality model and evaluate model performance against in situ water quality observations. Furthermore, we describe both the spatial patterns and temporal trends in TDS, BOD and FC concentrations for the period 1980–2019, and attribute the dominant contributing sectors to surface water pollution. Modelled output indicates that multi-pollutant hotspots are especially prevalent across northern India and eastern China, but that surface water quality issues exist across all world regions. Trends towards water quality deterioration have been most profound in the developing world, particularly Sub-Saharan Africa and southern Asia. The model code is available open source (https://github.com/UU-Hydro/DYNQUAL) and we provide global datasets of simulated hydrology, Tw, TDS, BOD and FC at 5 arc-min resolution with a monthly timestep (https://doi.org/10.5281/zenodo.7139222). These data have the potential to inform assessments in a broad range of fields, including ecological, human health and water scarcity studies.

Published: Jones, E.R., Bierkens, M.F.P., Wanders, N., Sutanudjaja, E.H., van Beek, L.P.H., and van Vliet, M.T.H. (2023) DynQual v1.0: a high-resolution global surface water quality model. *Geoscientific Model Development, 16*, pp. 4481–4500, DOI: 10.5194/gmd-16-4481-2023

3.1 Introduction

Maintaining good surface water quality is important for protecting ecosystem health and ensuring human access to safe water resources for a diverse range of sectoral needs (van Vliet et al., 2021; Jones et al., 2022). For example, high organic pollution can reduce oxygen availability and can lead to the suffocation of aquatic organisms (Sirota et al., 2013), while pathogen pollution represents a potential health risk for people exposed to this water. The consumption of contaminated drinking water can lead to the transmission of diseases such as cholera, dysentery and polio, which cause an estimated 485,000 deaths annually (Prüss-Ustün et al., 2019). Another example is salinisation of water resources, which can both limit irrigation water use (Thorslund et al., 2022) and threaten freshwater biodiversity where species cannot tolerate elevated salinity concentrations (Velasco et al., 2019). Similarly, increased water temperatures can disrupt energy production (van Vliet et al., 2016), and also provide more favourable conditions for cyanobacterial blooms that can lead to hypoxia which can disrupt freshwater habitats (Smucker et al., 2021).

Human activities, both directly and indirectly, cause changes in surface water quality relative to ambient ('pristine') conditions. Indirectly, altered precipitation patterns and the increased frequency of hydro-meteorological extremes that result from human-induced climate change can lead to fundamental changes in the hydrological regime (Wanders and Wada, 2015; Gudmundsson et al., 2021). Lower water levels due to altered seasonality patterns or droughts reduce the stream dilution capacity, which can increase the proportion of streamflow originating from (polluted) point sources (Wright et al., 2014; Luthy et al., 2015; Macedo et al., 2022). Both of these factors increase river water contamination, threatening both the safe usability of water and environmental health. Climate change is also altering the thermal regime of rivers (van Vliet et al., 2013), with higher temperatures also causing dissolved oxygen depletion (Ozaki et al., 2003).

More directly, sectoral activities generate return flows: water that is extracted for a specific purpose that is not consumed (evaporated) in the process but which has changed in composition as a result of the water use activity (Sutanudjaja et al., 2018; Jones et al., 2021). For example, the composition of domestic wastewater will reflect the various household water uses, including organic and fecal contamination from human waste (WWAP, 2017) and elevated nutrient concentrations from household chemicals and laundry detergents (van Puijenbroek et al., 2019). The reintroduction of these flows back to the environment represents a significant source of pollutant loadings that degrade river water quality (Jones et al., 2022). Collection and treatment of these flows, before their reintroduction to the environment, can help to minimise the impact on surface water quality (Jones et al., 2022). However, these processes can be economically expensive to establish and operate, and hence collection and treatment infrastructure is not ubiquitous worldwide (Jones et al., 2021; Jones et al., 2022).

Water quality is an integral part of the Sustainable Development Agenda, cross-cutting almost all Sustainable Development Goals (SDGs). Despite widespread recognition of its importance, water quality monitoring data are still severely lacking in several world regions – particularly Africa and central Asia (Damania et al., 2019). Furthermore, in regions where observation data are available, data are often sparse in both space and time. Water quality models offer opportunities to overcome these limitations (Hofstra et al., 2013; Beusen et al., 2015; UNEP, 2016; van Vliet et al., 2021). As opposed to statistical models which heavily rely on observed water quality data, physical models simulate the emission and transport of pollutant loadings along the river network directly based on climatic, hydrological and socioeconomic input data. This makes physically based model approaches especially advantageous when simulating water quality in ungauged catchments and for projecting water quality under future (uncertain) climatic and socioeconomic developments (Wanders et al., 2019).

A spatially and temporally detailed assessment of multiple water quality constituents at the global scale is lacking. Furthermore, only a few studies have quantitatively evaluated temporal dynamics and trends in water quality over extended time periods, particularly considering changes in factors that drive higher pollutant emissions (e.g. population growth, industrialisation) relative to factors that abate pollutant emissions (e.g. wastewater treatment). Lastly, few studies have assessed the spatio-temporal patterns in the specific sectoral activities that are driving patterns in surface water quality worldwide.

Here, we present a high-spatio-temporal-resolution surface water quality model (henceforth *DynQual*), which can currently be used to simulate water temperature (Tw), and concentrations of total dissolved solids (TDS) to represent salinity pollution, biological oxygen demand (BOD) to represent organic pollution and fecal coliform (FC) as a coarse indicator of pathogen pollution. All simulations are made at a daily timestep with a spatial resolution of 5 arc-min (∼10x10km at the equator). *DynQual* considers a wide range of hydro-climatic and socioeconomic drivers, spanning across the major contributing pollutant sources. The high spatio-temporal resolution of *DynQual*, combined with these features, allows the model to address scientific questions that are not currently possible using existing surface water quality models. For example, while previous work has compared pollutant loads (masses) originating from different sources at aggregated spatial scales (i.e. basin or sub-basin level), the impact on in-stream concentrations – which is also dependent upon spatio-temporal variability in dilution capacity and in-stream decay processes – has not been assessed.

The objectives of this study are to: 1) introduce a new open source global surface water quality model and evaluate model performance; 2) assess spatial patterns and trends in surface water quality, focussing on TDS, BOD and FC concentrations for the period 1980–2019; and 3) demonstrate additional model capabilities by assessing the sector-specific contributions towards surface water pollution across both space and time.

3.2 *DynQual* – model description

3.2.1 General overview

The newly developed *DynQual* model builds on the modelling framework of *DynWat*, a global water temperature model that solves the energy-water balance to simulate daily water temperature (Tw) and ice thickness (van Beek et al., 2012; Wanders et al., 2019). A full model description including the energy balance equations and the representation of ice cover, floodplains, channel roughness and lakes and reservoirs within *DynWat* is available in published literature (Wanders et al., 2019). *DynQual* further includes the impact of heat dumps produced in thermoelectric powerplants (van Vliet et al., 2012b; van Vliet et al., 2021) on water temperature. In addition to water temperature, *DynQual* simulates daily in-stream concentrations of three water quality constituents, namely, total dissolved solids (TDS), biological organic matter (BOD) and fecal coliform (FC), which are of key social and environmental relevance (van Vliet et al., 2021) (Fig. 3.1).

Two options for running *DynQual* are offered: 1) in a stand-alone configuration with specific discharge (i.e. baseflow, interflow and direct runoff in m day^{-1}) fed from any land surface or hydrological model; or 2) coupled with the global hydrological and water resources model *PCR-GLOBWB2* (Sutanudjaja et al., 2018). The routine for surface water (and pollutant) routing follows an eight-point steepest-gradient algorithm across the terrain surface (local drainage direction) in a convergent drainage network with the lowermost cell connected to either the ocean or an endorheic basin, as per *PCR-GLOBWB2* (Sutanudjaja et al., 2018) and *DynWat* (van Beek et al., 2012; Wanders et al., 2019). Routing within *DynQual* uses the kinematic wave approximation of the Saint-Venant equations with flow described by Manning's equation, solved using a time-explicit variable sub-time-stepping scheme based on the minimum Courant number (Sutanudjaja et al., 2018). In the coupled configuration, surface waters are subject to water withdrawals and return flows

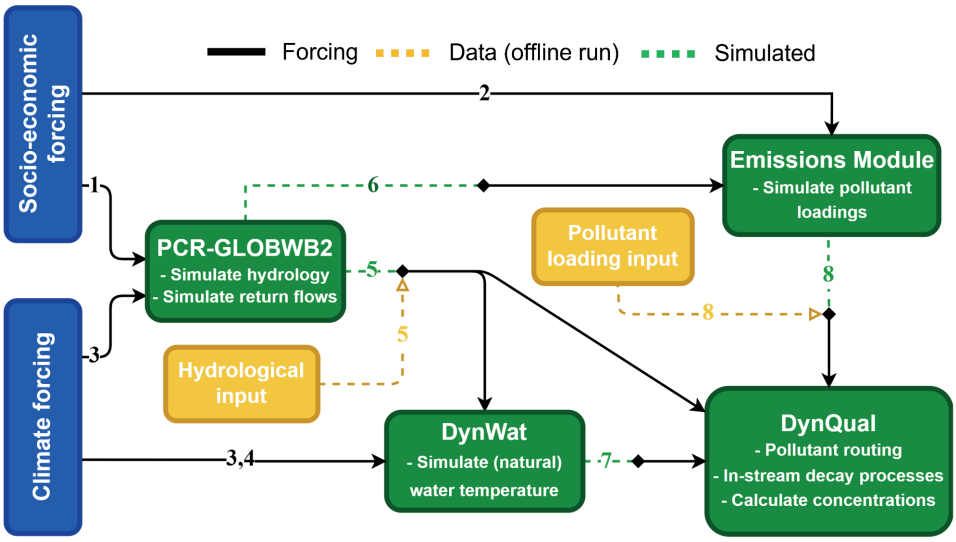

Socio-economic forcing

1. *Domestic gross and net water demand (m day^{-1}); industry gross and net water demand (m day^{-1}); livestock gross and net water demand (m day^{-1})*
2. *Population numbers; livestock numbers; urban fraction; thermo-electric power return flows (m^3 s^{-1}); excretion rates (g or cfu day^{-1}); mean effluent concentrations (mg l^{-1} or cfu 100ml^{-1})*

Climate forcing

3. *Air temperature (°C); precipitation (m day^{-1}); potential evapotranspiration (m day^{-1})*
4. *Solar radiation (W m^{-2}); annual average air temperature (°C); vapour pressure (kPa); cloud cover (%); sunlight hours (hours day^{-1})*

Hydrological data

5. *Baseflow or groundwater discharge (m day^{-1}); interflow (m day^{-1}); direct or surface runoff (m day^{-1})*
6. *Manufacturing return flows (m^3 day^{-1}); irrigation return flows (m^3 day^{-1}); urban surface runoff (m^3 day^{-1})*
7. *Water temperature (°C)*

Pollutant loading data

8. *Anthropogenic temperature loading (MW); TDS loading (g day^{-1}); BOD loading (g day^{-1}); FC loading (10^6 cfu day^{-1})*

Figure 3.1 Overview of the required input data for running *DynQual* in different model configurations. Runs coupled with *PCR-GLOBWB2* require socioeconomic (*arrow 1*) and climatic forcing (*3,4*) data as standard, with options to either 1) estimate loads based on additional socioeconomic (*2*) and simulated hydrological (*6*) data ; or 2) provide pollutant loadings directly as input data (*8*). Offline runs require both hydrological (*5*) and pollutant loading (*8*) input data to be provided directly.

from the domestic, industrial, livestock and irrigation sectors calculated within the water use module of *PCR-GLOBWB2*. A complete model description of *PCR-GLOBWB2* including detailed information on the model structure, individual modules (meteorology, land surface, groundwater, surface water routing and water use) and validation of hydrological output is available in published literature (Sutanudjaja et al., 2018). In both configurations of *DynQual*, pollutant loadings can be prescribed directly (akin to a forcing). Alternatively, when running *DynQual* coupled with *PCR-GLOBWB2* pollutant loadings can be simulated within the model runs by providing only simple input data (Appendix A.1). An overview of *DynQual*, which details the input data required for the different model configurations, is displayed in Fig. 3.1. By providing these options, we allow for flexibility – allowing pollutant loadings to be directly imposed on the model enables users to estimate loadings using their preferred methodology and assumptions, whereas the option to estimate pollutant loadings within the model run enables users to simulate water quality without any pre-processing requirements, but still provides flexibility to use their preferred input datasets. Parameter values related to pollutant emissions can be adjusted by the user, as desired. When simulating pollutant

loadings within model runs, it is also possible to quantify the contribution and relative importance of different water use sectors to the spatial patterns and temporal trends in surface water quality.

As per *PCR-GLOBWB2* (Sutanudjaja et al., 2018) and *DynWat* (Wanders et al., 2019), *DynQual* is written in Python 3 and is run using an initialization (.ini) file in which key aspects of the model run are defined (e.g. spatial extent, simulation period, paths to parameter and forcing files). Most input files required and all output files are in NetCDF format. Global 5 arc-min *DynQual* runs that are coupled with *PCR-GLOBWB2* have a wall-clock time of approximately 6 hours per year when run with parallelisation, due to the requirement to use the kinematic wave routing option for higher-accuracy discharge and water temperature simulations. This is approximately equivalent to the *PCR-GLOBWB2* run times given by Sutanudjaja et al. (2018). *DynQual* runs performed in the stand-alone configuration are faster (∼20%).

3.2.2 Water quality equations

Water temperature (Tw)

Water temperature (Tw) is simulated by solving the surface water energy balance using the *DynWat* model as basis (van Beek et al., 2012; Wanders et al., 2019). In addition to solving the surface water energy balance, *DynWat* also accounts for surface water abstraction, reservoirs, riverine flooding and the formation of ice (Wanders et al., 2019). Here, we further develop *DynWat* to include advected heat flows from thermoelectric powerplants, as per the method described in van Vliet et al. (2012b) and van Vliet et al. (2016). The modelling equations for Tw incorporated into *DynQual* are shown in Eq. 3.1 and are fully elaborated on in previous work (van Beek et al., 2012; van Vliet et al., 2012b; van Vliet et al., 2016; Wanders et al., 2019).

$$\begin{aligned} \rho_w C_p \frac{\partial(hT_w)}{\partial t} &= \rho_w C_p \frac{\partial(vT_w)}{\partial x} + H_{tot} + \rho_w C_p \int_{x=0}^{dx} q_s T_s + \frac{Tw_{pow_n}}{h \cdot w \cdot \partial x} \\ H_{tot} &= S_{in}(1 - a_w) + L_{in} - L_{out} - H - LE \\ Tw_{pow_n} &= \rho_w \cdot C_p \cdot RF_{pow,n} \cdot \Delta T_{pow_{rf}} \end{aligned} \tag{3.1}$$

where t is time, x is location along the drainage network, T_w is water temperature (K), C_p is the specific heat capacity of water (4,190 J kg^{-1} K^{-1}), ρ_w is the density of fresh water (1,000 kg m^{-3}), h is the stream water depth (m), v is the velocity of water (m^3 s^{-1}), H_{tot} is the heat flux at the air–water interface, S_{in} is the incoming shortwave radiation (J m^{-2} s^{-1}), $1 - a_w$ is the reflected shortwave radiation (J m^{-2} s^{-1}), L_{in} is the incoming longwave radiation (J m^{-2} s^{-1}), L_{out} is the outgoing longwave radiation (J m^{-2} s^{-1}), H is the sensible heat flux (J m^{-2} s^{-1}), LE is the latent heat flux (J m^{-2} s^{-1}), q_s is the lateral water fluxes from land to stream (m s^{-1}), T_s is the temperature of lateral water fluxes (K), Tw_{pow_n} is the heat dump from thermoelectric powerplants (J s^{-1}), $RF_{pow,n}$ is the return flows of cooling water from thermoelectric powerplants (m^3 s^{-1}), $\Delta T_{pow_{rf}}$ is the difference in water temperature between the return flows and ambient river water (K), w is the stream width (m) and dx is the distance between gridcell n and the upstream gridcell $n - 1$ (m).

Conservative (TDS) and non-conservative (BOD, FC) substances

Our modelling strategy for TDS, BOD and FC is a mass balance approach assuming transport by advection only, whereby sector-specific loadings (i.e. masses of pollutants generated from a particular human activity in a given time period) are accumulated from all contributing sectors and routed through the global stream network until outflow to the ocean or an endorheic basin (Thomann and Mueller, 1987; Chapra and Pelletier, 2004; Voß et al., 2012; UNEP, 2016; van Vliet et al., 2021).

TDS is modelled as a conservative substance, while BOD and FC are modelled as non-conservative substances that include first-order decay processes (Voß et al., 2012; Reder et al., 2015; UNEP, 2016;

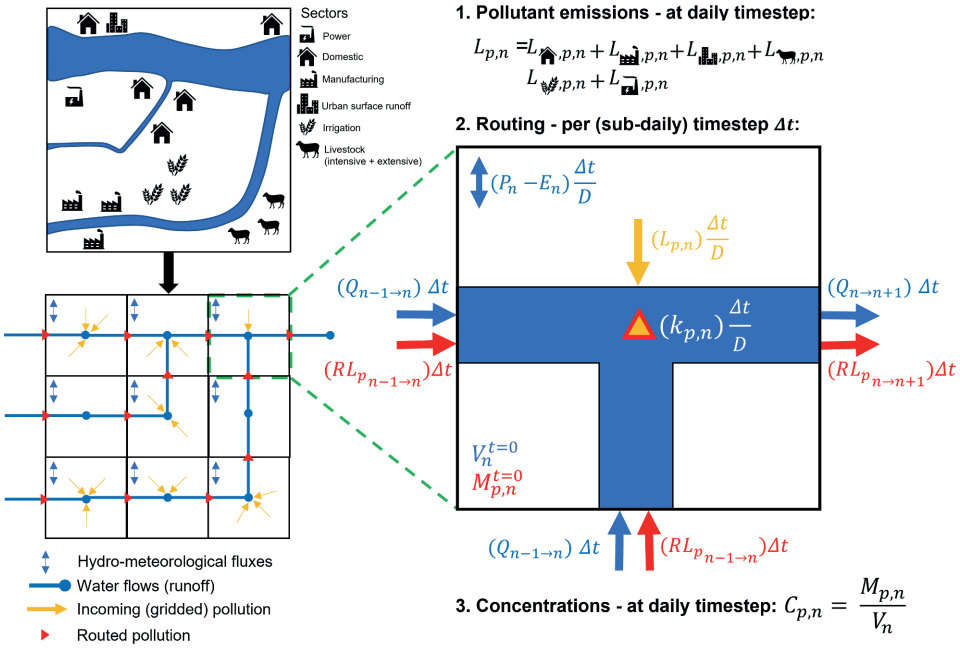

Figure 3.2 Schematic overview of *DynQual*, including a translation of local hydrological and socioeconomic situation into a local drain direction (LDD) map that includes hydrological and pollutant fluxes, and a representation of the gridcell based processes (pollutant emission calculation, routing procedure and computation of pollutant concentrations) in an individual DynQual gridcell. $C_{p,n}$ is the concentration of pollutant p (e.g. mg l^{-1}), while $M_{p,n}$ is the total mass of pollutant p (e.g. g) and V_n is the channel storage (m^3), all of which are in gridcell n. $V_n^{t=0}$ is the volume of channel storage from the previous timestep (m^3), while $Q_{n-1\to n}$ and $Q_{n\to n+1}$ are the discharge ($m^3\ s^{-1}$) into and out of gridcell n, respectively, per timestep Δt. $M_{p,n}^{t=0}$ is the mass of pollutant p from the previous timestep, while $RL_{p_{n-1\to n}}$ and $RL_{p_{n\to n+1}}$ are the loadings of pollutant p (e.g. g s^{-1}) that are routed into and out of gridcell n, per timestep Δt. $L_{p,n}$ are the combined local loadings of pollutant p (e.g. g day^{-1}) in gridcell n, which is the sum of loadings from all contributing sectors and urban surface runoff. $k_{p,n}$ represents a decay coefficient, which depends upon pollutant p. D is the length of a day in seconds (i.e. 86,400 s day^{-1}), while Δt is the length of the sub-timestep (s) which is linked to the internal routing regime within *DynQual* and *PCR-GLOBWB2*. P_n is precipitation (m^3 day^{-1}) and E_n is evapotranspiration (m^3 day^{-1}), with these terms included as an example of gridcell-specific hydrological fluxes. For a more detailed overview of the hydrological fluxes within a gridcell we refer to the *PCR-GLOBWB2* documentation (Sutanudjaja et al., 2018).

van Vliet et al., 2021). Our approach for both the conservative and non-conservative substances assumes instantaneous and full mixing of all streamflow and return flows in each gridcell. As per most water quality models, *DynQual* simulates water quality per individual gridcell over a consecutive series of discrete time periods (Loucks and van Beek, 2017). Each gridcell represents a volume element, which is in steady-state conditions within each time period and contains a (fully-mixed) pollutant mass (Fig. 3.2). In each consecutive timestep, there is an associated volume of water and mass of pollutant that flows into the gridcell from upstream and that flows out of the gridcell to the downstream gridcell. For non-conservative substances, there are also gridcell-specific in-stream decay processes that influence the total mass of pollutant in each sub-time interval. *DynQual* simulates these transport and decay processes with a sub-daily interval (Δt in seconds), the

length of which is determined with respect to channel characteristics and discharge (Appendix A.2 & Eq. A.9).

The pollutant concentration at each subsequent time interval ($t + \Delta t$) is calculated following Eq. 3.2. It should be noted that, while we simulate the terms of this equation with a sub-daily timestep interval, *DynQual* only reports concentrations in the final sub-daily interval of each day. This is due to the lack of sub-diurnal input data, for efficient data storage and the lack of relevance of such high-resolution simulations with respect to our large-scale modelling approach.

$$C_{p,n}^{t+\Delta t} = \frac{M_{p,n}^{t+\Delta t}}{V_n^{t+\Delta t}} + BG_{p,n} \tag{3.2}$$

Where $C_{p,n}^{t+\Delta t}$ and $M_{p,n}^{t+\Delta t}$ are the concentration and mass, respectively, of pollutant p in gridcell n at the consecutive time period ($t + \Delta t$), whereas $V_n^{t+\Delta t}$ is the volumetric channel storage (m^3) in this grdicell in the same time interval. $V_n^{t+\Delta t}$ is simulated directly within *PCR-GLOBWB2*, accounting for the initial storage, discharge into and out of gridcell n over time interval Δt and gridcell-specific hydrological fluxes including precipitation and evapotranspiration (Sutanudjaja et al., 2018). $M_{p,n}^{t+\Delta t}$ is simulated by solving the mass balance equation for pollutant p and accounting for in-stream decay processes following Eq. 3.3. $BG_{p,n}$ represents the background concentration of pollutant p in gridcell n. For TDS, these are estimated based on minimum observed EC-converted to TDS observations (Walton, 1989) contained in a new global salinity dataset (Thorslund and van Vliet, 2020) and are applied as a constant background concentration. Conversely, $BG_{BOD,n}$ and $BG_{FC,n}$ are assumed to be negligible relative to the mass of pollution produced by anthropogenic activities.

$$M_{p,n}^{t+\Delta t} = (M_{p,n}^{t=0} + (\sum (RL_{p_{n-1\rightarrow n}}) - RL_{p_{n\rightarrow n+1}}) + \frac{L_{pn}}{D}\Delta t) \cdot e^{-k_{pn}(\frac{\Delta t}{D})} \tag{3.3}$$

Where, at the subsequent timestep interval $t + \Delta t$, each gridcell n contains the mass of pollutant p from the previous timestep $M_{p,n}^{t=0}$ plus the pollutant load (mass second^{-1}) that has been transported from the immediately (adjacent) upstream gridcell(s) ($RL_{p_{n\rightarrow n-1}}$) and minus the pollutant load (mass second^{-1}) that has been transported downstream ($RL_{p_{n\rightarrow n+1}}$) in the time interval Δt (s). $L_{p,n}$ represents the daily influx of pollutant loadings produced into gridcell n (mass day^{-1}), which are added to the stream in equal increments per sub-daily timestep Δt (s) relative to the total length of a day D in seconds (i.e. 86,400 s day^{-1}). Our approach for adding local pollutant loadings in equal increments per sub-daily timestep is necessary as we lack information regarding the (sub-diurnal) timing at which pollution enters the stream network.

The variable $k_{p,n}$ represents a pollutant-specific p and gridcell-specific n decay rate (day^{-1}). While we model TDS as a conservative substance (i.e. $k_{TDS,n} = 0$), we determine the first-order degradation rate of BOD ($k_{BOD,n}$) as a function of water temperature (Eq. 3.4) and of FC ($k_{FC,n}$) as a function of water temperature, solar radiation and sedimentation (Eq. 3.5). Decay is implemented directly into *DynQual* by assuming that decay occurs at an equal rate over the course of a day ($\frac{\Delta t}{D}$). This assumption is necessary because we do not have sub-daily input data for some terms of the decay equations, such as Tw and incoming solar radiation (I_o).

$$\mathrm{k}_{BOD,n} = k(20) \cdot \Theta^{Tw_n - 20} \tag{3.4}$$

Where $k(20)$ is a first-order degradation rate coefficient at 20°C (day^{-1}) assumed at 0.35 (van Vliet et al., 2021), Tw_n is the water temperature (°C) in gridcell n and Θ is a temperature correction assumed to be 1.047 as per previous assessments (Wen et al., 2017; van Vliet et al., 2021).

$$\mathrm{k}_{FC,n} = k_d(20)\Theta^{Tw_n-20} + k_s\frac{I_o}{k_e H}(1 - e^{-k_e H}) + \frac{v}{H} \tag{3.5}$$

Where k_d is dark inactivation (day^{-1}), Θ is a temperature correction, Tw_n is the water temperature (°C) in gridcell n, k_s is sunlight inactivation ($\mathrm{m}^2\ \mathrm{W}^{-1}$), I_o is the surface solar radiation ($\mathrm{W\ m}^{-2}$), k_e is an attenuation coefficient (m^{-1}), H is stream depth (m) and v is the settling velocity ($\mathrm{m\ day}^{-1}$). Parameter values (Table 3.1) and mean basin average total suspended solids (Beusen et al., 2005) are based off previous fecal coliform modelling studies (Reder et al., 2015). Parameter values, including decay coefficients, can alternatively be defined by the user directly in the source code.

Table 3.1 Assumed parameter values for fecal coliform modelling.

Variable	Unit	Value
kd	day^{-1}	0.82
c	-	1
ks	$\mathrm{m}^2\ \mathrm{W}^{-1}$	0.0068
ke	m^{-1}	0.0931TSS + 0.881
v	$\mathrm{m\ day}^{-1}$	1.656

3.2.3 Pollutant loadings

In both model configurations (stand-alone or one-way coupled to *PCR-GLOBWB2*), user-defined pollutant loadings can be directly imposed on the model (akin to a forcing). Users can estimate pollutant loadings using their preferred methodology, and subsequently route these through the global stream network, account for in-stream decay processes and calculate in-stream pollutant concentrations using the *DynQual* model framework. Pollutant loadings that are prescribed to *DynQual* directly should have a daily temporal resolution (e.g. $\mathrm{g\ day}^{-1}$ or 10^6 $\mathrm{cfu\ day}^{-1}$).

Alternatively, when running *DynQual* coupled with *PCR-GLOBWB2*, pollutant loadings (with a daily temporal resolution) can be simulated within the model runs, requiring only simple input data (see Fig. 3.1 and Appendix A.1). This option is beneficial for users that do not have their own estimates of pollutant loadings. Furthermore, this option may be useful for those interested in scenario modelling, as input files related to different scenarios can be altered to reflect alternative climate and socioeconomic conditions.

In this set-up, *DynQual* estimates and routes pollutant loadings individually and combined for the main water use sectors (domestic, manufacturing, livestock and irrigation) and from urban surface runoff at 5 arc-min spatial resolution.

Loadings from the domestic sector are estimated by multiplying the gridded population with region-specific per capita excretion rates (Appendix A.1.1; Table A.1). For the manufacturing sector, a mean effluent concentration is multiplied by location-specific gridded estimates of return flows from the manufacturing sector (Appendix A.1.2; Table A.2). Urban surface return flows are approximated by multiplying surface runoff (simulated by *PCR-GLOBWB2*) with the gridded urban fraction, which are multiplied by a region-specific mean urban surface runoff effluent concentration (Appendix A.1.3; Table A.3). The livestock sector is sub-divided into 'intensive' and 'extensive' production systems based on livestock densities to better account for differences in the paths by which waste enters the stream network (Appendix A.1.4; Table A.4). Gridded livestock numbers for buffalo, chickens, cows, ducks, goats, horses, pigs and sheep are multiplied by pollutant excretion rates per livestock type and

by region (Appendix A.1.4; Tables A.5-A.7). TDS loadings from the irrigation sector are estimated by multiplying irrigation return flows simulated by *PCR-GLOBWB2* with spatially-explicit mean irrigation drainage concentrations based on salinity (as indicated by electrical conductivity) over the top- and sub- soil (Appendix A.1.5). Thermal effluents (heat dumps) from thermoelectric powerplants are included as point sources of advected heat by considering the temperature difference between the flows and ambient surface water temperature conditions (Appendix A.1.6). Pollutant loadings from the domestic, manufacturing and intensive livestock sectors, and from urban surface runoff, are abated based on gridcell-specific wastewater practices. The proportion of pollutant loadings removed by wastewater treatment practices is estimated by multiplying the fraction of each treatment level occurring in a gridcell by the pollutant removal efficiency associated with that treatment level, as described in detail in previous work (Jones et al., 2021; Jones et al., 2022).

A detailed explanation of how pollutant loadings are estimated within *DynQual* is provided in Appendix A.1, including equations (Eq. A.1-A.8), data sources and all parameter estimates (Tables A.1–A.7).

3.3 Model demonstration

3.3.1 Model run setup

DynQual is run for the time period 1980–2019 using W5E5 forcing data (Cucchi et al., 2020; Lange et al., 2021) in the configuration coupled with *PCR-GLOBWB2*. We used the standard parameterisation of *PCR-GLOBWB2* for hydrological simulations, as described in previous work (Sutanudjaja et al., 2018). The focus of our model demonstration is on TDS, BOD and FC, as results for Tw have been displayed extensively in previous work (Wanders et al., 2019). Pollutant loadings of TDS, BOD and FC are estimated within the model run at the daily timestep using input data summarised in Table 3.2, and as detailed in Section 3.2.3 and Appendix A.1. Both the meteorological forcing data and input data used for simulating pollutant loadings used in this study are accessible through links provided. We also provide the model code and full input data required for running an example catchment (Rhine basin) in the 'Code and data availability' statement.

As per *PCR-GLOBWB2* (Sutanudjaja et al., 2018), in addition to the original water temperature model *DynWat* (Wanders et al., 2019), no calibration was performed. The process-based nature and global scale of *DynQual*, combined with strong spatial biases in observations (Fig. A.2) and the large number of parameters that need to be estimated, complicate meaningful calibration. In addition, uncalibrated physical models can theoretically be applied in ungauged basins without loss of performance and are more preferable for global change assessments with different climatic and socioeconomic scenarios (Hrachowitz et al., 2013; Wanders et al., 2019).

Table 3.2 Summary of key input data used for the estimation of pollutant loadings in the presented model application.

Sector	Data	Source	Spatiotemporal resolution
Domestic	Population	Lange & Geiger (2020)	5 arc-min; annual
	Excretion rates	UNEP (2016) & van Vliet (2021)	Regional; constant
Manufacturing	Manufacturing return flows	PCR-GLOBWB2 (*simulated*)	5 arc-min; daily
	Effluent concentrations	UNEP (2016) & van Vliet (2021)	Global; constant
Urban surface runoff	Urban surface runoff	PCR-GLOBWB2 (*simulated*)	5 arc-min; daily
	Effluent concentrations	UNEP (2016)	Regional; constant
Livestock	Livestock population	Gilbert et al. (2018)	5 arc-min; annual
	Excretion rates	Weaver et al. (2005); Wilcock et al. (2006); Robinson et al. (2011); Wen et al. (2017); Vigiak et al. (2019); van Vliet et al. (2021)	Regional; constant
Irrigation	Irrigation return flows	PCR-GLOBWB2 (*simulated*)	5 arc-min; daily
	Effluent concentrations	Batjes (2005)	30 arc-min; constant
Power	Power return flows	Lohrmann et al. (2019)	5 arc-min; annual
	ΔT	van Vliet et al. (2012)	Global; constant

3.3.2 Model evaluation

Model simulations were compared to observations from surface water quality monitoring stations worldwide at daily temporal resolution. Observed data were obtained from various state-of-the-art databases (Appendix A.3.1). Water quality monitoring data cover the entire modelled time period (1980–2019) and include a far greater number of observations than in previous surface water quality modelling validation procedures (Table A.8). However, monitoring stations are unevenly distributed across space, with a strong bias towards North America and Western Europe for all water quality constituents (Fig. A.2). Furthermore, observations at monitoring stations are highly fragmented across time, particularly for BOD and FC.

The overarching purpose and applications of a model, including large-scale water quality models (Beusen et al., 2015; UNEP, 2016), must be considered for determining suitable metrics for model evaluation and judging model performance. Given the approximations in the model, uncertainties in input data and the overall complexity in the drivers of pollutant loadings, the purpose of global water quality models is not to compute daily concentrations exactly (UNEP, 2016). The modelling strategy is thus to focus on the main spatial and temporal drivers of pollution in river networks globally to facilitate first-order approximations of in-stream concentrations. A key reason for implementing *DynQual* at 5 arc-min spatial resolution is due to the marked improvement of the performance of both *PCR-GLOBWB2* (e.g. discharge) (Sutanudjaja et al., 2018) and *DynWat* (e.g. water temperature) (Wanders et al., 2019) at finer spatial extents. These two factors have an important influence on simulated in-stream concentrations due to dilution and in-stream decay processes, respectively.

Given these factors, combined with limitations in the observational records of surface water quality (Appendix A.3.1), global water quality models have typically not been evaluated with metrics commonly used for hydrological modelling such as coefficients of determination, Nash–Sutcliffe efficiency (NSE) and Kling–Gupta efficiency (KGE) (Voß et al., 2012; Beusen et al., 2015; UNEP, 2016; Wen et al., 2017; van Vliet et al., 2021), with the exception of water temperature simulations (van Vliet et al., 2012a; Wanders et al., 2019). The model evaluation approach adopted for *DynQual* combines methods applied for the evaluation of other global water quality modelling efforts. Simulated TDS, BOD and FC concentrations are evaluated with respect to pollutant classes linked to key sectoral water quality thresholds (UNEP, 2016; Wen et al., 2017) (Appendix A.3.2; Table A.9) and statistically using normalised-root-mean-square error (nRMSE) (Beusen et al., 2015; van Vliet et al., 2021) (Appendix A.3.2; Eq. A.11). This provides an indication of prediction errors across the different water quality constituents comparable with previous large-scale water quality assessments. Conversely, the quality of water temperature simulations is evaluated using KGE (Appendix A.3.2; Eq. A.10). All four water quality constituents are also evaluated by considering long-term time-series and multi-year annual cycles at individual monitoring stations (Appendix A.3.2), which we present for the station with the most data availability across all four constituents (see Fig. 3.5 for a station in the Mattaponi River in the USA) and for a selection of additional monitoring stations per water quality constituent (Figs. A.5–A.8).

Overall, a strong correspondence between simulated and observed concentrations classes is found, indicating that the model is (largely) able to simulate concentrations within the correct concentration range (Fig. 3.3). The simulated concentration class matches the observed concentration class exactly in 69%, 51% and 44% of instances for TDS, BOD and FC, respectively. When considering ±1 pollutant class, these percentages rise to 92%, 79% and 79%. Of the mismatches in simulated and observed concentration classes, *DynQual* tends to underestimate TDS and BOD concentrations relative to observed in-stream concentrations (i.e. difference in classification level >=1). This occurs for 75% of mismatches in simulated TDS classes and 69% of mismatches in BOD classes. Conversely, FC mismatches occur both for under-estimates (57% of cases) and over-estimates (43% of cases) in more equal proportions.

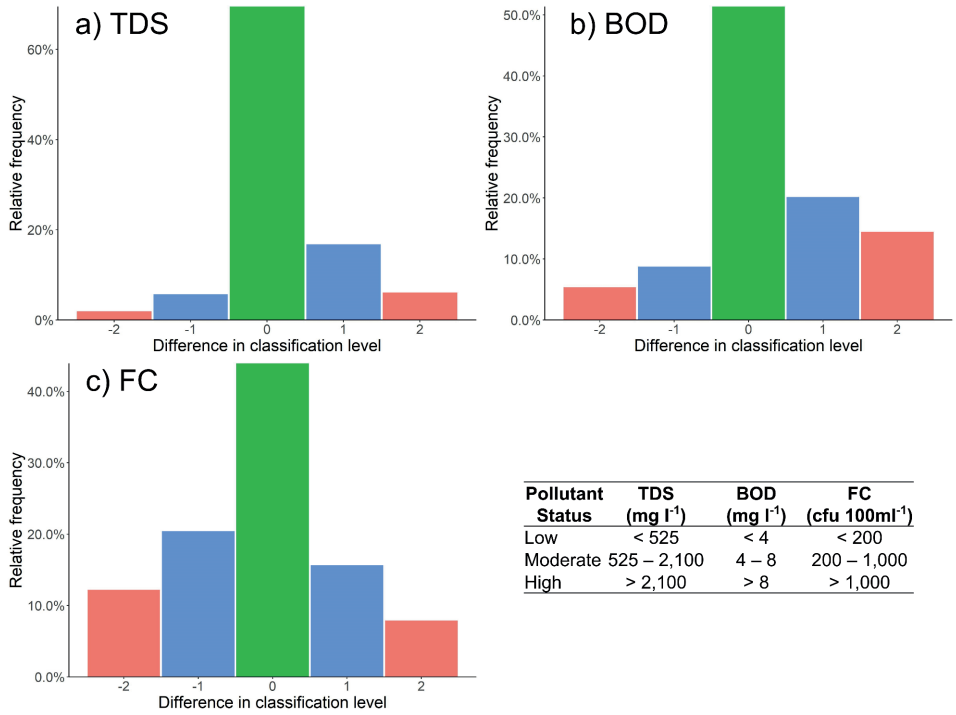

Pollutant Status	TDS (mg l^{-1})	BOD (mg l^{-1})	FC (cfu 100ml^{-1})
Low	< 525	< 4	< 200
Moderate	525 – 2,100	4 – 8	200 – 1,000
High	> 2,100	> 8	> 1,000

Figure 3.3 Differences in observed vs. simulated pollutant classes for a) total dissolved solids (TDS); b) biological oxygen demand (BOD); and c) fecal coliform (FC). Pollutant classes are defined based on water use and ecological limitations, as stated by governmental and international organisations. A difference in classification level of '0' indicates the simulated pollutant class matches the observed pollutant class, while negative differences indicate that observed concentrations exceeded simulated concentrations and vice versa for positive differences.

Statistical evaluation of the water temperature simulations using the KGE coefficient demonstrates the strong performance of *DynQual* (Fig. 3.4a) across all world regions (Fig. A.3). Across all observation stations, a median KGE of 0.72 is found (25th percentile = 0.52, 75th percentile = 0.83), with 32% of stations with KGE > 0.8, 83% of stations with KGE > 0.4 and 99% of stations with KGE values exceeding the performance threshold of > -0.41 (Knoben et al., 2019). Detailed time-series of individual rivers also demonstrate the ability of *DynQual* to closely replicate observed water temperature at the daily timestep, in addition to seasonal patterns, across different world regions (Fig. 3.5a; Fig. A.5). A detailed evaluation of water temperature simulations is available in previous work (Wanders et al., 2019).

The distribution of nRMSE values, sub-divided by annual average river discharge, for TDS, BOD and FC is displayed in Fig. 3.4b-d. Statistical evaluation of the simulations using nRMSE shows mixed results. A median nRMSE value of 0.76 is found for TDS across all observation stations, with 25th percentile of 0.79 and a 75th percentile of 1.83 (Fig. 3.4b). For BOD simulations, a median nRMSE of 0.98, 25th percentile of 0.76 and 75th percentile of 1.25 is found (Fig. 3.4c). A large spread is found for nRMSE values for FC simulations, with a median of 1.89, a 25th percentile of 1.16 and a 75th percentile of 3.53 (Fig. 3.4d). Simulated TDS concentrations are typically lower than observations in many locations that are proximate to the coastline, presumably due to a combination of background TDS concentrations based upon minimum observations (and applied constantly) and *DynQual* not accounting for the influence of saltwater intrusion. This may somewhat explain the long tail (nRMSE

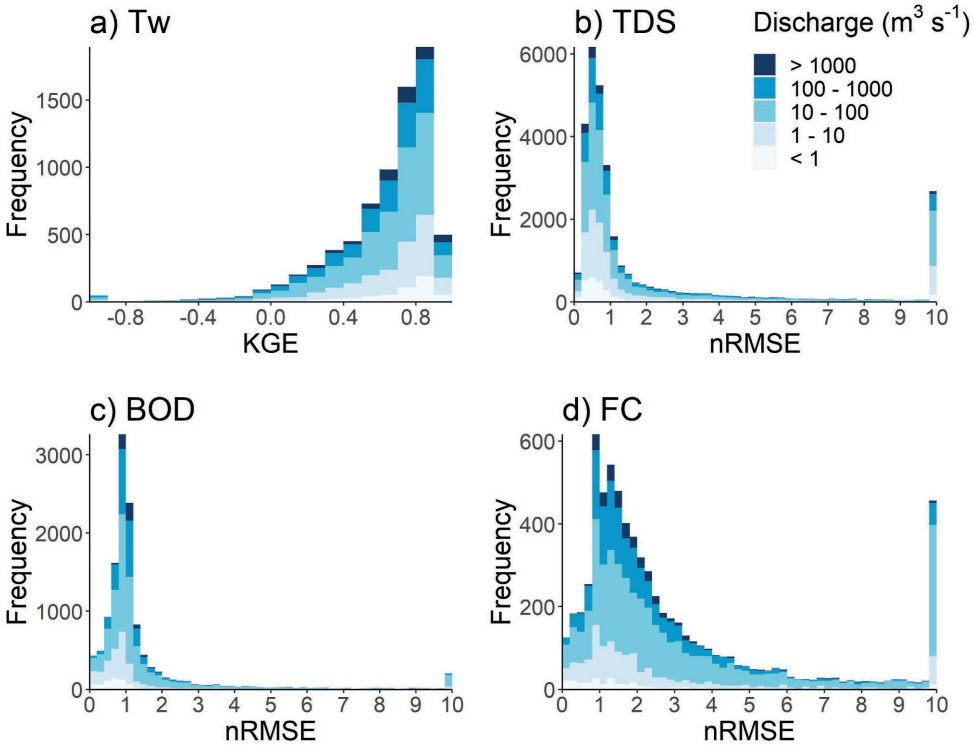

Figure 3.4 Evaluation of model performance using the Kling–Gupta efficiency (KGE) coefficient for a) water temperature (Tw); and normalised root mean square error (nRMSE) for b) total dissolved solids (TDS); c) biological oxygen demand (BOD); and d) fecal coliform (FC) simulations. Spatial patterns in KGE for Tw (Fig. A.3) and nRMSE for TDS, BOD and FC (Fig. A.4) are displayed in Appendix A.3.2

> 10) in the histogram for TDS (Fig. 3.4b) and the disproportionate tendency of *DynQual* to simulate TDS concentrations that are lower than observed concentrations (Fig. 3.3). Overall, no strong spatial patterns are found in the distribution of nRMSE values of BOD (Fig. A.4b) and FC (Fig. A.4c). For these water quality constituents, model simulations tend to represent the observed data better in larger streams (>100 m^3 s^{-1}). This is likely due to the influence of spatial mismatches between monitoring station locations and model simulations being especially important in smaller streams, where concentrations are more sensitive to natural dilution capacity (i.e. water availability) and variabilities in pollutant source contributions.

Long-term time-series and average annual cycle plots for TDS (Fig. 3.5b; Fig. A.6), BOD (Fig. 3.5c; Fig. A.7) and FC (Fig. 3.5d; Fig. A.8) show that *DynQual* can generally simulate in-stream concentrations within the correct range (e.g. min–max daily concentrations, 10th and 90th percentile average annual cycles). Simulated concentrations at the example monitoring station (Fig. 3.5) display that TDS, BOD and FC concentrations are largely simulated within plausible limits with strong overlaps in the average annual cycles, but the exact correspondence between observed and simulated concentrations at the daily timestep is relatively poor. For this observation station, simulated peaks in daily TDS, BOD and FC concentrations tend to exceed those in the observational record. However, given the incomplete nature of the observed records, it is problematic to draw conclusions on whether these concentrations are plausible but unrecorded, or if *DynQual* is simulating unrealistic peak

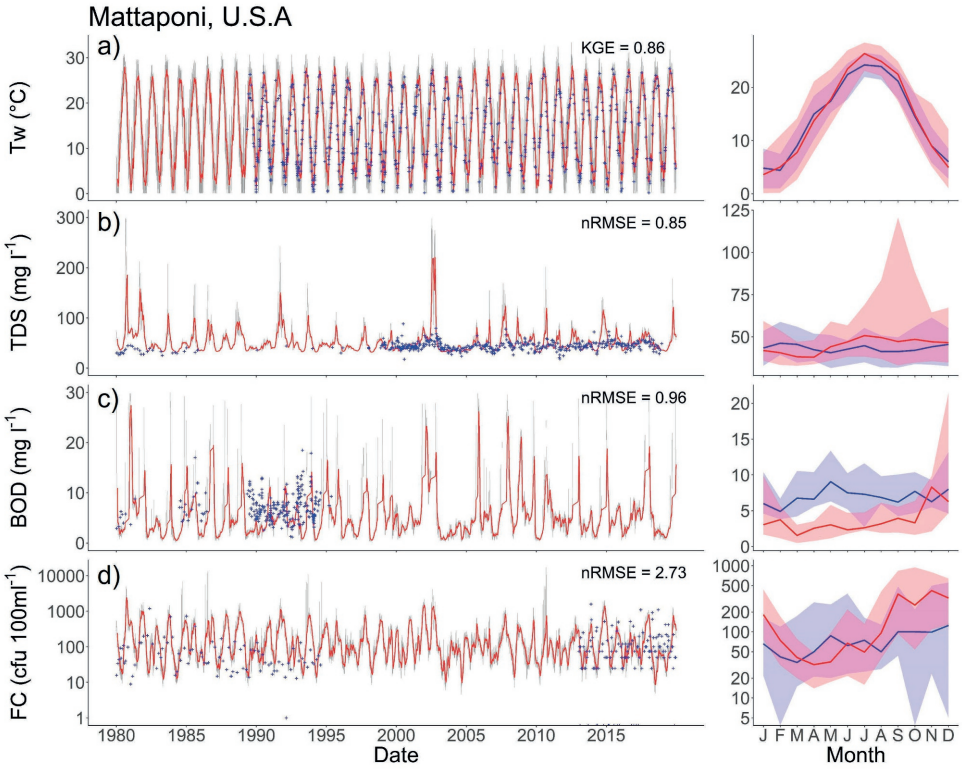

Figure 3.5 Time-series (left) and average annual cycles (right) of observed vs. simulated surface water quality as indicated by a) water temperature (Tw; °C); b) total dissolved solids (TDS; mg l^{-1}) concentrations; c) biological oxygen demand (BOD; mg l^{-1}) concentrations; and d) fecal coliform (FC; cfu 100ml^{-1}) concentrations at an example water quality monitoring station. In the time-series plots, observations are indicated by blue crosses, daily simulations are indicated by grey lines and 30 day running averages are indicated by red lines. In the average annual cycle plots, blue and red lines indicate the median observed and simulated values, respectively, while the shading represents the range in values as indicated by the 10th and 90th percentiles. More examples for Tw (Fig. A.5), TDS (Fig. A.6), BOD (Fig. A.7) and FC (Fig. A.8) across different world regions are displayed in Appendix A.3.2

concentrations. For example, while *DynQual* captures some of the peaks in observed daily BOD concentrations, simulated BOD concentrations exceed those in the observational record while simultaneously under-predicting average annual cycles in BOD concentrations (Fig. 3.5c). This pattern is also observable in TDS concentrations in the Mersey River (Fig. A.6) and FC concentrations in the Exe River (Fig. A.8).

While strong seasonality is present in the Tw observations, which is well captured by *DynQual* (Fig. 3.5a; Fig. A.5), and in TDS concentrations to a lesser extent (e.g. Mersey and Komati rivers in Fig. A.6), there is an overall lack of strong seasonal patterns in the observed records of BOD and FC concentrations. This, combined with large variability in the observed concentrations, results in large uncertainty in average annual cycles of observed concentrations across all months, as indicated by 10th and 90th percentiles (Fig. 3.5c-d; Figs. A.7–A.8). Annual average cycles in observed and simulated concentrations tend to strongly overlap for both BOD and FC. However, seasonal patterns are more evident in BOD simulations than observations (e.g. Mersey, Periyar in Fig. A.7) and the large variability in observed FC concentrations is not replicated by *DynQual* daily simulations (e.g.

Cauvery, Rhine in Fig. A.8). In the case of FC concentrations, for example, this could suggest that *DynQual* misses or under-represents the importance of pulse disturbances (e.g. high rainfall events causing sewer overflows) on the transport of pollutants to surface waters.

3.3.3 Spatial patterns

The spatial patterns in TDS (Fig. 3.6), BOD (Fig. 3.7) and FC (Fig. 3.8) concentrations show substantial variations both within and across world regions, driven by different sectoral activities (Fig. 3.9). The dilution capacity of rivers is also a major determinant of in-stream concentrations. Averaged at the annual time-scale this is particularly evident for BOD and FC where the large dilution capacity of some major rivers is sufficient to dilute concentrations to relatively low levels, despite often being fed by more polluted tributaries. However, it should also be noted that both river discharges and in-stream concentrations can exhibit substantial intra-annual variability, thus pollutant hotspots and the magnitude of pollutant levels must also be considered at finer temporal scales than presented here. Intra-annual variability can occur in the model due temporal variations in: 1) pollutant loadings; 2) water availability (i.e. dilution capacity); and 3) in-stream decay processes.

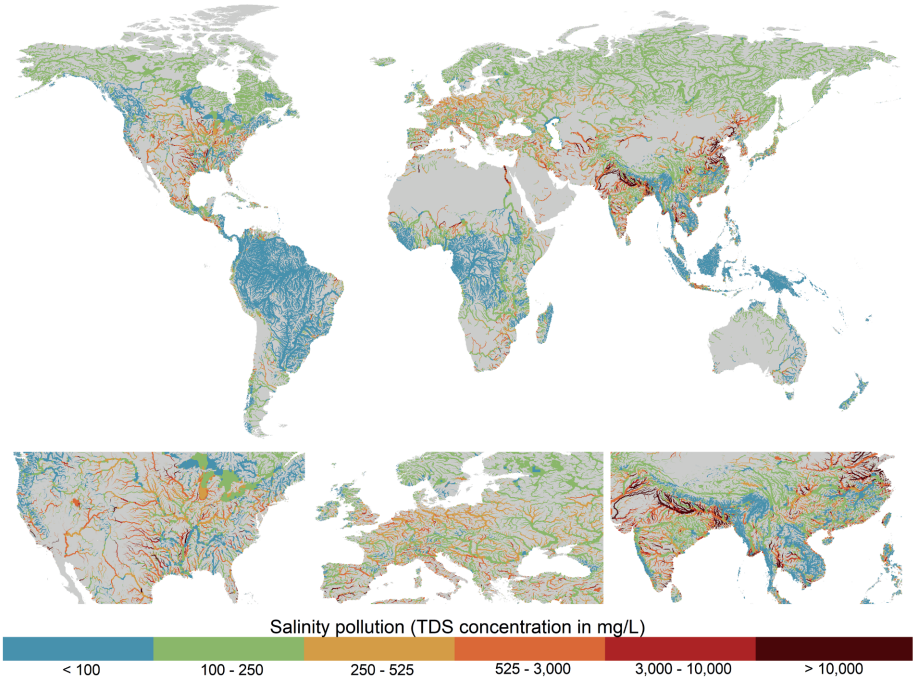

Figure 3.6 Annual average total dissolved solids (TDS) concentrations for the period 2010–2019. Plotted for rivers with > 10 m^3 s^{-1} annual average discharge.

TDS concentrations show strongly regional patterns, with key hotspots of salinity pollution located in southern Asia (Pakistan and northern India) and eastern China, and to a lesser degree across the United States and Europe (Fig. 3.6). High TDS concentrations in southeast Asia are predominantly driven by the irrigation sector and the presence of saline soils (Fig. 3.9a). While the irrigation sector is also an important driver of TDS pollution in eastern China, the contribution from manufacturing activities is also substantial (Fig. 3.9a). The manufacturing sector is the dominant contributor of TDS pollution across most of North America and Western Europe, accounting for >75% of in-stream

pollutant loadings in almost all major river segments in these regions (Fig. 3.9a). Aside from the lower Nile, where salinity pollution is predominantly from the manufacturing sector, the domestic sector is the key source of (non-natural) TDS loadings in Africa. However it should be noted that, aside from in the lower Nile, TDS concentrations are simulated to be relatively low across most of Africa (Fig. 3.6).

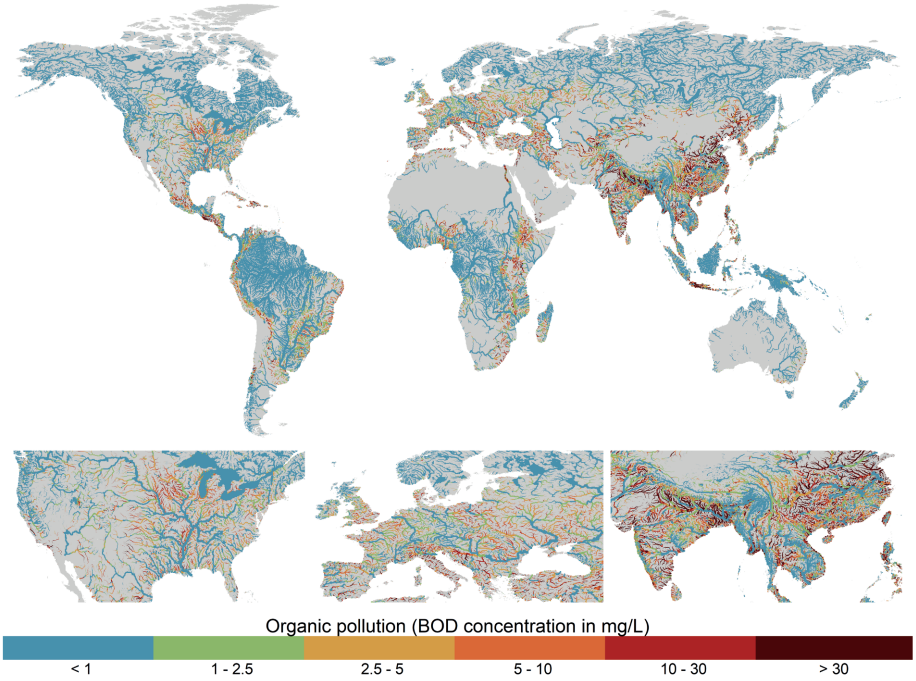

Figure 3.7 Annual average biological oxygen demand (BOD) concentrations for the period 2010–2019. Plotted for rivers with > 10 $m^3 s^{-1}$ annual average discharge.

While BOD concentrations show considerable diversity across the major world regions, a substantial proportion of river segments across populated areas of all continents experience moderate-to-high organic pollution (Fig. 3.7). There are clear spatial patterns in the dominant sectoral activities contributing BOD loadings worldwide, and it also evident that BOD pollution in most world regions is driven by a combination of multiple sectors opposed to from an individual dominant activity (Fig. 3.9b). Across Europe in particular, which sector is dominant varies both spatially and temporally and the contribution from the dominant sector is typically <50% (Fig. 3.9b). The manufacturing sector is the most significant source of BOD pollution across rivers in the United States; however the relative contribution commonly falls in the 20–50% or 50–75% categories (Fig. 3.9b). In the most polluted world regions, south and southeast Asia, the domestic sector is typically dominant. However, there are also significant contributions from manufacturing and extensive livestock activities (Fig. 3.7; Fig. 3.9b). Lastly, while its influence is highly localized, urban surface runoff can also represent an important source of BOD pollution in heavily urbanised gridcells across all world regions.

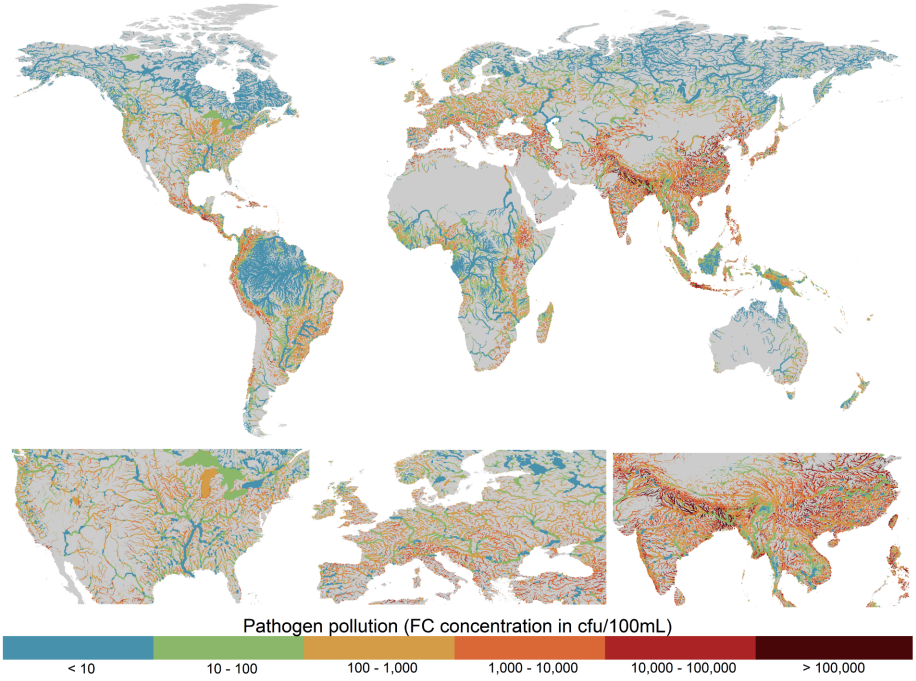

Figure 3.8 Annual average fecal coliform (FC) concentrations for the period 2010–2019. Plotted for rivers with > 10 m^3 s^{-1} annual average discharge.

FC pollution is particularly high across south and southeast Asia, with more localised hotspots found in parts of western Latin America, southern Europe, Middle East and eastern Africa (Fig. 3.8). Similar to BOD pollution, a large proportion of stream segments in south and southeast Asia are heavily polluted, with typically only rivers with extremely high dilution capacities appearing in the lower concentration classes. In this region, the domestic sector is predominantly responsible for FC pollution (commonly > 75%), attributed to large urban populations coupled with a large proportion of domestic wastewater being inadequately treated (Fig. 3.9c). In countries with high municipal wastewater collection and treatment rates, such as in Europe, the relative influence of livestock activities tends to be larger. While manufacturing activities remain the dominant source of FC pollution in North America, despite relatively high wastewater treatment rates, the percentage contribution is typically <50% and livestock activities also represent an important source of FC loadings (Fig. 3.9c). Despite variable municipal wastewater collection and treatment rates across Latin America, livestock activities appear to dominate FC loadings outside of the Amazon basin (Fig. 3.9c). This can be attributed to very high livestock numbers (particularly cattle), combined with the fact that the most of the large urban settlements (and thus domestic FC pollutant loadings) in Latin America are located in the coastal zone. As such, pollution from the domestic and manufacturing sectors typically enter the river network at downstream locations causing localised pollution before outflow to the ocean.

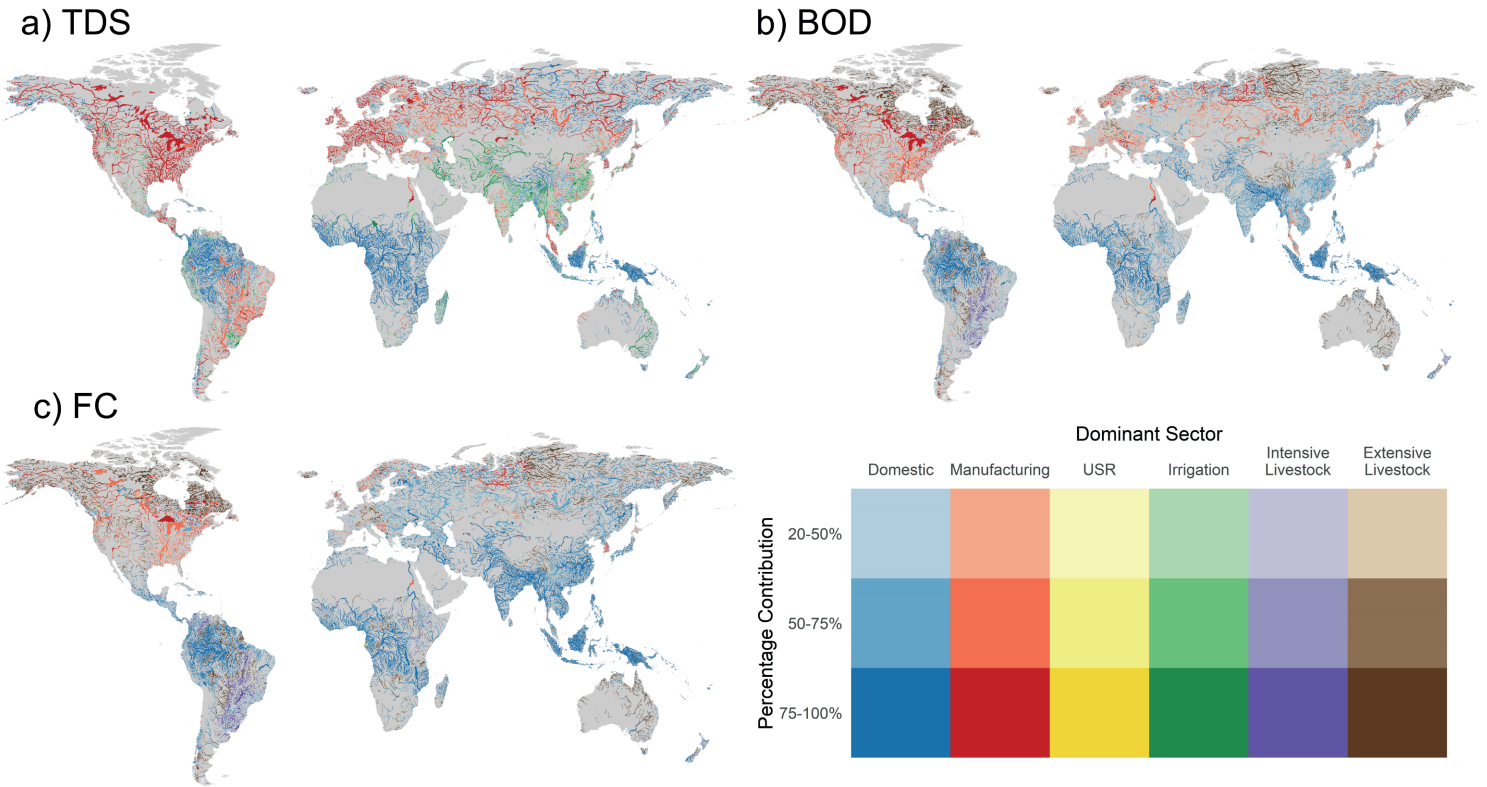

Figure 3.9 Dominant sectoral activity contributing towards a) total dissolved solids (TDS); b) biological oxygen demand (BOD); and c) fecal coliform (FC) pollution averaged over 2010–2019. Plotted for rivers with > 10 $m^3\ s^{-1}$ annual average discharge.

3.3.4 Trends

Long-term trends in TDS, BOD and FC concentrations over the simulated period (1980–2019) are also presented (Fig. 3.10). TDS concentrations in most world regions are either relatively constant or show relatively upward gradual trends (Fig. 3.10a). Typically, where TDS concentrations are increasing, the trend has been driven mainly by expansions in manufacturing or irrigation activities. Comparatively, trends in BOD (Fig. 3.10b) and FC (Fig. 3.10c) concentrations are larger in magnitude and exhibit substantially more spatial variation across the major world regions. Regionally, the strongest increases in BOD and FC concentrations are found in Sub-Saharan Africa, where wastewater treatment rates are low, and south Asia, where the rate of population growth and economic development has significantly outstripped the expansion of wastewater treatment infrastructure. Strong increasing trends are also found across most of Latin America, where a significant proportion of collected wastewater does not undergo wastewater treatment (UNEP, 2016; Jones et al., 2021). BOD and FC concentrations across North American rivers have typically remained relatively constant, or exhibit small decreasing trends. Strong decreasing trends are found across Europe, including the Danube and Rhine basins. In all world regions, the influence of reservoirs on BOD and FC concentrations is also evident, with increased water volumes (i.e. dilution) coupled with longer residence times (i.e. greater decay) reducing BOD and FC concentrations at these specific locations.

Complementary to the spatial analysis, we considered the proportion of the population that inhabits gridcells exhibiting different trends in pollutant concentrations, aggregated by geographical region and economic classification (Fig. 3.11). It should be noted that trends (Figs. 3.10–3.11) are not indicative of the degree of pollution directly and thus should also be considered with respect to in-stream concentrations (Figs. 3.6–3.8). Changes in TDS concentrations in the most populated areas worldwide are typically low, with increases of 0–1% most common across all geographical regions (Fig. 3.11a). Conversely, strong regional patterns are evident for BOD (Fig. 3.11b) and FC (Fig. 3.11c) concentrations. Particularly in Sub-Saharan Africa and southern Asia, BOD and FC concentrations in populated locations have been almost exclusively increasing. Over half of the population of Sub-Saharan Africa live in areas where BOD and FC concentrations have increased (on average) by >2% per year from 1980–2019. Conversely, in Western Europe, trends in BOD and FC have been negative for areas where 60% of the population lives.

When aggregating trends by country-specific economic classifications, trends in TDS, BOD and FC pollutant concentrations all display a clear correlation with level of economic development (Fig. 3.11). For the water quality constituents considered, the strongest and most widespread decreases in pollutant concentrations have been experienced by 'high income' countries, while 'low income' countries have experienced the greatest and most widespread degree of water quality degradation. These patterns are particularly clear for FC, where approximately 60% of the population in 'high income' countries live in gridcells displaying negative trends in FC concentrations, compared to 50%, 25%, and 10% in 'upper-middle income', 'lower-middle income' and 'low income' countries, respectively. Furthermore, in the 'low income' countries, 50% of the population live in areas where FC concentrations have increased (on average) by >2% each year from 1980 to 2019.

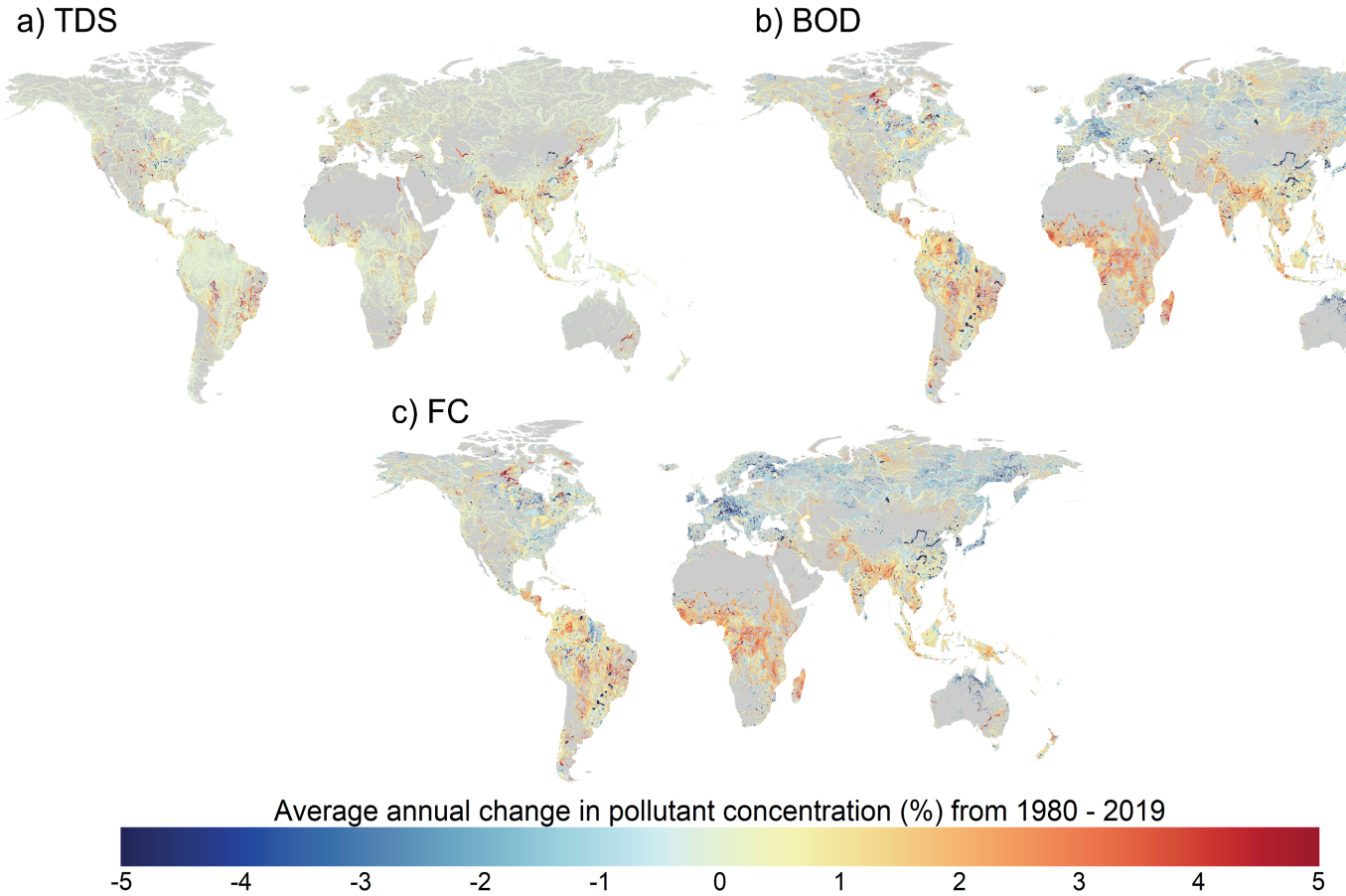

Figure 3.10 Average annual percentage changes in a) total dissolved solids (TDS); b) biological oxygen demand (BOD); and c) fecal coliform (FC) concentrations for the period 1980–2019. Plotted for rivers with > 10 $m^3\ s^{-1}$ annual average discharge.

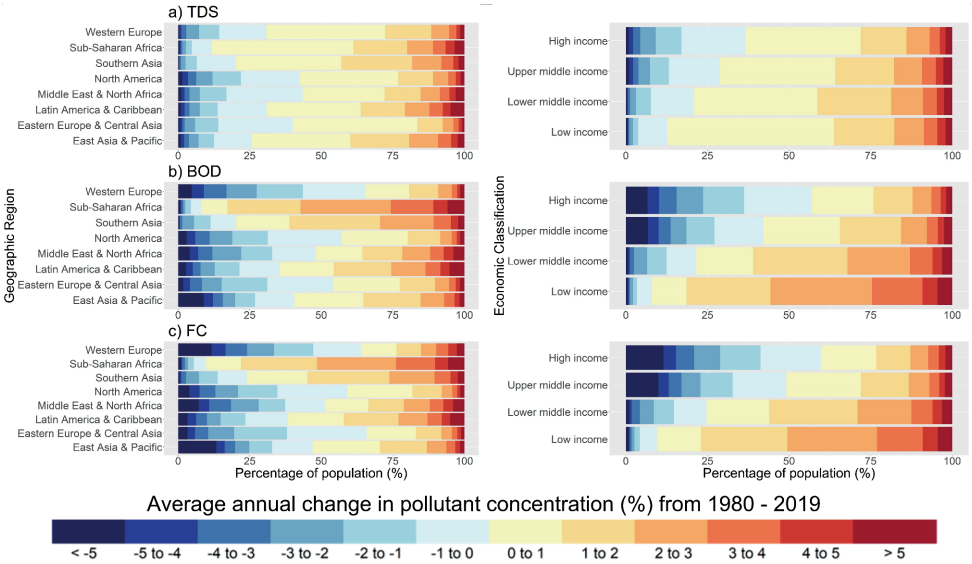

Figure 3.11 Average annual percentage changes in a) total dissolved solids (TDS); b) biological oxygen demand (BOD); and c) fecal coliform (FC) concentrations for the period 1980–2019. Plotted for rivers with > 10 m^3 s^{-1} annual average discharge.

Lastly, we present time-series of in-stream TDS, BOD and FC concentrations delineated by sector-specific contributions at three selected locations (Fig. 3.12) for which validation plots are also presented (Figs. A.6–A.8). While it is not our intention to explain the patterns in concentrations and sectoral drivers for the Mersey, Cauvery and Kiso rivers specifically, these plots are illustrative of the capabilities of *DynQual*. For example, these plots demonstrate the relative importance of different water use activities on in-stream concentrations dynamically, and also display changes over longer time periods. This is particularly evident in FC concentrations in the Mersey River, where decreasing loadings from the domestic and manufacturing sectors, primarily due to increases in wastewater treatment capacities, have driven an overall trend towards water quality improvements. Conversely, the manufacturing sector is simulated to have had an increasing influence on TDS concentrations in the Kiso River since ~2004, replacing the irrigation sector as the dominant driver of salinity pollution.

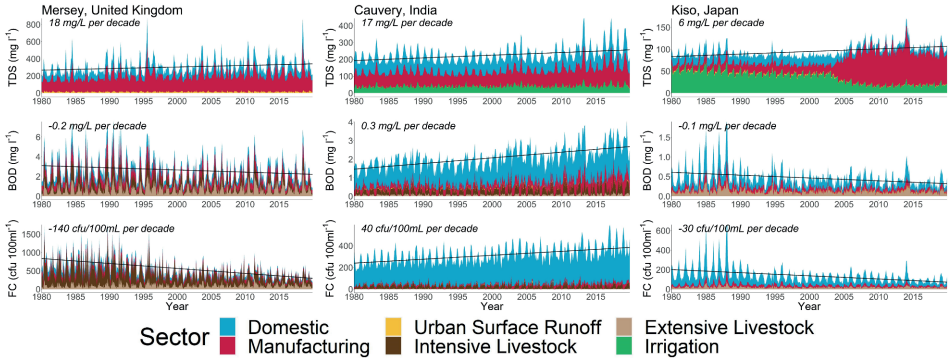

Figure 3.12 Simulated in-stream total dissolved solids (TDS), biological oxygen demand (BOD) and fecal coliform (FC) concentrations in selected rivers, disaggregated by contributing water use sectors and including linear decadal trends.

3.4 Discussion, conclusions and future work

To conclude, we have developed and evaluated a new global surface water quality model for simulating TDS, BOD and FC concentrations as indicators of salinity, organic and pathogen pollution, respectively. Building upon the water temperature model *DynWat* and utilising approaches developed in previous water quality model efforts, the open source code is structured in a way that allows for flexibility in both hydrological and pollutant loading inputs. Output data from *DynQual* has potential to inform assessments in a broad range of fields, including ecological, human health and water scarcity studies. Such work is not only relevant to the hydrological and water quality modelling communities but also has applications for the broader scientific community in addition to informing policy regarding water resources management.

DynQual is ambitious in its aim to model global surface water quality: 1) using a consistent approach; 2) dynamically; 3) considering multiple water quality constituents; and 4) at a high spatio-temporal (i.e. 5 arc-min and daily timestep) resolution. Any model must consider the trade-offs between model complexity and availability of input datasets and data to parameterise process descriptions of the model (Weaver and Zwiers, 2000; Wen et al., 2017), and the impact of this on model scope. Being a global model, *DynQual* is inherently unable to accurately represent all aspects relevant to the local context. Rather, the modelling strategy is to focus on the main spatial and temporal drivers of pollution in river networks globally to facilitate first-order approximations of in-stream concentrations at high spatial (5 arc-min) and temporal (daily) resolution with global coverage. As such, *DynQual* allows for the investigation of research questions that only large-scale modelling efforts can address. These include, as presented in the model application section, global pollution hot- and bright- spot identification (Figs. 3.6–3.8), the relative importance of different contributing sectors to water quality status across the globe (Fig. 3.9) and meta-trends in surface water quality dynamics (Figs. 3.10–3.11). The dynamic nature of *DynQual* can also facilitate analysis of intra- and inter- annual trends in surface water quality and help to further enhance the understanding of the main drivers of pollution via (dynamic) sectoral attribution (Fig. 3.12). Furthermore, this approach has particular value for simulating surface water quality in ungauged catchments, and our use of globally consistent input data facilitates meaningful comparisons across different world regions. Given severe limitations in observational records of surface water quality, both in terms of spatial coverage and the number of observations per water quality monitoring station (Appendix A.3.1), these are key strengths of *DynQual*. However, poor data availability is a severe limitation for both the development of global water quality models and their evaluation.

Uncertainties in surface water quality simulations arise from a combination of uncertainties associated with quantifications of pollutant loadings (e.g. pollutant excretion, emission rates and sector-specific return flows), the quality of hydrological simulations (e.g. discharge and velocities) and the representation of in-stream processes (e.g. decay coefficients). These uncertainties are especially prevalent when modelling at large spatial extents. In-stream pollutant concentrations are sensitive to dilution capacity and thus the quality of the hydrological simulations. This issue contributes to uncertainties in simulated concentrations particularly in headwater streams. Fixed estimates of decay coefficients are assumed, which contributes to uncertainties in simulations of reactive constituents such as BOD and FC. In addition, the representation of lakes and reservoirs in *DynQual* is rudimentary, with total (routed) loadings instantaneously averaged over the volume of the waterbody assuming full mixing.

With respect to pollutant loading quantifications, spatial mismatches between the generation of pollutant loadings and the location of entry to the stream network (return flows) can result in the simulation of unrealistic concentrations, particularly in gridcells with very low water availability (i.e. headwater streams). This can occur where the drivers of point source pollutant emissions (e.g. population) do not directly coincide with the location of wastewater treatment plant outlets. A lack of temporally-explicit input data can hinder proper representation of sectors with strong intra- or inter-annual variability. For instance, notable limitations for the livestock sector are the simplified assumptions made for livestock population numbers (assumed to be constant across days of the year), changes to livestock numbers across multi-year periods (applied annually and based on regional averages) and transportation pathways to the stream network (assumed to be a function of surface runoff excluding the representation of processes that affect pollutant retention in soils). Locally relevant sources of pollution may also be entirely excluded, such as the lack of information on TDS emissions from mining activities and road de-icing. Similarly, pulses of pollutant loadings occurring during extreme rainfall of flood events are also overlooked, such as those associated with sewer overflows or from inundated industrial areas.

Despite these uncertainties, *DynQual* has been demonstrated to perform with a reasonable level of performance, especially given the approximations of the model. Water temperature simulations closely match observations at daily resolution as indicated by KGE coefficients (Fig. 3.4a), which are high across all world regions (Fig. A.3). Furthermore, time-series and average annual plots (Fig. 3.5a; Fig. A.5) demonstrate that seasonal regimes present in observed water temperatures are well captured by the model. Simulated TDS, BOD and FC concentrations are largely within the correct concentration classes (Fig. 3.3) with nRMSE coefficients (Fig. 3.4b-d) deemed reasonable considering the challenges of comparing individual (instantaneous) observed daily TDS, BOD and FC concentrations against simulated daily concentrations. Long-term time-series and average annual cycle plots for TDS (Fig. 3.5b; Fig. A.6), BOD (Fig. 3.5c; Fig. A.7) and FC (Fig. 3.5d; Fig. A.8) show that *DynQual* can generally simulate in-stream concentrations within the correct range (e.g. min–max daily concentrations, 10^{th} and 90^{th} percentile average annual cycles), but simulations of in-stream concentrations timeseries on a daily timestep show relatively poor agreement with the observed timeseries. Observed data records also tend to display large variability in concentrations but little (systematic) seasonality, especially for BOD (Fig. A.7) and FC (Fig. A.8) concentrations. These factors have a strong influence on metrics including nRMSE but especially the other commonly used evaluation metrics in hydrology such as the Nash–Sutcliffe efficiency (NSE) and Kling–Gupta efficiency (KGE), and hence support our decision not to evaluate model performance using these metrics. Challenges related to the observational records themselves should also be acknowledged. These can relate to, for example, artefacts in observational records (Fig. A.9a), issues related to instrument detection limits and/or reporting accuracies (Fig. A.9b) and large variability in the observation records (Fig. A.9c). Lastly, given the approximations of the model, the overall complexity in the drivers of pollutant loadings and input data limitations, we reiterate that the current set-up of

DynQual is not suited to simulate daily TDS, BOD and FC concentrations that correspond exactly with in situ observational measurements.

With few comparable studies in the current literature, it is difficult to quantitatively assess the performance of *DynQual* relative to other large-scale surface water quality models. Overall, our modelled spatial patterns in surface water quality match well with previous regional and global assessments – showing multi-pollutant hotspots (e.g. TDS, BOD, FC) to be located across northern India and eastern China in particular (UNEP, 2016; Wen et al., 2017; van Vliet et al., 2021). Consistent with a recent data-driven (machine learning) approach (Desbureaux et al., 2022), albeit for some different water quality constituents (e.g. total phosphorus), we find a general trend towards surface water quality improvement in developed countries and deterioration in developing countries. Water temperature (Tw) simulations closely match those of the global water temperature models upon which *DynQual* is based (van Vliet et al., 2012a; Wanders et al., 2019; van Vliet et al., 2021). For total dissolved solids (TDS) and biological oxygen demand (BOD) concentrations, values of and patterns in nRMSE are similar to previous work (van Vliet et al., 2021), with reasonable model performance (<1 nRMSE) exhibited at monitoring locations across all continents. Other large-scale surface water quality models have validated simulated concentrations with respect to concentration classes linked to sectoral water use and environmental health limits. Following this approach, Wen et al. (2017) reported BOD concentrations simulated within the same classification in 94% of instances; however this is based on only 760 measurements of which 91% are modelled in the lowest pollutant class (0–5 mg l^{-1}). More comparable to our simulations, UNEP (2016) compared modelled and observed pollutant classes for TDS, BOD and fecal coliform (FC) concentrations across Latin America, Africa and Asia, achieving largely comparable model performance. Comparing our simulations to output from other global water quality models modelling Tw, BOD, TDS and FC, when available, will provide further insights into model performance.

Meaningful comparisons to other surface water quality models are challenging due to the high diversity in terms of: 1) spatial extent (e.g. lumped vs. distributed); 2) temporal resolution (e.g. daily vs. monthly vs. annual vs. decadal); and 3) water quality constituent and reporting form (e.g. loads vs. concentrations). Similarly, watershed-scale surface water quality models are constructed for different purposes than large-scale (continental to global) surface water quality models. These watershed models can better incorporate locally relevant input data and processes, are parameterized for local conditions and typically have data of good quality and record length for calibration and validation – which facilitates higher precision and accuracy in both hydrological and water quality simulations. However, these models are reliant upon detailed local knowledge which is severely lacking for many (particularly ungauged) catchments worldwide (e.g. large parts of Africa).

Despite their limitations, process-based large-scale water quality models can facilitate first-order assessments of global water quality dynamics that are consistent across both space and time, such as those demonstrated in the model application section of this study. Future applications of *DynQual* may include: 1) expanding the number of modelled water quality constituents; 2) further spatio-temporal analysis of surface water quality; and 3) investigating the impact of uncertain climatic and socioeconomic change on future surface water quality.

Code and data availability

DynQual v1.0 is open source and distributed under the terms of the GNU General Public License version 3, or any later version, as published by the Free Software Foundation. The full model code, configuration INI files and a user manual are provided through a GitHub repository: https://githubv.com/UU-Hydro/DYNQUAL. The model code presented in this paper is archived at https://doi.org/10.5281/zenodo.7398410.

A full set-up with all required input datasets for running *DynQual* for the Rhine–Meuse basin is provided as an example (https://doi.org/10.5281/zenodo.7027242). Monthly water temperature (Tw) and salinity (TDS), organic (BOD) and pathogen (FC) concentrations are available directly via https://doi.org/10.5281/zenodo.7139222. Here, we also provide the output hydrological data (discharge and channel storage) simulated within the model run.

Acknowledgements

MTHvV was financially supported by a VIDI grant (project no. VI.Vidi.193.019) of the Netherlands Scientific Organisation (NWO). NW acknowledges funding from the NWO (project no. 016.Veni.181.049). We acknowledge the NWO for the grant that enabled us to use the national supercomputer Snellius (EINF. 3999).

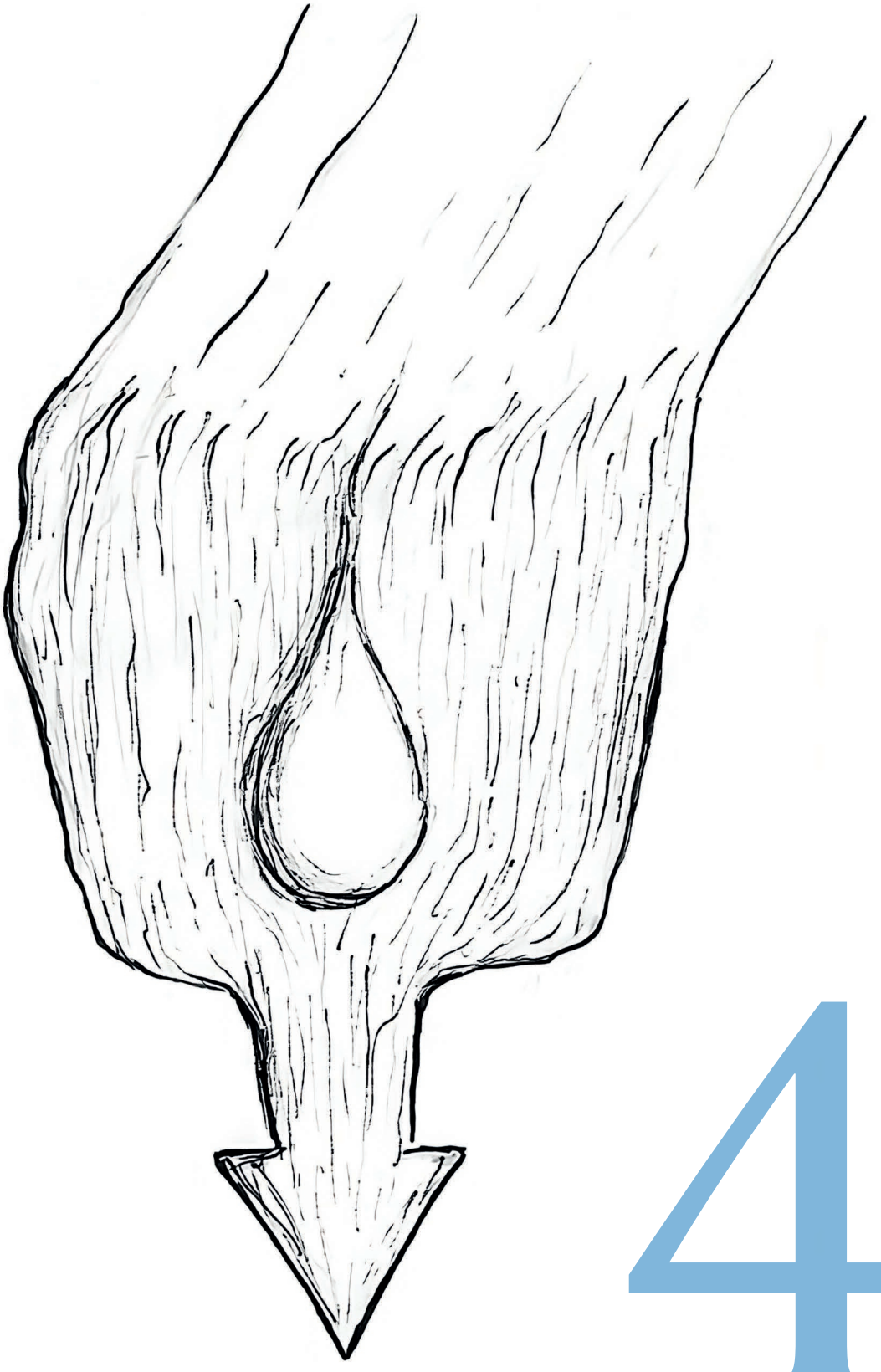

4

Chapter 4 | Current wastewater treatment targets are insufficient to protect surface water quality

Abstract

The quality of global water resources is increasingly strained by socioeconomic developments and climate change, threatening both human livelihoods and ecosystem health. With inadequately managed wastewater being a key driver of deterioration, Sustainable Development Goal (SDG) 6.3 was established to halve the proportion of untreated wastewater discharged to the environment by 2030. Yet, the impact of achieving SDG 6.3 on global ambient water quality is unknown. Addressing this knowledge gap, we develop a high-resolution surface water quality model for salinity as indicated by total dissolved solids (TDS), organic pollution as indicated by biological oxygen demand (BOD) and pathogen pollution as indicated by fecal coliform (FC). Our model includes a novel spatially-explicit approach to incorporate wastewater treatment practices, a key determinant of in-stream pollution. We show that achieving SDG 6.3 reduces water pollution, but is still insufficient to improve ambient water quality to below key concentration thresholds in several world regions. Particularly in the developing world, reductions in pollutant loadings are locally effective but transmission of pollution from upstream areas still leads to water quality issues downstream. Our results highlight the need to go beyond the SDG-target for wastewater treatment in order to achieve the overarching goal of clean water for all.

Published: Jones, E.R., Bierkens, M.F.P., Wanders, N., Sutanudjaja, E.H., van Beek, L.P.H. & van Vliet, M.T.H. (2022) Current wastewater treatment targets are insufficient to protect surface water quality. *Communications Earth & Environment, 3(1)*, pp. 1–8, DOI: 10.1038/s43247-022-00554-y

4.1 Introduction

Compared to water availability (e.g. river discharge), few observations and large-scale modelling assessments exist for understanding global surface water quality (Alcamo et al., 2010). Inadequate water quality for different sectoral purposes poses a variety of constraints across the water-food-energy-ecosystem nexus (Heal et al., 2021): organic and pathogen pollution causes risks to human health (Ashbolt, 2004), increased salinity levels threaten agricultural productivity (Rietz and Haynes, 2003) and increased water temperatures can disrupt thermoelectric power plants that depend on surface water resources for cooling (van Vliet et al., 2012b; van Vliet et al., 2016). Moreover, all these pollutants can adversely affect the aquatic environment (Englert et al., 2013). Improving our ability to accurately simulate in-stream pollutant concentrations is therefore key to improved understanding of the threats to global clean water resources and to devise management options that safeguard clean water for all (UNEP, 2016; van Vliet et al., 2021).

Sectoral activities artificially increase surface water pollutant concentrations by discharging polluted water back to the environment, particularly in regions with limited wastewater treatment (UNEP, 2016; Wen et al., 2017; van Vliet et al., 2021). The existence of and degree to which treatment practices reduce contaminant levels (Jones et al., 2021) and the proportion of (treated) wastewater relative to streamflow (Macedo et al., 2022) are crucial determinants of the quality of receiving waters (Mateo-Sagasta et al., 2015; Jones et al., 2021). The importance of wastewater management practices is recognised in Sustainable Development Goal (SDG) target 6.3 (UN, 2015), which sets the target of halving the proportion of untreated wastewater released to the environment by 2030. With inadequately managed wastewater being the key driver of water pollution, this target represents the principal action for achieving the overarching goal of improved ambient water quality. Yet, no study has quantitatively assessed the effectiveness of achieving SDG 6.3 on global ambient water quality.

Here we develop a high-resolution surface water quality model (henceforth *DynQual*) that is essential for addressing this knowledge gap. *DynQual* simulates surface water temperature (Tw), salinity as indicated by total dissolved solids (TDS), organic pollution as indicated by biological oxygen demand (BOD) and pathogen pollution as indicated by fecal coliform (FC) concentrations (Fig. B.1). The model is unique in that it operates at an unprecedented spatial resolution of 5x5 arc-min (~10km at the equator) and simulates water quality dynamically at daily temporal resolution globally. Water temperature (Tw) is simulated using a heat-advection approach (van Beek et al., 2012; Wanders et al., 2019) with thermoelectric powerplant effluents added as an additional point source of advected heat (Fig. B.2). Pollutant loadings of TDS, BOD and FC are calculated per sector following previous approaches (UNEP, 2016; van Vliet et al., 2021) (Appendix B.1). The high spatial resolution of our model allows for meaningful inclusion of a novel spatially-explicit wastewater treatment dataset (Jones et al., 2021), further disaggregated by treatment level (Appendix B.4, Fig. B.12), that is more representative of the real-world situation compared to existing approaches. Pollutant loadings are subsequently routed through the global stream network to calculate in-stream concentrations at the daily timestep. The model accounts for both the dilution capacity of the rivers and natural degradation processes (see Materials & Methods and Appendix B.2).

4.2 Results

4.2.1 Global surface water quality

Modelled water temperature (Tw) and in-stream concentrations of TDS, BOD and FC show overall good agreement with the observed data (Appendix B.3). Global patterns in salinity, organic and pathogen pollution at the high spatial resolution (Fig. 4.1) are consistent with previous work (UNEP, 2016; van Vliet et al., 2021). While TDS concentrations are strongly influenced by geological factors, hotspots of high salinity pollution (> 2,100 mg l^{-1} TDS) correspond to heavily industrialised regions,

such as northeastern China and the contiguous United States, and to heavily irrigated regions such as northern India (Fig. 4.1a; Fig. B.3; Fig. B.6). Exceedance of the salinity threshold in these regions tends to occur for more than half the year (>6 months) and occasionally year-round. More localised salinity pollution is also common in the tributaries to some major European rivers, before dissipating due to the increased dilution capacity of the main stream. Exceedance of the salinity threshold between 1–3 months per year occur in the Mediterranean and across large swathes of Africa. Exceedance of salinity thresholds are relatively low across Latin America, although some seasonal exceedances do occur in the more populated and industrialised regions.

Global patterns in the exceedance of BOD (8 mg l^{-1}) and FC (1,000 cfu $100ml^{-1}$) thresholds follow similar patterns, attributed to the pollutant loadings originating from similar sectoral sources (Fig. 4.1b-c; Figs. B.4–B.6). However, both the frequency and magnitude of FC threshold exceedances are larger than for TDS and BOD. Modelled FC concentrations can occasionally exceed 10,000 cfu $100ml^{-1}$, with the most polluted river stretches having FC concentrations surpassing 1 million cfu $100ml^{-1}$. Exceedances of BOD and FC thresholds are typically very low in sparsely populated locations, such as in northern high-latitudes and wet-tropical rainforests. In most other world regions, exceedance of organic and pathogen pollution thresholds are commonplace for at least some part of the year. Across east and southern Asia, in-stream concentrations of BOD and FC that exceed quality thresholds are occurring both frequently and across many streams irrespective of river discharge (i.e. dilution capacity). Year-round exceedances of thresholds, especially for FC, are very high across China. Frequent exceedances are also widespread across Africa, such as in the tributaries of the Nile and the Niger, with typically more seasonal exceedances in the main channels of these rivers. BOD and FC thresholds are also exceeded across many parts of Western Europe, Japan and the Eastern Seaboard of the USA, despite wastewater treatment rates already being high. However, exceedances in these regions tend to be more seasonal and do not typically occur in rivers with large year-round discharges. Statistics aggregated by geographical region are displayed in Fig. B.7.

Fig. 4.1d displays the incidences of threshold exceedance in any month of the year aggregated across multiple water quality constituents. Thus, a value of 2 denotes that 2 out of 3 of the water quality constituent thresholds are jointly exceeded in at least one month, with monthly concentrations averaged over 2006–2015. In line with the analysis of individual water quality constituents, no exceedances in any of the water quality thresholds considered are found for large portions of the high-latitude and wet tropical regions. Conversely, in most other populated regions, one or more water quality thresholds are exceeded in at least one month per year. Simultaneous exceedances of all three water quality constituents (i.e. TDS, BOD, FC) mostly occur where large seasonal variations in river discharge (e.g. Africa, India) exist. High TDS loadings can be mostly attributed to either large-scale irrigation systems (e.g. northern India) or manufacturing activities (e.g. eastern China). Exceedances in BOD and FC concentrations are commonplace both where wastewater treatment rates are low (e.g. East Asia and Pacific, Southern Asia) and high (e.g. Western Europe, North America). This demonstrates the importance of dilution (i.e. river discharge) in determining in-stream concentrations. Incidences where only one water quality constituent shows exceeded concentrations are mostly attributed to FC, and mostly during low-flow seasons.

4.2.2 Halving the proportion of untreated wastewater (SDG 6.3)

Expansions in wastewater treatment capacities to achieve SDG 6.3 are designated at the country-level and delineated to gridcells based upon where pollutant loadings are highest (Appendix B.5, Figs. B.14–B.15). Fig. 4.2a displays the top 30 countries with the largest required expansions in wastewater treatment. Together, these 30 countries account for ~87% of the total required expansions to achieve SDG 6.3. The largest expansions required before 2030 are in China (40 billion m^3 yr^{-1}), the USA (16 billion m^3 yr^{-1}) and India (15 billion m^3 yr^{-1}), with these three countries alone accounting for ~45% of the required expansions. Expansions are required across many regions in the

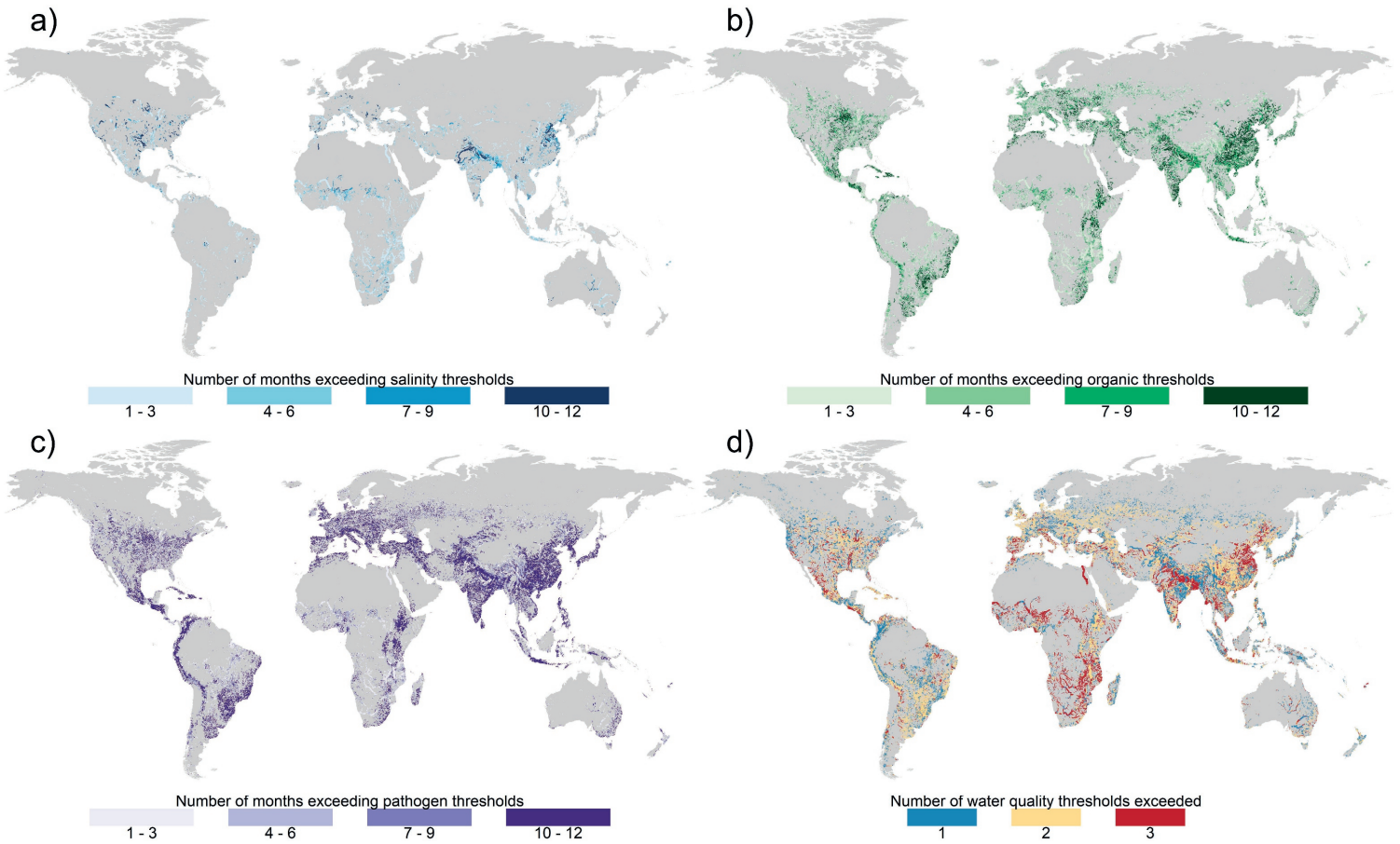

Figure 4.1 Number of months per year exceeding key water quality thresholds for a) total dissolved solids (TDS) (2,100 mg l^{-1}); b) biological oxygen demand (BOD) (8 mg l^{-1}); and c) fecal coliform (FC) (1,000 cfu 100ml^{-1}), averaged over 2006–2015. d) the combined number of water quality thresholds (i.e. TDS, BOD and FC) exceeded in any month of the year, averaged over 2006–2015. Only streams with an average annual discharge >1 m^3 s^{-1} are displayed.

populated areas of North America and Europe, particularly where (a proportion of) the collected wastewater is still released to the environment without treatment. Conversely, in world regions with little or no wastewater treatment in 2015, the expansions required to achieve SDG 6.3 are fulfilled by establishing wastewater treatment in only a few, densely populated locations. While high percentage reductions in pollutant loadings are achieved in these specific locations, achieving SDG 6.3 in these regions has a more limited impact on pollutant loadings across geographical space (Fig. B.16).

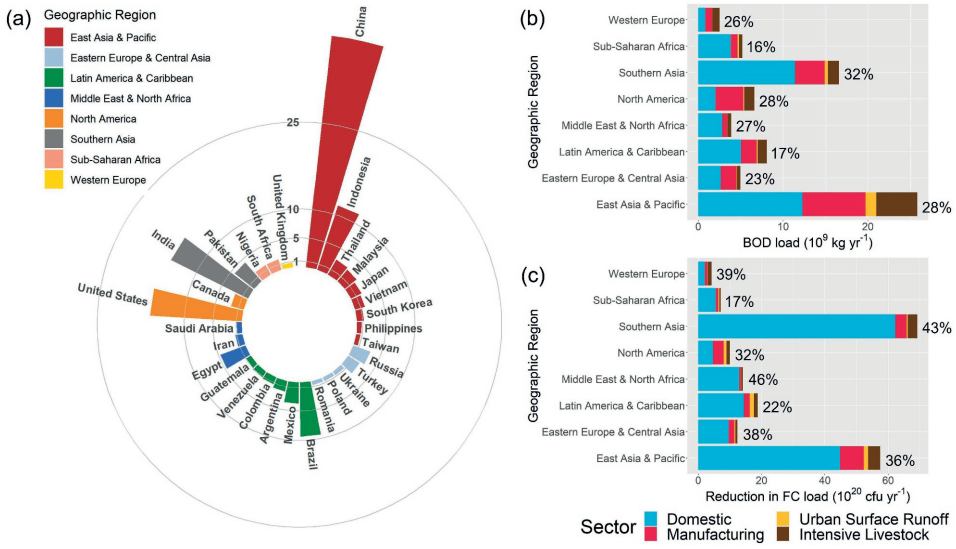

Figure 4.2 a) Expansions in annual wastewater treatment capacity (10^9 m^3 yr^{-1}) required by 2030 to achieve SDG 6.3 for the top 30 countries; and the associated absolute and percentage reductions in b) biological oxygen demand (BOD) and c) fecal coliform (FC) pollutant loadings per sector, aggregated by geographical region

As we assume that secondary wastewater treatment practices do not influence TDS loadings (van Vliet et al., 2021), the expansions in wastewater treatment influence BOD and FC loadings and concentrations only. This assumption also means that reductions in gridded pollutant loadings are capped at 85% and 97.5%, which are the assumed pollutant removal efficiencies for secondary wastewater treatment for BOD and FC, respectively (Table B.4). Fig. 4.2b and Fig. 4.2c display the region-aggregated reductions in BOD and FC pollutant loadings relative to loadings without expansions in wastewater treatment. Strong (absolute) reductions are achieved in the East Asia and Pacific and Southern Asia regions. Reductions in total BOD loadings range from 16% to 32% across the different regions; and reductions in total FC loadings from 17% to 43%. While increases in wastewater treatment capacities reduce point source pollution locally, the benefits to surface water quality also propagate downstream. The average annual reductions in BOD and FC concentrations when achieving SDG 6.3 are displayed in Fig. 4.3a and Fig. 4.3b, respectively (see Fig. B.17 and Fig. B.18 for zoom-in panels).

While Fig. 4.3a and Fig. 4.3b are very similar, variations between BOD and FC reductions occur due to: 1) the different removal efficiencies associated with secondary wastewater treatment; 2) the differences in proportion of loadings originating from sectors influenced by wastewater treatment; and 3) interplay with the decay processes. Reductions in BOD and FC concentrations are particularly large in northern India, eastern China and the Eastern Seaboard of the USA, corresponding to the countries requiring the largest volumetric expansions in wastewater treatment (Fig. 4.2a). SDG 6.3 expansions led to very high localised reductions in BOD and FC concentrations, which also translate

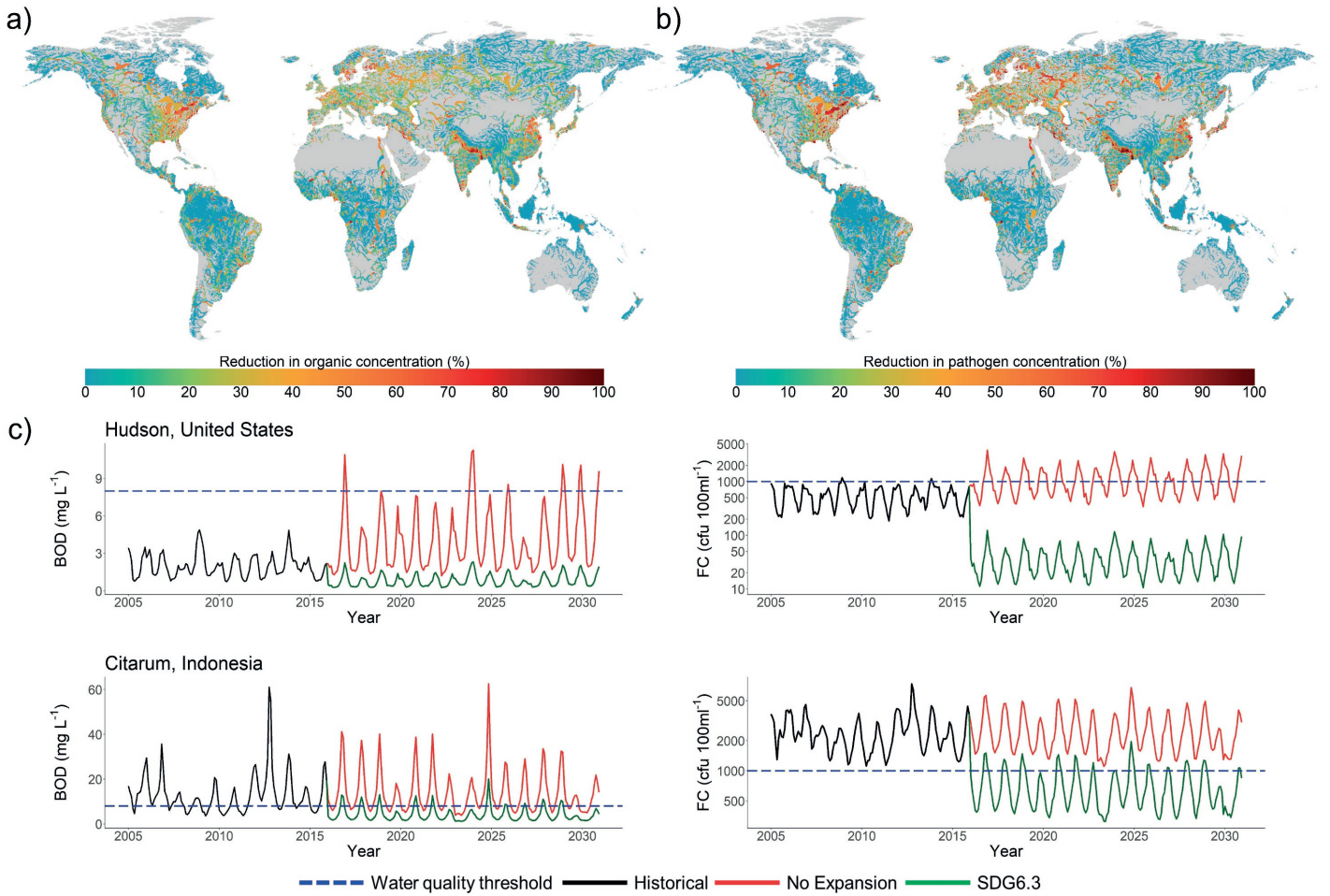

Figure 4.3 Average annual percentage reductions in a) organic pollution as indicated by biological oxygen demand (BOD) concentrations; and b) pathogen pollution as indicated by fecal coliform (FC) concentrations, assuming no expansions in wastewater treatment vs. achieving SDG 6.3. Percentage reductions displayed in a) and b) are averaged over multiple general circulation models (GCMs) for the time period 2021–2030 and are only displayed for streams with an average annual discharge >10 $m^3 s^{-1}$. More detailed maps displaying percentage reductions in BOD and FC concentrations in key world regions are available Fig. B.17 and Fig. B.18, respectively. Panel c) displays in-stream BOD (left) and FC (right) concentrations under historical, no expansion and SDG 6.3 conditions. Additional time-series plots across more world regions are displayed in Fig. B.19.

into substantial improvements in the river water quality of the regions' major rivers e.g. Mississippi (USA), Ganges (India) and Yellow (China). Improvements in water quality associated with SDG 6.3 can be seen in most streams across Europe, with reductions of ∼40% for BOD and ∼50% for FC concentrations are achieved in the major rivers. The fact that such substantial reductions are achieved in both the tributaries and main channels of European river networks is attributed to the fact that the required increases in wastewater treatment capacities for SDG 6.3 are widespread in space, following the extensive treatment capacity currently in place.

Conversely, in regions where SDG 6.3 can be achieved by expanding wastewater treatment capacities at a small number of locations – particularly Africa – reductions in BOD and FC concentrations are less ubiquitous. Here, the concentrations in a greater proportion of stream segments are unaffected by achieving SDG 6.3. Nevertheless, the benefit of achieving SDG 6.3 on BOD and FC concentrations can still be seen in both localised stream segments (where expansions are occurring) and also for major rivers, such as the lower Nile and parts of the Niger. In countries with highly concentrated populations, such as Australia, SDG 6.3 expansions in wastewater treatment are also confined to a small number of locations. Therefore, very high localised reductions in BOD and FC concentrations are achieved, but only in the major urban settlements.

Time-series of in-stream concentrations at selected locations (Fig. 4.3c; Fig. B.19) show that SDG 6.3 can drastically reduce in-stream concentrations and reduce the frequency and magnitude of water quality threshold exceedance. For example, BOD concentrations in the Citarum River, Indonesia can be reduced to below the 8 mg l^{-1} threshold in almost all months of the year under SDG 6.3, whereas year-round exceedance is commonplace under current wastewater treatment levels. Similarly, without expansions in wastewater treatment, FC concentrations in the Hudson River, USA begin to frequently exceed the 1,000 cfu 100ml^{-1} threshold (typically 4–6 months per year), whereas these exceedances are entirely prevented under SDG 6.3. Such exceedances of water quality thresholds are important as they may result in the surface water being unsuitable for sectoral uses, or threaten environmental health.

The percentage reductions in BOD (Fig. 4.3a; Fig. B.17) and FC (Fig. 4.3b; Fig. B.18) also translate into changes in the frequency and magnitude of water quality threshold exceedances. We demonstrate these changes with respect to the percentage of surface water abstractions that exceed quality thresholds under historical, no expansion and SDG 6.3 conditions (Fig. 4.4; Figs. B.20–B.21). With no reductions in TDS loadings assumed with secondary wastewater treatment, no variation in TDS exceedances under the two scenarios are found. Furthermore, only small changes are found in these scenarios relative to the historical conditions.

In terms of BOD and FC threshold exceedance, reductions in the proportion of surface water extractions exceeding quality thresholds are highest in developed regions of North America, Western Europe and Eastern Europe and Central Asia. In these regions, expansions in wastewater treatment for SDG 6.3 are widespread in space, achieved through a combination of expanding wastewater treatment in gridcells where wastewater collection is already present ('collected, untreated', Fig. B.13) and establishing wastewater treatment facilities in new locations. Furthermore, in-stream concentrations of BOD and FC are typically lower in these regions attributed to the wastewater collection and treatment infrastructure that is already established. Thus, SDG 6.3 expansions in wastewater treatment are more frequently sufficient for achieving reductions beneath quality thresholds. Conversely, in world regions with more limited existing wastewater treatment (e.g. Sub-Saharan Africa), achieving SDG 6.3 leads to relatively fewer changes in threshold exceedances. While wastewater treatment expansions in these regions causes substantial reductions in localised pollutant loadings, these are often insufficient to reduce in-stream concentrations to levels beneath quality thresholds. This primarily occurs due to the propagation of pollution originating in upstream areas where expansions in wastewater treatment are not allocated.

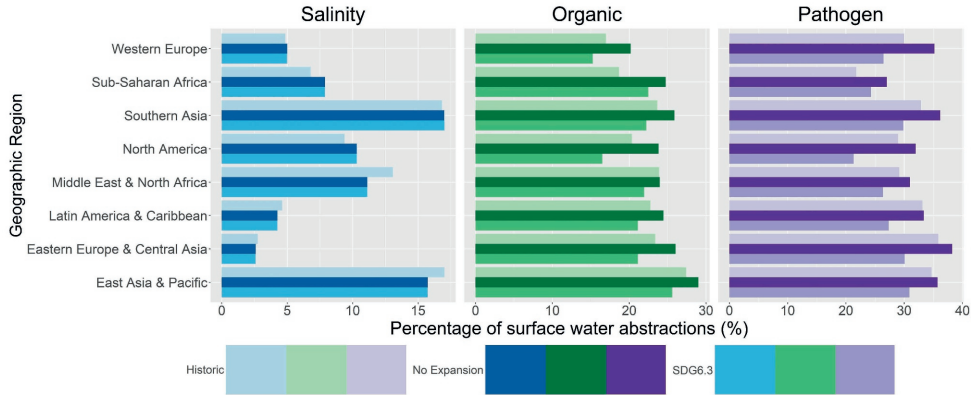

Figure 4.4 Percentage of surface water abstractions exceeding critical water quality thresholds for salinity pollution as indicated by total dissolved solids (TDS) concentrations (2,100 mg l^{-1}), organic pollution as indicated by biological oxygen demand (BOD) concentrations (8 mg l^{-1}) and pathogen pollution as indicated by fecal coliform (FC) concentrations (1,000 cfu 100ml^{-1}) under historical and near-future (no expansions and SDG 6.3) conditions. Water quality threshold exceedance and surface water abstractions are assessed at monthly temporal resolution, and subsequently aggregated per geographic region across all months. Results are averaged across multiple general circulation models (GCMs) using 2005–2014 as the historical and 2021–2030 as the future time period.

4.3 Conclusions

Our findings show that substantial reductions in organic and pathogen pollution, as indicated by BOD and FC concentrations in surface waters, are achieved under SDG 6.3. The achieved water quality improvements, to differing extents across regions, reduce the frequency and magnitude of water quality threshold exceedances for sectoral uses and aquatic ecosystem health (Fig. 4.4; Fig. B.20). Reductions in threshold exceedances are typically largest where wastewater treatment rates are already high, such as North America and Western Europe. Conversely, in world regions with limited existing wastewater treatment, the impact of achieving SDG 6.3 on threshold exceedance is more modest. This occurs due to SDG 6.3 being met by expanding wastewater treatment in a relatively limited number of locations. Furthermore, volumes of untreated wastewater (and the associated pollutant loadings) can still be very large under SDG 6.3 – in a country without any existing wastewater treatment facilities, 50% of the total produced wastewater is still released to the environment untreated. With propagation of pollution from upstream areas still resulting in widespread exceedances of key water quality thresholds, the suitability of SDG 6.3 as a global sustainability target for improving ambient water quality must be considered. Based on our study, it can be concluded that SDG 6.3 can substantially improve ambient water quality worldwide, but that in many world regions improvements are still insufficient to meet water quality requirements for human use and aquatic ecosystem health.

As we enter the 'Decade of Action (2021–2030)' for achieving the Sustainable Development Agenda, now is the time to renew global efforts to go above and beyond the wastewater treatment target stipulated by SDG 6.3. While achieving the required expansions in wastewater treatment will poses serious economic challenges, extracting the economic value inherent within wastewater flows (e.g. water, nutrients and energy recovery) can provide funding opportunities compatible with a circular economy. Yet, our results also demonstrate that in addition to expanding and improving our 'hard infrastructure' (i.e. sewer networks and wastewater treatment facilities), a strong focus on reducing pollutant emissions at source will also be required to achieve the overarching goal of SDG6 – clean water and sanitation for all.

4.4 Materials and methods

4.4.1 Wastewater treatment and pollutant loadings

Pollutant loadings are considered from six distinct sources, namely from the domestic, manufacturing, irrigation, livestock and thermoelectric power sectors, and from urban surface runoff (Fig. B.1). Pollutant loadings of water temperature (Tw), total dissolved solids (TDS), biochemical oxygen demand (BOD) and fecal coliform (FC) are calculated at a gridcell resolution of 5x5 arc-min (∼10km at the equator) with a monthly timestep. Socioeconomic and hydroclimatic data are used as basis from 1980–2015 (historical), with data for 2016–2030 based on future projections associated with RCP7.0 and SSP3 (Lange and Buchner, 2021). This combination represents an intermediate-high emissions and development scenario, characterised by regional rivalry (Fujimori et al., 2017). Loadings from the domestic and livestock sectors are estimated by multiplying the gridded population (Jones and O'Neill, 2016) with a pollutant-specific per capita excretion rate (UNEP, 2016; van Vliet et al., 2021). Conversely, loadings from the manufacturing and irrigation sectors, and from urban surface runoff, are estimated by multiplying a return flow volume, simulated with the global hydrology and water resources model *PCR-GLOBWB2* (Sutanudjaja et al., 2018), with a pollutant-specific mean effluent concentration (UNEP, 2016; van Vliet et al., 2021). Heat dumps from the power sector are estimated by multiplying the associated return flows with an estimated difference in water temperature between the return flows and the receiving waters (van Vliet et al., 2012b; van Vliet et al., 2021). More information on the datasets used and methodology for calculating pollutant loadings per sector are presented in Appendix B.1 (Figs. B.2–B.6).

Sector-specific pollutant loadings can be abated based upon their transmission paths to receiving waters (Appendix B.4, Fig. B.1). Pollutant loadings from the domestic and manufacturing sectors, and from urban surface runoff, can be heavily influenced by wastewater management plants where wastewater collection (e.g. in sewers) and subsequent treatment (e.g. in sewage treatment works) practices are occurring (Fig. B.11). The specific path via which municipal wastewater is disposed, including the treatment level (i.e. removal efficiency) of collected wastewater, is therefore key to determining the resultant pollutant loadings. Previous global water quality studies have used country-level data to represent this process (van Vliet et al., 2012b; van Vliet et al., 2021). Here, we use a newly developed global wastewater collection and treatment dataset (Jones et al., 2021), further disaggregated by treatment level (primary, secondary, tertiary+), to delineate these wastewater pathways at 5 arc-min (Figs. B.12–B.13). This is a substantially higher spatial resolution than previously captured. For detailed information on the spatially-explicit wastewater dataset, we refer to the original publication (Jones et al., 2021).

4.4.2 Surface water quality modelling (*DynQual*)

A new surface water quality model, named *DynQual*, has been developed in this study to simulate surface water temperature (Tw), water salinity as indicated by total dissolved solids (TDS), organic pollution as indicated by biological oxygen demand (BOD) and pathogen pollution as indicated by fecal coliform (FC) concentrations at a spatial resolution of 5x5 arc-min and daily temporal resolution globally. These water quality constituents are selected because they are key in constraining different sector water uses and ecosystem health (Dumont et al., 2012; Damania et al., 2019). *DynQual* has been developed in a flexible way to allow for the addition of more water quality constituents, which could include nutrients, dissolved oxygen and emerging contaminants.

DynQual builds on recent water quality model developments (UNEP, 2016; Wen et al., 2017; van Vliet et al., 2019; van Vliet et al., 2021) and the water temperature modelling framework *DynWat* (van Beek et al., 2012; Wanders et al., 2019). *DynWat* solves the surface water energy balance at the daily timestep, while also accounting for surface water abstractions, reservoirs, riverine flooding and the formation of ice, giving Tw at a spatial resolution of 5x5 arc-min (Wanders et al., 2019). We further

include advected flow from heat effluents of thermoelectric powerplants, following previous work (van Vliet et al., 2012a; van Vliet et al., 2021). Daily surface water concentrations of TDS (mg l^{-1}), BOD (mg l^{-1}) and FC (cfu $100ml^{-1}$) are simulated by using a mass balance approach, combining the sectoral pollutant loadings routed over the stream network with the dilution capacity of the receiving stream. We assume instantaneous and full mixing of all pollutant loadings in each gridcell. TDS is simulated using a conservative substances approach, whereas BOD and FC are simulated using a non-conservative substances approach with first-order decay during downstream water transport (Reder et al., 2015; UNEP, 2016; van Vliet et al., 2021). The decay coefficient for FC is a function of water temperature, solar radiation and the settling rate of bacteria (sedimentation) (Reder et al., 2015; UNEP, 2016), whereas the decay coefficient for BOD is water-temperature dependent only (Wen et al., 2017; van Vliet et al., 2021). Hydrology (e.g. surface runoff, interflow, baseflow, channel storage) and surface water abstractions are simulated by the global hydrology and water resources model *PCR-GLOBWB2*, for which we refer to the original publication (Sutanudjaja et al., 2018). More information on the surface water quality modelling approach is presented in Appendix B.2.

In this study, *DynQual* is run for a historical time period of 1980–2015 using W5E5 forcing data (Cucchi et al., 2020; Lange et al., 2021) (Appendix B.2). *DynQual* is uncalibrated to facilitate application in ungauged basins (e.g. parts of Africa with limited water quality monitoring availability) without loss of performance (Wanders et al., 2019). In-stream concentrations for the historical time period are validated against in situ surface water quality monitoring data from the Global Environment Monitoring System (GEMS) (UNEP, 2019) (Table B.1). Overall, modelled Tw and in-stream concentrations of TDS, BOD and FC show good agreement with the observed data, as indicated by calculated Kling Gupta Efficiency coefficients. In accordance with the focus of our study – the exceedance of key water quality thresholds under past and near-future conditions – we also present our validation results with respect to pollutant classes (UNEP, 2016). More information on the validation of the water quality model from 1980–2015 is presented in Appendix B.3 (Figs. B.8–B.10).

Future projections of water quantity, surface water temperature and pollutant (i.e. TDS, BOD and FC) concentrations are made up to 2030, including the impact of climate change following the representative concentration pathway RCP 7.0 (Lange and Buchner, 2021). We use bias-corrected CMIP6 forcing data from 5 GCMs (Lange et al., 2021) for the time period 2006–2030. Future pollutant loadings are simulated following the shared socioeconomic pathway SSP3 (Jones and O'Neill, 2016; Lange and Buchner, 2021) under two different assumptions considering 1) no expansion in wastewater treatment ('*no expansion*'); and 2) expansions to halve the proportion of untreated wastewater globally by 2030 ('*SDG 6.3*'). We compare our water quality simulations under these two assumptions to evaluate the relative impact of halving the proportion of untreated wastewater on global surface water quality. Surface water quality simulations are linked to concentration thresholds relevant for sectoral water use (Table B.2) (UNEP, 2016) to determine the frequency and magnitude of their exceedance. This allows for evaluation of the constraints posed to sectoral water users from a water quality perspective. Future work should also assess pollution status from an ecological perspective, whereby the assimilative capacity of the receiving waters (aside from just the dilution component) is a key additional consideration.

4.4.3 Halving the proportion of untreated wastewater (SDG 6.3)

SDG 6.3 sets the target of halving the proportion of untreated wastewater that is released to the environment and improve ambient water quality by 2030 (UN, 2015). We only consider wastewater undergoing secondary or higher treatment practices in 2015 as adequately treated for SDG 6.3, as a substantial proportion of pollutant loadings are abated only at these treatment levels. We calculate the volumetric expansion required in domestic and manufacturing sectors to achieve SDG 6.3 at the country level using trend analysis, and subsequently delineate these expansions hierarchically to

gridcells with the highest pollutant loadings in 2015. We focus our expansions on gridcells with high pollutant loadings as collection and treatment is assumed to be both more desirable and economically feasible (and hence more likely) where the strongest reductions in pollutant loadings are achieved. Expansions in wastewater treatment are assumed to be at the secondary level. An overarching assumption is that SDG 6.3 is met by all countries by 2030. Given current progress towards this target, particularly against the backdrop of financial challenges of COVID-19 (Kantur and Özcan, 2021), we acknowledge the likelihood of SDG 6.3 achievement to be low. Nevertheless, this assumption allows for quantitative assessment of the suitability of SDG 6.3 for improving ambient water quality. Detailed information and results regarding the spatial expansions in wastewater treatment associated with achieving SDG 6.3 is presented in Appendix B.5 (Figs. B.14–B.15).

Data availability

Data used in this study for water quality simulations is primarily available open-access and is accessible from the original sources: climate forcing (Lange and Buchner, 2021), population (O'Neill et al., 2016), livestock numbers (Gilbert et al., 2018), powerplants (Lohrmann et al., 2019) and wastewater collection and treatment (Jones et al., 2020; Jones et al., 2021). Global water quality output data from 1980 to 2015 at 10km resolution is available at: https://doi.org/10.6084/m9.figshare.20486277, while simulated water quality under the two wastewater treatment scenarios for all 5 GCMs is available at: https://doi.org/10.6084/m9.figshare.20486310. Further information is available in the Appendix B or upon reasonable request.

Code availability

The global hydrological model *PCR-GLOBWB2* (Sutanudjaja et al., 2018), which is used for hydrological simulations, is available at: https://github.com/UU-Hydro/PCR-GLOBWB_model/. The code of the water quality model is available upon request to the corresponding author.

Acknowledgements

We thank the Global Environment Monitoring System for providing observed water quality data for our model validation. MTHvV was financially supported by a VIDI grant (Project No. VI.Vidi.193.019) of the Netherlands Scientific Organisation (NWO). NW acknowledges funding from NWO 016.Veni.181.049. We acknowledge the Netherlands Organisation for Scientific Research (NOW) for the grant that enabled us to use the national supercomputer Snellius.

5

Chapter 5 | Sub-Saharan Africa will increasingly become the dominant hotspot of surface water pollution.

Abstract

Human activities greatly impact surface water quality, while being reliant upon it for water supply. Surface water quality is expected to change in the future as a result of alterations to pollutant loadings, surface water withdrawals and hydrological regimes, driven by both climate change and socioeconomic developments. Here, we use a high-resolution global surface water quality model to project water temperature, and indicators of salinity (total dissolved solids), organic (biological oxygen demand) and pathogen (fecal coliform) pollution until 2100. Results show that while surface water quality, as indicated by these pollutants, will improve in most advanced economies, the outlook for poorer nations is bleak. The proportion of the global population exposed to salinity, organic and pathogen pollution by the end of the century ranges between 17–27%, 20–37% and 22–44%, respectively, with poor surface water quality disproportionately affecting people living in developing countries. Exhibiting the largest increases in both the absolute and relative number of people exposed, irrespective of climate change and socioeconomic development scenario, we conclude that Sub-Saharan Africa will become the new hotspot of surface water pollution globally.

Published: Jones, E.R., Bierkens, M.F.P., van Puijenbroek, P.J.T.M., van Beek, L.P.H., Wanders, N., Sutanudjaja, E.H., and van Vliet, M.T.H. (2023) Sub-Saharan Africa will increasingly become the dominant hotspot of surface water pollution. *Nature Water, 1*, pp. 602–613, DOI: 10.1038/s44221-023-00105-5

5.1 Introduction

Alterations to global water resources are expected in the coming decades as a result of climate change and socioeconomic developments (Arnell, 1999; Haddeland et al., 2014). Global warming is projected to cause fundamental shifts in hydrological regimes worldwide, including altered precipitation and evaporation patterns (Konapala et al., 2020), changes to snowmelt regimes (Kraaijenbrink et al., 2021) and an increase in the frequency and magnitude of hydrological extremes (e.g. droughts, floods) (Trenberth et al., 2014). Simultaneously, population and economic growth are projected to alter water demands for different sectoral uses (e.g. agriculture, domestic, energy), leading to greater water withdrawals and exacerbated competition for global water resources in some world regions (Wada et al., 2016).

In addition to water availability, human activities also greatly impact water quality (Jones et al., 2022; van Vliet et al., 2021). Pollutants originating from different water use sectors are often discharged to surface waters, causing water quality degradation (Jones et al., 2022; Jones et al., 2023; van Vliet et al., 2021). Proper management of pollution from water use sectors, including domestic, manufacturing, livestock and irrigation activities, is crucial for minimising the impact on receiving aquatic ecosystems, but the prevalence of these practices is highly unequal across the globe (Jones et al., 2021; Jones et al., 2022). Changes in future pollutant concentrations are also strongly driven by the dilution capacity of rivers, and thus sensitive to changes in the hydrological regime induced by both climatological changes and increased sectoral water abstractions. Furthermore, projected changes in abiotic conditions (e.g. water temperature, incoming solar radiation) can exert considerable influence over in-stream physical, chemical and biological processes that also determine in-stream pollutant concentrations (Reder et al., 2015; Bosmans et al., 2022).

The impacts of future climate change on hydrological regimes have been assessed extensively (Caretta et al., 2022), predominantly using numerical hydrological models forced with projections of future climatic conditions (e.g. precipitation, air temperature, evapotranspiration) under different 'Representative Concentration Pathways' (RCPs) (Schewe et al., 2014; Bosmans et al., 2022). Future changes to water demands are typically based on quantitative projections of socioeconomic drivers, particularly population, GDP and land use, associated with different development scenarios such as those described by the 'Shared Socioeconomic Pathways' (SSPs) (Wada et al., 2016; O'Neill et al., 2017; Riahi et al., 2017). Water scarcity assessments have typically combined these factors to evaluate spatial and temporal mismatches in water demand and supply (Wada et al., 2014; Döll et al., 2018; Hanasaki et al., 2018).

Conversely, quantitative projections of future water quality are sparse, particularly at the global scale (Caretta et al., 2022). Yet, akin to water availability, future changes in water quality will have direct consequences for both human water uses (van Vliet et al., 2021; Jones et al., 2022) and freshwater ecosystems (van Vliet et al., 2013; Bosmans et al., 2022). This study represents a comprehensive assessment of the impacts of long-term climate and socioeconomic change on future surface water quality globally. We use a new high-resolution global surface water quality model (*DynQual*) (Jones et al., 2022; Jones et al., 2023), which is coupled to a global hydrological and water resources model (*PCR-GLOBWB2*) (Sutanudjaja et al., 2018), to simulate hydrology (e.g. discharge, channel storage, runoff), sectoral water use and return flows, and multiple water quality constituents that are relevant for human uses and ecosystem health (UNEP, 2016; van Vliet et al., 2021; Jones et al., 2022). We focus on water temperature (Tw) and total dissolved solids (TDS), biological oxygen demand (BOD) and fecal coliform (FC) concentrations as indicators of salinity, organic and pathogen pollution, respectively. Global model simulations are made for the time period 2005–2100 with a daily timestep and at 5 arc-min (∼10 km) spatial resolution. We consider multiple RCP-SSP scenarios to explore a range of possible surface water quality futures based on (uncertain) future developments in societal and climatic conditions (O'Neill et al., 2017), and use bias-corrected output from five

general circulation models (GCMs) to account for uncertainties inherent in the climatological projections (Lange and Buchner, 2021). To assess the potential impact of future changes in surface water quality, we link simulated in-stream pollutant concentrations to key water quality thresholds for human uses and environmental health.

5.2 Results

5.2.1 Pollutant loadings

Future loadings of pollutants depend strongly on the rate and direction of change in socioeconomic drivers (e.g. population, prosperity) relative to developments in wastewater management practices, as dictated by the SSPs (Fig. 5.1). In general, pollutant loadings of BOD and FC are projected to reduce in most world regions. Conversely, TDS loadings are projected to increase, except under SSP1-RCP2.6, predominantly due to population increase and the associated rise in irrigation and manufacturing activities. The sharpest and largest reductions in global loadings of all three pollutants (TDS, BOD and FC) are achieved under SSP1-RCP2.6, resulting from a combination of a stable and prosperous world population acting as sustainable consumers (O'Neill et al., 2017), achieved via inclusive and equitable development that respects environmental boundaries. These factors drive substantial reductions in loadings from domestic, manufacturing and intensive livestock activities, with global BOD and FC loadings under SSP1-RCP2.6 reduced by ∼25% by the mid-century, and by more than half by 2100. BOD and FC loadings also substantially decrease under SSP5-RCP8.5, particularly by the end of the century. Rapid growth of the global economy, albeit driven by fossil-fuelled development and resource intensive lifestyles, facilitate widespread development of advanced wastewater treatment practices. Yet, compared to SSP1-RCP2.6, loadings from the livestock sector are especially high under SSP5-RCP8.5 reflecting the high and increasing demand for meat products worldwide. Furthermore, global TDS loadings are highest under SSP5-RCP8.5, predominantly driven by increased manufacturing activities associated with the resource intensive lifestyle of the global population.

While global pollutant loadings under SSP3-RCP7.0 are comparable to historical conditions, strong regional differences exist (Figs. C.1–C.3). Reductions in pollutant loadings achieved in the developed world are offset by increases in developing nations, particularly in Sub-Saharan Africa and Southern Asia. For example, BOD loadings in Sub-Saharan African more than quadruple by the end of the century (Fig. C.2), predominantly due to rapid population growth massively outstripping the development of wastewater treatment infrastructure. Under SSP3-RCP7.0, the percentage of global BOD loadings originating in Sub-Saharan Africa increases from <10% historically to >25% by the end of the 21st century. Strong regional differences also exist under SSP1-RCP2.6 and SSP5-RCP8.5. In regions where wastewater treatment rates are already high, such as North America and Western Europe, pollutant loadings are consistently highest under SSP5-RCP8.5. Conversely, in countries with low wastewater treatment rates, slower population growth combined with the development of wastewater infrastructure facilitated by strong economic growth under SSP1-RCP2.6 and SSP5-RCP8.5 result in lower pollutant loadings relative to SSP3-RCP7.0. Yet, it should be noted that pollutant loadings in most developing nations will continue to rise until the mid-century (Latin America and Caribbean, Southern Asia, Middle East and North Africa) or the end of the century (Sub-Saharan Africa) even under the most optimistic future scenario (RCP1-SSP2.6).

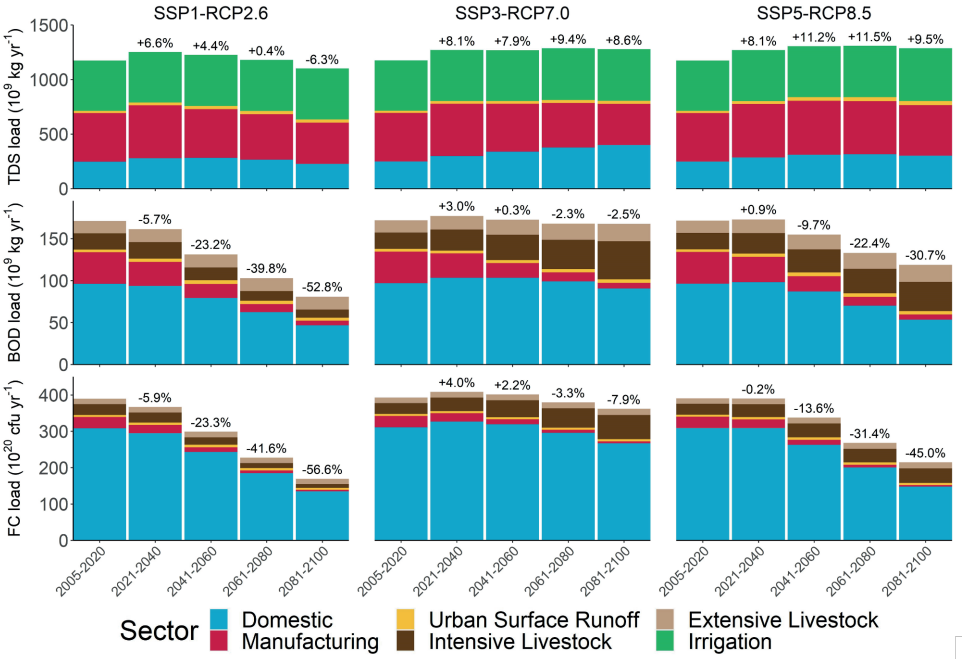

Figure 5.1 Future pollutant loadings by contributing water use sector under three combined climate and socioeconomic scenarios, disaggregated by water use sector. Displayed percentages show the change in pollutant loadings relative to the reference period (2005–2020). More detailed line plots displaying changes in pollutant loadings, disaggregated by geographic region, are displayed in Appendix C.1 (Figs. C.1–C.3).

5.2.2 Future surface water quality

Patterns in future surface water quality are driven by a complex balance of changes in pollutant loadings (Fig. 5.1; Figs. C.1–C.3), the dilution capacity of streams (Fig. C.4) and in-stream decay processes, which are strongly dependent on water temperature (Fig. C.5) under global change. Our projected changes to global TDS, BOD and FC concentrations under different combined climate and socioeconomic development scenarios exhibit patterns of both water quality improvement and deterioration, which vary greatly across world regions (Fig. 5.2; Figs. C.6–C.11) and individual river basins (Figs. C.3–C.4). To evaluate the impact of these relative changes on surface water quality, we also consider the number of months that concentration thresholds are exceeded under the climatic and socioeconomic scenarios (Fig. 5.5; Figs. C.12–C.13).

Water quality deterioration is projected across most of Sub-Saharan Africa, irrespective of the future climate and socioeconomic scenario (Fig. 5.2). Increases in TDS, BOD and FC concentrations are largely ubiquitous in space, including the outlets of major river basins such as the Niger, Congo and Jubba (Fig. 5.3). While variability exists, some general patterns are evident. Water quality deterioration of all three constituents is typically strongest and most widespread for all three constituents under SSP3-RCP7.0. The strongest percentage increases mostly occur for BOD concentrations, with in-stream concentrations across many rivers projected to more than double by the end of the century. Some reductions in FC concentrations are projected under SSP5-RCP8.5, mostly related to improvements in wastewater treatment practices that are facilitated by the strong economic growth under this scenario.

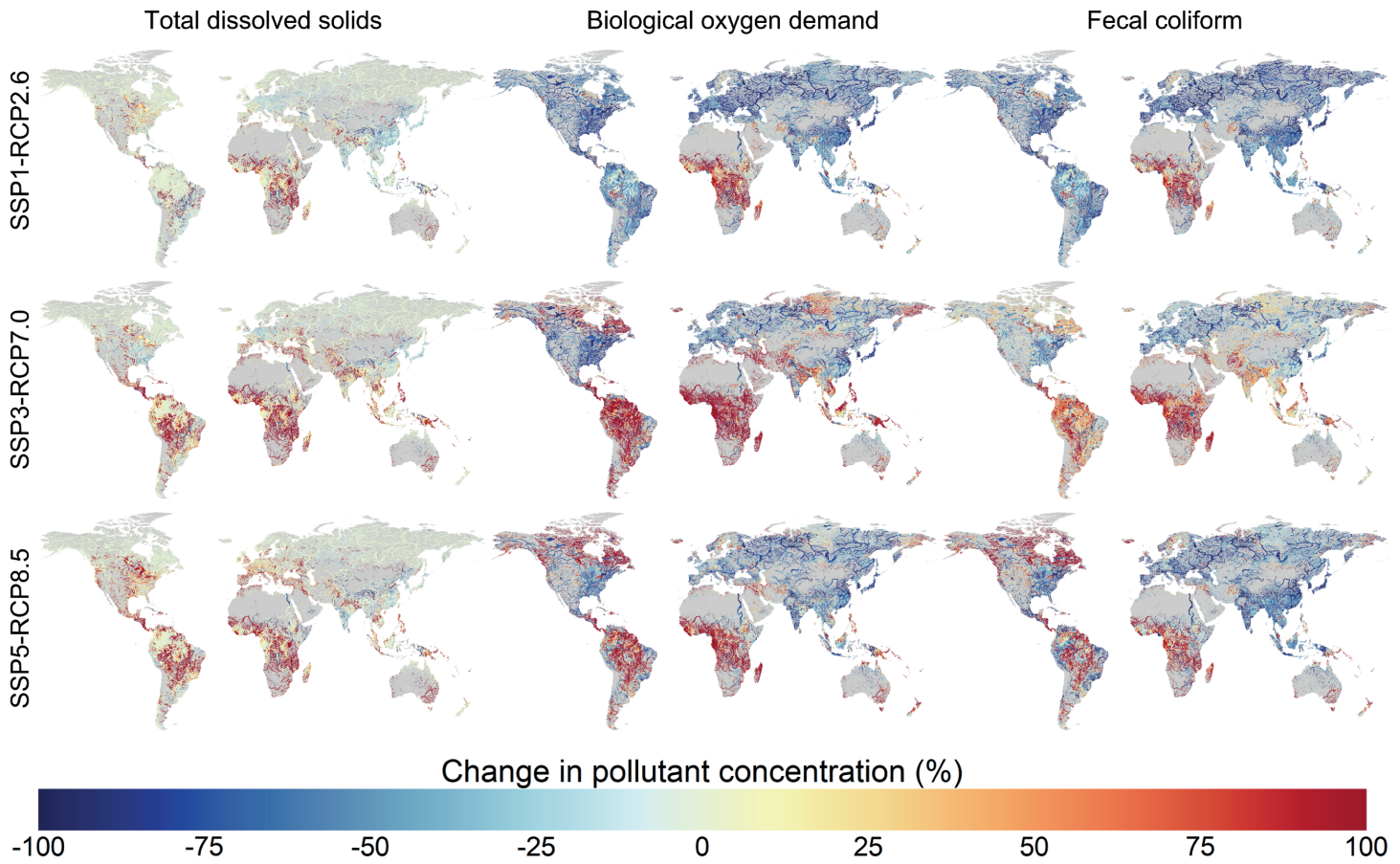

Figure 5.2 Percentage changes in total dissolved solids (TDS), biological oxygen demand (BOD) and fecal coliform (FC) concentrations in the future time period 2081–2100, relative to a historical reference period (2005–2020) under three combined climate and socioeconomic scenarios. Larger versions of these maps, in addition to maps displaying relative changes in streamflow and water temperature and absolute concentrations of TDS, BOD and FC, are displayed in Appendix C.2 (Figs. C.4–C.11).

While most African rivers are projected to become more saline, increases in TDS concentrations are lowest under SSP1-RCP2.6. These conclusions are further supported by seasonal patterns in individual gridcells, located at major African cities (Fig. 5.4). For example, water quality deterioration is projected for Addis Abada in Ethiopia irrespective of global change scenario, with average monthly TDS, BOD and FC concentrations consistently highest under SSP3-RCP7.0.

Future water quality deterioration results in river stretches in most African basins exhibiting multi-seasonal or year-round exceedances of key water quality thresholds. For BOD, this is both most extreme and widespread under SSP3-RCP7.0 with similar (albeit dampened) patterns under SSP5-RCP8.5 (Fig. 5.5). While deterioration is projected even under the most optimistic scenario (SSP1-RCP2.6), exceedances of BOD thresholds are less frequent and widespread, with some rivers across Sub-Saharan Africa (e.g. White Nile) displaying some water quality improvements (Fig. 5.5). Similar patterns exist for exceedances of TDS (Fig. C.12) and FC (Fig. C.13) thresholds. While water quality deterioration across Sub-Saharan Africa appears inevitable as the continent develops demographically and economically, the spatial extent, frequency and magnitude of exceedances is sensitive to the future climate and socioeconomic scenarios.

Contrasting patterns in surface water quality are projected for Latin America under the different scenarios. Strong reductions in BOD and FC concentrations occur under SSP1-RCP2.6 (Fig. 5.2), which decrease both the spatial extent and frequency of BOD and FC threshold exceedances (Fig. 5.5), while there are relatively minor changes in TDS concentrations and exceedances. Conversely, substantial increases in both concentrations and threshold exceedances of all three water quality constituents (TDS, BOD and FC) are widespread under SSP3-RCP7.0 and SSP5-RCP8.5 (Fig. 5.2). This is driven both by socioeconomic developments and climate change. In particular, an increase in livestock activities in Latin America to meet the increased global demand for animal products (e.g. meat) leads to increased BOD and FC loadings, while TDS concentrations mostly increase due to climate-change induced reductions in streamflow (Fig. C.4). While water quality deterioration is projected across most of the Latin America, some water quality improvements are projected for BOD and FC in downstream locations. This corresponds to a reduction in BOD and FC loadings from coastal urban areas (e.g. Rio de Janeiro, São Paulo, Buenos Aires) as a result of improved wastewater treatment practices and a reduction in the proportion of wastewater that is collected but not treated. This explains why reductions are projected at the outlet of the Amazon and Parana rivers (Fig. 5.3), despite many upstream regions becoming more polluted (Fig. 5.2). This spatial pattern is also reflected in the changes in the number of months that BOD (Fig. 5.5) and FC (Fig. C.13) concentration thresholds are exceeded.

Water quality patterns also vary across the other world regions. Typically, improvements in surface water quality are projected in developed countries under all the future climate and socioeconomic scenarios (Fig. 5.2). This translates into a reduction in the number of months exceeding water quality thresholds (Fig. 5.5, Figs. C.12–C.13).

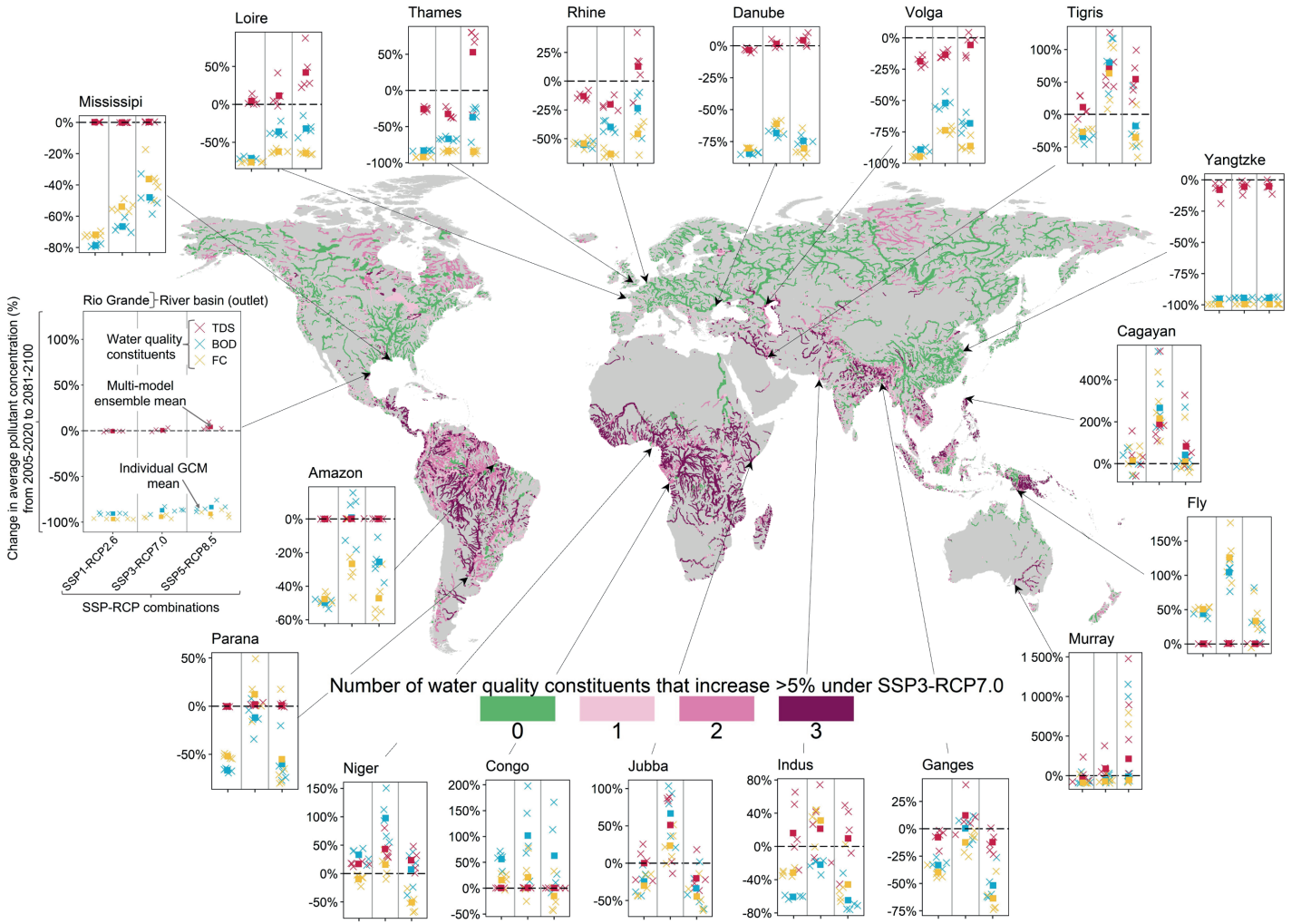

Figure 5.3 Percentage change in average annual mean pollutant concentrations over 2081–2100, relative to a historical reference period (2005–2020), under three combined climate and socioeconomic scenarios. Sinaplots display individual model outcomes (crosses) and a combined ensemble mean (squares) at various river mouths. The water quality constituent is indicated using colours: total dissolved solids (red), biological oxygen demand (blue) and fecal coliform (yellow). The map displays the number of water quality constituents that increase by a multi-model ensemble average >5% under SSP3-RCP7.0.

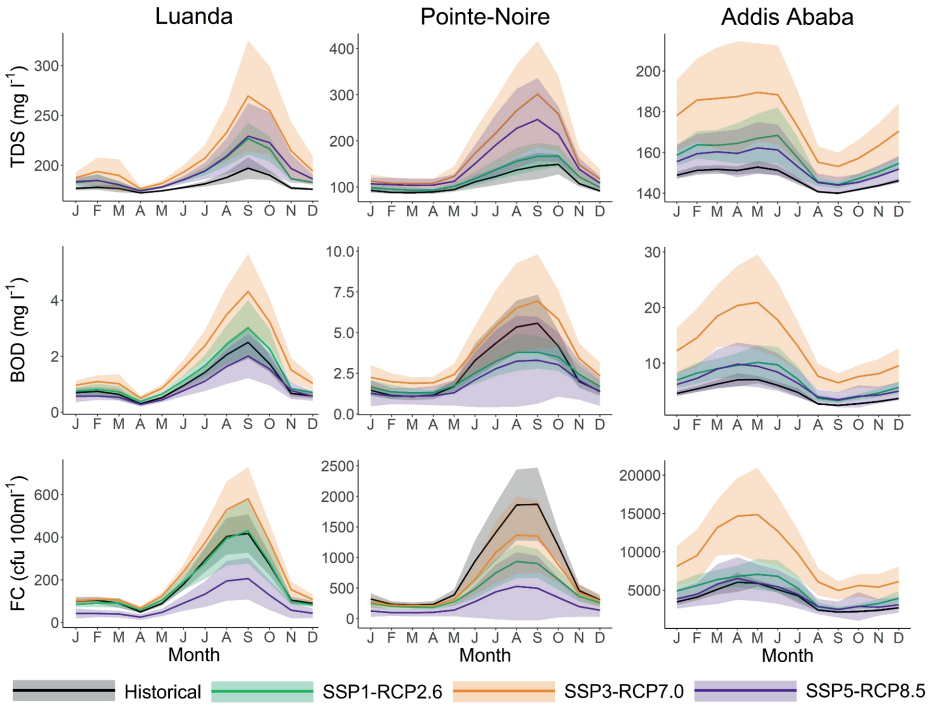

Figure 5.4 Seasonal variability in total dissolved solids (TDS), biological oxygen demand (BOD) and fecal coliform (FC) concentrations in selected African cities averaged over a historical reference period (2005–2020) and in the future time period 2081–2100 under three combined climate and socioeconomic scenarios. Lines display the mean average over the 5 general circulation models (GCMs) considered, while shaded areas represent the uncertainty arising from variations in GCM simulations as ±1 standard deviation.

Surface water quality improvements are strongest under SSP1-RCP2.6, and occur to a lesser extent under SSP3-RCP7.0. While reductions in BOD and FC concentrations are strong under SSP5-RCP8.5 due to very high wastewater treatment rates, TDS concentrations tend to increase due to high demands for manufactured goods (Figs. C.6–C.7). These patterns are reflected in changes in pollutant concentrations in outlets of major European (e.g. Rhine, Danube) and North American (e.g. Mississippi, Rio Grande) rivers (Fig. 5.3). High percentage reductions in BOD and FC concentrations occur across China under all scenarios (Fig. 5.2), as displayed for the outlet of the Yangtze (Fig. 5.3). This is driven by both reductions in pollutant loadings, occurring mostly due to vastly improved wastewater treatment services, but also partly due to projected increases in streamflow. Surface water quality improvements translate into widespread reductions in exceedances of water quality thresholds, which were mostly ubiquitous in space and time in the reference period (2005–2020) (Fig. 5.5). The same patterns do not hold true for the rest of east and southeast Asia, where mixed patterns for different constituents are observed across the region (Fig. 5.2) and at the outlets of individual river basins (e.g. Cagayan, Fly, Ganges) (Fig. 5.3). Lastly, water quality improvements in the Middle East are predominantly only projected under SSP1-RCP2.6. In this region, severe water quality deterioration is projected under SSP3-RCP7.0 which occurs due to a combination of increased pollutant loadings and streamflow reduction.

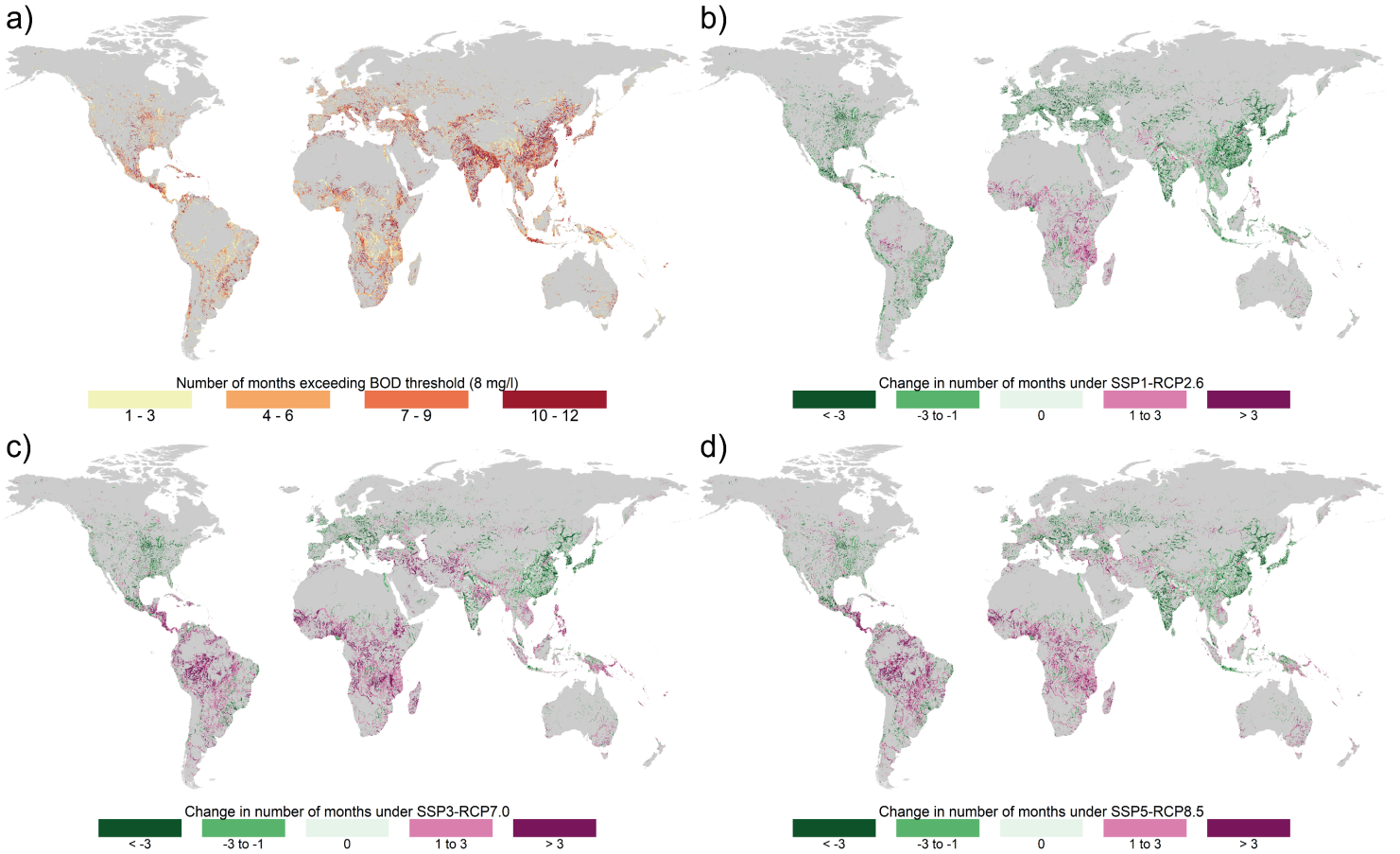

Figure 5.5 a) Number of months per year that surface waters exceed a biological oxygen demand (BOD) threshold of 8 mg l^{-1} under a historical reference period (2005–2020). Panels b), c) and d) display the change in number of months that BOD thresholds are exceeded in a future time period (2081–2100) under three combined climate and socioeconomic scenarios, relative to historical exceedances (i.e. panel a). The same plots for total dissolved solids (TDS; 2,100 mg l^{-1}) and fecal coliform (FC, 1,000 cfu $100ml^{-1}$) are displayed in Appendix C.2 (Figs. C.12–C.13).

5.2.3 Population at risk

For an indication of the potential impact of future changes in surface water quality on humankind, we quantify the number of people living in areas exposed to concentrations that exceed thresholds for safe use (Fig. 5.6a; Figs. C.14–C.16) and the relative change in exposed population per geographic region and water quality constituent (i.e. TDS, BOD and FC) (Fig. 5.6b-d).

The number of people exposed to surface water pollution varies greatly per water quality constituent, RCP-SSP scenario and geographic region (Fig. 5.6a; Figs. C.14–C.16). Substantial decreases in the number of people exposed to surface water BOD and FC pollution are achieved by the end of the century under SSP1-RCP2.6 (BOD: 1.6 ±0.1 billion; FC: 2.0 ±0.1 billion) and SSP5-RCP8.5 (BOD: 1.6 ±0.3 billion; FC: 1.9 ±0.3 billion), relative to historical conditions (BOD: 2.7 ±0.1 billion; FC: 3.7 ±0.1 billion). Changes in exposure to BOD and FC pollution roughly follow consistent patterns per geographic region, with exposure becoming negligible in Western Europe and North America and strong percentage reductions in the historically polluted regions of East Asia and Latin America. Reductions in exposure across Eastern Europe, Central Asia and Southern Asia are more modest, but are still substantial. Under SSP1-RCP2.6 and SSP5-RCP8.5, changes in the proportion of the population exposed to BOD and FC pollution in Sub-Saharan Africa are also modest, although there is substantial spread across the GCMs. The global population exposed to TDS pollution at the end of the century under SSP1-RCP2.6 (1.3 ±0.1 billion) and SSP5-RCP8.5 (1.4 ±0.3 billion) is comparable to historic levels (1.3 ±0.1 billion people), with small increases (∼5%) in exposed population across most world regions counterbalanced by the reductions in East Asia and Pacific.

Conversely, substantial increases in the total number of people exposed to surface water pollution occur under SSP3-RCP7.0. The number of people exposed to TDS, BOD and FC pollution increases to 2.9 (±0.4), 4.2 (±0.4) and 5.1 (±0.4) billion people, respectively. Compared to the most optimistic future scenario, the total population exposed to BOD and FC pollution approximately triples, while also more than doubling for TDS pollution. In some world regions, such as South Asia, the Middle East and North Africa, rapid population growth in regions under SSP3-RCP7.0 leads to an overall increase in absolute number of people exposed to BOD and FC pollution despite decreases in the percentage of the population exposed (Fig. 5.6).

Multi-pollutant threshold exceedances at the end of the century are projected to be widespread in Sub-Saharan Africa, irrespective of the climate and socioeconomic scenario (Fig. 5.7). This pattern is not replicated in any other world region, with the exception of more localised pockets in south and south-east Asia, central America and continental Latin America (Fig. C.17). Across all scenarios for Sub-Saharan Africa, rapid population growth is coupled with strong water quality deterioration. This leads to large increases in the absolute number of people exposed to pollution issues, with hotspots coinciding with major urban centres where rapid population growth is projected, such as Kinshasa, Nairobi and Addis Ababa (Fig. 5.7).

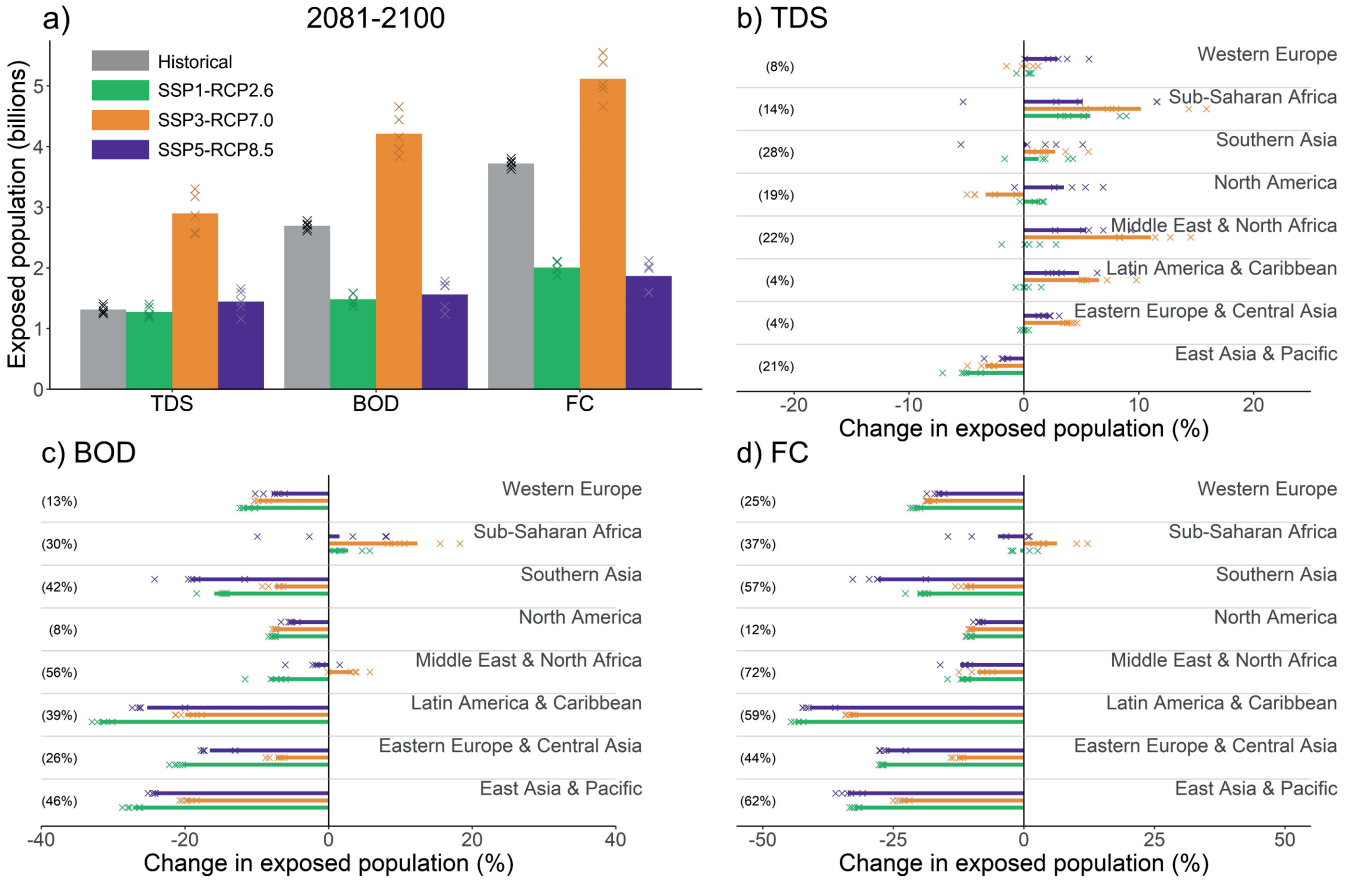

Figure 5.6 a) Number of people exposed to surface water quality that exceeds concentration thresholds for total dissolved solid (TDS; 2,100 mg l^{-1}), biological oxygen demand (BOD; 8 mg l^{-1}) and fecal coliform (FC; 1,000 cfu 100ml^{-1}) in a historical reference period (2005–2050) and in the time period 2081–2100 under three combined climate and socioeconomic scenarios. Panels b), c) and d) display the percentage change in exposed population in the time period 2081–2100 relative to 2005–2020 per geographic region, for TDS, BOD and FC respectively. Error bars in panel a) display the uncertainty as ±1 standard deviation, arising from variations in general circulation models (GCM) simulations. Crosses in panels b), c) and d) represent the results per individual GCM, with the percentage values on the lefthand side displaying percentage exceedance in the historic reference period. Bars in all panels display the ensemble mean value averaged over the 5 GCMs.

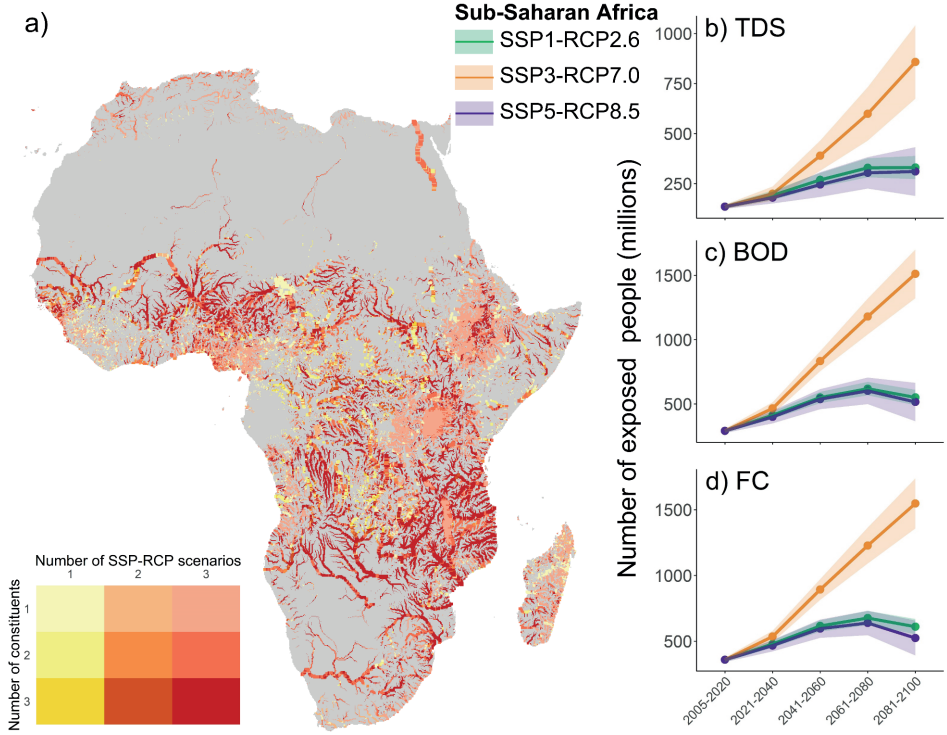

Figure 5.7 a) Combined number of constituents that exceed water quality thresholds, and under how many scenarios, for the African continent, averaged over 2081–2100. Water quality thresholds considered are 2,100 mg l^{-1}, 8 mg l^{-1} and 1,000 cfu $100ml^{-1}$ for total dissolved solids (TDS), biological oxygen demand (BOD) and fecal coliform (FC), respectively. Line plots display the number of people in Sub-Saharan Africa exposed to in-stream concentrations that exceed b) TDS, c) BOD and d) FC thresholds under the different combined climate and socioeconomic scenarios, averaged over multi-year periods. Lines display the mean average over the 5 general circulation models (GCMs) considered, while shaded areas represent the uncertainty arising from variations in GCM simulations as ±1 standard deviation. Line plots for all world regions (Figs. C.14–C.16) and the same map at the global extent (Fig. C.17) are displayed in Appendix C.3.

Even under the most optimistic future scenario (SSP1-RCP2.6) the number of people exposed to TDS, BOD and FC exceedances in Sub-Saharan Africa will more than double. Under SSP5-RCP8.5, the population exposed to surface water pollution peaks in the mid-late century (2061–2080). By the end of the century projections of population exposure under SSP5-RCP8.5 are comparable to SSP1-RCP2.6. This is due to strong (fossil-fuelled) economic developments under SSP5-RCP8.5 facilitating the development of wastewater treatment infrastructure to a level that can counteract the trend of increasing pollution. Conversely, extreme population growth combined with restricted and more regional economic development under SSP3-RCP7.0 leads to a continuously increasing trend in the number of people exposed to surface water pollution. An estimated 1.5 (±0.2) billion people in Sub-Saharan Africa alone are exposed to surface waters with BOD concentrations exceeding 8 mg l^{-1} under SSP3-RCP7.0, approximately three times that under SSP1-RCP2.6 (550 ±60 million people) and SSP5-RCP8.5 (515 ±149 million people) (Fig. 5.7c), and over five times that in the historical reference period (290 ±16 million people). Overall, similar patterns exist for both TDS (Fig. 5.7b) and FC (Fig. 5.7d).

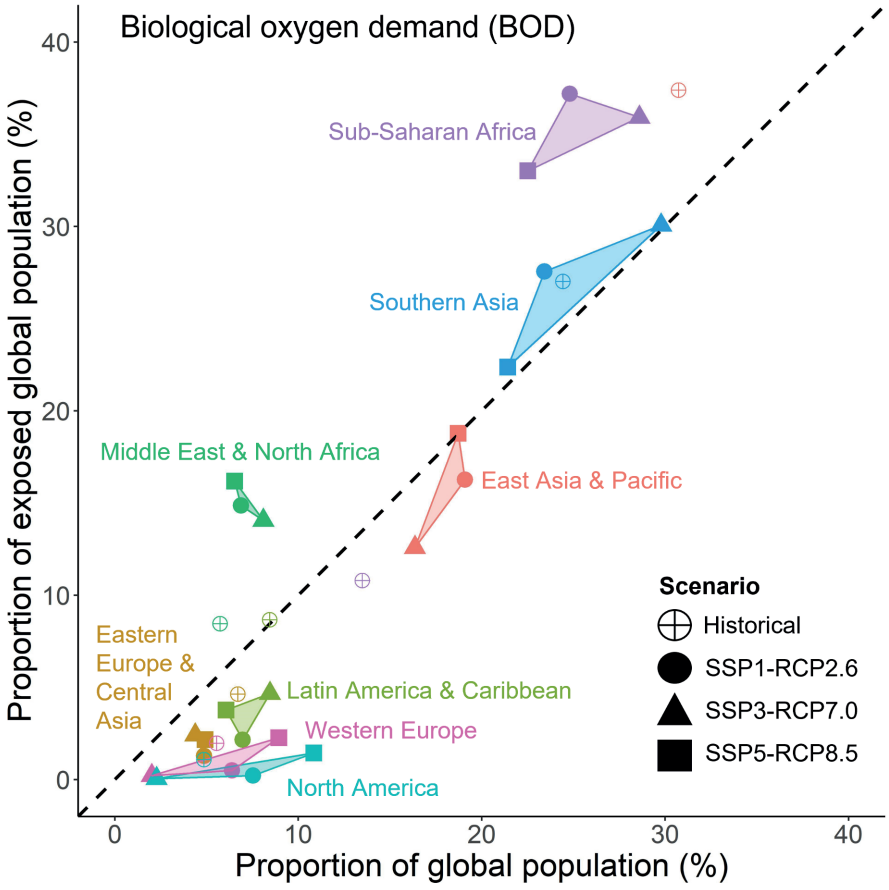

Figure 5.8 Percentage of the total global population versus the percentage of the global population that are exposed to surface waters that exceed a biological oxygen demand (BOD) concentration of 8 mg l^{-1}, disaggregated by world region. Results are for averaged over multi-year periods for both a historical reference period (2005–2020) and for the time period 2081–2100 under the three different combined climate and socioeconomic scenarios. The same plots for total dissolved solids (TDS; 2,100 mg l^{-1}) and fecal coliform (FC, 1,000 cfu 100ml^{-1}) are displayed in Appendix C.3 (Figs. C.18–C.19).

The global aggregation (Fig. 5.6a) thus conceals the substantial regional variability that exists in both the percentage and absolute number of people exposed to surface water pollution, particularly for BOD and FC. Aforementioned increases in Sub-Saharan Africa, in addition to in Southern Asia, the Middle East and North Africa, mask the vast improvements projected in other world regions. This is particularly true for the East Asia and Pacific region, which was the dominant pollution hotspot in the reference period. Here, exposed populations are projected to substantially decrease across all climate and socioeconomic scenarios. As an illustration, the proportion of people exposed to organic pollution in the East Asia and Pacific region drops from 46% in the historical period to 18–20%, 25–27% and 21–23% under SSP1-RCP2.6, SSP3-RCP7.0 and SSP5-RCP8.5, respectively. This represents a drop from 36% of the total global exposed population to between 13–19%, depending on the global change scenario (Fig. C.8). By contrast, a disproportionately high share of the global

population exposed to organic pollution will live in Sub-Saharan Africa by the end of the century irrespective of future scenarios: 36–38% under SSP1-RCP2.6, 35–37% under SSP3-RCP7.0 and 29–36% under SSP5-RCP8.5, with the region containing just 25%, 29% and 23% of the global population, respectively (Fig. 5.8). This represents a prominent shift from historical conditions, where the Sub-Saharan Africa region contained 14% of the global population but just 10% of the population exposed to organic surface water pollution (Fig. 5.8). Similar patterns exist for exposure to both salinity (Fig. C.18) and pathogen (Fig. C.19) pollution. Therefore, irrespective of climate and socioeconomic scenario, our results suggest a shift in the dominant hotspot of surface water pollution from the East Asia and Pacific region to Sub-Saharan Africa. While Southern Asia, the Middle East and North Africa are also important hotspots of future surface water quality pollution, trends towards further deterioration in these regions are mainly projected under SSP3-RCP7.0.

5.3 Discussion

This work represents the first study to comprehensively evaluate the impact of uncertain climate and societal change on global surface water quality, as indicated by TDS, BOD and FC, at high spatial and temporal resolution. The global outlook is mixed, exhibiting strong regional trends in surface water quality improvements and deterioration, while also sensitive to scenarios of climate change (based on the RCPs) and socioeconomic developments (SSPs). It should also be noted that the analysis displayed in this paper focuses on concentrations averaged over aggregated periods (i.e. annual, monthly), and thus not on extreme values. With expected changes in the frequency and magnitude of both droughts and floods under climate change (Trenberth et al., 2014), intensification of surface water quality issues that occur on shorter time periods are expected.

Uncertainties in surface water quality simulations arise from a combination of uncertainties associated with estimates of pollutant loadings (e.g. pollutant excretion rates, emission rates and sector-specific return flows), the quality of hydrological simulations (e.g. discharge and velocities) and the representation of in-stream processes (e.g. decay coefficients). These uncertainties are further amplified when modelling at large spatial extents. Our modelling strategy is thus to focus on the main spatial and temporal drivers of pollution in large-scale river networks to facilitate first-order approximations of in-stream concentrations, using globally consistent input data to facilitate meaningful comparisons of in-stream concentrations across different world regions. We opt to implement *DynQual* at 5 arc-min spatial resolution as the performance of both *PCR-GLOBWB2* (Sutanudjaja et al., 2018; Hoch et al., 2023) and *DynWat* (Wanders et al., 2019) have been demonstrated to markedly improve at finer spatial extents, which have a strong influence on simulated surface water pollutant concentrations due to dilution and in-stream decay processes, respectively.

Our results are sensitive to the structural uncertainty of the global hydrological model (GHM) *PCR-GLOBWB2* (Sutanudjaja et al., 2018) and the water quality model *DynQual* (Jones et al., 2023). This is important to acknowledge as all models are imperfect, with errors and biases arising from aspects such as model parameterisation and inaccuracies in the representation of physical processes (van der Wiel et al., 2019). Severe limitations in observational surface water quality data, both in terms of spatial coverage and with respect to the number of observations per water quality monitoring station (UNEP, 2016; Damania et al., 2019), make systematically quantifying these factors challenging. Overall, TDS, BOD and FC simulations are consistently better in larger streams than gridcells with low water availability (e.g. headwater streams) (Jones et al., 2023). This is likely due to spatial mismatches between the generation of pollutant loadings and the location of entry to the stream network (return flows), which become less influential on simulated concentrations as pollutants are routed downstream (Jones et al., 2023). Given this, combined with the overall research

aims of global water quality models, our analysis of future water quality focuses on large rivers. We also focus on relative changes (Figs. 5.2–5.3), using an absolute concentration plot (aggregated over a 20-year period) as a means to communicate variability under the global change scenarios (Fig. 5.4) rather than as a projection or prediction of future in-stream concentrations. Similarly, we use a simple binary threshold exceedance (i.e. exceedance vs. no exceedance) approach, as opposed to specifically considering changes to absolute concentrations when analysing surface water quality with respect to concentration thresholds (Fig. 5.5) and population exposure to polluted surface waters (Figs. 5.6–5.8). Repeating the analysis with hydrological simulations from different GHMs (as facilitated by the model structure of *DynQual*) could provide further insights into model sensitivity (van der Wiel et al., 2019). Furthermore, comparing our simulations to output from other global water quality models, when available, will be crucial for understanding uncertainties in the underlying assumptions for estimating pollutant loadings and in the representation of in-stream decay processes.

As few studies have projected global surface water quality into the future, there is limited scope to compare our results to the existing scientific literature. Recent work using CMIP5 climate forcing has simulated changes in water temperature under future climate change (Barbarossa et al., 2021; Bosmans et al., 2022) with similar results to ours, hence our decision not to present detailed analysis here. Previous work estimated that 2.5 billion people will be affected by organic (BOD) surface water pollution in 2050 (Wen et al., 2017), with developing countries disproportionality affected, which is comparable to our estimates of between 1.8–3.6 billion people depending on the combined climate and socioeconomic scenario. No previous studies have simulated TDS or FC concentrations into the future. However, there is historical precedent for improvements in surface water quality associated with economic development (Damania et al., 2019), particularly with respect to the so called 'pollutants of poverty' (e.g. BOD, FC), as demonstrated in studies using both modelling (Jones et al., 2023) and data-driven approaches (Desbureaux et al., 2022).

While we use TDS, BOD and FC to draw conclusions on future global surface water quality, they do not represent the full suite of contaminants that pose risks to human water use and environmental health. The diversity in pollutants, their drivers and the associated impacts to humans and the environment make the establishment of all-encompassing metric to assess surface water quality extremely challenging. As an illustration, the global repository for water quality data (GEMStat) contains observations for more than 220 different water quality constituents (UNEP, 2019), while thousands of extra constituents have been identified by organisations such as the World Health Organisation (WHO) (Damania et al., 2019). Furthermore, the US Environmental Protection Agency (EPA) set maximum concentrations for 125 individual pollutants based on human health criteria under the Clean Water Act.

Of these, nutrient pollution is of particular concern, with the associated eutrophication and loss of ecosystems services posing both serious economic and environmental problems (Xie and Ringler, 2017; Beusen et al., 2022). The Integrated Model to Assess the Global Environment - Global Nutrient Model (*IMAGE-GNM*) is similarly coupled to *PCR-GLOBWB2* and has been used extensively to assess the delivery of nitrogen (N) and phosphorus (P) to surface waters under different socioeconomic developments globally (van Drecht et al., 2009; Morée et al., 2013; Beusen et al., 2022). Future trends in N and P are largely driven by changes in agricultural practices (Xie and Ringler, 2017), making direct comparisons to our selected constituents (i.e. TDS, BOD and FC) difficult. However a general pattern of the most severe degradation in surface water quality with respect to nutrients occurring in developing nations is consistent with our findings (Beusen et al., 2022). Patterns in other constituents, particularly those that are not typically removed at conventional wastewater treatment plants, likely exhibit vastly different trends. These include so called 'pollutants of prosperity', such as pharmaceuticals, plastics and industrial chemicals, which will pose their own challenges and risks for humans and ecosystems (Damania et al., 2019; Desbureaux et al., 2022).

Future work could explore expanding physically-based modelling approaches such as *DynQual* to include a greater range of water quality constituents, thus enhancing our overall understanding of global water quality dynamics.

5.4 Methods

5.4.1 Surface water quality model (*DynQual*)

We use the new physically-based Dynamical Surface Water Quality (*DynQual*) model to simulate in-stream water temperature (Tw) and concentrations of total dissolved solids (TDS), biological oxygen demand (BOD) and fecal coliform (FC) at daily timestep and 5 arc-min spatial resolution (Jones et al., 2022; Jones et al., 2023). These water quality constituents are selected due to their key role in constraining different sector water uses and environmental health (van Vliet et al., 2021), in addition to acting as proxies for other pollutants and more generally as overarching indicators of water quality status. The open source model *DynQual* is coupled to the global hydrological and water resources model *PCR-GLOBWB2* (Sutanudjaja et al., 2018), which simulates hydrological variables (e.g. discharge, channel storage) including the influence of human activities (e.g. sectoral water withdrawals, consumption and return flows). Pollutant loadings are estimated within *DynQual* based on sectoral water use activities (domestic, manufacturing, irrigation, livestock and power generation) and from urban surface runoff, accounting for wastewater collection and treatment practices. Pollutant loadings are routed through the hydrological network, with in-stream concentrations computed considering both the dilution capacity and pollutant-specific decay processes (Jones et al., 2023). As with all modelling studies, and particularly those at the global scale, we must acknowledge uncertainties in our water quality simulations. Uncertainties arising from the representation of physical processes within *DynQual*, as well as an extensive validation using observed water temperature and TDS, BOD and FC concentrations, are described and presented in previous work (Wanders et al., 2019; Jones et al., 2022; Jones et al., 2023).

5.4.2 Future climate and socioeconomic change

Shared Socioeconomic Pathways (SSPs) and Representative Concentration Pathways (RCPs) describe future possible developments in socioeconomic and climatic conditions, respectively, to provide integrated scenarios to explore uncertain future change in a consistent framework (O'Neill et al., 2017). In this study, we simulate surface water quality under (uncertain) climate change and socioeconomic scenarios for the time period 2005–2100, considering three combined SSP-RCP scenarios: SSP1-RCP2.6, SSP3-RCP7.0 and SSP5-RCP8.5. Each scenario is run using bias-corrected daily CMIP6 climate output (precipitation, air temperature and solar radiation) from the five General Circulation Models (GCMs) included in the Inter-Sectoral Impact Model Intercomparison Project (ISIMIP3b) database (GFDL-ESM4; UKESM1-0-LL; MPI-ESM1-2-hr; IPSL-CM6A-LR and MRI-ESM2-0) (Lange and Buchner, 2021).

The required socioeconomic data for simulating pollutant loadings under the different SSPs is derived from various data sources. Datasets for gridded population (Jones and O'Neill, 2016) and urban fraction (Hurtt et al., 2020) are derived at the annual time-step, while return flows from the manufacturing and irrigation sectors are simulated by *PCR-GLOBWB2* with a daily timestep (Sutanudjaja et al., 2018; Jones et al., 2023). Country-level rates of change in livestock numbers up to 2050 (Beusen et al., 2022) are applied to 2010 livestock populations at 5 arc-min resolution (Gilbert et al., 2018), extended to 2100 by assuming a continuation of the rate of change in the final available timestep (2049–2050) for all subsequent years. We apply regional and sub-regional decadal rates of change in water withdrawals for thermoelectric power generation that include variations in technological change under the SSPs (Graham et al., 2018) to return flows from the thermoelectric

power sector in 2020 (Lohrmann et al., 2019). Human and livestock excretion rates per capita and effluent concentrations from the different sectors are assumed to remain constant and follow previous work (UNEP, 2016; van Vliet et al., 2021; Jones et al., 2022; Jones et al., 2023).

5.4.3 Wastewater management scenarios

The mass of pollution discharged to surface waters is strongly influenced by the transmission path (van Puijenbroek et al., 2019; Beusen et al., 2022; Jones et al., 2022). Collection and subsequent treatment of wastewater can remove a substantial proportion of the loadings, depending on the removal efficiency (i.e. treatment level). Thus, how wastewater treatment infrastructure develops under different socioeconomic assumptions has a strong influence on future surface water quality. We account for seven different wastewater management practices in three categories: 1) collection and treatment (primary, secondary, tertiary and quaternary); 2) collected but untreated; and 3) uncollected (basic sanitation, open defecation). These wastewater management practices are reported at country-level per SSP with a decadal time-step and are derived as a function of GDP (van Puijenbroek et al., 2019). Country-level estimates are downscaled to 5 arc-min following previous work (Jones et al., 2021; Jones et al., 2022). Removal efficiencies of pollutants from different wastewater management practices are also based on previous work (Jones et al., 2023). To account for future technological improvement, the practice 'quaternary treatment' was introduced (van Puijenbroek et al., 2019) for which we assume almost complete removal of BOD (up to 99%) and FC pollution (99.99%), and 65% removal of TDS (based on the removal efficiency of TDS from wastewater via reverse osmosis (Jones et al., 2019).

5.4.4 Future surface water quality and exposed population

Future surface water quality is assessed with respect to multi-year periods, in accordance with the WorldClim (Fick and Hijmans, 2017) time periods (2005–2020, 2021–2040, 2041–2060, 2061–2080 and 2081–2100). We select a 20-year time interval to account for natural inter-annual variability in the climatology and associated hydrological regimes, while still being short enough to observe changes in the socioeconomic drivers of pollutant loadings that typically occur on shorter timescales (e.g. population growth, expansions in wastewater treatment). The displayed results are based on the average of the multi-model ensembles. Where possible, we display the uncertainty arising from the different GCMs as either ±1 standard deviation (e.g. Fig. 5.4; Fig. 5.6a; Fig. 5.7b-d) or by displaying results for the entire range of simulations (e.g. Fig. 5.3; Fig. 5.6b-d).

In order to assess the potential impacts of future changes in surface water quality, we assess in-stream concentrations with respect to quality thresholds that are derived from extensive literature research (UNEP, 2016; Jones et al., 2022). A TDS threshold of 2,100 mg l^{-1} is used, reflecting the concentration at which water becomes 'unsuitable' for irrigation purposes (Fipps, 2003; Zaman et al., 2018). Consumption of saline water at this level has also been linked to negative human health impacts, with a 42% increase in the prevalence of hypertension associated with consumption of water >2,000 mg l^{-1} TDS in Bangladesh (Nahian et al., 2018). For BOD, a threshold of 8 mg l^{-1} is used, which is representative of 'high pollution' that can pose risks to both the domestic sector and ecosystem health (UNEP, 2016; Wen et al., 2017). The threshold of 1,000 cfu $100ml^{-1}$ for FC is based on human health concerns associated with direct contact (UNEP, 2016; Jones et al., 2022). The selected concentration thresholds are further elaborated on in previous work (Jones et al., 2022). The population exposed to surface water pollution, as defined by these thresholds, is estimated per abstraction zone. Abstraction zones represent groups of gridcells which relate water availability to human demands, in order to match local demand to available water resources in nearby cells. Abstraction zones are inherent to the water demand module of *PCR-GLOBWB2* (Sutanudjaja et al., 2018), with approximately 60,000 defined globally.

Code and data availability

The surface water quality model used in this study, *DynQual*, is available open-access through a GitHub repository (https://github.com/UU-Hydro/DYNQUAL/). Input data is available through the references provided in the methods section. Global hydrological and surface water quality output at 10km resolution, per general circulation model (GCM) and global change scenario (RCP-SSP), is available open-access at: https://doi.org/10.5281/zenodo.7811612.

Acknowledgements

MTHvV was financially supported by the Netherlands Scientific Organisation (NWO) by a VIDI grant (VI.Vidi.193.019) and European Research Council (ERC) under the European Union's Horizon Europe research and innovation program (grant agreement 101039426). We acknowledge and thank the Netherlands Organisation for Scientific Research (NWO) for the grant that enabled us to use the national supercomputer Snellius (project: EINF-3999).

6

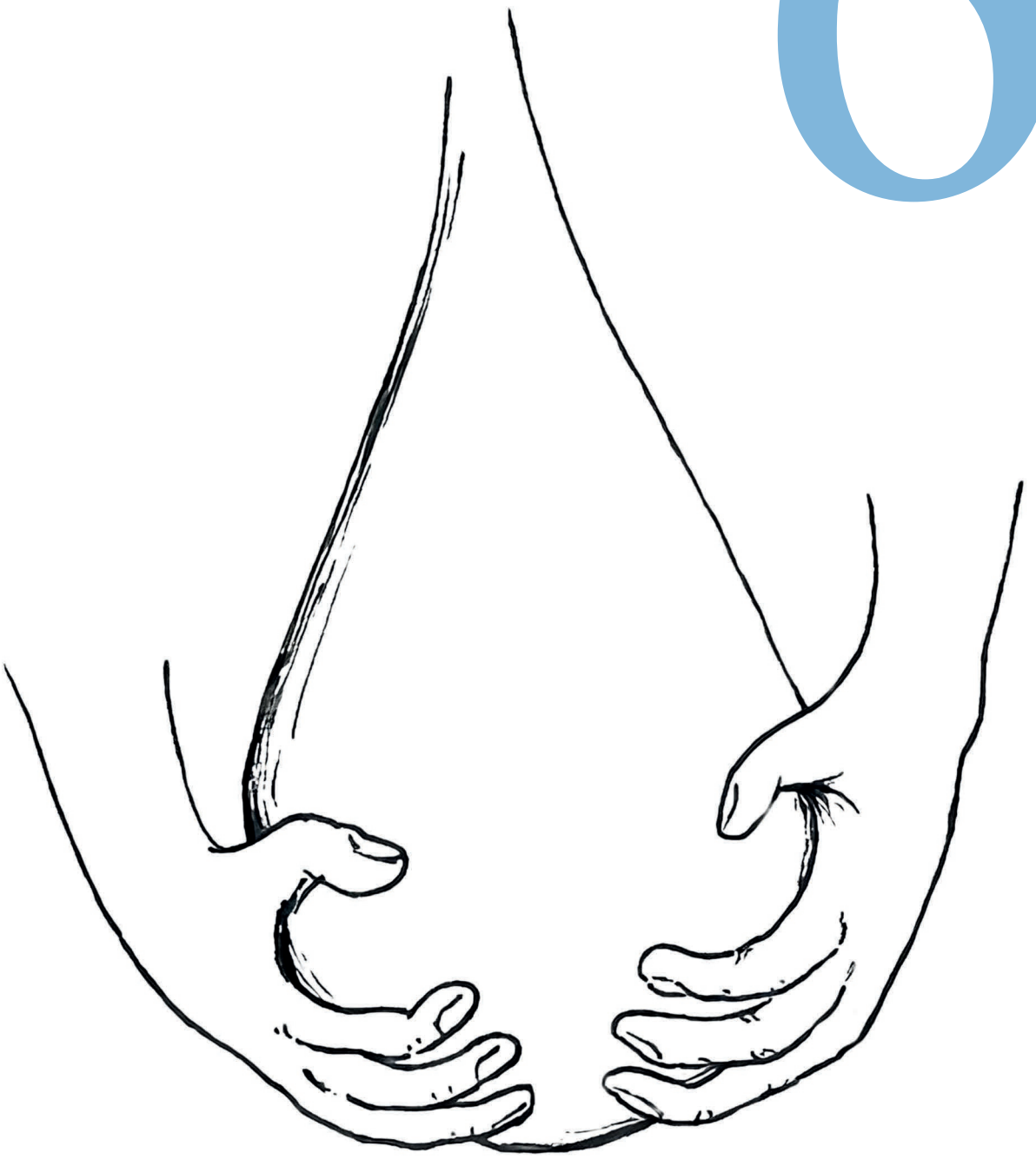

Chapter 6 | Synthesis

Water pollution is a globally-relevant problem, affecting developed and developing countries alike, yet one that has proven difficult for researchers and society to fully grasp. The diversity in pollutants, their drivers and the associated impacts to humans and the environment exacerbate the challenge further (Rode et al., 2010; UNEP, 2016), and is at least partly why global water quality monitoring has been so difficult (Damania et al., 2019). Being largely under-monitored, difficult to detect and often imperceptible to the human eye, the World Bank has branded water quality issues as an 'invisible crisis' (Damania et al., 2019).

Techniques that can improve our understanding of global water quality dynamics without requiring in situ measurements are rapidly emerging, facilitated by technological advancements. Rapid developments in hardware and software architecture, reductions in the cost of high-performance computing and improved access to these resources offer increased opportunities for (process-based) modelling of global surface water quality, as has been well-utilised by the global atmospheric and hydrological modelling communities (Bierkens, 2015).

Leveraging these capabilities, the objective of this thesis was:

To assess the past and current status of surface water quality globally, and to evaluate the impact of (uncertain) global change on future surface water quality.

In this Chapter, the key findings of this thesis are summarised, together with a wider discussion on the implications for science and society. Bringing together the novel findings of this thesis, a preliminary assessment of future water scarcity that includes water quality projections is presented. Lastly, an outlook of the opportunities and challenges for future research in large-scale water quality modelling is provided.

6.1 Main results: contribution to science and society

The key results of this thesis, disaggregated by research question, are summarised in Table 6.1.

Table 6.1 Overview of the main results and conclusions of this thesis, disaggregated by research question.

Research question	Main results
Q1: What is the current global status of wastewater management (i.e. production, collection, treatment and reuse)? (Chapters 2 and 3)	The proportion of wastewater undergoing treatment varies strongly with level of economic development, estimated at 74% for high-income countries, 43% for upper-middle income countries, 23% for lower-middle income countries and 4.2% for low-income countries.
	Approximately half (52%) of global wastewater undergoes treatment, opposed to previous estimates of 20%.
	Treated wastewater re-use already represents an important source of freshwater for human uses at ~111 million m^3 day^{-1}, exceeding the volume of water produced by desalination (~95 million m^3 day^{-1}).
Q2: What is the past and current status of global surface water quality, as indicated by water temperature (Tw) and indicators of salinity (total dissolved solids), organic (biological oxygen demand) and pathogen (fecal coliform) pollution? (Chapters 3 and 4)	Current multi-pollutant hotspots are especially prevalent in northern India and eastern China, but surface water quality issues exist across all world regions.
	In highly developed economies, organic (BOD) and pathogen (FC) pollution have decreased over time, particularly due to expansions in wastewater collection and treatment, while TDS concentrations have marginally increased, predominantly due to expansions in manufacturing activities.
	Recent trends towards surface water quality deterioration are most profound in the developing world, particularly Sub-Saharan Africa and southern Asia. Here, increases in TDS concentrations are predominantly driven by irrigation activities, while increases in BOD and FC pollution are driven by the domestic sector.
	Process-based global modelling approaches (e.g. *DynQual*) can facilitate surface water quality dynamics with a consistent spatial and temporal resolution, but challenges remain for simulating in-stream pollutant concentrations that correspond exactly with in-situ observations at high temporal (e.g. daily) resolution.
Q3: How does global surface water quality change in the future under near-term sustainability targets (Chapter 4) and long-term scenarios (Chapter 5) of climate and socioeconomic change?	Future surface water pollution will disproportionately affect people living in developing countries, with a widening gap in exposure rates between rich and poor countries.
	While achieving the UN's wastewater treatment target by 2030 would substantially improve surface water quality globally, this is insufficient to safeguard human water uses and environmental health - particularly in developing countries.
	The proportion of the global population exposed to salinity (TDS), organic (BOD) and pathogen (FC) pollution by the end of the century ranges between 17 – 27%, 20 – 37% and 22 – 44%, respectively, under the three combined climate and socioeconomic scenarios (SSP1-RCP2.6, SSP3-RCP7.0 and SSP5-RCP8.5)
	A combination of surface water quality deterioration and demographic changes will increasingly make Sub-Saharan Africa the new global hotspot of surface water pollution, irrespective of climate change and socio-economic development scenarios.

6.1.1 Current status of wastewater practices (RQ1)

This thesis provides the first comprehensive and consistent global outlook on the state of wastewater production, collection, treatment and reuse. The open-access databases (country-level and 5 arc-min) have a broad range of applications, such as serving as a reference for understanding the global wastewater situation, identifying hotspots where untreated wastewater enters the environment and for evaluating progress towards policy goals that are both directly and indirectly related to wastewater management (e.g. SDG 6.3). Spatially-explicit results are well-suited for detailed hydrological analysis, such as the surface water quality model simulations presented in this thesis (Chapters 3–5).

Global wastewater production is estimated at 359 billion m^3 yr^{-1}, with 63% collected (225 billion m^3 yr^{-1}) and 52% treated (188 billion m^3 yr^{-1}). Therefore, our results imply that globally 48% is released to the environment untreated – far lower than the commonly cited statistic of ∼80%. However, global wastewater statistics are skewed by the large amount of wastewater produced in the developed world, where wastewater collection and treatment rates are high. For example, 'high-income' countries produce 41% of wastewater globally, but contain just 16% of the global population. Conversely, countries classified as 'lower-middle' and 'low-income' contain ∼50% of the global population but produce just ∼20% of the world's wastewater. While per capita wastewater production rates in the developing world are much lower, wastewater treatments are also extremely low (e.g. 'low-income' countries treat just 4.2% of the wastewater produced). Thus, while this thesis showed that more wastewater is collected and treated than previously thought, significant volumes of wastewater enter the environment untreated – particularly in the poorest countries.

Improved wastewater management is required to protect human and environmental health, while simultaneously providing opportunities to promote sustainable development and support the transition to a circular economy. A key opportunity associated with wastewater, particularly in water scarce regions, is to augment freshwater supplies by treated wastewater reuse. In this thesis, the first global estimate of treated wastewater reuse is made (∼111 million m^3 day^{-1}), which exceeds the global desalination capacity (∼95 million m^3 day^{-1}) (Jones et al., 2019). In addition to demonstrating the importance of treated wastewater for clean water provision, the results highlight the enormous potential for expansions in treated wastewater reuse capacities. Wastewater treatment also presents opportunities for the recovery of by-products, such as energy and nutrients. This thesis echoes calls for a paradigm shift in water resources management, whereby wastewater is viewed as a resource rather than as 'waste' (WWAP, 2017; Qadir et al., 2020).

6.1.2 Global surface water quality (RQ2)

This thesis contributes to the advancement of the (emerging) field of large-scale surface water quality modelling through the introduction of a new open-source model (*DynQual*) for simulating water temperature (Tw) and concentrations of total dissolved solids (TDS), biological oxygen demand (BOD) and fecal coliform (FC) (https://github.com/UU-Hydro/DYNQUAL). The model is structured in a flexible way to allow both hydrological and pollutant loadings to either be simulated within the model run or user-defined as a forcing. This facilitates the estimation of pollutant loadings using a different methodology and the use of a different land-surface or global hydrological model to simulate hydrological fluxes, respectively. These features could also prove to be advantageous for simulating surface water quality in world regions where locally-specific input data (compared to the globally consistent datasets) or higher fidelity models are available.

In this thesis, *DynQual* was applied to provide a long-term global assessment of surface water quality (1980–2019), using state-of-the-art climate and socioeconomic forcing data. For example, hydrological simulations are made with the most recent W5E5 climate forcing data (Cucchi et al., 2020; Lange et al., 2021). Similarly, pollutant loading estimates leverage novel gridded datasets on wastewater management practices (Chapter 2), to more realistically account for the impact of these

practices on pollutant delivery to surface waters. This represents an advancement on existing methods adopted by large-scale water quality models, which typically estimate the abatement of pollutants at wastewater treatment plants based on country-level or regional average rates.

Historical simulations of global surface water quality display past and current hot- and bright-spots of surface water pollution, providing insights into the sectoral drivers of these patterns and also linking in-stream concentrations to water quality thresholds. Modelled results demonstrate that surface water quality issues are globally relevant, with in-stream TDS, BOD and FC concentrations exceeding key thresholds across all world regions, albeit with different frequencies and magnitudes. Globally, TDS pollution is predominantly driven by the irrigation and manufacturing sectors, while hotspots of BOD and FC pollution are largely driven by (untreated) wastewater from domestic and livestock activities. Current year-round multi-pollutant hotspots are particularly prevalent across northern India and eastern China, while trends towards surface water quality deterioration in the last ~40 years have been most profound in the developing world, particularly Sub-Saharan Africa and southern Asia. While modelled results demonstrate that improvements to wastewater collection and treatment practices, particularly in the developed world, have been successful for improving in-stream water quality (e.g. BOD and FC), trends are also strongly pollutant-specific. However, this thesis reiterates assertions that surface water pollution does not necessarily disappear with economic development, but rather evolves (Desbureaux et al., 2022). *DynQual* provides a framework for process-based modelling of additional constituents, which may be particularly relevant for emerging contaminants and other so-called *pollutants of prosperity* (Damania et al., 2019), which are not typically well-monitored (Deblonde et al., 2011; Geissen et al., 2015).

This thesis also elucidates some of the challenges of large-scale water quality assessments. The dearth of in situ observations of water quality across both space and time severely limit the understanding that can be gained from in situ measurements alone, motivating approaches such as process-based modelling. However, the lack of water quality observations complicate model development and evaluation. Furthermore, there are significant limitations associated with the poor availability of and uncertainties in input data for model simulations. This thesis advocates for improved global monitoring, in addition to the public and free dissemination of existing data, of both observed surface water quality (e.g. in-stream concentrations, pollutant loadings) and pollutant fluxes originating from sectoral activities (e.g. effluent concentrations from wastewater treatment plants and industrial facilities, management practices of livestock waste). These data are crucial for advancing our knowledge of global surface water quality and for facilitating the development of effective policies and intervention strategies to tackle surface water pollution.

6.1.3 Future global surface water quality (RQ3)

The IPCC AR6 report describes existing attempts to quantify future changes in water quality as 'incipient' and 'sparse', noting a 'dearth of quantification at the global scale' (Caretta et al., 2022). Future in-stream pollutant concentrations are dependent upon changes in the mass of pollution discharged to surface waters, which is strongly driven by anthropogenic activities, in combination with climate-change induced changes to hydrological regimes (e.g. dilution capacities) and abiotic conditions (e.g. water temperature) – all of which are simulated by *DynQual*. This enables the use of *DynQual* for assessments of future surface water quality, driven by multiple interconnected factors, under global change.

The need for short-term improvements to surface water quality is recognised in the Sustainable Development Agenda, with related impacts cross-cutting almost all Sustainable Development Goals (SDGs) (UN, 2015) – including food (SDG 2), water (SDG 6) and energy (SDG 7) security (Wang et al., 2022). The target to halve the proportion of untreated wastewater released to the environment by 2030 (SDG 6.3) represents the principal action to achieve the overarching goal of improved

ambient water quality. In this thesis, *DynQual* was applied to provide the first quantitative assessment of the effectiveness of SDG 6.3 for improving global surface water quality by 2030. Results indicate that while substantial reductions in organic (BOD) and pathogen (FC) concentrations are achieved across all world regions, the effectiveness of this measure for protecting surface water quality (i.e. meeting concentration thresholds for sectoral use and environmental health) is highly variable. If existing wastewater treatment rates in a country are low, the volume of untreated wastewater (and the associated pollutant loadings) can still be very large under SDG 6.3. Here, halving the proportion of untreated wastewater can also be achieved by establishing wastewater treatment in a relatively limited number of locations. As such, while achieving SDG 6.3 is locally effective in reducing pollutant loadings, transmission of pollution from upstream can still result in widespread exceedances of key water quality thresholds. The suitability of SDG 6.3 as a global sustainability target for improving water quality must therefore be considered. The findings also demonstrate that, in addition to expanding centralised collection networks and treatment facilities, alternative measures are also required to protect the quality of surface waters. These could include both preventative (e.g. measures to reduce pollutant emissions at source) and reactive (e.g. constructed wetlands) measures, with a strong focus on nature-based solutions (Jarosiewicz et al., 2022).

While scenario-based modelling has been applied to assess future changes in hydrology at the global scale (Schewe et al., 2014), it has rarely been applied for projections of future water quality. In this thesis, *DynQual* is applied to assess global surface water quality, as indicated by multi-pollutants (i.e. Tw, TDS, BOD, FC), considering three combined climate and socioeconomic scenarios (SSP1-RCP2.6, SSP3-RCP7.0 and SSP5-RCP8.5). This work represents the first quantitative assessment of the impact of climate and socioeconomic change on global surface water quality until the end of the century. While projections indicate strong and robust trends towards surface water quality improvement in most developed countries, widespread deterioration is projected in the poorest nations. Coupled with the fact that most of the future population growth will occur in 'low income' to 'lower-middle income' countries, future water pollution issues will disproportionately impact people living in developing countries. This is particularly true for Sub-Saharan Africa, where there will be a strong increase in the number of people who are exposed to poor surface water quality irrespective of the climate change and socio-economic scenario considered. As such, this thesis concludes that Sub-Saharan Africa will become the key hotspot of surface water pollution in the future.

6.2 (Re-)evaluating water scarcity in the 21st century

6.2.1 Rationale and approach

Human activities rely upon the availability of water in both adequate quantities and of acceptable quality for an intended use (van Vliet et al., 2017; van Vliet et al., 2021). However, existing water scarcity assessments have predominantly focused on water quantity aspects only (Liu et al., 2017). This includes the water scarcity indicator adopted by the United Nations in SDG 6.4.2, whereby water scarcity is defined as the ratio of water withdrawal to the overall water availability (UN, 2015). The suitability of this indicator has been critiqued for a number of reasons, including that aspects related to water quality are largely ignored (Vanham et al., 2018). Methods that have incorporated water quality aspects include the water poverty index (Sullivan et al., 2003), threat indices (Vörösmarty et al., 2010) and approaches building on the grey-water footprint concept (Liu et al., 2016; Zhao et al., 2016; van Vliet et al., 2017; van Vliet et al., 2021). These studies have consistently demonstrated that poor water quality intensifies water scarcity problems.

While previous studies have assessed future water scarcity from a quantity perspective (Schewe et al., 2014; Greve et al., 2018; He et al., 2021), these approaches have not included water quality in their

projections. The preliminary results presented in this Chapter represent the first attempt to quantity future water scarcity including both quantity and quality aspects.

To this end, the approach developed in van Vliet et al. (2017) and van Vliet et al. (2021) has been further modified (Appendix D.1). Water scarcity is assessed considering quantity aspects only (*WS*) (Eq. D.1) and also including water quality (*WSq*) (Eq. D.2) for current conditions (2005–2020), and for the end of the century (2081–2100) under (uncertain) climate and socioeconomic change scenarios. All input data used is as described in Chapter 5, mostly simulated by *PCR-GLOBWB2* and *DynQual*. The population exposed to water scarcity issues, as indicated by *WS* and *WSq* values exceeding 1, are quantified for each scenario.

6.2.2 Preliminary results

Water scarcity, as indicated by both (*WS*) and (*WSq*), varies drastically across the year (Fig. 6.1). Inter-annual patterns in water scarcity are influenced by multiple factors: for *WS* these are reflective of changes in water demand and the availability of surface and groundwater resources, while changes in surface water quality are also included in *WSq*. As such, exacerbation of *WS* indicates more frequent and widespread water gaps (i.e. instances where human water demands exceed the renewable water supply), while increases in *WSq* indicates that in-stream concentrations are more commonly exceeding critical water quality thresholds.

With surface water quality issues currently ubiquitous across the globe (Chapters 3 and 4), the inclusion of water quality exacerbates water scarcity in all world regions. The impact is strongest in the current hotspots of surface water pollution (Chapters 3 and 4): such as northern India, eastern China and coastal Latin America. This pattern is reflected in the increase in people exposed to water scarcity when including water quality, which occurs year-round in the East Asia and Pacific (mean monthly increase: +24%, minimum monthly increase: +18%, maximum monthly increase: +28%) and Latin America and Caribbean (mean: +23%, min: +17%, max: +29%) regions, and more seasonally in southern Asia (mean: +19%, min: +12%, max: +30%) (Fig. 6.1). These regions also correspond with those where wastewater production is rising at a faster pace than the development of wastewater collection and treatment infrastructure (Chapter 2).

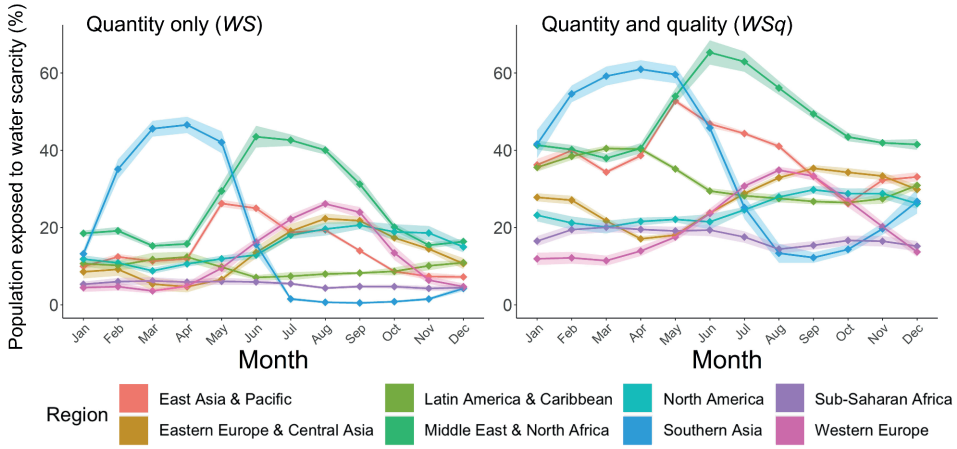

Figure 6.1 Percentage of the population exposed to water scarcity based on water quantity aspects only (*WS*) and including water quantity and quality (*WSq*) in the historical reference period (2005–2020), disaggregated by geographic region. Shaded areas represent the uncertainty as ±1 standard deviation.

Comparatively, exacerbation of water scarcity due to water quality is more limited in regions where pollution is less widespread, such as Western Europe (mean: +9%, min: +7%, max: +14%) and North America (mean: +10%, min: +7%, max: +11%). While trends towards water quality deterioration since 1980 have been most profound in Sub-Saharan Africa, in-stream concentrations remain below key thresholds (Chapter 3 and 4). Thus, this region is not (yet) identified as a dominant hotspot of surface water quality pollution (Chapter 3). This is also reflected in the relatively limited influence of water quality on current quantifications of water scarcity in the region, with an average increase of +12% (min: +10%, max: +14%) (Fig. 6.1).

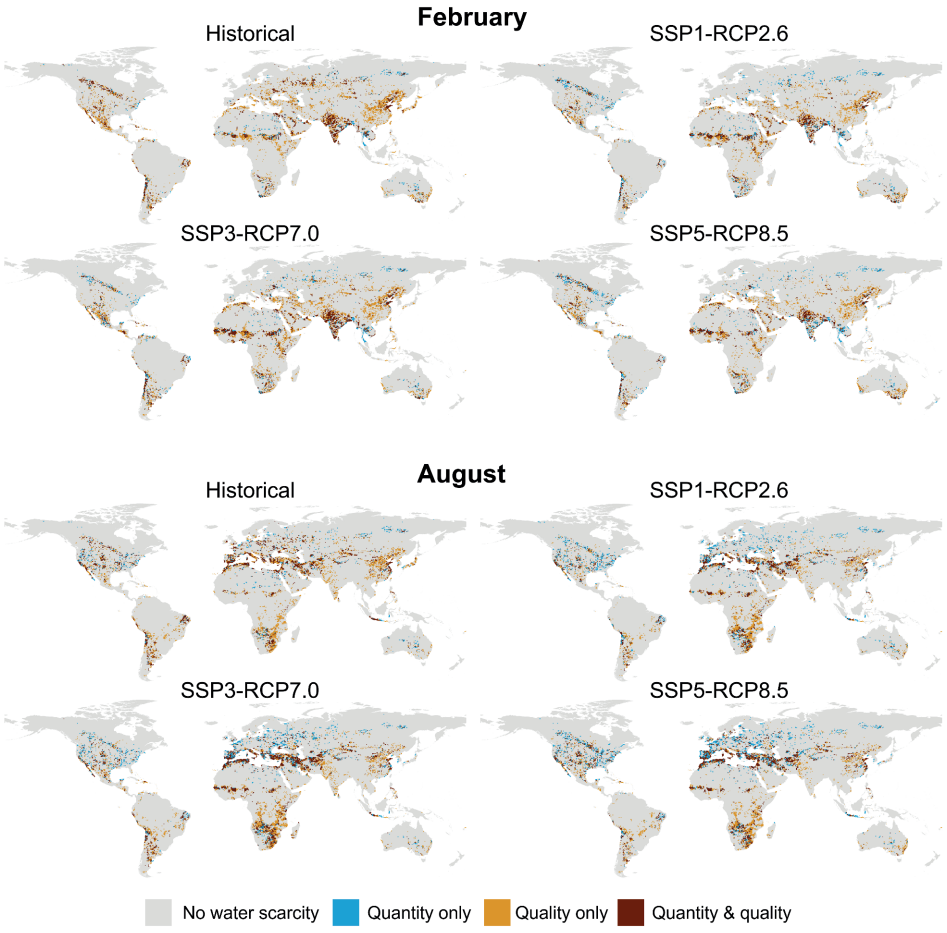

Figure 6.2 Water quality hotspots and their drivers, designated as 'quantity only' (i.e. insufficient water availability, no quality issues), 'quality only' (i.e. sufficient water availability, quality issues) and 'quantity and quantity' (i.e. insufficient water availability, further exacerbated by quality issues). Hotspots are displayed for two months (February and August) averaged over a historical reference period (2005–2020) and at the end of the century under three combined climate and socioeconomic scenarios (2081–2100).

However, projected changes in surface water quality under various climate and socioeconomic changes scenarios suggest Sub-Saharan Africa will increasingly become the dominant hotspot for surface water pollution (Chapter 5). This is reflected by the spatial patterns of water scarcity (Fig. 6.2) and the exacerbation in the population exposed to water scarcity issues when including water quality (Fig. 6.3).

Across all months, the proportion of the population exposed to water scarcity issues (as indicated by both *WS* and *WSq*) in Sub-Saharan Africa by 2081–2100 is substantially greater than in the historical period under all future scenarios (Fig. 6.1). Thus, water scarcity is driven by both water quantity and quality issues (Fig. 6.2). High levels of (year-round) exposure in the future, coupled with the rapid population growth projected for the region, leads to a huge increase in the number of people living in Sub-Saharan Africa that are exposed to water scarcity issues (Fig. 6.3).

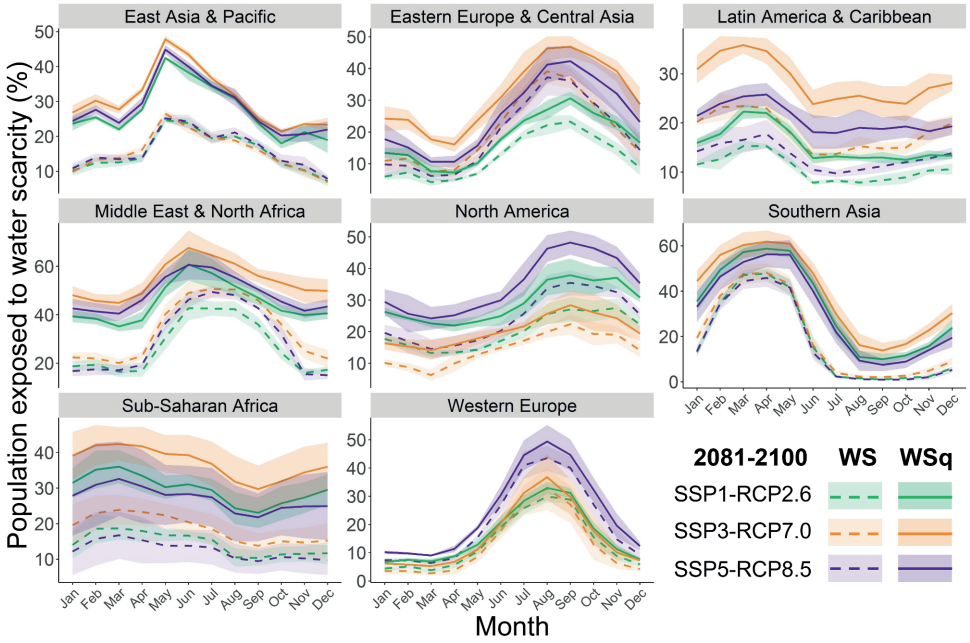

Figure 6.3 Percentage of the population exposed to water scarcity based on water quantity aspects only (*WS*) and including water quantity and quality (*WSq*) at the end of the century under three combined climate and socioeonomic scenarios, disaggregated by geographic region. Lines display the mean average over the 5 general circulation models (GCMs) considered, while shaded areas represent the uncertainty arising from variations in GCM simulations as ±1 standard deviation.

Compared to Sub-Saharan Africa, most world regions display stronger inter-annual patterns in future water scarcity. For example, there are stark differences between spatial patterns in Western Europe and North America in February and August (Fig. 6.2). Despite widespread improvements to surface water quality in both regions (Chapter 5), water scarcity increases under all scenarios. This is predominantly water quantity-driven, and is especially prevalent in the summer months. Conversely, improvements in surface water quality across the East Asia and Pacific region (Chapter 5), combined with limited changes to quantity-driven water scarcity, reduce *WSq* with respect to historical conditions.

6.2.3 Next steps

The presented water scarcity framework accounts for aspects related to both water quantity (water demands vs. renewable supply) and surface water quality (usability of water based on key thresholds for safe use). In this preliminary study, 'safe' water quality thresholds of 2,100 mg l^{-1}, 8 mg l^{-1} and 1,000 cfu 100ml^{-1} for TDS, BOD and FC, respectively, are used in the quantification of water scarcity. As water quality requirements differ by intended use (van Vliet et al., 2017; van Vliet et al., 2021), this represents a gross simplification. However, including sector-specific concentration thresholds in global assessments remains challenging due to: 1) high uncertainty as to what constitutes a 'safe' level of pollution per sector; 2) large variations in water quality requirements within individual sectors (e.g. different crop water quality requirements); and 3) large uncertainties in the water demands and withdrawals for specific (sub-)sectors, particularly in the future. A simplified approach is therefore adopted for this preliminary water scarcity assessment, using concentration thresholds that are consistent with other analyses presented in this thesis (e.g. Chapters 4 and 5). Future work should aim to advance our understanding of (sub)-sector specific water requirements from both quantity and quality perspectives, enabling improved inclusion of water quality in global clean water scarcity assessments.

Secondly, the role of unconventional water resources, which can alleviate water scarcity (van Vliet et al., 2021), is currently overlooked. This is a common oversight and a weakness of current water scarcity assessments (Vanham et al., 2018). Wastewater undergoing treatment, when to an appropriate level, can be directly reused to fulfil sector-specific water demands. Similarly, desalination can supplement existing (conventional) water supplies by making previously unusable water resources (e.g. seawater, brackish water) appropriate for fulfilling sectoral demands (Jones et al., 2019). These technologies already represent important sources of freshwater for human uses, with 95.4 million m^3 day^{-1} produced via desalination (Jones et al., 2019) and 111 million m^3 day^{-1} of treated wastewater reused (Chapter 2). Future work will aim towards the meaningful inclusion of these resources in this water scarcity assessment.

Theoretical maximum expansions in treated wastewater reuse to 4.0 billion m^3 $month^{-1}$ and desalination to 13.6 billion m^3 $month^{-1}$ could significantly reduce water scarcity levels (van Vliet et al., 2021). However, an assessment of how these technologies will change in the future under various climatic and socioeconomic scenarios is lacking. Therefore, while future scenarios of water scarcity presented in this Chapter include the impact of changes in water demands, water availability (surface and groundwater) and surface water quality under uncertain climate and socioeconomic change, the influence of changes to the use of unconventional water resources for water scarcity alleviation is overlooked. Future work will aim to quantify these changes and assess the associated impact on clean water scarcity quantifications.

6.3 Future directions: opportunities and challenges

The complexity of water quality, the diversity in constituents and uncertainties in impacts make understanding global water quality dynamics a significant challenge. With no silver bullet available to solve global water quality problems, these represent a large threat to both humans and the environment – but one that is often overlooked on account of its imperceptible nature.

Making progress to improve the quality of global surface waters is contingent upon understanding of the problem and its drivers. In this thesis, a new tool for enhancing our knowledge of global surface water quality dynamics is presented. The focus of this thesis is on modelling Tw and TDS, BOD and FC concentrations, primarily in rivers, with results mostly displayed for multi-year periods to be representative of 'average' conditions. However, the presented modelling framework has the potential to be expanded in multiple ways to help address other aspects of global surface water quality.

For example, opportunities exist for expanding the model framework to include a greater number of water quality constituents. With many pollutants having common sources, combined with the co-simulation of variables (e.g. flow velocities, water depth, water temperature) that can influence in-stream processes (e.g. decay, growth, sedimentation), the *DynQual* framework may be particularly advantageous for modelling other water quality constituents. This could include water quality constituents such as nutrients, dissolved oxygen and heavy metal concentrations, but also emerging contaminants such as pharmaceuticals, plastics and industrial chemicals. While the *DynQual* framework provides a strong technical basis for this, the major challenge here will be in the development of methods for pollutant loading estimates and for the adequate representation of pollutant specific in-stream processes. Challenges may be especially large for the emerging contaminants due to lack of knowledge on these aspects, combined with the scarce availability of observation data for model development and evaluation.

Similarly, the analysis presented in this thesis is predominantly on average conditions (e.g. monthly, annual), both in the past and future. Quantifying the impact of extreme events (floods, droughts, heatwaves) on surface water quality is, however, also key. With climate change projected to increase the frequency and magnitude of extreme events (Trenberth et al., 2014), robust understanding of these responses will become increasingly important in the future. Simulating hydrology, water temperature and pollutant concentrations with a daily timestep, *DynQual* has potential to be used for this purpose. However, the challenges posed by data scarcity in observational records of water quality are exacerbated further when considering extreme events. Similarly, a lack of temporally explicit input data for quantifying pollutant loadings and transmission pathways to surface waters is already a major challenge for large-scale water quality modelling, and one that is only amplified further under extremes. For example, contaminant pulses (i.e. large changes in pollutant loadings and concentrations over a short period) can occur under extreme conditions, due to factors such as sewer overflows, inundation and overload of wastewater treatment plants or the increased mobilisation and transport of pollutants (Kaushal et al., 2008; Whitehead et al., 2009; Kaushal et al., 2014; Miller and Hutchins, 2017; van Vliet et al., 2023). Changes to hydrological conditions (i.e. dilution capacity) under extreme events is also uncertain, particularly for low flows (Staudinger et al., 2011), yet have a strong influence over in-stream pollutant concentrations. Improved understanding and representation of these processes in hydrological and water quality models is therefore a prerequisite for applying large-scale modelling approaches to quantify the impact of extreme events on in-stream pollutant concentrations.

Therefore, while the modelling framework presented in this study has the potential to address a variety of aspects, this will not be without challenges. It should also be noted that process-based models, such as *DynQual*, are not a panacea for understanding global water quality dynamics. As advocated by the World Water Quality Alliance, more efforts are required to combine existing knowledge gained from in situ observations, remote sensing and modelling approaches via a so-called *triangulation* approach (WWQA, 2021). Improvements to the measurement and reporting of water quality are desperately required, particularly in developing countries. In situ data both provides the ground truth on which water quality assessment and management is based in its own right and is also irreplaceable for the development and evaluation of water quality models and remote sensing approaches. Open dissemination of in situ measurement data is therefore essential, yet it is often prohibited for political or economic reasons (Damania et al., 2019).

In addition to measurement data for model evaluation, the availability of good quality, freely available and easily accessible global input datasets remains one of the biggest challenges for large-scale water quality modelling approaches (UNEP, 2016). Aiming for global consistency, the large-scale water modelling community is strongly reliant on globally available datasets of socioeconomic drivers (e.g. population, urbanisation, GDP) to represent drivers of pollution.

However, the translation of these drivers into pollutant loadings introduces substantial uncertainty (Tang et al., 2019). Access to more detailed data, such as inflow and outflow concentrations at wastewater treatment plants and industrial facilities, could facilitate better estimates of pollutant loadings. In addition to the uncertainties in pollutant loading estimates, the high variability of biogeochemical processes and the propagation of prediction errors from climate and hydrological models translate into relatively large uncertainties in global water quality model output (van Griensven and Meixner, 2006; Tang et al., 2019). Better understanding and representation of processes in these models would therefore have a beneficial knock-on effect on water quality simulations. There is also high uncertainty with regards to impacts and safe thresholds of water pollutants. Robust scientific understanding of the dose-response relationships are required to inform pollution reduction plans, and therefore in for the design and implementation of measures to safeguard the quality of surface water resources for human use and environmental health. As such, it is essential to research the problem and impacts of poor surface water quality in tandem.

Successful implementation of measures to improve water quality, whether proactive (i.e. prevent or mitigate pollution at source) or reactive (i.e. treat or purify effluent before environmental discharge), is contingent upon having sufficient economic capacity, and societal and political willpower. With these factors being highly heterogenous across and within countries, effective pollution reduction schemes will require a mix of approaches. These must be tailored to the local conditions and based on risk, feasibility and cost-effectiveness. Water pollution can also be driven by far-end consumption. Globalisation has effectively enabled wealthy countries to outsource some of their pollution overseas through trade (Wan et al., 2016). Efforts that also transcend national boundaries are therefore required to address the global challenge of water pollution, which is crucial for fulfilling the UN's 2030 Agenda for Sustainable Development and to secure a safe and equitable future for all.

Appendix A | Supplementary information to Chapter 3

Supplementary to: Jones, E.R., Bierkens, M.F.P., Wanders, N., Sutanudjaja, E.H., van Beek, L.P.H., and van Vliet, M.T.H. (2023) DynQual v1.0: a high-resolution global surface water quality model. *Geoscientific Model Development, 16*, pp. 4481–4500, DOI: 10.5194/gmd-16-4481-2023

A.1 Pollutant loadings

Pollutant loadings can be either be: 1) prescribed by the user directly; or 2) calculated within the *DynQual* run by providing simple input data. When loadings are prescribed directly to the model, the user is only required to provide input files on the total (i.e. combined) pollutant loadings of TDS (in g day^{-1}), BOD (in g day^{-1}), FC (in 10^6 cfu day^{-1}) and Tw (in MW). Conversely, when pollutant loadings are calculated within *DynQual*, a variety of input data is required to reflect both pollutant emissions from sectoral activities and the transmission of pollution to the environment (Jones et al., 2022). Loadings calculated using *DynQual* are in consistent units across all sectors: g day^{-1} for TDS and BOD and 10^6 cfu day^{-1} for FC. The subsequent routing of pollutants through the stream network and the calculation of in-stream concentrations follows the same approach in both configurations.

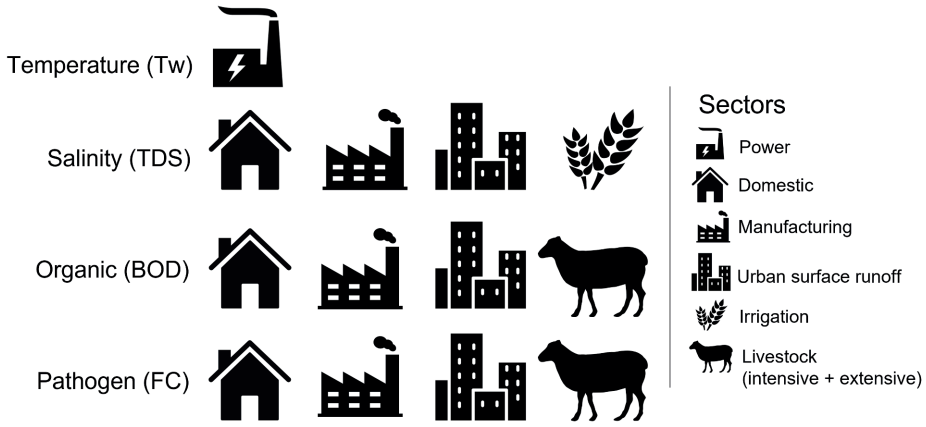

Figure A.1 Sectoral sources of salinity (TDS), organic (BOD), pathogen (FC) and temperature (Tw) pollution.

The following section describes the approach used and assumptions made for calculating pollutant loadings dynamically within a *DynQual* model run. *DynQual* considers pollutant emissions from five distinct sectors (domestic, manufacturing, livestock, irrigation and thermoelectric power generation) and from urban surface runoff (Fig. A.1). The prevalence of wastewater collection and treatment, combined with their associated pollutant removal efficiencies, are key factors controlling subsequent delivery of pollution to surface waters (Jones et al., 2022).

The fraction of pollutant loadings removed by wastewater treatment (-) are estimated for the domestic ($R_{dom,p,n}$), manufacturing ($R_{man,p,n}$) and extensive livestock ($R_{intLiv,p,n}$) sectors, and from urban surface runoff ($R_{USR,p,n}$), by multiplying the fraction of each treatment level occurring in a gridcell by the pollutant removal efficiency associated with that treatment level (Eq. A.1). For more detailed information about the development and implementation of gridcell-specific wastewater treatment practices and their inclusion in *DynQual*, we refer to previous work (Jones et al., 2021; Jones et al., 2022).

$$R_{dom,p,n} = f_{ter_n} \cdot r_{ter_p} + f_{sec_n} \cdot r_{sec_p} + f_{pri_n} \cdot r_{pri_p} + (f_{bs_n} \cdot r_{bs_p}) + (f_{od_n} \cdot (1 - s_n))$$
$$R_{man,p,n} = f_{ter_n} \cdot r_{ter_p} + f_{sec_n} \cdot r_{sec_p} + f_{pri_n} \cdot r_{pri_p}$$
$$R_{urb,p,n} = f_{ter_n} \cdot r_{ter_p} + f_{sec_n} \cdot r_{sec_p} + f_{pri_n} \cdot r_{pri_p}$$
$$R_{intLiv,p,n} = (f_{sec_n} + f_{ter_n}) \cdot r_{sec_p} \quad \text{(A.1)}$$

Where: f is the fraction of tertiary+ treatment (f_{ter_n}), secondary treatment (f_{sec_n}) and primary treatment (f_{pri_n}) within gridcell n, and r is the removal efficiency associated with teriary (r_{ter_p}), secondary (r_{sec_p}) and primary (r_{pri_p}) treatment per pollutant p. f_{bs_n} and f_{od_n} is the fraction of basic sanitation and open defecation, respectively, within gridcell n. r_{bs_p} is the reduction of pollutant p from basic sanitation collection facilities, and s_n is the gridcell-specific surface runoff fraction.

A.1.1 Domestic

Pollutant loadings from the domestic sector ($L_{dom,p,n}$) are calculated by multiplying the total population (Pop_n) in gridcell n by a regional-specific per capita excretion rate ($E_{dom,p,n}$) of pollutant p (TDS and BOD in g capita^{-1} day^{-1}; FC in cfu capita^{-1} day^{-1}) (Eq. A.2). Pollutant loadings are abated based upon gridcell-specific domestic wastewater collection and treatment practices, represented by $R_{dom,p,n}$ (-), which depends upon the wastewater pathway(s) in gridcell n and the pathway-specific removal efficiency of pollutant p (Jones et al., 2021; Jones et al., 2022).

$$\mathrm{L}_{dom,p,n} = Pop_n \cdot E_{dom,p,n} \cdot (1 - R_{dom,p,n}) \quad \text{(A.2)}$$

Gridded population data at 5 arc-min and annual temporal resolution was obtained from ISIMIP3a (Lange and Geiger, 2020). Per capita pollutant loadings are prescribed per water quality constituent at the regional scale (Table A.1). Per capita excretion rates of BOD and FC vary at the regional level due to differences in diet, climate and health status (Williams et al., 2012; UNEP, 2016). Conversely, due to a lack of more detailed data, an average global value for per capita excretion of TDS was used. Pollutant loadings per capita are based on extensive literature research conducted for previous global water quality modelling studies (UNEP, 2016; van Vliet et al., 2021) and are assumed to remain constant throughout the study period.

Table A.1 Per capita excretion rates of total dissolved solids (TDS), biological oxygen demand (BOD) and fecal coliform (FC) loadings per geographic region.

Geographic Region	Domestic		
	TDS[1] (g day^{-1} capita^{-1})	BOD[2] (g day^{-1} capita^{-1})	FC[3] (cfu day^{-1} capita^{-1})
North America	100	65	$1.3 \cdot 10^{10}$
Latin America & Caribbean	100	56	$1.4 \cdot 10^{10}$
Western Europe	100	60	$1.3 \cdot 10^{10}$
Middle East & North Africa	100	45	$1.8 \cdot 10^{10}$
Sub-Saharan Africa	100	37	$4.7 \cdot 10^{9}$
Southern Asia	100	40	$1.9 \cdot 10^{10}$
Eastern Europe & Central Asia	100	50	$1.6 \cdot 10^{10}$
East Asia & Pacific	100	50	$1.6 \cdot 10^{10}$

[1]as per UNEP (2016) & van Vliet et al., (2021); [2]as per UNEP (2016) & Williams et al., (2012); [3]as per UNEP (2016) & Reder et al., (2015)

A.1.2 Manufacturing

Pollutant loadings from the manufacturing sector ($L_{man,p,n}$) are calculated by multiplying the manufacturing wastewater flows (return flows) in gridcell n ($WW_{man,n}$ in m^3 day^{-1}) by a mean manufacturing effluent concentration ($C_{man,p,n}$) for pollutant p (TDS and BOD in mg l^{-1}; FC in cfu 100ml^{-1}) (Eq. A.3). Pollutant loadings are abated based upon gridcell-specific manufacturing wastewater collection and treatment practices, represented by $R_{man,p,n}$ (-) which depends upon the wastewater pathway(s) in gridcell n and the pathway-specific removal efficiency of pollutant p (Jones et al., 2021; Jones et al., 2022).

$$\mathrm{L}_{man,p,n} = WW_{man,n} \cdot C_{man,p,n} \cdot (1 - R_{man,p,n}) \tag{A.3}$$

As *PCR-GLOBWB2* does not distinguish explicitly between the manufacturing and thermoelectric power sectors (lumped together as the 'industrial' sector), we estimate the percentage of total industrial flows that originate specifically from manufacturing activities and apply this to *PCR-GLOBWB2* simulated industrial return flows at the country level. To make this distinction, we subtract power return flows derived from an external source (Lohrmann et al., 2019) from *PCR-GLOBWB2* industrial return flows, to provide an estimate of manufacturing return flows. We further cross-checked these estimated manufacturing return flows against a spatially-explicit municipal wastewater dataset (Jones et al., 2021).

Lacking more detailed information regarding both the specific manufacturing processes and the associated effluent quality, globally consistent effluent concentrations are applied for all manufacturing return flows worldwide (Table A.2), consistent with previous work (UNEP, 2016; van Vliet et al., 2021). Mean effluent concentrations are derived from literature review and are assumed to remain constant throughout the study period.

Table A.2 Effluent concentrations of total dissolved solids (TDS), biological oxygen demand (BOD) and fecal coliform (FC) from the manufacturing sector.

	Manufacturing[1]		
	TDS (mg l^{-1})	BOD (mg l^{-1})	FC (cfu 100ml^{-1})
Global	3000	400	$3.55 \cdot 10^6$

as per UNEP (2016) & van Vliet et al., (2021)

A.1.3 Urban surface runoff

Pollutant loadings from urban surface runoff ($L_{USR,p,n}$) are calculated by multiplying urban surface return flows ($RF_{USR,n}$ in m^3 day^{-1}) in gridcell n by a mean urban runoff effluent concentration ($C_{USR,p,n}$) for pollutant p (TDS and BOD in mg l^{-1}; FC in cfu 100ml^{-1}) (Eq. A.4). Pollutant loadings are abated based upon gridcell-specific wastewater collection and treatment practices, represented by $R_{USR,p,n}$ (-) which depends upon the wastewater pathway(s) in gridcell n and the pathway-specific removal efficiency of pollutant p (Jones et al., 2021; Jones et al., 2022).

$$\mathrm{L}_{USR,p,n} = RF_{USR,n} \cdot C_{USR,p,n} \cdot (1 - R_{USR,p,n}) \tag{A.4}$$

Urban surface runoff flows are simulated within *PCR-GLOBWB2* (Sutanudjaja et al., 2018), calculated by multiplying the fraction of the gridcell that is urban by the simulated surface runoff. Mean urban surface runoff pollutant concentrations are taken from existing work (UNEP, 2016), based on extensive literature review. TDS and BOD concentrations vary at the regional level whereas, lacking detailed data, FC is assumed to be constant across all regions (Table A.3). Mean urban surface runoff concentrations are assumed to remain constant throughout the study period.

Table A.3 Urban surface runoff total dissolved solids (TDS), biological oxygen demand (BOD) and fecal coliform (FC) mean concentrations per geographic region.

Geographic Region	Urban surface runoff[1]		
	TDS (mg l^{-1})	BOD (mg l^{-1})	FC (cfu 100ml^{-1})
North America	205	12	$1 \cdot 10^6$
Latin America & Caribbean	205	12	$1 \cdot 10^6$
Western Europe	205	12	$1 \cdot 10^6$
Middle East & North Africa	212	19	$1 \cdot 10^6$
Sub-Saharan Africa	178	62	$1 \cdot 10^6$
Southern Asia	246	105	$1 \cdot 10^6$
Eastern Europe & Central Asia	246	19	$1 \cdot 10^6$
East Asia & Pacific	246	105	$1 \cdot 10^6$

[1]as per UNEP (2016)

A.1.4 Livestock

For calculating pollutant loadings from the livestock sector, the sector is sub-divided into intensive and extensive systems based on livestock population density. For defining intensive livestock systems, a minimum threshold density of 25 livestock units per km^2 was set with one livestock unit equivalent to ~250kg (1 bovine) (Wen et al., 2017; Vigiak et al., 2019). Average animal mass equivalent coefficients were taken from literature (Robinson et al., 2011; Wen et al., 2017) to convert this threshold density into a livestock-type specific threshold density per km^2 (Table A.3) (Wen et al., 2017; Vigiak et al., 2019). Gridcells exceeding this threshold density (per livestock type) were designated as intensive livestock systems, whereas gridcells below this threshold were designated as extensive livestock systems.

Table A.4 Threshold density for designation of livestock activities as intensive systems, per livestock type.

Livestock type	Animal mass equivalent coefficient[1]	Threshold density (stock km^{-2})
Buffalo	1	25
Chicken	0.01	2500
Cow	1	25
Duck	0.01	2500
Goat	0.1	250
Horse	1	25
Pig	0.3	83
Sheep	0.1	250

[1]as per Robinson et al., (2012) & Wen et al., (2017)

The distinction between intensive and extensive livestock systems is made to account for the differences in the paths by which livestock waste (manure) enters the stream network, namely whether there is transportation by surface runoff (for extensive systems) or whether there is collection (and potentially subsequent treatment) of livestock waste (for intensive systems). Abation of collected livestock waste is all assumed to be at the same level as secondary treatment in line with Wen et al. (2017) and occurs only in gridcells where municipal wastewater treatment is also occurring. The waste is subsequently assumed to be spread to land as manure and transported to surface water via surface runoff. This approach for calculating pollutant loadings from the livestock sector is line with previous work (Wen et al., 2017; Vigiak et al., 2019).

Pollutant loadings from the livestock sector are calculated as per Eq. A.5, in line with the previous approaches for calculating pollutant loadings from intensive (Wen et al., 2017; Vigiak et al., 2019) and extensive (van Vliet et al., 2021) livestock systems.

$$L_{intLiv,p,n} = \Sigma_y(LivPop_{y,n} \cdot E_{liv,y,p,n}) \cdot (1 - R_{intLiv,p,n}) \cdot s_n$$
$$L_{extLiv,p,n} = \Sigma_y(LivPop_{y,n} \cdot E_{liv,y,p,n}) \cdot s_n \quad \text{(A.5)}$$

Where $L_{intLiv,p,n}$ and $L_{extLiv,p,n}$ represent the loadings of pollutant p in gridcell n from the intensive and extensive livestock sectors, respectively. $LivPop_{y,n}$ is the total livestock population in gridcell n per livestock type y, with 8 separate livestock types considered (buffalo, chicken, cow, duck, goat, horse, pig, sheep). $E_{liv,y,p,n}$ is the per stock excretion rate of pollutant p (BOD in g stock^{-1} day^{-1}; FC in cfu stock^{-1} day^{-1}) of livestock type y and gridcell n. S_n is the fraction surface runoff in gridcell n and $R_{intLiv,p,n}$ is the removal fraction of pollutant p due to livestock waste management practices in gridcell n (Jones et al., 2021; Jones et al., 2022).

Gridded livestock numbers at 5 arc-min are derived at the annual timescale from a global dataset for the reference year of 2010 (Gilbert et al., 2018). Thus, we do not account for intra-annual variations in livestock numbers. For the quantification of past gridded livestock numbers, a region-specific (annual) constant percentage change in the number of animals per livestock type is applied to all gridcells based on data from the FAO (Thomson, 2003) (Table A.5).

Table A.5 Annual growth in livestock type (population number) between 1999–2030 (%), applied to gridded livestock populations for 1980–2019 (Thomson 2003).

Geographic Region	Livestock type (% annual change)				
	Cattle & Buffalo	Sheeps & Goats	Pigs	Horses	Chickens & Ducks
North America	-0.1	0.2	0.1	0.0	0.6
Latin America & Caribbean	1.0	0.6	1.1	0.0	1.9
Western Europe	-0.1	0.2	0.1	0.0	0.6
Middle East & North Africa	1.5	1.0	0.0	0.0	2.1
Sub-Saharan Africa	1.1	1.2	1.4	0.0	2.2
Southern Asia	0.3	1.1	1.0	0.0	3.6
Eastern Europe & Central Asia	1.2	1.2	0.8	0.0	1.5
East Asia & Pacific	1.2	1.2	0.8	0.0	1.5

Excretion rates of BOD (Table A.6) and FC (Table A.7) per livestock type y and per region were determined through literature study, as per previous global water quality modelling studies (UNEP, 2016; van Vliet et al., 2021). Excretion rates of pollutants per livestock type is assumed constant throughout the study period.

Table A.6 Biological oxygen demand (BOD) loadings per animal per livestock type and geographic region.

Geographic Region	Biological oxygen demand (g day^{-1} $stock^{-1}$)[1]							
	Buffalo	Chicken	Cow	Duck	Goat	Horse	Pig	Sheep
North America	400	8.3	400	8.3	50	300	233	50
Latin America & Caribbean	280	8.3	280	8.3	50	300	233	35
Western Europe	400	8.3	400	8.3	50	300	233	50
Middle East & North Africa	280	8.3	280	8.3	50	300	186.4	35
Sub-Saharan Africa	240	8.3	240	8.3	50	300	186.4	35
Southern Asia	200	8.3	200	8.3	50	300	233	35
Eastern Europe & Central Asia	240	8.3	240	8.3	50	300	233	35
East Asia & Pacific	280	8.3	280	8.3	50	300	233	35

[1]as per Robinson et al., (2011), Wen et al., (2017), Vigiak et al., (2019) & van Vliet et al., (2021).

Table A.7 Fecal coliform (FC) loadings per animal per livestock type and geographic region.

Geographic Region	Fecal coliform (cfu $stock^{-1}$ day^{-1})[1]							
	Buffalo	Chicken	Cow	Duck	Goat	Horse	Pig	Sheep
North America	$1.01{\cdot}10^{11}$	$1.36{\cdot}10^{8}$	$1.01{\cdot}10^{11}$	$2.43{\cdot}10^{9}$	$1.20{\cdot}10^{9}$	$1.40{\cdot}10^{9}$	$1.08{\cdot}10^{10}$	$1.12{\cdot}10^{9}$
Latin America & Caribbean	$6.06{\cdot}10^{10}$	$1.36{\cdot}10^{8}$	$6.06{\cdot}10^{10}$	$2.43{\cdot}10^{9}$	$1.20{\cdot}10^{9}$	$1.40{\cdot}10^{9}$	$8.64{\cdot}10^{9}$	$7.84{\cdot}10^{8}$
Western Europe	$5.05{\cdot}10^{10}$	$1.36{\cdot}10^{8}$	$5.05{\cdot}10^{10}$	$2.43{\cdot}10^{9}$	$1.20{\cdot}10^{9}$	$1.40{\cdot}10^{9}$	$1.08{\cdot}10^{10}$	$7.84{\cdot}10^{8}$
Middle East & North Africa	$1.01{\cdot}10^{11}$	$1.36{\cdot}10^{8}$	$1.01{\cdot}10^{11}$	$2.43{\cdot}10^{9}$	$1.20{\cdot}10^{9}$	$1.40{\cdot}10^{9}$	$1.08{\cdot}10^{10}$	$1.12{\cdot}10^{9}$
Sub-Saharan Africa	$7.07{\cdot}10^{10}$	$1.36{\cdot}10^{8}$	$7.07{\cdot}10^{10}$	$2.43{\cdot}10^{9}$	$1.20{\cdot}10^{9}$	$1.40{\cdot}10^{9}$	$8.64{\cdot}10^{9}$	$7.84{\cdot}10^{8}$
Southern Asia	$7.07{\cdot}10^{10}$	$1.36{\cdot}10^{8}$	$7.07{\cdot}10^{10}$	$2.43{\cdot}10^{9}$	$1.20{\cdot}10^{9}$	$1.40{\cdot}10^{9}$	$1.08{\cdot}10^{10}$	$7.84{\cdot}10^{8}$
Eastern Europe & Central Asia	$6.06{\cdot}10^{10}$	$1.36{\cdot}10^{8}$	$6.06{\cdot}10^{10}$	$2.43{\cdot}10^{9}$	$1.20{\cdot}10^{9}$	$1.40{\cdot}10^{9}$	$1.08{\cdot}10^{10}$	$7.84{\cdot}10^{8}$
East Asia & Pacific	$7.07{\cdot}10^{10}$	$1.36{\cdot}10^{8}$	$7.07{\cdot}10^{10}$	$2.43{\cdot}10^{9}$	$1.20{\cdot}10^{9}$	$1.40{\cdot}10^{9}$	$1.08{\cdot}10^{10}$	$7.84{\cdot}10^{8}$

[1]as per Weaver et al., (2005) & Wilcock et al., (2006)

A.1.5 Irrigation

$$\mathrm{L}_{irr,p,n} = RF_{irr,n} \cdot C_{irr,p,n} \tag{A.6}$$

The only pollutant considered from the irrigation sector in *DynQual* is TDS. To calculate TDS from the irrigation sector, the return flows from the irrigation sector ($RF_{irr,n}$) in gridcell n is multiplied by a mean irrigation drainage concentration $C_{irr,p,n}$ for pollutant p, which for TDS is in mg l^{-1} (Eq. A.6). As irrigation runoff is rarely collected or treated (WWAP, 2017), no abation due to wastewater management practices occurs.

Irrigation return flows are simulated by *PCR-GLOBWB2*, under the assumption that withdrawn water that is not consumed (via plant transpiration and open water or soil evaporation) is lost via percolation and contributes to groundwater recharge (Sutanudjaja et al., 2018). Mean irrigation drainage concentrations are derived from the electrical conductivity (dS m^{-1}) averaged over the topsoil (0–30cm) and subsoil (30–100cm) at 0.5^0 resolution from the ISRIC-WISE global soil database (Batjes, 2005), as per previous work (van Vliet et al., 2021). Electrical conductivity (EC) is converted to TDS using a TDS/EC ratio for freshwater of 0.7 (Walton, 1989). Mean irrigation drainage concentration is assumed to be constant throughout the study period.

A.1.6 Power

The only pollutant considered from the thermoelectric power sector is water temperature (Tw). Thermal pollution (heat dumps) from the power sector (Eq. A.7) is calculated based on a spatially-explicit powerplant database containing 13,506 powerplants with detailed information on fuel type and cooling type, representing an estimated 87% of the global thermoelectric capacity in 2015 (Lohrmann et al., 2019).

$$\mathrm{L}_{pow,Tw,n} = \rho_w \cdot C_p \cdot RF_{pow,n} \cdot \Delta T_{pow_{rf}} \tag{A.7}$$

Where $L_{pow,Tw,n}$ is the heat dump from thermoelectric powerplants (W) in gridcell n, C_p is the specific heat capacity of water (4,190 J kg^{-1} K^{-1}), ρ_w is the density of fresh water (1,000 kg m^{-3}), $RF_{pow,n}$ is the return flows of cooling water (m^3 s^{-1}) in gridcell n and $\Delta T_{pow_{rf}}$ is the difference in water temperature between the return flows and ambient river water (K).

Water withdrawals and consumption per powerplant are from a spatially explicit powerplant dataset (Lohrmann et al., 2019). These estimates are quantified as a function of plant capacity, load hours and water use intensity, which depends primarily on fuel type and cooling system. The dataset considers five types of cooling systems (wet cooling towers, dry cooling systems, inlet cooling systems, once through cooling and recirculating cooling-pond systems) and four fuel types (nuclear, coal, gas and oil). Power return flows $RF_{pow,n}$ are subsequently calculated by subtracting water consumption from the water withdrawal. We aggregated these power return flows at the gridcell level (5 arc-min) and delineate them in time based upon the construction year of the powerplant. The construction year is derived by cross-referencing powerplant coordinates with information from various other sources (http://GlobalEnergyObservatory.org/; https://datasets.wri.org/dataset/globalpowerplantdatabase).

A range of values for $\Delta T_{pow_{rf}}$ were found in the literature, varying from between 3 K based upon maximum permissible limits for powerplants in the US as per the Clean Water Act (van Vliet et al., 2012b) to 10 K from once-through systems in the USA in summer months between 2001–2005 (Madden et al., 2013). We selected an intermediate value of 7 K for $\Delta T_{pow_{rf}}$, as this falls within the range of reported values in the literature and matches well with more recent global thermal emission rates of ~480 GW (Raptis et al., 2016). Results of a sensitivity analysis also suggests that values for $\Delta T_{pow_{rf}}$ of between 3–7 K have relatively moderate impacts on simulated water temperature in thermally polluted basins (van Vliet et al., 2012b).

A.1.7 Combined sectoral loadings

Sectoral loadings of each water quality constituent per gridcell n are converted into consistent units (MW for Tw; g day^{-1} for TDS and BOD; 10^6 cfu day^{-1} for FC) and aggregated across the contributing sectors, with $L_{TDS,n}$, $L_{BOD,n}$, $L_{FC,n}$, $L_{Tw,n}$ representing the combined local TDS, BOD, FC and Tw loads in gridcell n (Eq. A.8).

$$\begin{aligned}
L_{TDS,n} &= L_{dom,TDS,n} + L_{man,TDS,n} + L_{USR,TDS,n} + L_{irr,TDS,n} \\
L_{BOD,n} &= L_{dom,BOD,n} + L_{man,BOD,n} + L_{USR,BOD,n} + L_{intLiv,BOD,n} + L_{extLiv,BOD,n} \\
L_{FC,n} &= L_{dom,FC,n} + L_{man,FC,n} + L_{USR,FC,n} + L_{intLiv,FC,n} + L_{extLiv,FC,n} \\
L_{Tw,n} &= L_{pow,Tw,n}
\end{aligned} \tag{A.8}$$

A.2 Implementation of water quality equations

DynQual uses a numerical scheme (time-explicit fine differences) to simulate the routing of both water and pollutants through the surface water network (based on a local drain direction map), including in-stream processes, with a sub-daily timestep.

The length of the time interval (Δt_n in seconds) is estimated with respect to both channel storage and discharge (Eq. A.9). This ensures that the length of the time interval is small enough to ensure that flow from gridcell n only flows into the immediately downstream gridcell $n+1$, and not further (i.e. $\Delta t_n > T_n$, where T_n represents the residence time of gridcell n).

$$\Delta t_n = \frac{h_n \cdot A_n \cdot (\frac{w_n \cdot l_n}{A_n})}{Q_n} \tag{A.9}$$

Where h_n is the water height (m), A_n is the gridcell area (m^2), w_n is the channel width (m), l_n is the channel length (m) and Q_n is the discharge (m^3 day^{-1}) simulated at the sub-daily timestep using the simplified kinematic wave routing, all in gridcell n.

While Δt_n is initially initially determined per individual gridcell, the shortest calculated interval is used consistently for all gridcells within the simulation extent (Δt). We also set a maximum time-interval (Δt) of 720s (i.e. to ensure that the routing procedure happens at least once every 12 minutes). While we could further increase the numerical accuracy of our simulations by introducing shorter time intervals, this also increases computational times, and thus a balance must be struck (Loucks and van Beek, 2017). More information on the implementation of water quality equations within *DynQual* is available in the open-access model code (https://github.com/UU-Hydro/DYNQUAL).

A.3 Model validation

A.3.1 Water quality observations

Tw and BOD data was downloaded from the Global River Water Quality Archive (GRQA) (Virro et al., 2021), which aggregates data from a variety of datasets including GEMStat (Global Freshwater Quality Database) (UNEP, 2019), GLORICH (GLObal River CHemistry) (Hartmann et al., 2014) and WQP (Water Quality Portal) (Read et al., 2017). Electrical conductivity (EC) data was obtained from a global surface water database (Thorslund and van Vliet, 2020), which we additionally supplemented with GEMStat data (UNEP, 2019), and converted to TDS using a conversion factor of 0.7 (Walton, 1989). FC data was obtained from GEMStat (UNEP, 2019), additionally supplemented with data from the National Water Information System (NWIS) from the United States Geological Survey (USGS). The total number of water quality modelling stations and associated observations collated for *DynQual* validation is presented in Table A.8. The number of stations with >30 and >90 measurements across the time period 1980–2019 and the associated number of observations are also presented (Table A.8).

Table A.8 Number of water quality monitoring stations and measurements used for *DynQual* model validation.

Constituent	All stations		Stations > 30 obs		Stations > 90 obs	
	N Stations	N Obs	N Stations	N Obs	N Stations	N Obs
Tw	22,990	841,781	7,312	729,813	2,194	474,567
TDS	31,509	6,809,700	26,615	6,722,775	10,494	5,921,049
BOD	12,604	312,019	2,735	233,169	636	133,106
FC	7,917	246,652	2,263	213,705	863	136,961

Both the number of water quality monitoring stations and the length of the observation record are highly unequally distributed across space (Fig. A.2). Spatial patterns are relatively consistent across all four water quality constituents. North America is by far the most data-rich world region, with 45%, 76%, 62% and 92% of all monitoring stations for Tw, TDS, BOD and FC located in this region, respectively, accounting for 39%, 32%, 50% and 83% of the total number of observations, respectively. Observations made across Western Europe account for 28%, 14% and 4% of Tw, BOD and FC of the total data availability, respectively, but just 3% of the TDS observations. Conversely, 58% of total TDS observations are from the East Asia and Pacific region, but just 14%, 7% and 3% of the Tw, BOD and FC observations, respectively. However strong spatial biases within individual regions must also be considered, particularly for TDS observations in East Asia and Pacific where >99% of these observations are from Australia. The Latin America and Caribbean region also accounts for a small but significant share of total Tw, TDS, BOD and FC observations, at 13%, 1%, 15% and 3% of total observations, respectively.

Data is extremely scarce across other world regions, especially when also considering the length of observation records (Fig. A.2). While there are some localised pockets of high data availability in different regions (e.g. TDS measurements in South Africa), publicly accessible observational data records are mostly non-existent. For example, the number of stations in Sub-Saharan Africa with >30 observations of Tw, BOD and FC is just 10, 1 and 1, respectively. When considering stations with >90 observations, these numbers drop to 6, 1 and 0. Similar patterns in data availability are observed for the Middle East and North Africa and Southern Asia regions.

The spatial biases in the observed data, combined with data availability issues in general (especially for BOD and FC), provide acute challenges for the evaluation of global water quality models across different world regions (Appendix A.3.2).

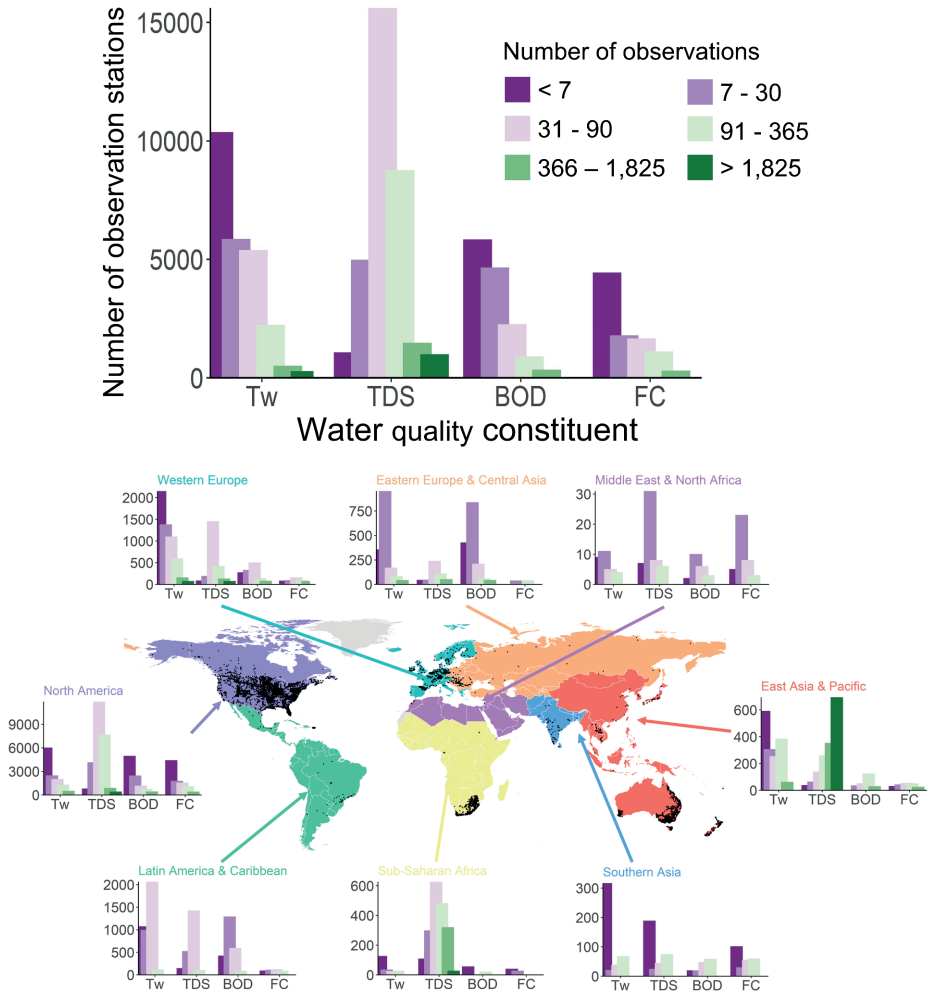

Figure A.2 Number of surface water quality monitoring stations per world region, disaggregated by the total number of observations made at each site from 1980–2019. Black dots on the map display the locations of water quality monitoring stations with > 90 observations of any water quality constituent. Please note that different numbers are used on the vertical axis for bar charts displaying the number of observation stations for different world regions.

A.3.2 Model evaluation

Concentration classes

As per Jones et al. (2022), we evaluate model performance for TDS, BOD and FC with respect to pollutant classes linked to key sectoral water quality thresholds (Table A.9), which are derived from extensive literature research (UNEP, 2016). TDS thresholds are based upon irrigation water quality standards (Fipps, 2003; Zaman et al., 2018), with < 525 mg l^{-1} designated as 'good', 525–2,100 mg l^{-1} as 'permissible to doubtful' and > 2,100 mg l^{-1} as 'unsuitable'. BOD thresholds are linked to environmental standards, with < 4 mg l^{-1} designating low pollution ('sufficient oxygen and high species diversity'), 4–8 mg l^{-1} designating moderate pollution ('suspended discharges occur but have no major effect on biota') and > 8 mg l^{-1} designating high pollution ('depletion of oxygen can result in fish kills') (UNEP, 2016). FC thresholds are based upon human health concerns related to direct contact, with high pollution designated as >1,000 cfu 100ml^{-1} ('unsuitable for direct human contact'), and < 200 cfu 100ml^{-1} representing no risk to human health (UNEP, 2016).

Table A.9 Total dissolved solids (TDS), biological oxygen demand (BOD) and fecal coliform (FC) concentration thresholds denoting the pollution status of a freshwater body as 'low', 'moderate' or 'high'.

Pollutant Status	TDS (mg l^{-1})	BOD (mg l^{-1})	FC (cfu 100ml^{-1})
Low	< 525	< 4	< 200
Medium	525 – 2,100	4 – 8	200 – 1,000
High	> 2,100	> 8	> 1,000

Statistical evaluation metrics

For Tw, model performance is evaluated statistically using the Kling-Gupta efficiency (KGE) coefficient (Eq. A.10) (Gupta et al., 2009).

$$KGE = 1 - \sqrt{(r-1)^2 + (\alpha-1)^2 + (\beta-1)^2} \tag{A.10}$$

Where r is the linear correlation between observations and simulations, is a measure of the flow variability error, and a bias term. KGE values of 1 indicate perfect agreement between observations and simulations, while KGE values exceeding -0.4 indicate that a model improved upon a mean benchmark (Knoben et al., 2019).

Spatial patterns in KGE for water temperature simulations by *DynQual* are displayed in Fig. A.3 and are described in the manuscript.

Time-series and average annual cycles

Supplementing the time-series and average annual cycles displayed in the manuscript (Fig. 3.5), results from additional stations are presented for Tw (Fig. A.5), TDS (Fig. A.6), BOD (Fig. A.7) and FC (Fig. A.8).

For TDS, BOD and FC, model performance is evaluated statistically using the root mean square error normalised by the mean (nRMSE) (Eq. A.11).

$$\mathrm{n}RMSE = \frac{\sqrt{\frac{\sum_{i=1}^{N}(Sim_i - Obs_i)^2}{n}}}{\overline{Obs}} \tag{A.11}$$

Patterns in nRMSE for TDS, BOD and FC simulations are displayed in Fig. A.4 and are described in the manuscript.

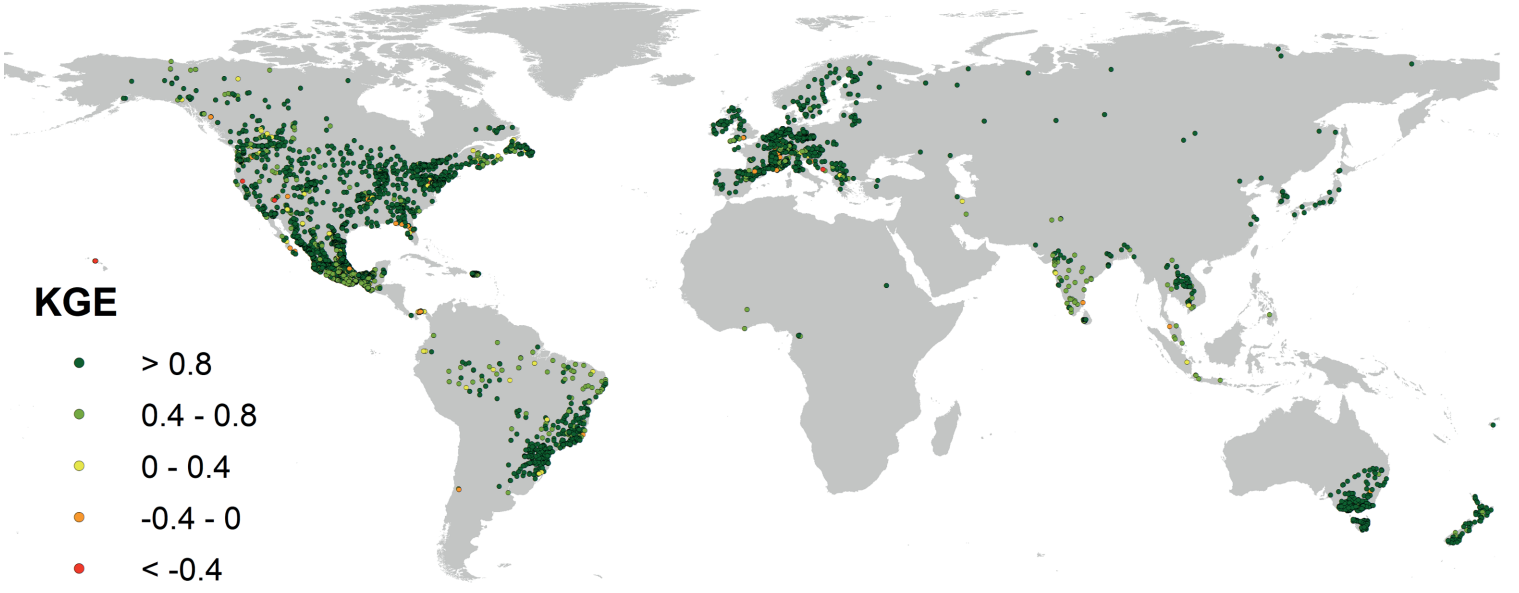

Figure A.3 Spatial validation of water temperature (Tw) observations versus simulations using the Kling-Gupta efficiency (KGE) at for observation stations with > 30 observations over 1980–2019.

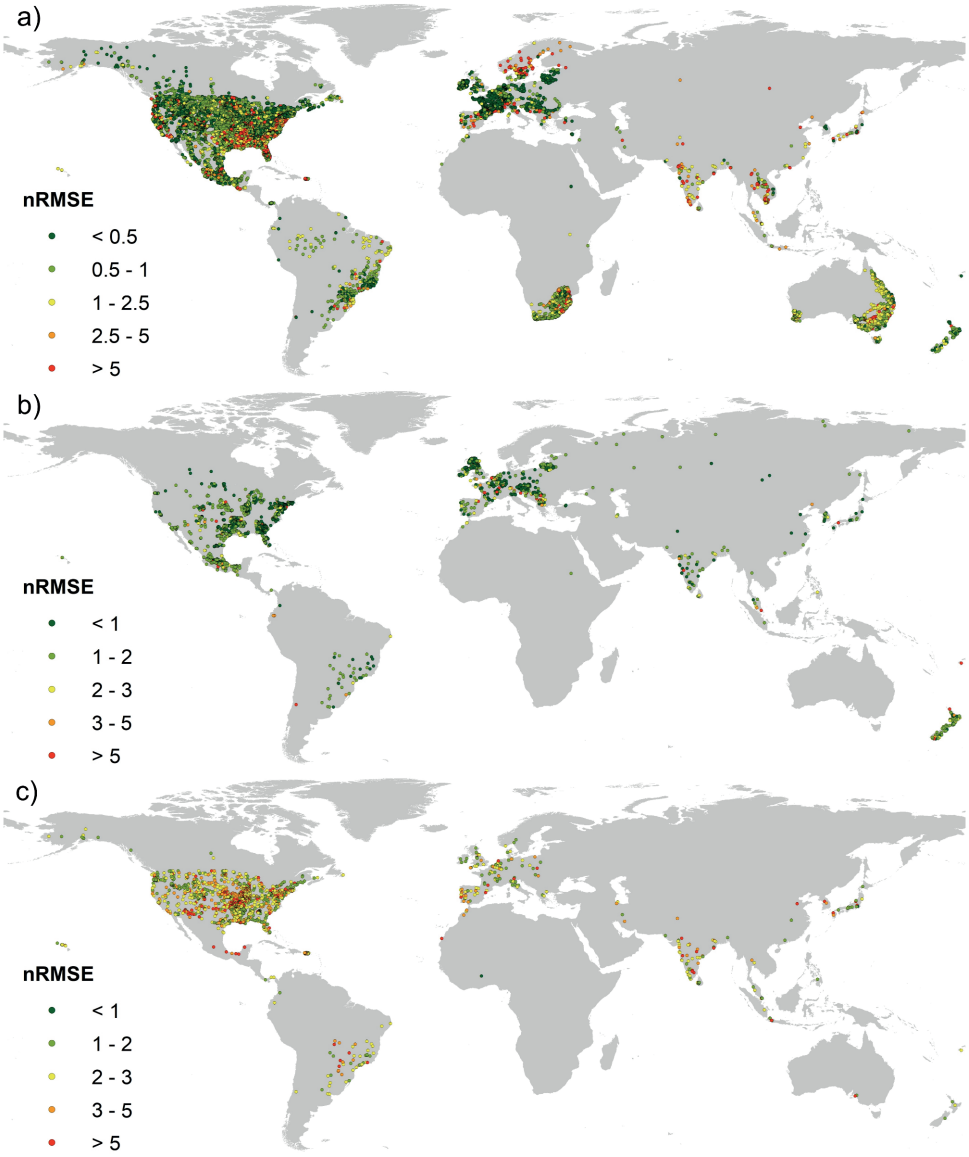

Figure A.4 Spatial validation of a) total dissolved solids (TDS); b) biological oxygen demand; and c) fecal coliform (FC) observations versus simulations using the normalised root mean square error (nRMSE) at for observation stations with > 30 observations over 1980–2019.

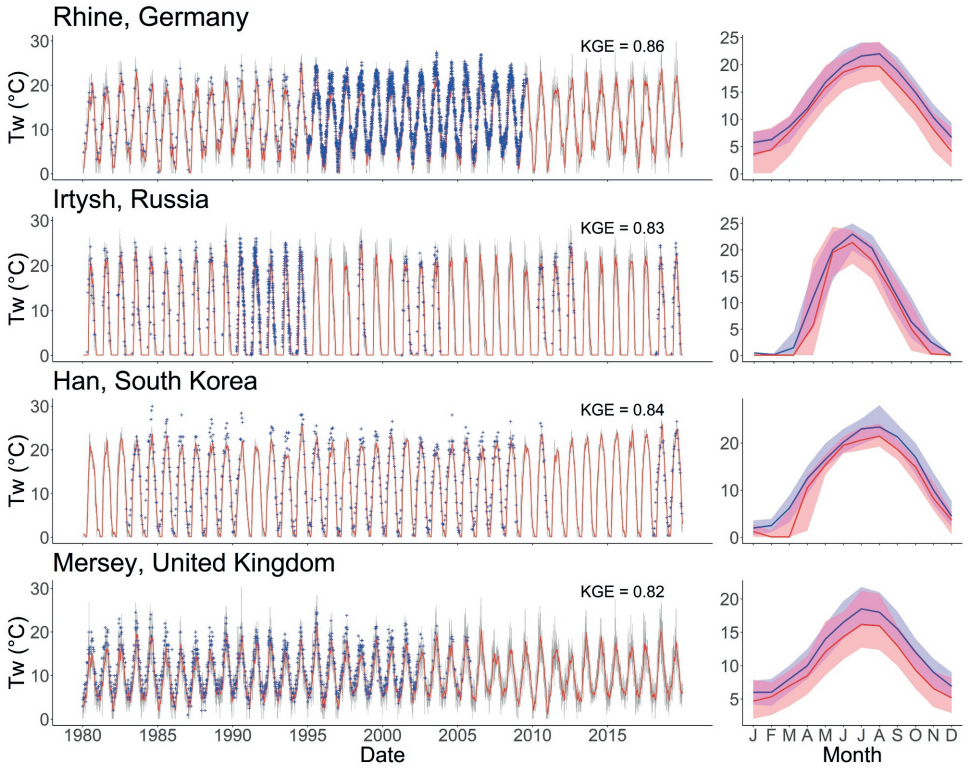

Figure A.5 Time-series (left) and average annual cycles (right) of observed versus simulated water temperature (°C) at four selected monitoring stations. In the time-series plots, observations are indicated by blue crosses, daily simulations by grey lines and 30 day running averages by red lines. In the average annual cycles plots, blue and red lines indicated the median observed and simulated water temperature, respectively, while the shading represents the range in water temperatures as indicated by the 10th and 90th percentiles.

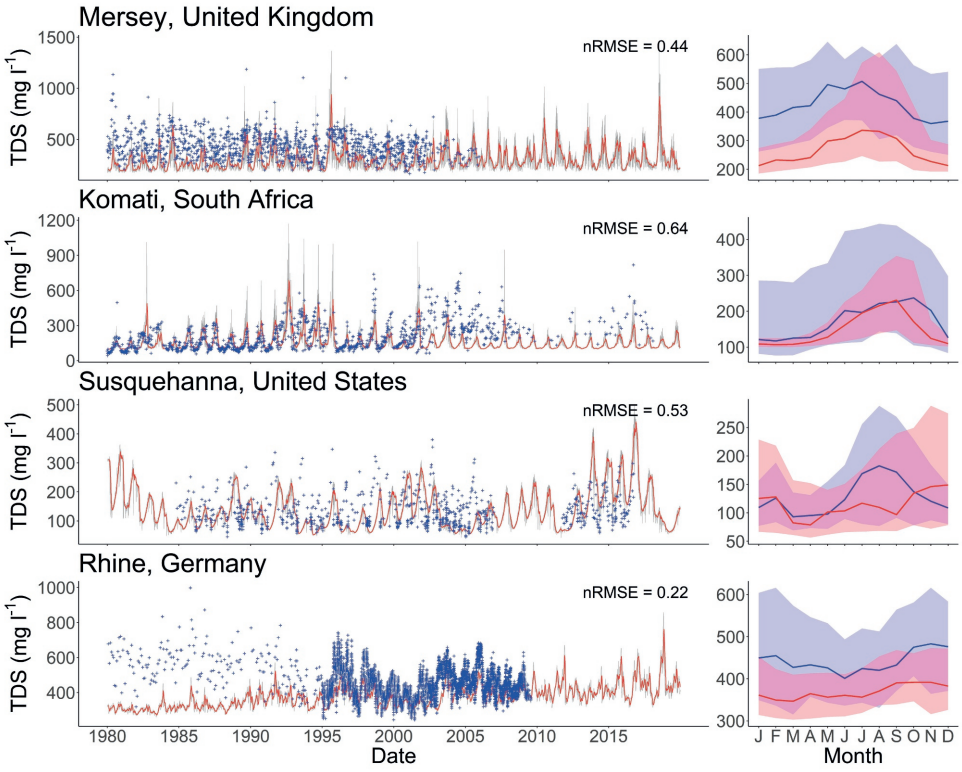

Figure A.6 Time-series (left) and average annual cycles (right) of observed versus simulated total dissolved solids (TDS) concentrations (mg l^{-1}) at four selected monitoring stations. In the time-series plots, observations are indicated by blue crosses, daily simulations by grey lines and 30 day running averages by red lines. In the average annual cycles plots, blue and red lines indicated the median observed and simulated concentrations, respectively, while the shading represents the range in concentrations as indicated by the 10th and 90th percentiles.

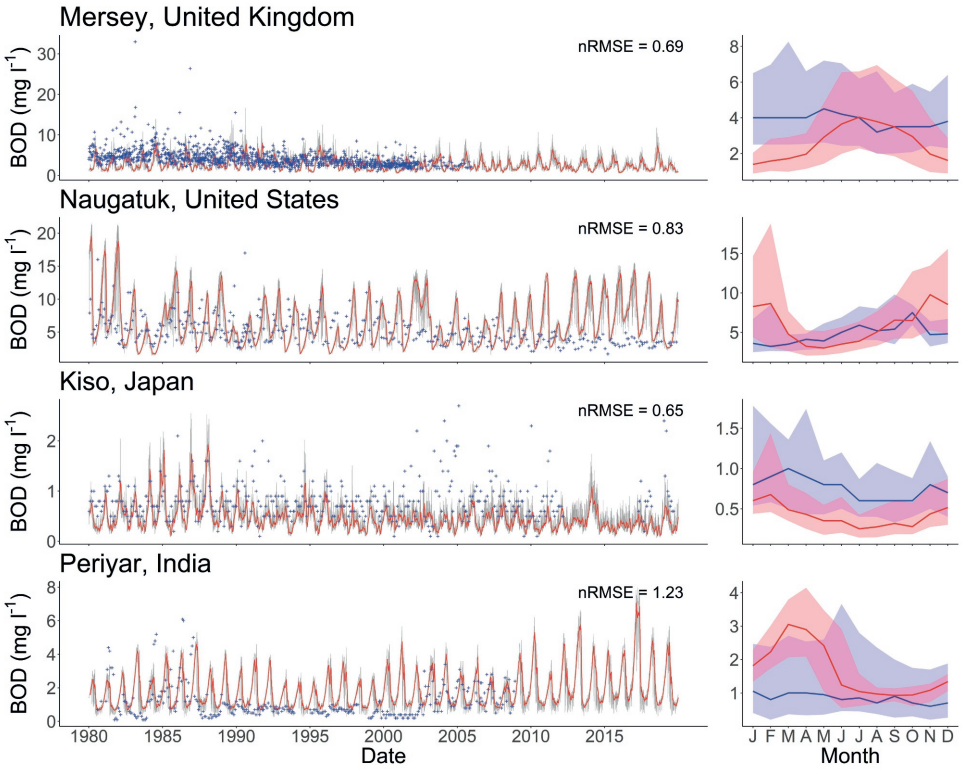

Figure A.7 Time-series (left) and average annual cycles (right) of observed versus simulated biological oxygen demand (BOD) concentrations (mg l^{-1}) at four selected monitoring stations. In the time-series plots, observations are indicated by blue crosses, daily simulations by grey lines and 30 day running averages by red lines. In the average annual cycles plots, blue and red lines indicated the median observed and simulated concentrations, respectively, while the shading represents the range in concentrations as indicated by the 10th and 90th percentiles.

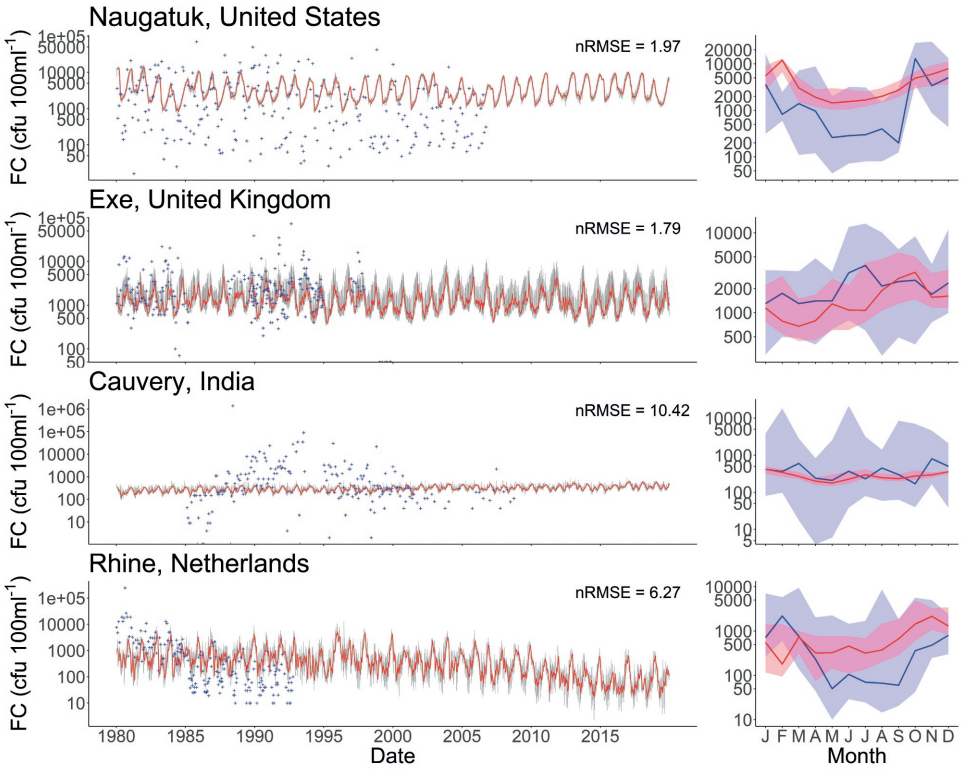

Figure A.8 Time-series (left) and average annual cycles (right) of observed versus simulated fecal coliform (FC) concentrations (cfu $100ml^{-1}$) at four selected monitoring stations. In the time-series plots, observations are indicated by blue crosses, daily simulations by grey lines and 30 day running averages by red lines. In the average annual cycles plots, blue and red lines indicated the median observed and simulated concentrations, respectively, while the shading represents the range in concentrations as indicated by the 10th and 90th percentiles.

A.3.3 Examples of issues in observational records

To evaluate the performance of DynQual, data from ~57,000 individual water quality monitoring stations was collated from various data sources (Appendix A.3.1). While this is beneficial for having a greater number of observations, this procedure also introduces additional challenges for model evaluation. We illustrate some examples of issues within the observational records themselves in Fig. A.9, including a) artefacts in data records; b) issues related to detection limits or reporting accuracies; and c) large variability in the observational records.

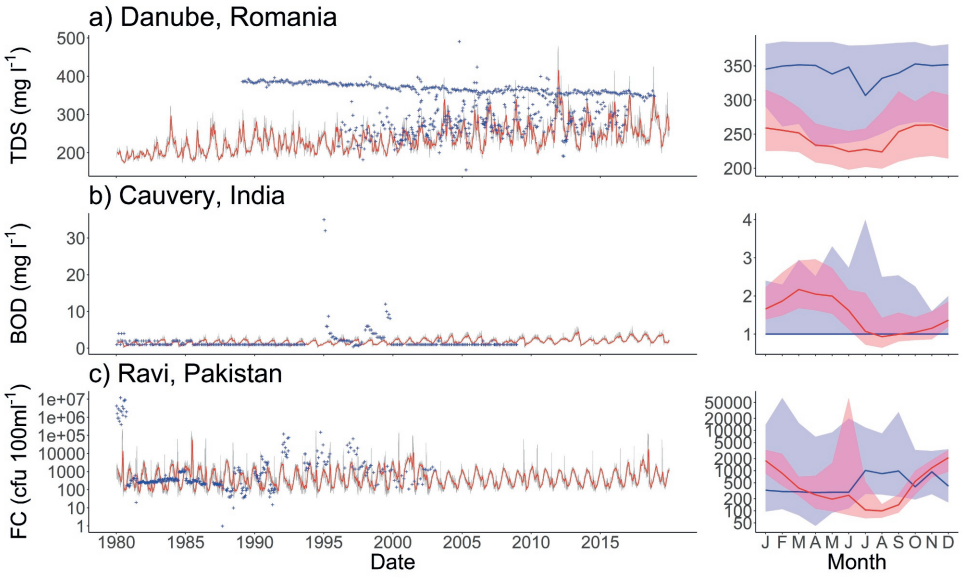

Figure A.9 Examples of challenges associated with observation data when evaluating global surface water quality models: a) artefacts in the data; b) detection limits or reporting accuracy; c) large variability in the observed record.

Appendix B | Supplementary information to Chapter 4

Supplementary to: Jones, E.R., Bierkens, M.F.P., Wanders, N., Sutanudjaja, E.H., van Beek, L.P.H. & van Vliet, M.T.H. (2022) Current wastewater treatment targets are insufficient to protect surface water quality. *Communications Earth & Environment, 3(1)*, pp. 1–8, DOI: 10.1038/s43247-022-00554-y .

B.1 Pollutant loading calculations

We have developed a new water quality model, named *DynQual*, to simulate surface water temperature (Tw), salinity (total dissolved solids; TDS), organic pollution (biochemical oxygen demand; BOD) and pathogen pollution (fecal coliform; FC). These water quality constituents are selected because they are key in constraining different sector water uses and ecosystem health (Dumont et al., 2012; Damania et al., 2019), and most of these water quality constituents are also part of SDG indicator 6.3.2 ('Proportion of bodies of water with good ambient water quality').

Sector specific pollutants loadings of Tw, TDS, BOD and FC are calculated at the monthly timestep for the years 1980–2030. Historical socioeconomic data (e.g. population, GDP) (Jones and O'Neill, 2016) and hydrological data from the *PCR-GLOBWB2* hydrology and water resources model (Sutanudjaja et al., 2018) are used as basis for pollutant loading calculations. W5E5 v2.0 forcing data is used for the historical period from 1980–2015 (Cucchi et al., 2020), whereas data from 2016–2030 are based on future projections associated with RCP 7.0 and SSP 3 (Fujimori et al., 2017; Lange et al., 2021), representing an intermediate-high emissions and development scenario. We simulate water quantity and quality using forcing from the five GCMs included in ISIMIP3b (Lange et al., 2021), namely GFDL-ESM4, IPSL-CM6A- LR, MPI-ESM1-2-HR, MRI-ESM2-0, UKESM1-0-LL, which is bias corrected using W5E5 v2.0 as the observational reference dataset (Cucchi et al., 2020; Lange et al., 2021). It should also be noted that there is low variability in both greenhouse gas concentrations and socioeconomic drivers (e.g. population, GDP) associated with the different RCPs and SSPs up until 2030, with significant deviations occurring mainly beyond our chosen study period. An overview of the sectoral pollutant loadings per water quality constituent is provided in Fig. B.1.

The overarching approaches for calculating sector-specific pollutant loadings for Tw (van Vliet et al., 2012b; van Vliet et al., 2021), TDS (Williams et al., 2012; UNEP, 2016; van Vliet et al., 2021), BOD (Williams et al., 2012; UNEP, 2016; Wen et al., 2017; Vigiak et al., 2019; van Vliet et al., 2021) and FC (Reder et al., 2015; UNEP, 2016) loadings closely follow previous work. Loadings from the domestic sector are calculated by multiplying the gridded population numbers (Jones and O'Neill, 2016) with a (regional-specific) per capita excretion rate derived from previous work (UNEP, 2016; van Vliet et al., 2021). Pollutant loadings from the manufacturing sector are calculated by multiplying gridded manufacturing wastewater flows with a mean manufacturing effluent concentration derived from previous work (UNEP, 2016; van Vliet et al., 2021). As *PCR-GLOBWB2* does not simulate manufacturing return flows directly, and rather 'industrial' flows (which combines the manufacturing and power sectors), we subtract power return flows, derived from an external source (Lohrmann et al., 2019), as an estimate of manufacturing return flows.

Pollutant loadings from urban surface runoff are calculated by multiplying gridcell-specific urban surface return flows, as simulated by *PCR-GLOBWB2* on 5x5 arcminutes, with a mean urban runoff effluent concentration, derived from previous studies (UNEP, 2016). Following Wen et al. (2017), we sub-divide the livestock sector into 'intensive' and 'extensive' systems based on livestock density to account for differences in the paths by which livestock waste enters the stream network. A minimum threshold density of 25 livestock units per km^2 was set with one livestock unit equivalent to $\sim$250kg (1 bovine) with average animal mass equivalent coefficients from literature (Robinson et al., 2011; Wen et al., 2017; Vigiak et al., 2019). Gridcells exceeding this threshold density (per livestock type) were designated as intensive livestock systems, whereas gridcells below this threshold were designated as extensive livestock systems. Gridded livestock numbers for buffalo, chickens, cows, ducks, goats, horses, pigs and sheep are obtained from a 5 arc-min global dataset for the reference year of 2010 (Gilbert et al., 2018), with a region-specific constant percentage change in the number of animals per livestock type applied to gridcells based on data from the FAO (Bruinsma, 2003). Livestock numbers are multiplied by excretion rates per livestock type and per region, obtained from previous work (UNEP, 2016; van Vliet et al., 2021). To calculate TDS from the irrigation sector, return flows from

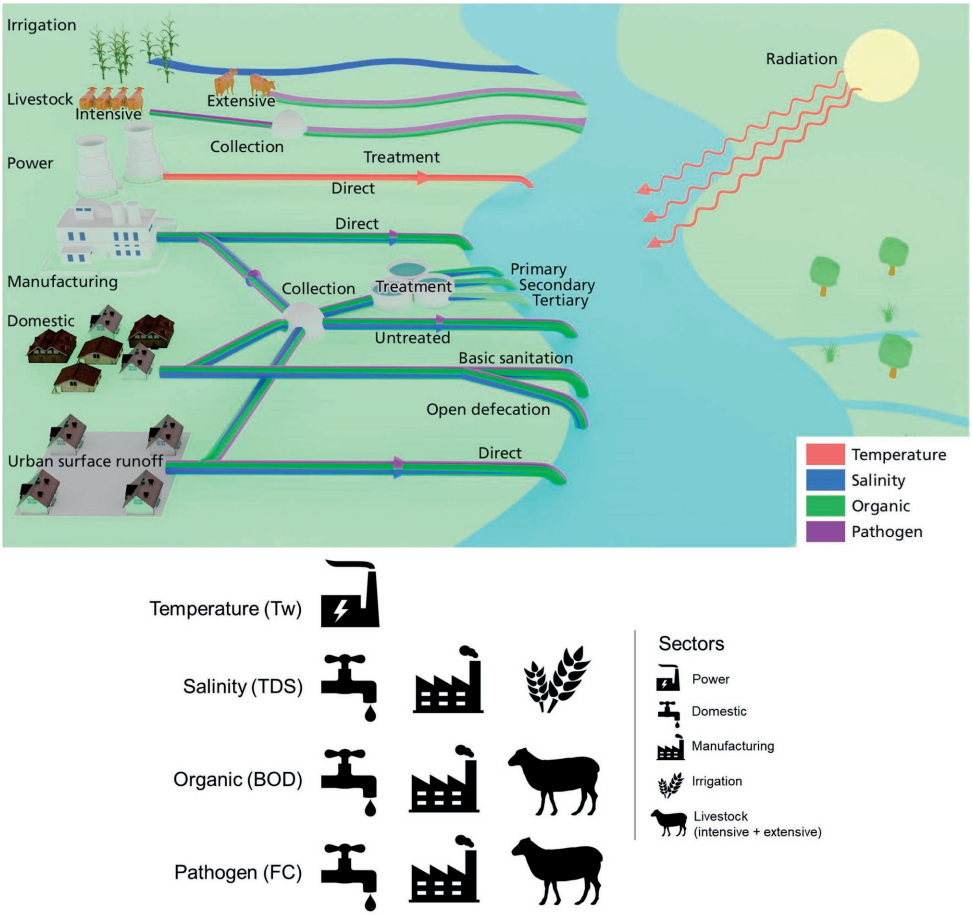

Figure B.1 Sources of salinity (TDS), organic (BOD), pathogen (FC) and temperature (Tw) pollution by sector and including wastewater management pathways.

the irrigation sector, calculated by *PCR-GLOBWB2*, were multiplied by a mean irrigation drainage concentration (TDS in mg l^{-1}). The mean irrigation drainage concentration is derived from the electrical conductivity (dS m^{-1}) averaged over the topsoil (0–30cm) and subsoil (30–100cm) at 0.5x0.5 degree spatial resolution from the ISRIC-65 WISE global soil database (Batjes, 2005), as per previous work (van Vliet et al., 2021). Lastly, thermal pollution (heat dumps) from the thermoelectric power sector were calculated based on a spatially-explicit powerplant database with detailed information on fuel and cooling system type (Lohrmann et al., 2019). Return flows from powerplants, calculated by subtracting water consumption from water withdrawal, are multiplied by the specific heat capacity of water (4,190 J kg^{-1} K^{-1}), the density of freshwater (1,000 kg m^{-3}) and the difference in water temperature between return flows and ambient river water (assumed to be 7 K) to obtain spatially-explicit estimates of thermal pollution (van Vliet et al., 2012b; van Vliet et al., 2021).

The path by which contaminated wastewater re-enters the environment can have a large influence on the eventual pollutant loading to the stream, especially where systems of wastewater collection and treatment exist. Pollutant loadings from the domestic, manufacturing and intensive livestock sectors, as well as from urban surface runoff, are abated based on gridcell-specific wastewater collection and

treatment practices. This is implemented per sector by multiplying by the complement of the removal ratio, the calculations of which are detailed in Section B.4 (Eqs. B.1–B.5). As irrigation runoff is rarely collected or treated, no abatement due to wastewater management practices occurs (WWAP, 2017). Similarly, no abatement in temperature loadings from the thermoelectric power sector are considered due to wastewater management practices.

Thermoelectric power generation is the only sectoral activity that is considered as a source of temperature loadings and we therefore display the gridded heat dumps from thermoelectric powerplants for the year 2015 in Fig. B.2. For other pollutants, gridded (5 arc-min) pollutant loadings of each water quality constituent are aggregated over the contributing sectors to give a total pollutant load per gridcell. The spatial distribution of combined pollutant loadings and the sector-specific loadings per geographical region, averaged for the year 2015, are displayed for salinity pollution as indicated by TDS (Fig. B.3), organic pollution as indicated by BOD (Fig. B.4) and pathogen pollution as indicated by FC (Fig. B.5).

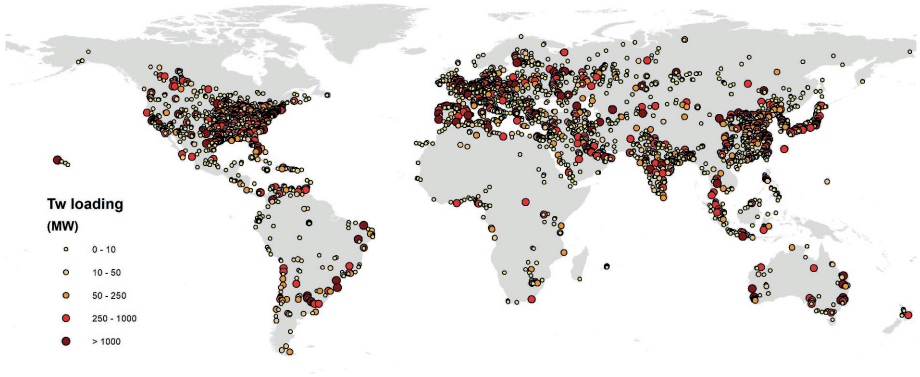

Figure B.2 Gridded heat dumps from thermoelectric powerplants (MW) in 2015.

The geographic locations of temperature pollution (Fig. B.2) match the point locations of thermoelectric powerplants (Lohrmann et al., 2019), which are located across much of the developed world, particularly in North America, Western Europe and Eastern China. Temperature loadings from individual powerplants depend upon factors including powerplant size (i.e. volume of return flows), cooling system technology and fuel type. These factors differ both within and across world regions, particularly related to the year that the powerplant was commissioned. Generally, thermoelectric powerplants are less prevalent across Sub-Saharan Africa, whereby energy demands are lower and mostly fulfilled by hydro-electric power, and unpopulated continental areas such as Australian Outback and the Tibetan Plateau.

Gridded TDS loadings (in 10^3 kg day^{-1}) are displayed in Fig. B.3a. Across most world regions, TDS loadings are dominated by the irrigation (e.g. Southern Asia, Middle East and North Africa) and manufacturing (e.g. Western Europe, North America) sectors (Fig. B.3b). The location of loadings within countries and regions strongly reflects these activities – with the heavily irrigated areas of Northern India and the large cities of North America and Europe clearly visible as salinity hotspots. A combination of both irrigation and manufacturing activities contribute to the high TDS loadings seen across China, thus high TDS loadings are more ubiquitous across the country. With the exception of the major cities of South America and Africa, and the lower Nile, TDS loadings across these regions are relatively low.

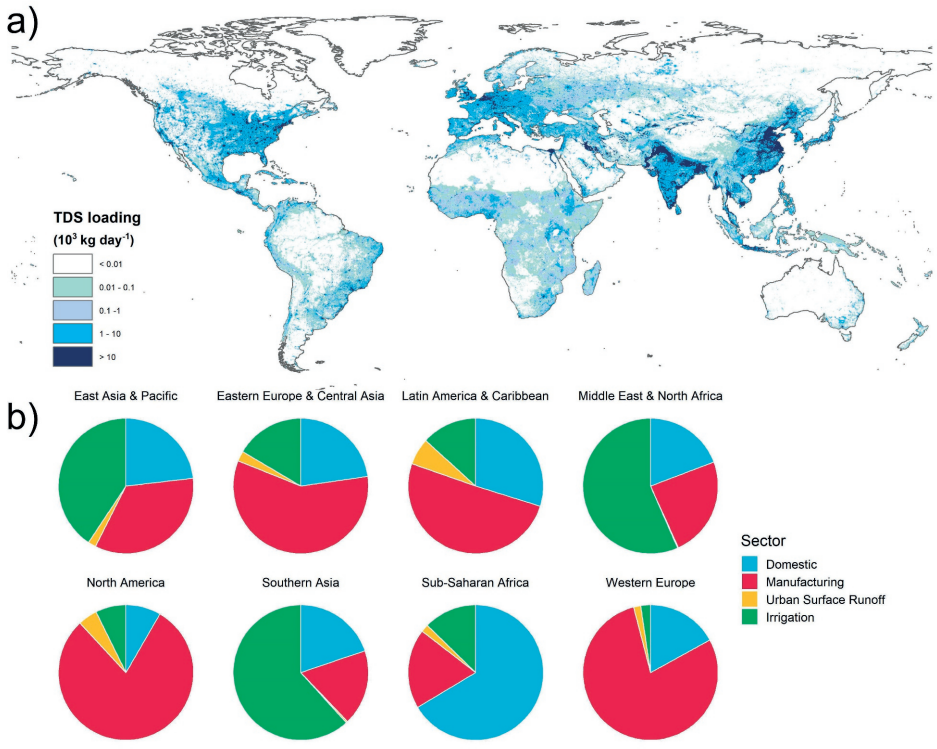

Figure B.3 a) Average TDS loadings averaged for 2015 from all contributing sectors at 5 arc-min spatial resolution; and b) sector-specific contributions aggregated per region.

Spatial patterns in BOD loadings (Fig. B.4a) are closely related to of the distribution of urban and livestock activities, but also to wastewater treatment rates (Fig. B.12), with dominant sectoral sources varying slightly across different regions (Fig. B.4b). Generally, the proportional contribution of the domestic sector is highest in regions with low wastewater treatment rates (e.g. Southern Asia, Sub-Saharan Africa). The manufacturing sector dominates BOD loadings in North America, despite high wastewater treatment rates. In most world regions, extensive livestock systems contribute a significant proportion of BOD loadings – however it should be noted these are typically spread out over large geographical extents.

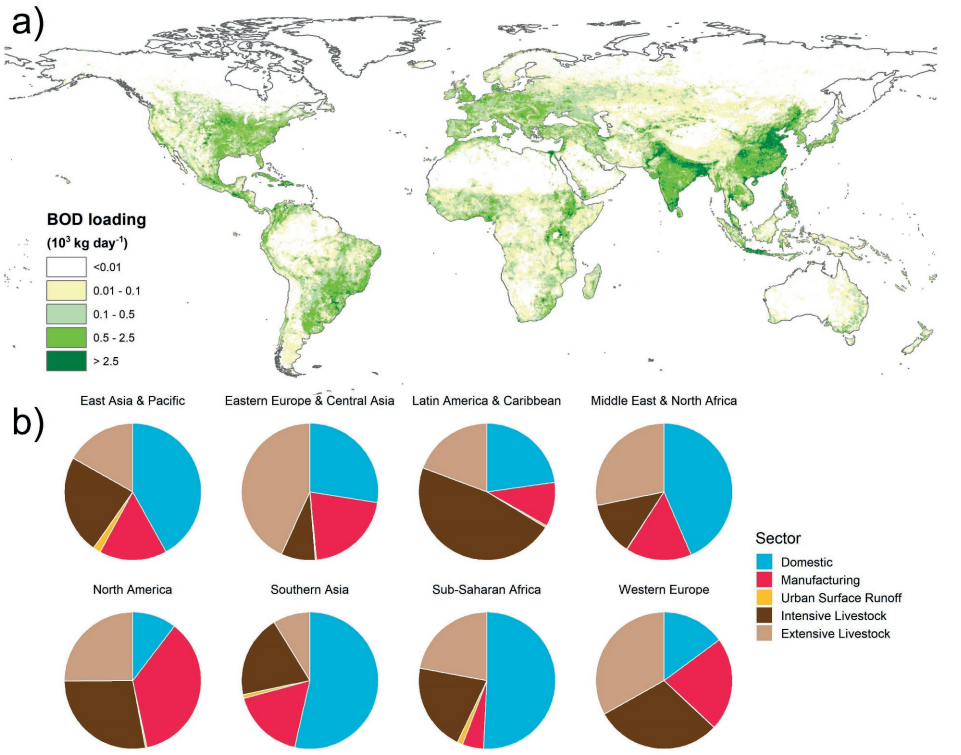

Figure B.4 a) Average BOD loadings averaged for 2015 from all contributing sectors at 5 arc-min spatial resolution; and b) sector-specific contributions aggregated per region.

Spatial patterns in FC loadings (Fig. B.5a) closely match patterns in BOD loadings, attributed to common sources of organic and pathogen pollution and contributing sectors. Again, geographical patterns in FC are strongly influenced by wastewater treatment pathways and levels (Fig. B.12). Compared to BOD loadings, FC loadings are more strongly dominated by the domestic sector across all world regions (Fig. B.5b). Besides the domestic sector, intensive and extensive livestock activities are the major sources of FC pollution across most world regions.

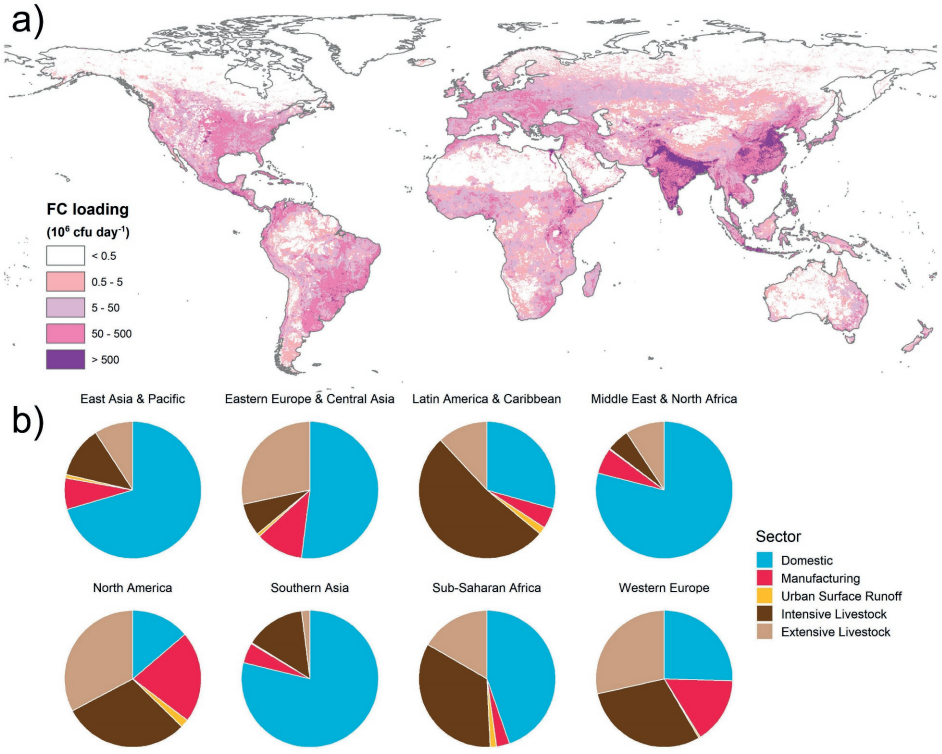

Figure B.5 a) Average FC loadings averaged for 2015 from all contributing sectors at 5 arc-min spatial resolution; and b) sector-specific contributions aggregated per region.

The emissions and pollutant loadings differ substantially, both in magnitude and by sectoral sources, across geographic regions (Fig. B.6). Highest pollutant loading estimates are typically found in Southern Asia and East Asia and Pacific regions, with highest TDS loadings originating from the irrigation sector and BOD and FC loadings from domestic and intensive livestock production sectors. The domestic sector is the dominant contributor of BOD and FC loads in East Asia and Pacific and Southern Asia in particular, resulting from a combination of large populations and relatively low wastewater treatment rates (Jones et al., 2021). Municipal sewerage systems that are not connected to wastewater treatment also act as large point sources of BOD and FC (UNEP, 2016; Jones et al., 2021), which is commonplace in Southern Asia (51% of collected wastewater is untreated) and in Latin America and the Caribbean (61% of collected wastewater is untreated) (Jones et al., 2021). Loadings of BOD and FC are notably lower in Western Europe and North America, relative to population size, where wastewater treatment practices are more widespread and typically have higher removal efficiencies (Section B.4, Fig. B.12, Table B.4). TDS loadings in these world regions are also more dominated by the manufacturing sector opposed to irrigation activities.

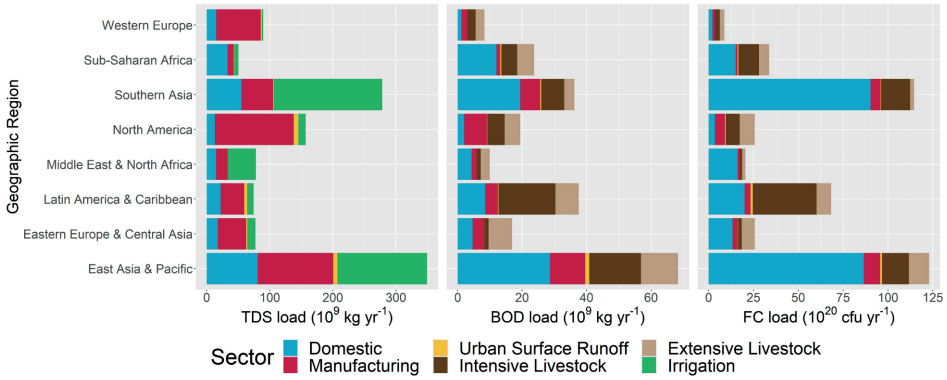

Figure B.6 Sector-specific contributions (aggregated per region) to pollutant loadings for salinity (total dissolved solids; TDS), organic pollution (biological oxygen demand; BOD) and pathogen pollution (fecal coliform; FC) averaged for 2015.

B.2 In-stream water quality

Water temperature is simulated building on the method developed for *DynWat*, solving the surface water energy balance at the daily timestep and at 5 arc-min spatial resolution (van Beek et al., 2012; Wanders et al., 2019). The exchange of heat between the atmosphere and the river is a key determinant of river temperature in naturalized river systems (Wanders et al., 2019). *DynWat* also accounts for surface water abstraction, reservoirs, riverine flooding and the formation of ice (Wanders et al., 2019). Impacts of from heat effluents of thermoelectric powerplants are also included as advected heat sources, following previous work (van Vliet et al., 2012b; van Vliet et al., 2021).

While pollutant loadings are used to quantify the mass of pollutant that is discharged to surface waters in a given period of time, in-stream concentrations represent the mass of pollutant in a defined volume of water. Salinity (TDS) is modelled using a mass balance and conservative substances approach, relating TDS concentrations in a downstream gridcell to concentrations in upstream gridcells, assuming instantaneous full mixing of all streamflow and wastewater flows in each gridcell and including dilution (van Vliet et al., 2021). Organic (BOD) and pathogen (FC) pollution are modelled using a non-conservative mass balance approach, equally relating pollutant loadings in a downstream gridcell to concentrations in upstream gridcells and assuming instantaneous full mixing of all streamflow and wastewater flows in the gridcell. BOD decay during downstream transport is simulated as a function of water temperature, following previous assessments (Wen et al., 2017; van Vliet et al., 2021). FC bacteria decay during downstream transport is simulated as a function of solar radiation, water temperature and the settling rate of bacteria (sedimentation) (Reder et al., 2015; UNEP, 2016). Water quality equations to simulate daily TDS (mg l^{-1}), BOD (mg l^{-1}) and FC (cfu 100 ml^{-1}) concentrations are implemented within the modelling framework of *DynWat* (van Beek et al., 2012; Wanders et al., 2019), with a spatial resolution of 5 arc-min. For numerical stability, a sub-timestep was used for both solving the surface water energy balance (for Tw) and for pollutant loading routing (of TDS, BOD and FC) (Wanders et al., 2019).

Aside from pollutant loadings from the different human sectors, background processes can also be important determinants of in-stream water quality. All surface waters contain a natural concentration of salts, with variations in geology, soils, climate and vegetation causing variations in background salinity of freshwater systems to span over at least two orders of magnitude (Olson and Hawkins, 2012). Background TDS concentrations are inferred based on minimum observed EC-converted to TDS data (Walton, 1989), contained in a new global salinity dataset (Thorslund and van Vliet, 2020), with spatial interpolation for pixels without observed data conducted using ordinary kriging.

Complementing Fig. 4.1, Fig. B.7 displays the percentage of gridcells within each geographical region that exceed a water quality threshold for high pollution (Table B.2) and the number of months of exceedance. All geographical regions experience frequent exceedances across the considered water quality constituents. Exceedances of TDS thresholds are particularly common across Southern Asia, while more limited in the East Europe and Central Asia region. Exceedance patterns in BOD and FC are closely related, attributed to common sectoral sources of pollution. It should however be noted that these results display the proportion of gridcells exceeding water quality thresholds, and thus are not directly linked to water availability or surface water abstractions in the region for which we refer to Fig. 4.4.

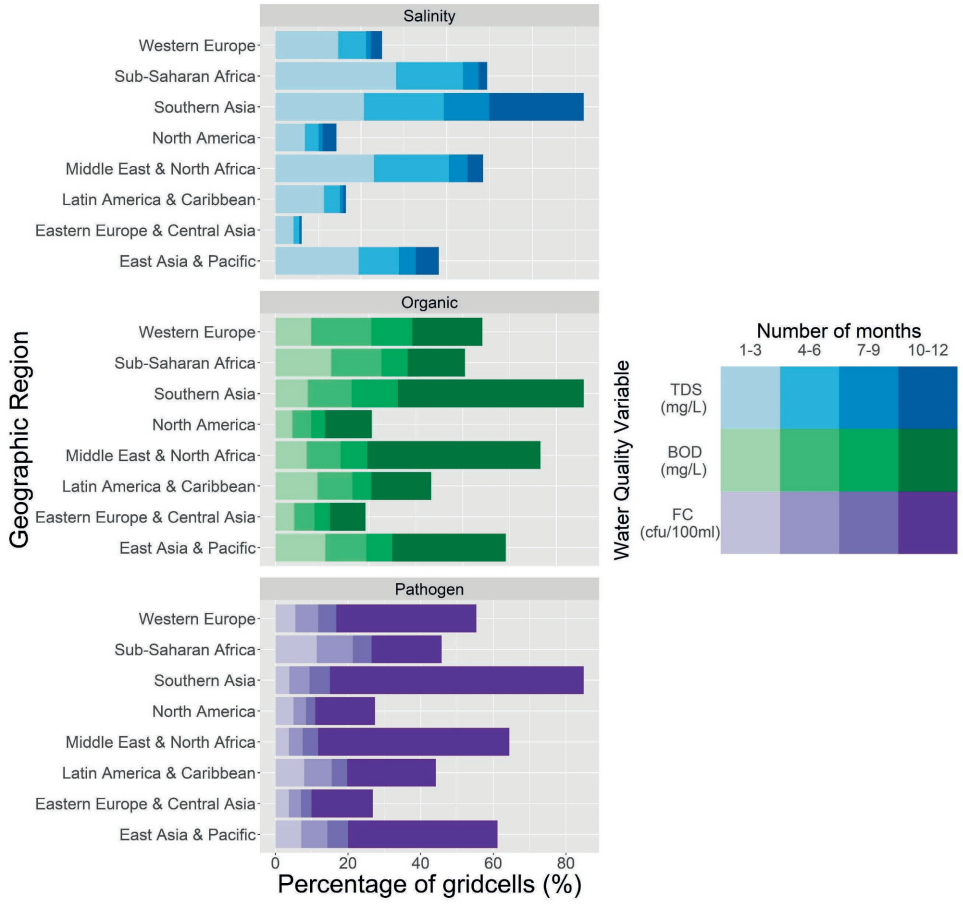

Figure B.7 Percentage of gridcells (average annual discharge >1 $m^3\ s^{-1}$) exceeding critical water quality thresholds (high pollution; see Table B.2) for salinity (TDS; 2,100 mg l^{-1}), organic (BOD; 8 mg l^{-1}) and pathogen (FC; 1,000 cfu $100ml^{-1}$) averaged for 2005–2014. Water quality threshold exceedance are assessed at monthly temporal resolution.

B.3 Model validation

For model validation, observed water quality data was obtained from the Global Environment Monitoring System for freshwater (GEMS/Water), part of the United Nations Environment Programme (UNEP, 2019). Observed water temperature (Tw) and salinity (EC), organic (BOD) and pathogen (FC) concentrations were downloaded from all water quality monitoring stations with > 30 measurements in the time period 1980–2014. Observed EC measurements were subsequently converted to TDS using a conversion factor of 0.7, following Walton (1989). The number of water quality modelling stations meeting this criteria, together with the total number of measurements aggregated at the regional level is presented in Table B.1. The spatial distribution of water quality monitoring stations can be inferred from Fig. B.8 and Fig. B.9.

Table B.1 Number of water quality monitoring stations and measurements considered per water quality constituent, aggregated per geographic region.

	Temperature (Tw)		Salinity (EC)		Organic (BOD)		Pathogen (FC)	
	N stations	N Obs	N stations	N Obs	N stations	N Obs	N stations	N Obs
Global	711	119,106	903	137,346	529	78,988	340	36,825
Geographic Region								
Western Europe	208	33,186	216	30,077	180	23,397	115	9,746
Sub-Saharan Africa	3	199	21	8,171	1	110	1	34
Southern Asia	84	14,182	85	13,833	84	14,117	79	11,096
North America	40	5,803	199	26,630	2	172	27	2,206
Middle East & North Africa	7	740	7	774	7	673	5	472
Latin America & Caribbean	148	13,209	135	10,800	87	8,029	71	6,584
Eastern Europe & Central Asia	42	13,482	16	4,901	42	11,331	8	1,413
East Asia & Pacific	179	38,373	224	42,160	126	21,159	34	5,274

We assess the performance of Tw simulations statistically by calculating normalised Root Mean Square error (nRMSE) and qualitatively using a confusion matrix (Fig. B.8). Observed water temperatures closely match model simulations, with nRMSE values of below 0.25 at 68% of stations and below 0.5 at 94% of stations. nRMSE values indicate particularly strong performance at monitoring stations located across South America, Europe, India and Japan. Poorer model performance occurs especially in high-latitude rivers. The confusion matrix demonstrates that, in the majority of cases, water temperature simulations are within 5°C of observed temperatures. Very few cases of large mismatches between observations and simulations occur. For an in-depth validation of the water temperature model, excluding thermoelectric powerplants as an additional source of heat, we refer to the original *DynWat* publications (van Beek et al., 2012; Wanders et al., 2019).

We assess model performance for TDS, BOD and FC statistically by calculating Kling Gupta Efficiency (KGE) coefficients, a widely used metric for evaluating the performance of hydrological model output 30. We chose KGE, as opposed to nRMSE (as used for Tw) due to the importance of the hydrological simulations for calculating in-stream concentrations of TDS, BOD and FC. KGE values greater than -0.41 indicate that a model improves upon using the mean as a benchmark, up to a theoretical maximum of 1 if simulations exactly match observations (Knoben et al., 2019). The three KGE terms (correlation, variability bias and mean bias) can be weighted to allow specification of the relative importance of each term based on the application (Gupta et al., 2009; Knoben et al., 2019). In this study, we opt for a weighting scheme of 0.2, 0.4 and 0.4 for correlation, variability bias and mean bias, respectively. We reduce the relative importance of correlation (timing) with respect to the other terms as we validate at the daily timestep, whereby in-stream concentrations are sensitive to short-term fluctuations in water availability (channel storage).

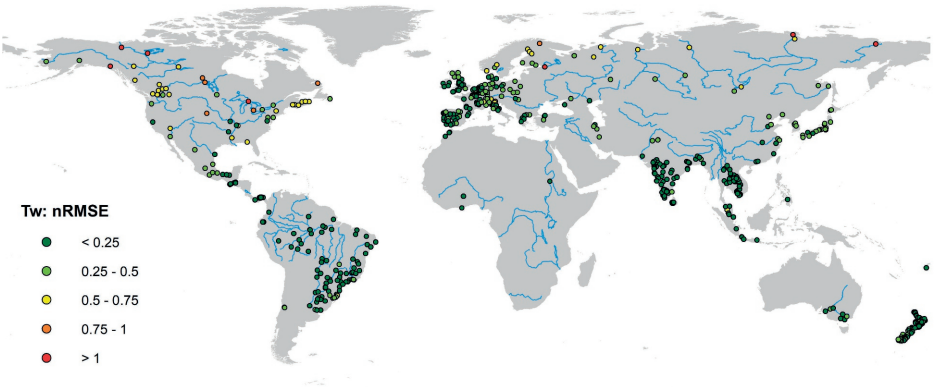

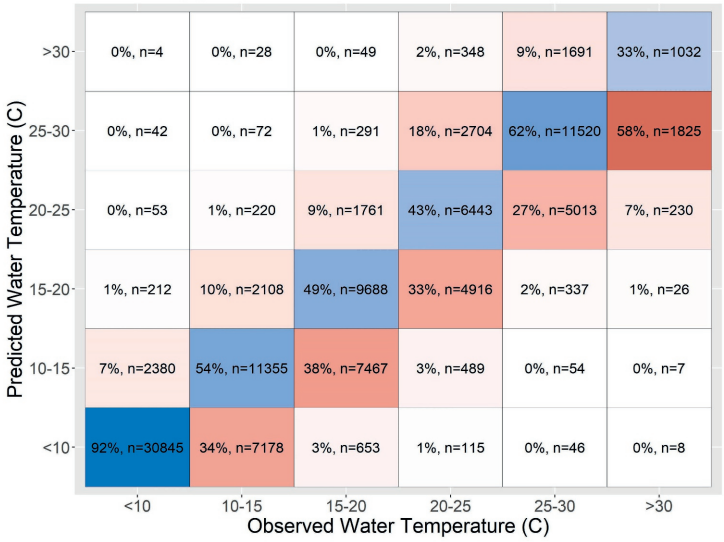

Figure B.8 Calculated normalised root mean square error (nRMSE) coefficients and confusion matrix for water temperature.

For TDS, BOD and FC, we also evaluate model performance with respect to pollutant classes, which are linked to key sectoral water quality thresholds (Table B.2) imposed by governments and international organisations. In-stream concentrations are translated into pollutant classes that denote 'low', 'moderate' and 'high' pollution status for freshwater bodies, based upon sectoral water use or environmental water quality thresholds.

Table B.2 TDS, BOD and FC concentration thresholds denoting the pollution status of a freshwater body as low, moderate or high.

Pollutant status	Total dissolved solids (TDS; mg l^{-1})	Biological oxygen demand (BOD; mg l^{-1})	Fecal coliform (FC; cfu 100 ml^{-1})
Low pollution	< 525	< 4	<100
Moderate pollution	525 - 2100	4 - 8	100 - 1000
High pollution	> 2100	> 8	> 1000

The water quality thresholds associated with pollutant classes, which are derived from extensive literature research (UNEP, 2016), considered in this study are shown in Table B.2. Salinity thresholds used are based upon irrigation water quality standards (Fipps, 2003; Zaman et al., 2018), which classify TDS concentrations below 525 mg l^{-1} as 'good', 525–2,100 mg l^{-1} as 'permissible-to-doubtful' and >2,100 mg l^{-1} as 'unsuitable'. These standards also closely reflect those recommended by the FAO (Ayers and Westcot, 1985). For organic pollution, we follow the threshold classifications used by UNEP (UNEP, 2016) which are based on analysis of water quality standards in 11 countries. BOD concentrations below 4 mg l^{-1} are designated as 'low pollution' (sufficient oxygen supply and high species diversity), 4–8 mg l^{-1} as 'moderate pollution' (suspended discharges occur but have no major effect on biota) and > 8 mg l^{-1} as 'high pollution' (depletion of dissolved oxygen can result in fish kills). Our selected thresholds are also in a similar range as to those used in other studies, which have used 5 mg l^{-1} as indicative of high pollution based on adverse effects to the domestic sector and to ecosystem health (Wen et al., 2017; van Vliet et al., 2021). For pathogen pollution, we also closely follow thresholds developed by UNEP (2016) which are based on analysis of water quality standards in 17 countries. These standards are primarily based on concentrations that pose human health concerns associated with direct contact. FC concentrations above 1,000 cfu $100ml^{-1}$ are deemed unsuitable for contact, thus used in this study as the threshold level for 'high pollution'. We take a slightly more stringent concentration range of 100–1,000 cfu 100 ml^{-1} to designate moderate pollution, opposed to 200 cfu $100ml^{-1}$ as used by UNEP (2016), based on the interim criteria for recreational waters (Bartram and Rees, 1999). Beneath 100 cfu $100ml^{-1}$ is considered in this study as indicative of 'low pollution'.

Overall, calculated Kling Gupta Efficiency coefficients indicate reasonable model performance (Fig. B.9). In line with other studies, the best validation results are achieved for TDS, followed by BOD and then FC (UNEP, 2016; van Vliet et al., 2021). For TDS, KGE coefficients exceed 0.4 in 65% of stations and are below -0.41 in only 22% of cases. For BOD and FC, KGE coefficients of > 0.4 are calculated at 42% and 33% of stations, respectively. KGE values below -0.41, indicating very low agreement between observed and simulated concentrations, occur at 27% and 18% of monitoring stations, respectively.

Overall, a very strong correspondence between simulation and observed performance for simulated versus observed pollutant classes is found for TDS and BOD, indicating strong model performance (Fig. B.9). The model simulates the same pollutant class as the observed pollutant class in 84% and 75% of cases for TDS and BOD, respectively. When considering ±1 pollutant class, these numbers rise to 98% and 91%, respectively. Simulated versus observed pollutant classes are less well simulated for FC, with just 41% of simulated pollutant classes exactly matching observations. When also considering ±1 pollutant class, this rises to 79%.

As displayed in Fig. B.9, the poorest model performance obtained in this study is for FC. We attribute this to a combination of both uncertainty in the modelling approach, including both quantification of pollutant loadings and decay processes (Reder et al., 2015), and uncertainties in reported FC concentrations. FC concentrations that span across all three pollutant classes (i.e. observations that are <100, 100–1,000 and >1,000) are present in the data in 74% of water quality stations, and 88% of water quality monitoring stations report FC concentrations ranging over three or more orders of magnitude. To illustrate this, we present the time-series for modelled and observed fecal coliform concentrations at three water quality monitoring stations (Fig. B.10). These plots display that while, in general, the model is able to model observations within the correct concentration range, it underestimates the temporal variability represented by the measured timeseries data – especially when measured concentrations are low.

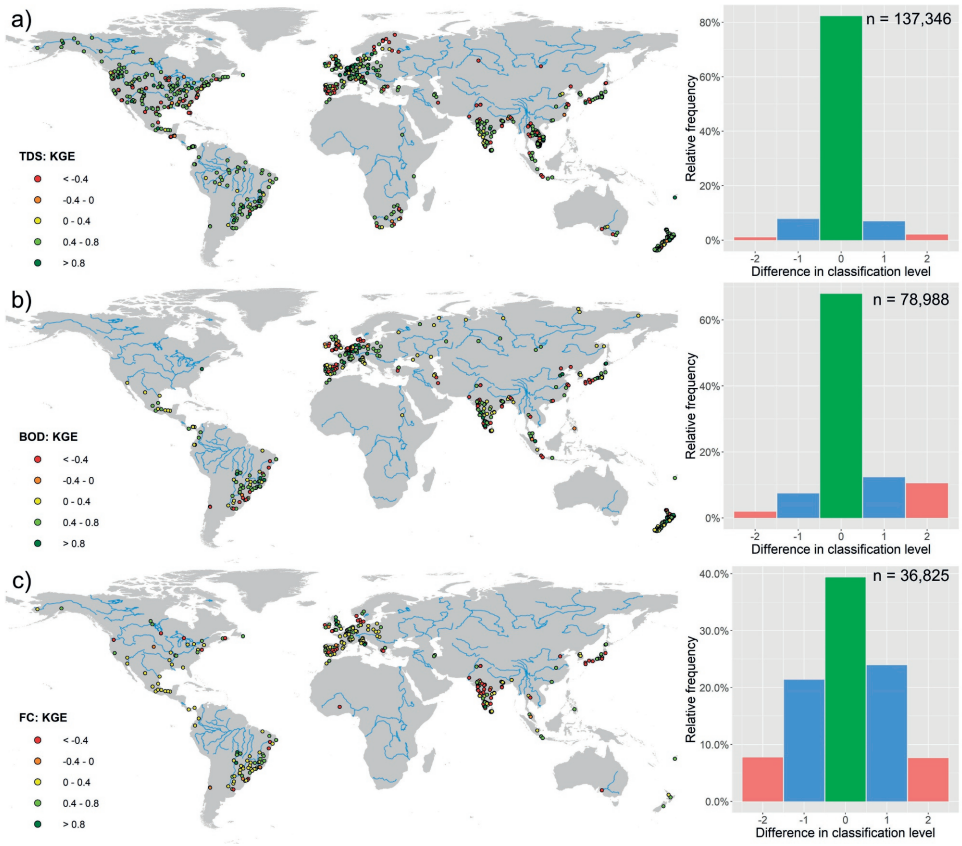

Figure B.9 Calculated Kling Gupta Efficiency (KGE) coefficients and differences in observed and simulated pollutant classes for a) TDS; b) BOD; and c) FC. Pollutant classes are defined based on thresholds imposed by governmental bodies and international organisations, separated into three classes, and are as follows: TDS (mg l^{-1}): < 525, 525–2,100, >2,100; BOD (mg l^{-1}): < 4, 4–8, >8; FC (cfu $100ml^{-1}$): < 100, 100–1,000, >1,000. A difference in classification level of '0' indicates no difference in pollutant class between simulations and observations, negative differences indicate that the observed concentration was higher than the simulated concentration, and positive differences indicate that simulated concentration was higher than the observed concentration.

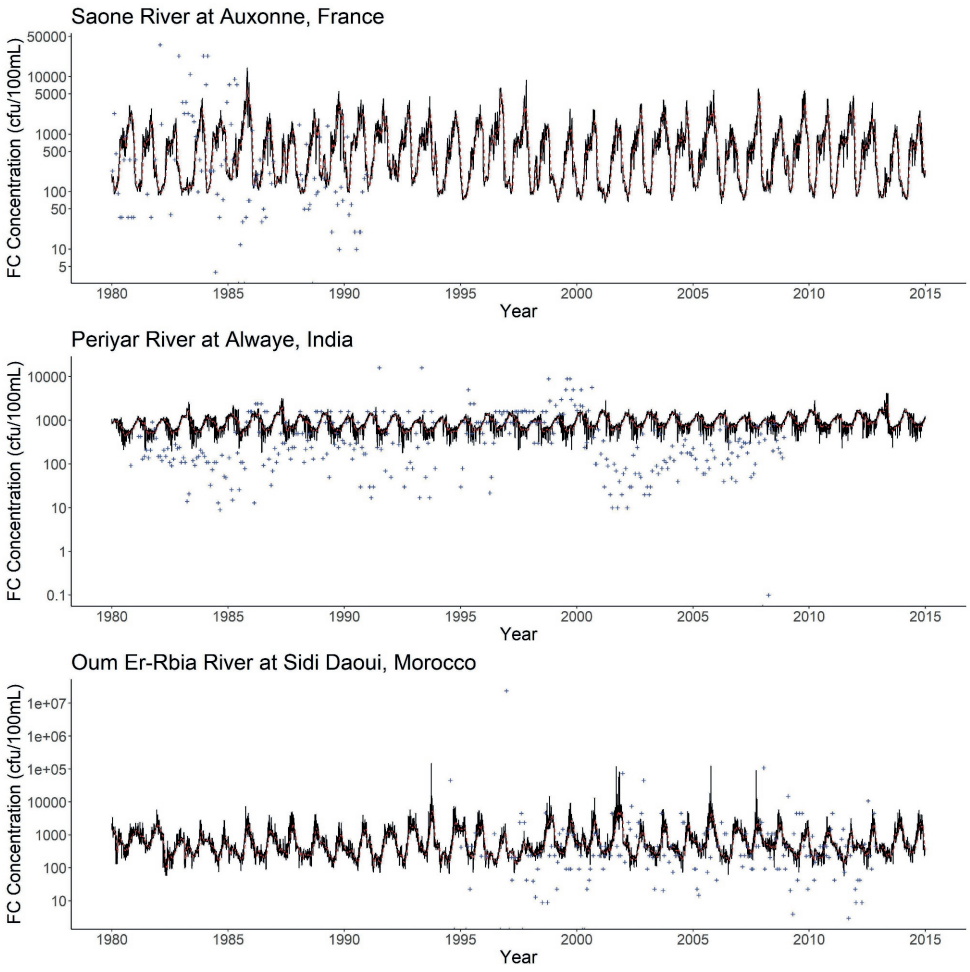

Figure B.10 Selected time series of observed vs. simulated fecal coliform (FC) concentrations (cfu $100ml^{-1}$). Black (daily) and red (rolling 30-day average) lines indicated simulated FC concentrations; whereas blue crosses are observed concentrations.

B.4 Wastewater collection and treatment pathways

Following production, wastewater from domestic and manufacturing activities can follow a number of collection and treatment pathways (Fig. B.11). Wastewater from both domestic and manufacturing activities can be collected, typically in a sewered system or septic tanks, and subsequently undergo treatment practices to reduce pollutant loadings that are subsequently introduced to the environment. Treatment practices include primary, secondary and tertiary+ processes. Wastewater that is collected but untreated is not associated with a reduction in pollutant loadings, while having a significant effect in concentrating the discharge of pollutants (UNEP, 2016).

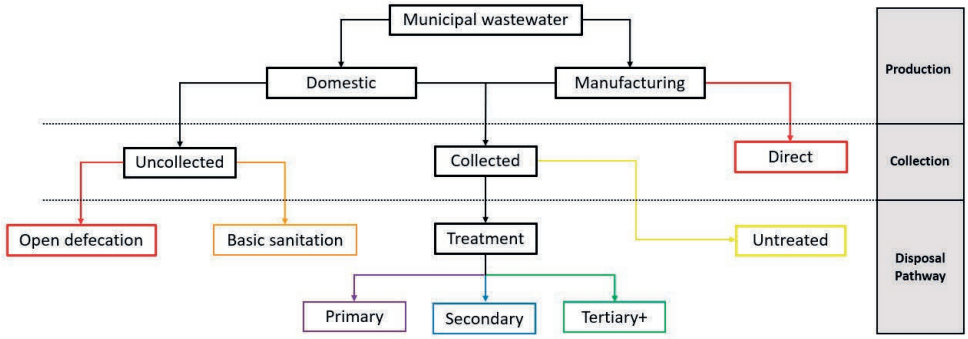

Figure B.11 Wastewater disposal pathways for the domestic and manufacturing sectors.

Primary treatment processes aims to settle and remove suspended solids, including processes of screening, comminution and sedimentation (Mateo-Sagasta et al., 2015). Secondary treatment uses biological processes to degrade and remove organic matter, typically using bacteria or protozoa (Mateo-Sagasta et al., 2015). Treatment techniques can include using activated sludge, aerated lagoons or constructed wetlands. Tertiary treatment processes represent a broad range of techniques, including membrane filtration, disinfection and carbon adsorption. Tertiary treatment is particularly used for the removal of inorganic materials and nutrients (especially nitrogen and phosphorus), and an important step for ensuring the safety of wastewater for reuse (Mateo-Sagasta et al., 2015).

Country-level wastewater production, collection and treatment were determined at the annual timestep for 1980–2015 following the methodology described and validated in previous work (Jones et al., 2021). Treated wastewater flows are further disaggregated by treatment level (primary, secondary and tertiary+) based on country-level statistics. Reported data on the ratio of primary, secondary and tertiary+ treatment was obtained from Eurostat (38 countries) and Global Water Intelligence (42 countries) for the year 2015. Supplemented with the 38 countries with no wastewater treatment (Jones et al., 2021), these 118 countries account for ~89% of the global population. For countries where reported data was not available, proportions are applied to the country-level treatment rates based on ratios averaged by income level from the reported data (Table B.3). It should be noted that these ratios are only applied to countries containing ~11% of the global population, and predominantly for countries where treatment rates are low. The ratio of primary, secondary and tertiary+ treatment levels within a country are assumed to remain constant throughout the study period 1980–2015.

Table B.3 Ratio of primary, secondary and tertiary + treatment applied to countries without data.

	Treatment ratio[1]		
Economic classification	**Primary**	**Secondary**	**Tertiary+**
High	0	0.33	0.67
Upper-middle	0	0.87	0.13
Lower-middle	0.54	0.44	0.02
Low	1	0	0

[1]These ratios are applied to treatment rates within a country.

We derive gridcell-specific flows of produced, collected and treated wastewater for 1980–2015 using the methodology developed and validated in Jones et al. (2021). Treated wastewater flows are then disaggregated by treatment level at 5 arc-min by hierarchically assigning the highest treatment levels to gridcells with the largest treated wastewater flows. Treated wastewater flows, disaggregated by treatment level for 2015, are displayed in Fig. B.12. High spatial coverage of tertiary treatment practices are found across North America and Western Europe. Conversely, across South America, India and China, the dominant wastewater treatment level is secondary and these practices occur across a smaller number of gridcells. Very little wastewater treatment to any level is displayed across much of Sub-Saharan Africa, whereby the majority of wastewater treatment (if any) is occurring in the major cities. Volumetric wastewater flows, disaggregated by treatment level, are subsequently divided by the total gridded wastewater production to give the fraction of each treatment level occurring in a gridcell.

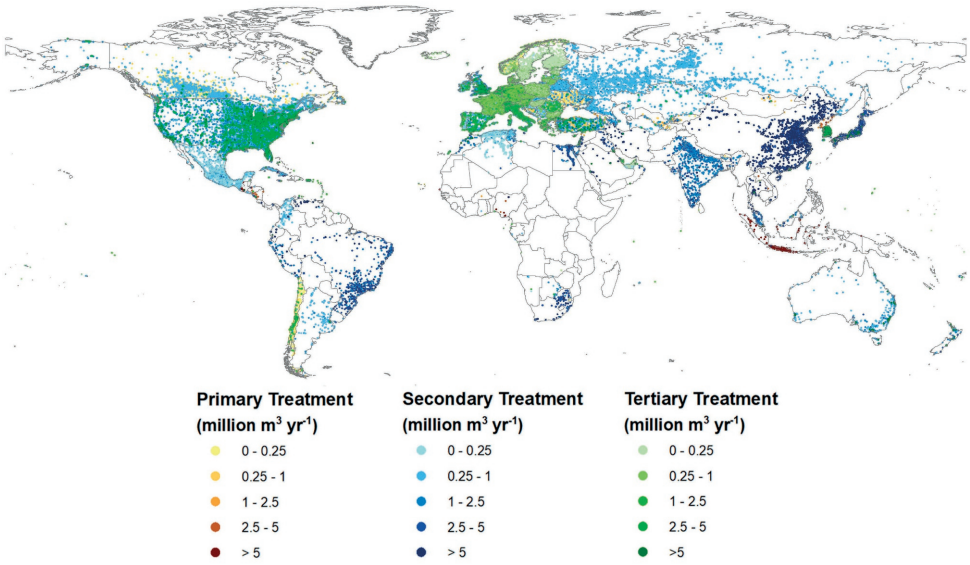

Figure B.12 Gridded treated municipal (domestic and manufacturing) wastewater flows by treatment level (primary, secondary, tertiary+) in 2015.

Gridcell-specific reductions in pollutant loadings from wastewater collection and treatment are determined by multiplying the fraction of each treatment level occurring in a gridcell by the pollutant removal efficiency associated with that treatment level (Eq. B.1). Tertiary+ practices are typically associated with the highest level of pollutant removal, followed by secondary and primary treatment (Table B.4).

$$\mathrm{R}_{p,n} = f_{ter_n} \cdot r_{ter_p} + f_{sec_n} \cdot r_{sec_p} + f_{pri_n} \cdot r_{pri_p} \tag{B.1}$$

Where: f is the fraction of tertiary+ treatment (f_{ter_n}), secondary treatment (f_{sec_n}) and primary treatment (f_{pri_n}) within gridcell n, and r is the removal efficiency associated with teriary (r_{ter_p}), secondary (r_{sec_p}) and primary (r_{pri_p}) treatment per pollutant p. Pollutant removal efficiencies per wastewater treatment level are based on extensive literature research in previous global water quality modelling studies (Williams et al., 2012; UNEP, 2016; van Vliet et al., 2021) and are displayed in Table B.4. Notably, no removal of TDS is assumed across any treatment level. This follows previous studies (UNEP, 2016; van Vliet et al., 2021), and is assumed due to limited information on specific technologies that reduce TDS loadings at individual wastewater treatment plants.

Table B.4 Pollutant removal efficiency by wastewater treatment level.

Treatment level	Pollutant removal efficiency (%)		
	Salinity (TDS)	Organic (BOD)	Pathogen (FC)
Tertiary+	0	99	99.99
Secondary	0	85	97.45
Primary	0	25	42.79

The difference between collected and treated wastewater per gridcell represents the collected but untreated flows, while the difference between the produced and treated wastewater represents the uncollected flows. Uncollected domestic wastewater is further disaggregated into two categories: basic sanitation and open defecation. Country-level data for open defecation rates are for 1980–2015, while basic sanitation practices account for all the wastewater produced that is not either collected or accounted for by open defecation. No further segregation between different basic sanitation practices (e.g. pit latrines, composting toilets) is made due to lack of data. Basic sanitation and open defecation flows are downscaled to 5 arc-min based on gridded untreated wastewater flows for the domestic sector, with gridcells with the highest flows allocated to basic sanitation and the remaining gridcells designated to open defecation (Fig. B.13a).

The reduction in pollutant loadings from the domestic sector is also dependent on wastewater following these uncollected pathways. While basic sanitation and open defecation practices are not associated with any direct reductions in pollutant loadings due to treatment practices, these pathways can delay or reduce the entry of wastewater into the environment, which can affect the loading. No abatement of TDS, BOD or FC loadings from basic sanitation practices are assumed. However, only a portion of loadings from open defecation will enter the stream network, for which we use the surface runoff fraction as per previous work (UNEP, 2016).

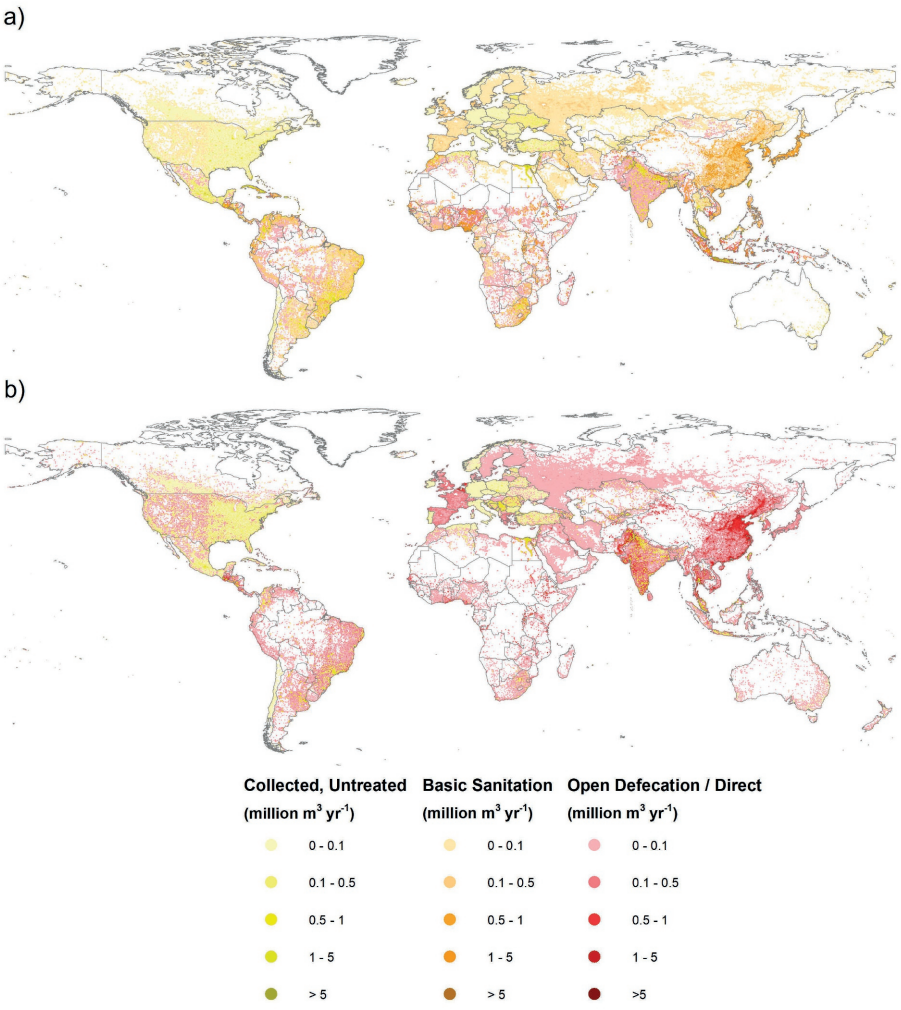

Figure B.13 Gridded untreated wastewater flows in 2015 by pathway for the a) domestic; and b) manufacturing sectors.

As such, the reduction in pollutant loadings from the domestic sector ($R_{dom,p,n}$) is calculated as per Eq. B.2.

$$\mathrm{R}_{dom,p,n} = R_{p,n} + (f_{bs_n} \cdot r_{bs_p}) + (f_{od_n} \cdot (1 - s_n)) \tag{B.2}$$

Where: f_{bs_n} and f_{od_n} is the fraction of basic sanitation and open defecation, respectively, within gridcell n, r_{bs_p} is the reduction of pollutant p from basic sanitation collection facilities (assumed to be 0 for TDS, BOD and FC), and s_n is the gridcell-specific surface runoff fraction as simulated by *PCR-GLOBWB2*.

Conversely, all uncollected manufacturing wastewater is assumed to be discharged directly to surface waters (Fig. B.13b). With this pathway, no reduction in pollutant loadings is assumed. Therefore, abatement of pollutant loadings from the manufacturing sector ($R_{man,p,n}$) depends only upon centralised (gridcell-specific) wastewater collection and treatment practices (Eq. B.3).

$$\mathrm{R}_{man,p,n} = R_{p,n} \tag{B.3}$$

As per previous studies (Williams et al., 2012; UNEP, 2016) and due to data limitations, gridded municipal (domestic and manufacturing) wastewater collection and treatment rates are applied to urban surface runoff. The reduction of pollutants from urban surface runoff ($R_{urb,p,n}$) depend only upon centralised (gridcell-specific) wastewater collection and treatment practices (Eq. B.4). Urban surface runoff flows that are designated as uncollected are assumed to enter the surface water network directly without abatement.

$$\mathrm{R}_{urb,p,n} = R_{p,n} \tag{B.4}$$

The distinction between intensive and extensive livestock systems is made to account for the differences in the paths by which livestock waste enters the stream network, namely whether there is transportation by surface runoff (for extensive systems) or whether there is collection (and potentially subsequent treatment) of livestock waste (for intensive systems). For extensive livestock systems, only a portion of loadings will be transported to the surface water network, which we account for by multiplying by the fraction surface runoff from *PCR-GLOBWB2* (in line with the approach used for domestic pollutant loadings from open defecation practices).

Due to data limitations, and in line with previous studies (Wen et al., 2017; Vigiak et al., 2019) intensive livestock farming was considered akin to a manufacturing activity for the purposes of determining livestock waste treatment rates. The reduction of pollutant loadings from intensive livestock activities ($R_{intLiv,p,n}$) (Eq. B.5) was calculated at the gridcell level, occurring in line with the location where municipal wastewater treatment of secondary level or higher is occurring. All treatment of wastewater from the intensive livestock sector is assumed to be to the secondary level, as per previous work (Wen et al., 2017; Vigiak et al., 2019).

$$\mathrm{R}_{intLiv,p,n} = (f_{sec_n} + f_{ter_n}) \cdot r_{sec_p} \tag{B.5}$$

Where $R_{intLiv,p,n}$ is the reduction in pollutant loadings from the intensive livestock sector, f_{sec_n} and f_{ter_n} are the fraction of secondary and tertiary+ treatment, respectively, in gridcell n, and r_{sec_p} is the removal efficiency associated with secondary treatment per pollutant p.

B.5 Towards SDG 6.3 and improved wastewater treatment

SDG 6.3 aims to improve ambient water quality by halving the proportion of untreated wastewater released to the environment by 2030, relative to 2015. The volume of wastewater from 2016–2030 is projected based on trend analysis of wastewater flows from 2011–2015, which are estimated based on population, GDP per capita and access to basic sanitation (Jones et al., 2021). Projections for 2016–2030 wastewater flows are downscaled to 5 arc-min proportionally following the method implemented for 1980–2015, as discussed in Section B.4.

Only wastewater undergoing secondary or higher treatment practices in 2015 is considered adequately treated for SDG 6.3, as only these treatment levels represent abate a substantial proportion of pollutant loadings. As such, the required additional volume of wastewater that must be treated in 2030 ($req\_WWt_{SDG6.3_{2030,c}}$) to meet SDG 6.3 in country c is calculated (Eq. B.6), where WWp_{2030} is the wastewater production in 2030, and $WWt_{secondary}$ and $WWt_{tertiary}$ is the total volume of wastewater treated to secondary and tertiary+ treatment levels in 2015, respectively. The required treatment to meet SDG 6.3 is thus half of the difference between the wastewater produced in 2030 and the wastewater treated to above secondary level in 2015.

$$\text{req\_}WWt_{SDG63_{2030}} = \frac{WWp_{2030} - \left(WWt_{\text{secondary }2015} + WWt_{\text{tertiary }2015}\right)}{2} \tag{B.6}$$

The required volumetric expansion in municipal wastewater treatment, aggregated by geographic region and by level of economic development, are displayed in Fig. B.14.

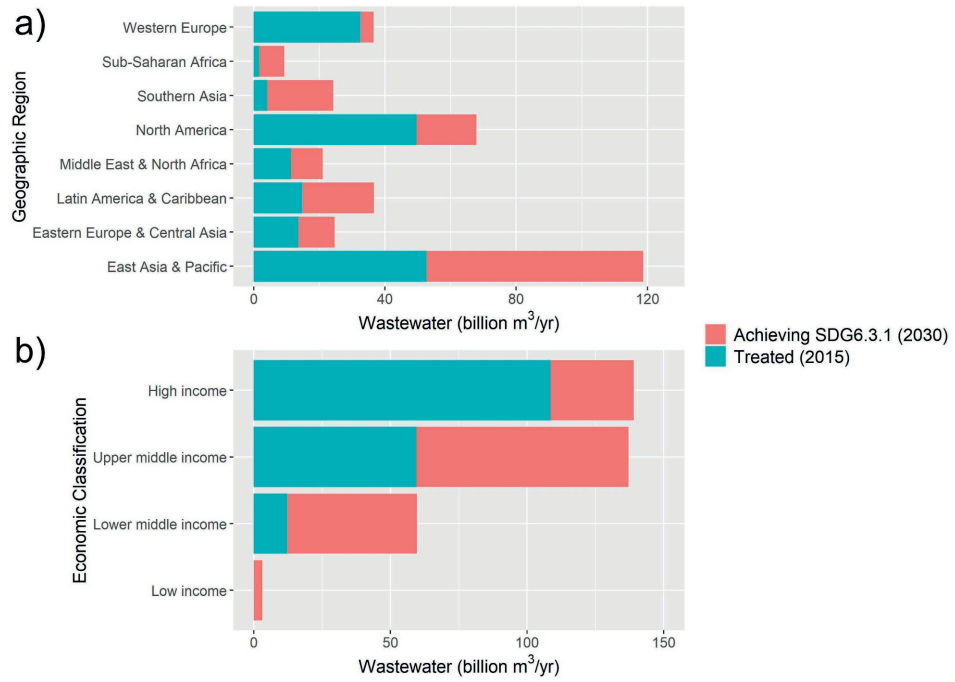

Figure B.14 Required expansions in wastewater treatment in order to achieve SDG 6.3 (i.e halving the proportion of untreated waste water) aggregated by a) geographical region; and b) economic classification.

The increase in wastewater treatment is delineated within countries to 5 arc-min by hierarchically assigning expansions to gridcells where 2015 pollutant loadings are highest, until the required volume of wastewater treatment expansion is met. The gridded percentage expansions in wastewater treatment required for SDG 6.3 at 5 arc-min is displayed in Fig. B.15. We focus our expansions on gridcells with high pollutant loadings as collection and treatment is assumed to be both more desirable and economically feasible, and hence more likely, where the strongest reductions in pollutant loadings will be achieved. Expansions in wastewater treatment are assumed to be to secondary level, the minimum treatment level required by SDG 6.3 and in lieu of the prohibitive economic costs of tertiary treatment for all but the most developed nations.

For determining pollutant loadings in 2030, the loadings for domestic ($R_{dom,p,n}$) and manufacturing ($R_{man,p,n}$) are recalculated under these (SDG 6.3-realised) conditions to account for the increased abatement of pollutant loadings associated with the expansions in wastewater treatment capacities. The pollutant loadings from urban surface runoff ($R_{urb,p,n}$) and intensive livestock ($R_{intLiv,p,n}$) also increase, in in line with the assumptions associated with treatment in these particular sectors. As this study assumes that secondary treatment practices do not influence loadings of salinity (TDS) or water temperature (Tw), only changes in organic pollution (BOD) and pathogen (FC) loads and concentrations occur as a result of expanding wastewater treatment. The gridded percentage changes in pollutant loadings as a result of achieving SDG 6.3, opposed to no additional expansions in wastewater treatment capacity over 2015 levels, is displayed in Fig. B.16. In countries where wastewater treatment rates are already high, SDG 6.3 is achieved by both expanding treatment capacities in gridcells with existing wastewater treatment facilities are already established and in gridcells without existing treatment. Conversely, in countries with limited existing wastewater treatment, SDG 6.3 is achieved by treating all wastewater produced in a smaller number of gridcells.

Fig. B.17 and Fig. B.18, derived directly from Fig. 4.3a and Fig. 4.3b respectively, display 'zoomed-in' panels for a) United States; b) Europe; c) South and East Asia and d) North and Central Africa.

Fig. B.19 is complementary to Fig. 4.3c, displaying in-stream concentrations for six additional rivers (Rhine-Meuse, Thames, Ogan, Qiantang, Vaal, Karnaphuli).

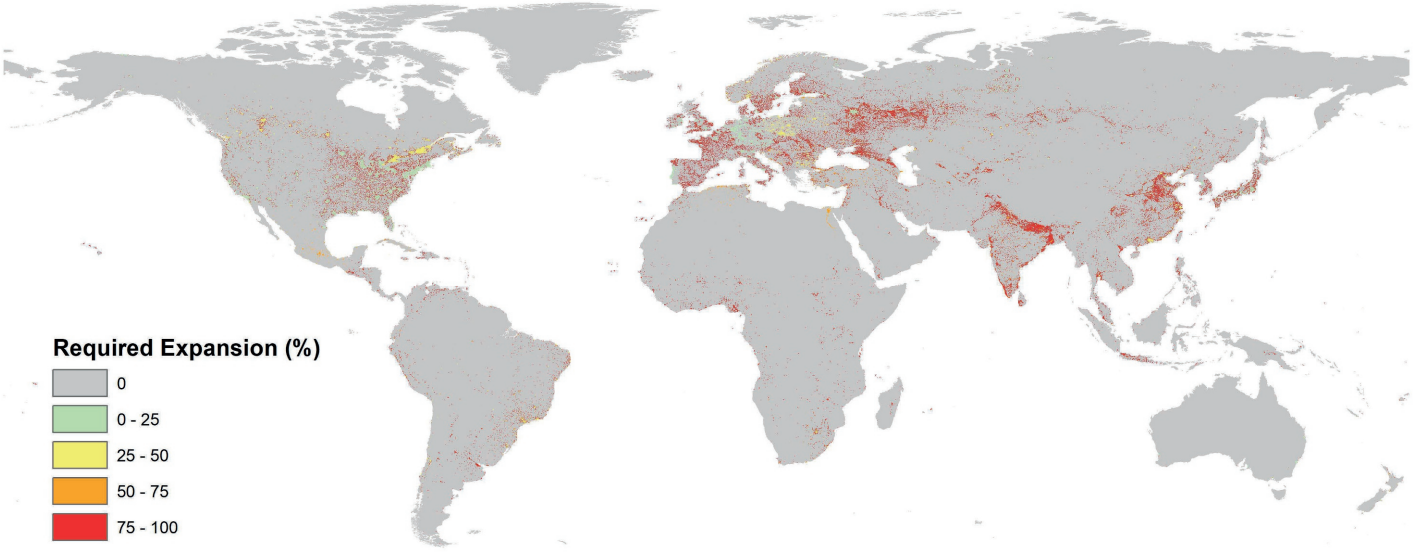

Figure B.15 Gridded percentage expansions in wastewater treatment capacities required to achieve SDG 6.3. A required percentage expansion of 100% indicates that required expansions are equal to the volume of wastewater produced.

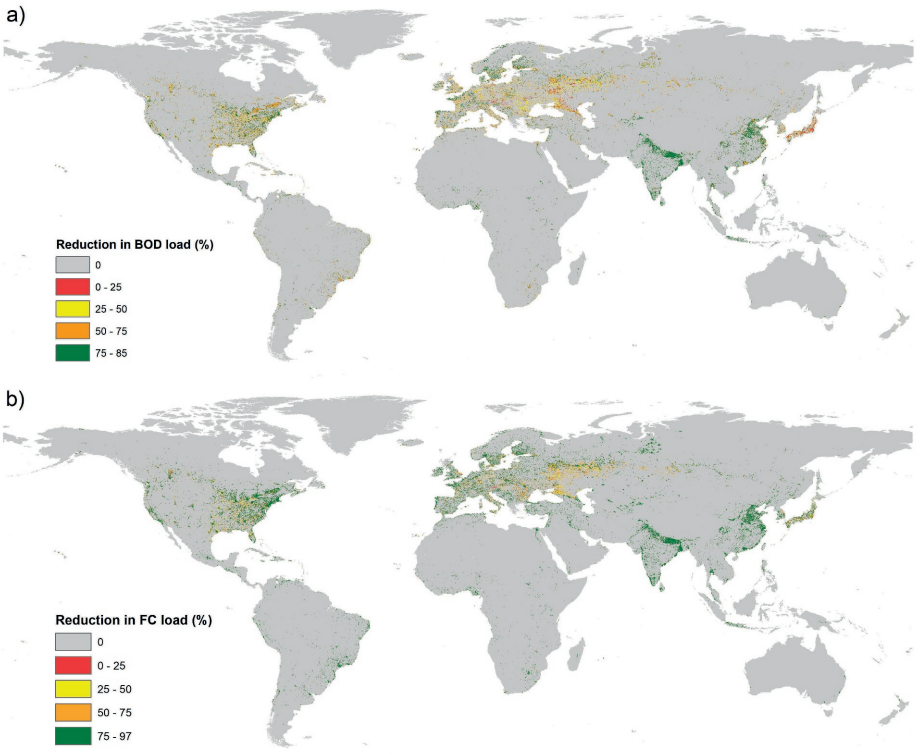

Figure B.16 Percentage reductions in (unrouted) pollutant loadings of a) BOD; and b) FC per gridcell due to wastewater treatment expansions required to achieve SDG 6.3.

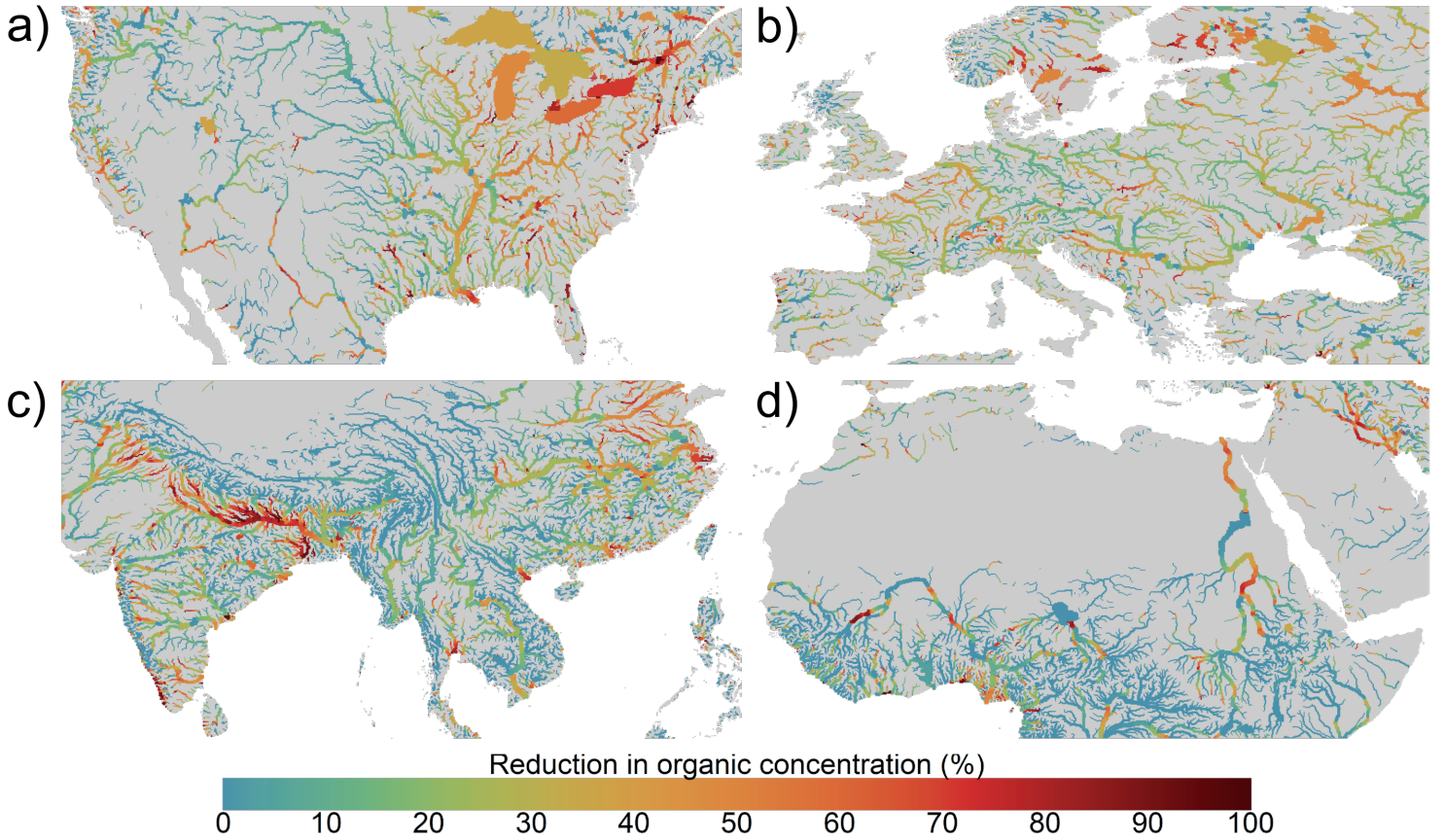

Figure B.17 Average annual percentage reductions in organic pollution as indicated by BOD concentrations assuming no expansions in wastewater treatment vs. achieving SDG 6.3. Percentage reductions displayed in panels are averaged over multiple GCMs for the time period 2021–2030 and are only displayed for streams with an average annual discharge >10 $m^3 s^{-1}$.

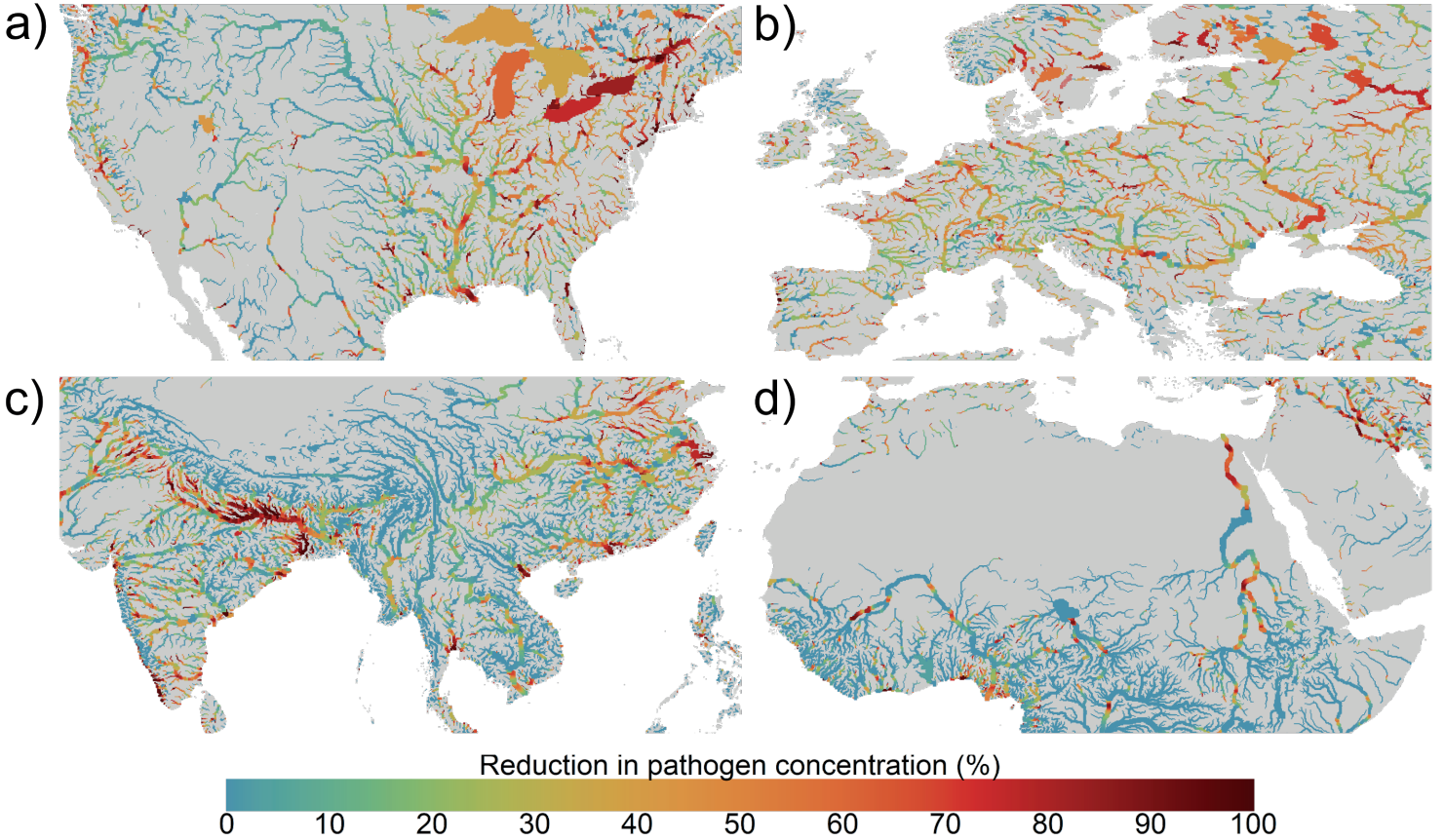

Figure B.18 Average annual percentage reductions in pathogen pollution as indicated by FC concentrations assuming no expansions in wastewater treatment vs. achieving SDG 6.3. Percentage reductions displayed in panels are averaged over multiple GCMs for the time period 2021–2030 and are only displayed for streams with an average annual discharge >10 $m^3 s^{-1}$.

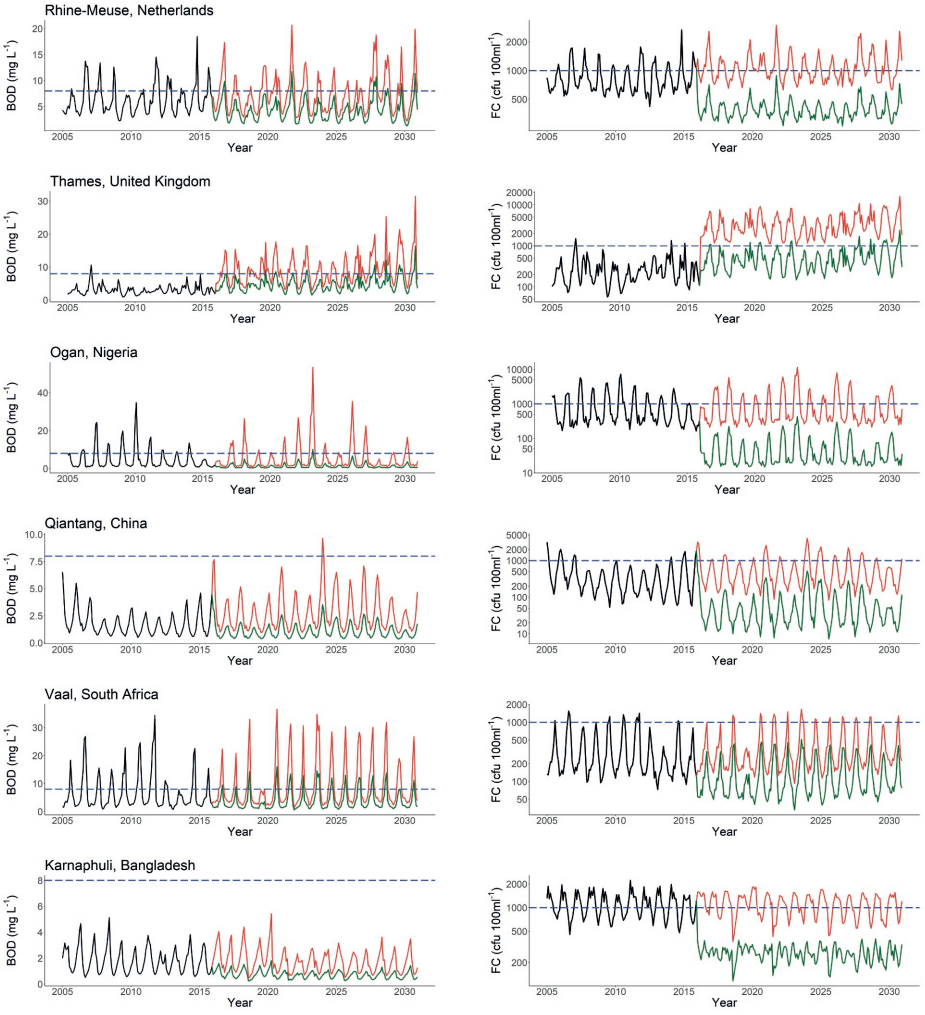

Figure B.19 In-stream BOD (left) and FC (right) concentrations under historical (black), no expansion (red) and SDG 6.3 (green) conditions at selected locations.

We also consider the exceedance of key surface water quality thresholds with respect to surface water abstractions (Fig. B.20). For the historical period, surface water abstractions that exceed the moderate TDS threshold vary from 8% in Eastern Europe and Central Asia to 31% in Southern Asia. Exceedance of high or very high salinity levels are largest in the regions of Southern Asia (17%), East Asia and Pacific (17%) and the Middle East and North Africa (13%). Volumetrically, the largest surface water abstractions exceeding 2,100 mg l^{-1} TDS are in East Asia and Pacific (119 km^3 yr^{-1}) and Southern Asia (47 km^3 yr^{-1}) regions – dominated by China and India, respectively.

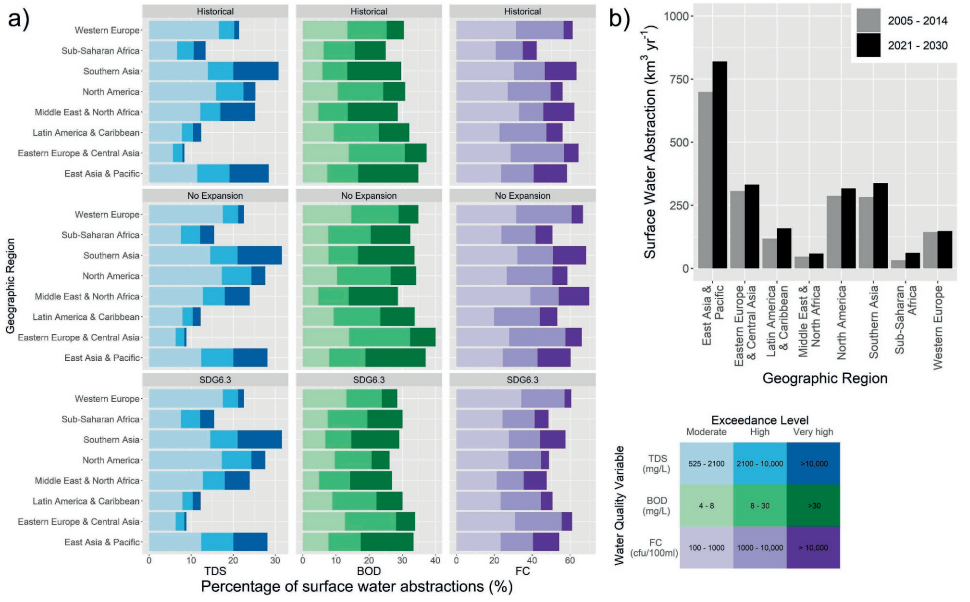

Figure B.20 a) Percentage of surface water abstractions exceeding multiple critical water quality thresholds for salinity (TDS), organic (BOD) and pathogen (FC) pollution under historical and near-future (no expansions and SDG 6.3) conditions. Water quality threshold exceedance and surface water abstractions are assessed at monthly temporal resolution, and subsequently aggregated per geographic region across all months. b) Total annual surface water abstractions (km^3 yr^{-1}) per geographic region. All results are averaged across multiple GCMs using 2005–2014 as the historical and 2021–2030 as the future time period.

The percentage of surface water abstractions exceeding the moderate BOD threshold (4 mg l^{-1}) in the historic period is relatively consistent across all world regions, ranging from 25% to 37% (Fig. B.20). Similarly, exceedances of the moderate FC threshold (1,000 cfu 100 ml^{-1}) are similar across world regions, and are also notably high at between 42–65%. Larger differences between the regions emerge when considering stricter water quality thresholds. 18% and 16% of surface water abstractions in East Asia and Pacific and Southern Asia, respectively, exceed 30 mg l^{-1} BOD compared to just 5% in Western Europe and 7% in North America. This pattern, which is also reflected in the FC statistics, can be largely attributed to the higher wastewater treatment rates in these regions.

Without expansions in wastewater treatment (scenario 'No Expansion'), both the percentage of surface water abstractions and the degree of exceedance increase across all world regions, commensurate with factors such as population growth (Fig. B.20). This is particularly true for the Sub-Saharan Africa region, whereby the total surface water abstractions exceeding >4 mg l^{-1} BOD rises from 25% to 32% and abstractions exceeding 8 mg l^{-1} from 19% to 25%. Increases in surface water abstractions exceeding FC thresholds are also highest in Sub-Saharan Africa. Furthermore,

without expansions in wastewater treatment, the Western Europe and North America regions also see a substantial rise in the percentage of surface water abstractions that exceed quality thresholds. This occurs as current wastewater treatment capacities become increasingly insufficient to treat rising loadings, particularly from the domestic sector.

The average volumes of polluted surface water abstractions under SDG 6.3 and no expansions in wastewater treatment are displayed for BOD (Fig. B.21a) and FC (Fig. B.21b). Fewer surface water abstractions are polluted in all world regions under SDG 6.3, indicating that expansions in wastewater treatment do have some impact for reducing pollutant concentrations below key quality thresholds. Yet, these impacts strongly differ per region. Most notably, surface water abstractions polluted with BOD (>8 mg l^{-1}) reduce from 76 km^3 yr^{-1} without expansions to 52 km^3 yr^{-1} under SDG 6.3 in Northern America – a 31% reduction. Similarly, a 24% reduction is achieved in Western Europe. More moderate, yet still considerable, improvements are found for other world regions – with a decrease of 28 km^3 yr^{-1} in East Asia and Pacific being the largest volumetrically. Reductions are even larger with respect to the FC threshold (1,000 cfu $100ml^{-1}$), ranging from 10% in Sub-Saharan Africa to 33% in Northern America.

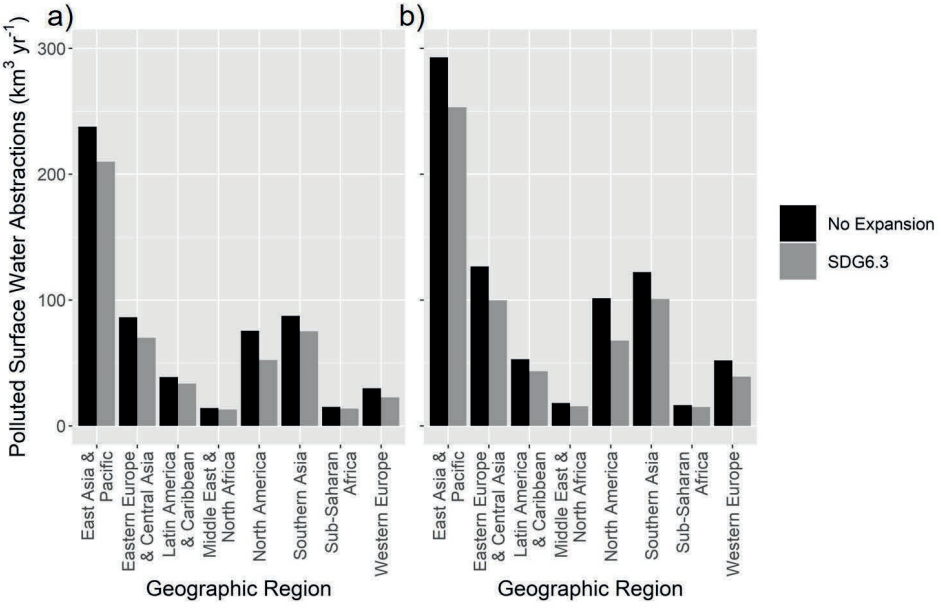

Figure B.21 Average annual volumes of surface water abstractions exceeding quality thresholds for a) BOD (8 mg l^{-1}); and b) FC (1,000 cfu $100ml^{-1}$).

Appendix C | Supplementary information to Chapter 5

Supplementary to: Jones, E.R., Bierkens, M.F.P., van Puijenbroek, P.J.T.M., van Beek, L.P.H., Wanders, N., Sutanudjaja, E.H., and van Vliet, M.T.H. (2023) Sub-Saharan Africa will increasingly become the dominant hotspot of surface water pollution. *Nature Water, 1*, pp. 602-613, DOI: 10.1038/s44221-023-00105-5

C.1 Future pollutant loadings

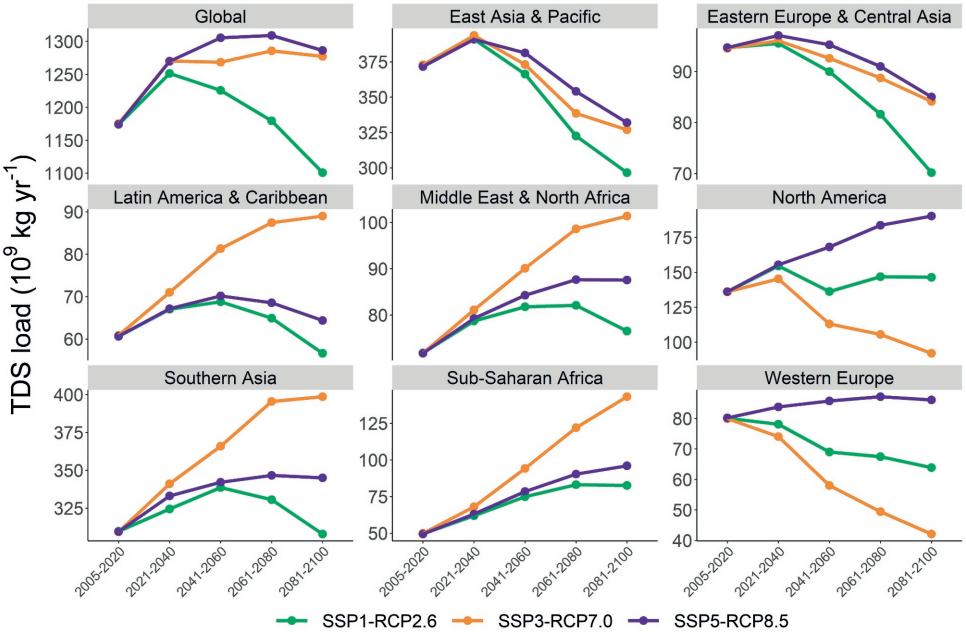

Figure C.1 Changes in total dissolved solids (TDS) loadings under the different combined climate change and socioeconomic scenarios, disaggregated by geographic region.

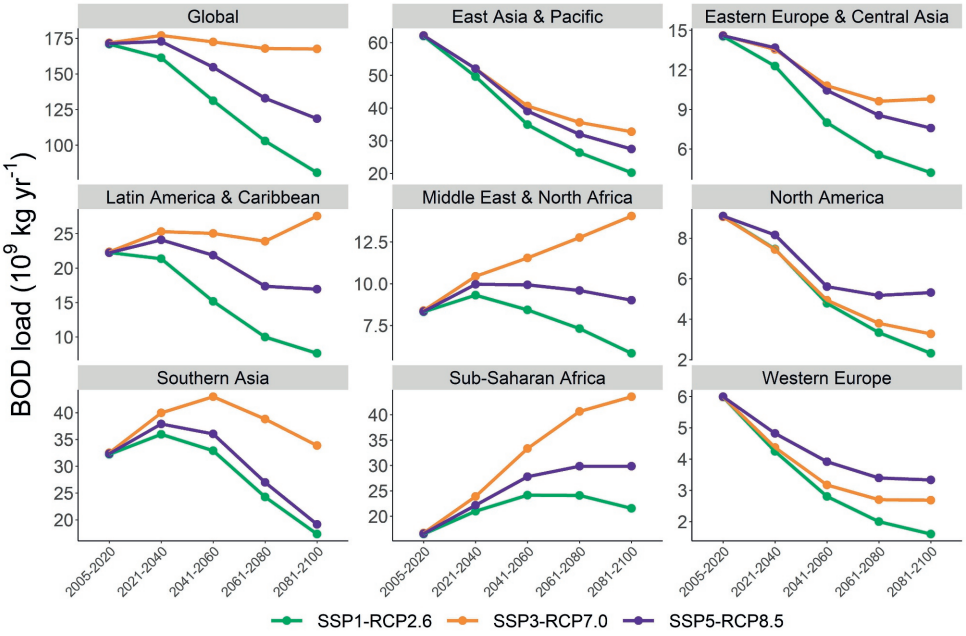

Figure C.2 Changes in biological oxygen demand (BOD) loadings under the different combined climate change and socioeconomic scenarios, disaggregated by geographic region.

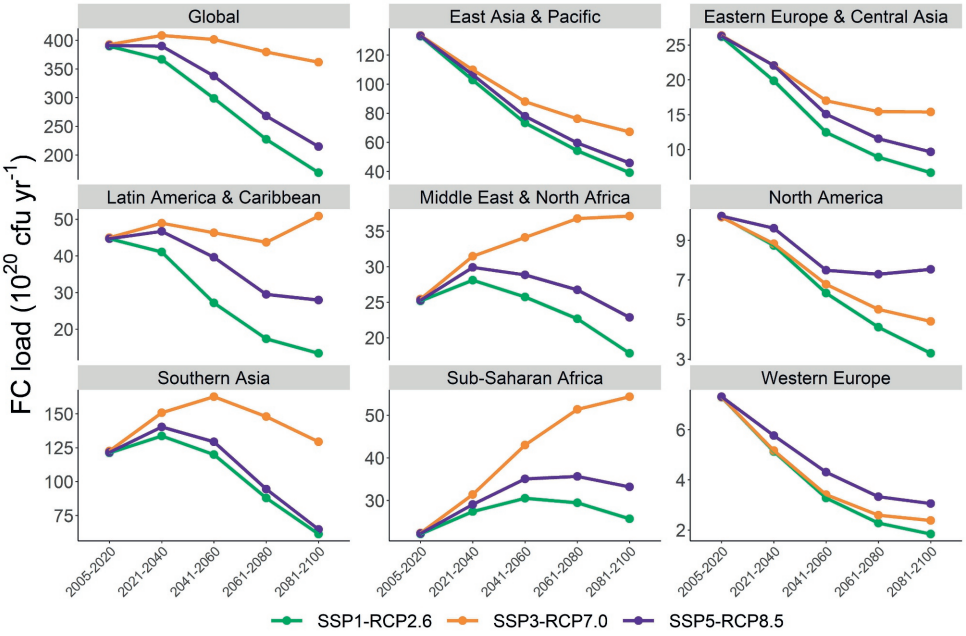

Figure C.3 Changes in fecal coliform (FC) loadings under the different combined climate change and socioeconomic scenarios, disaggregated by geographic region.

C.2 Future hydrology and water quality

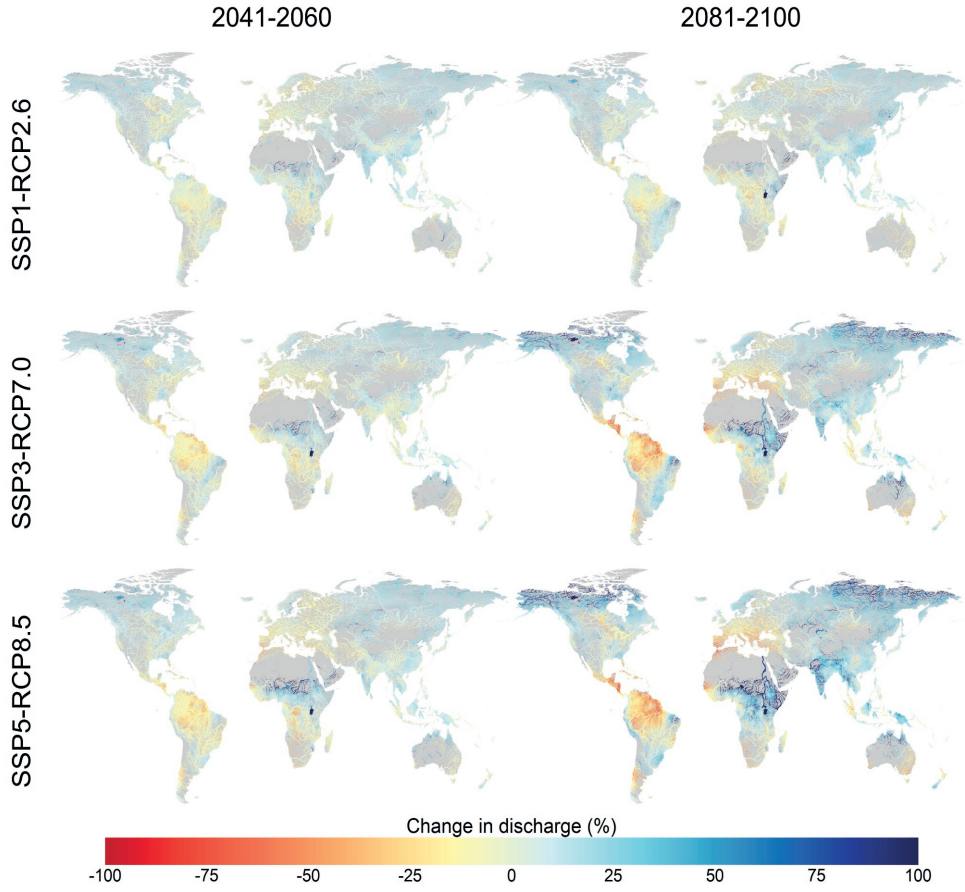

Figure C.4 Percentage changes in discharge in the time periods 2041–2060 and 2081–2100 under three combined climate and socioeconomic scenarios, relative to a historical reference period (2005–2020).

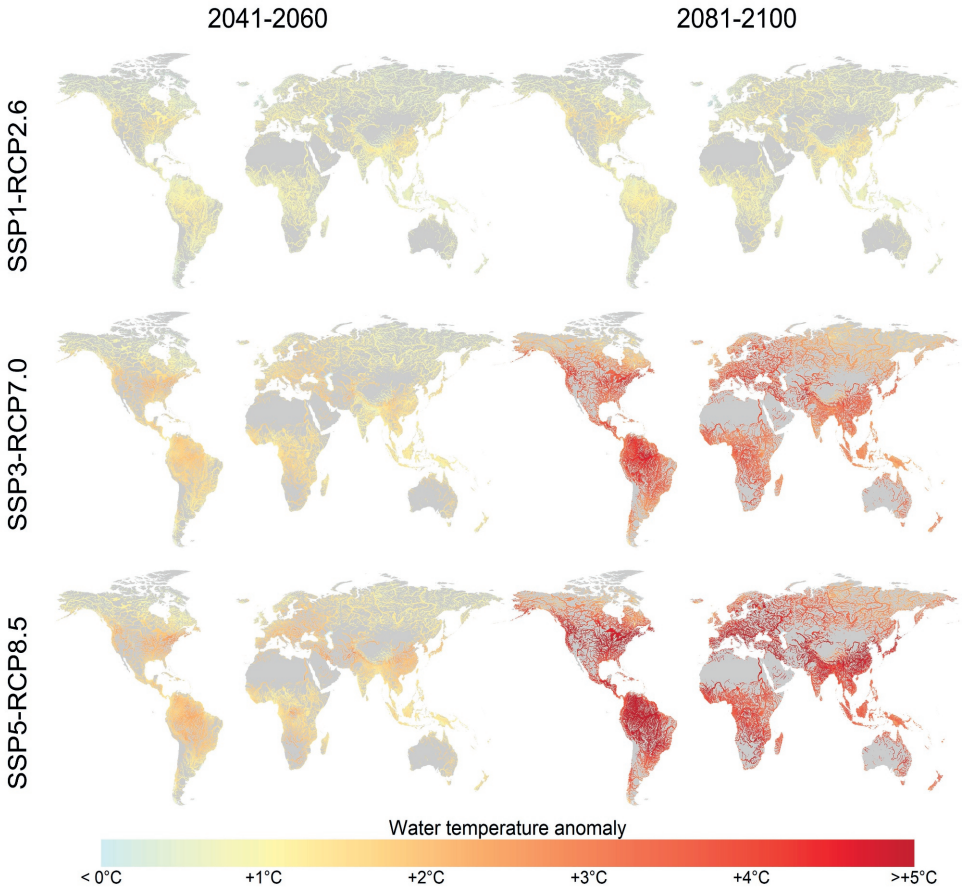

Figure C.5 Water temperature (Tw) anomaly (°C) in the time periods 2041–2060 and 2081–2100 under three combined climate and socioeconomic scenarios, relative to a historical reference period (2005–2020).

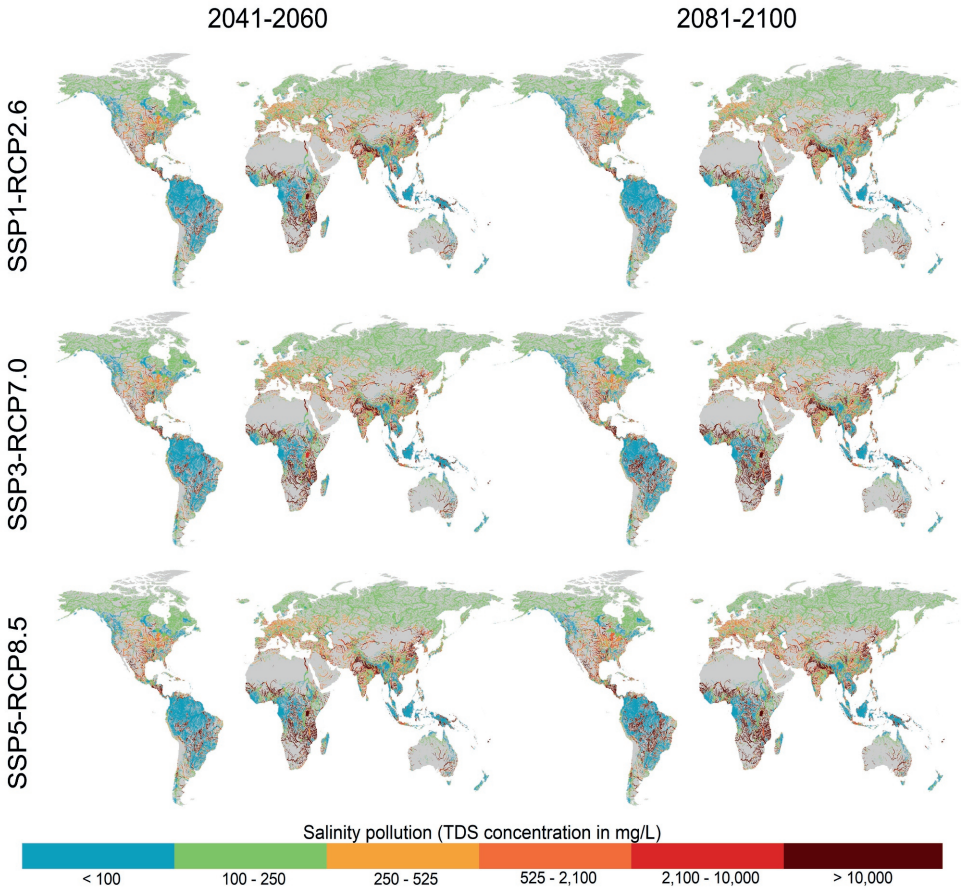

Figure C.6 Average annual total dissolved solids (TDS) concentrations (mg l^{-1}) in the time periods 2041–2060 and 2081–2100 under three combined climate and socioeconomic scenarios.

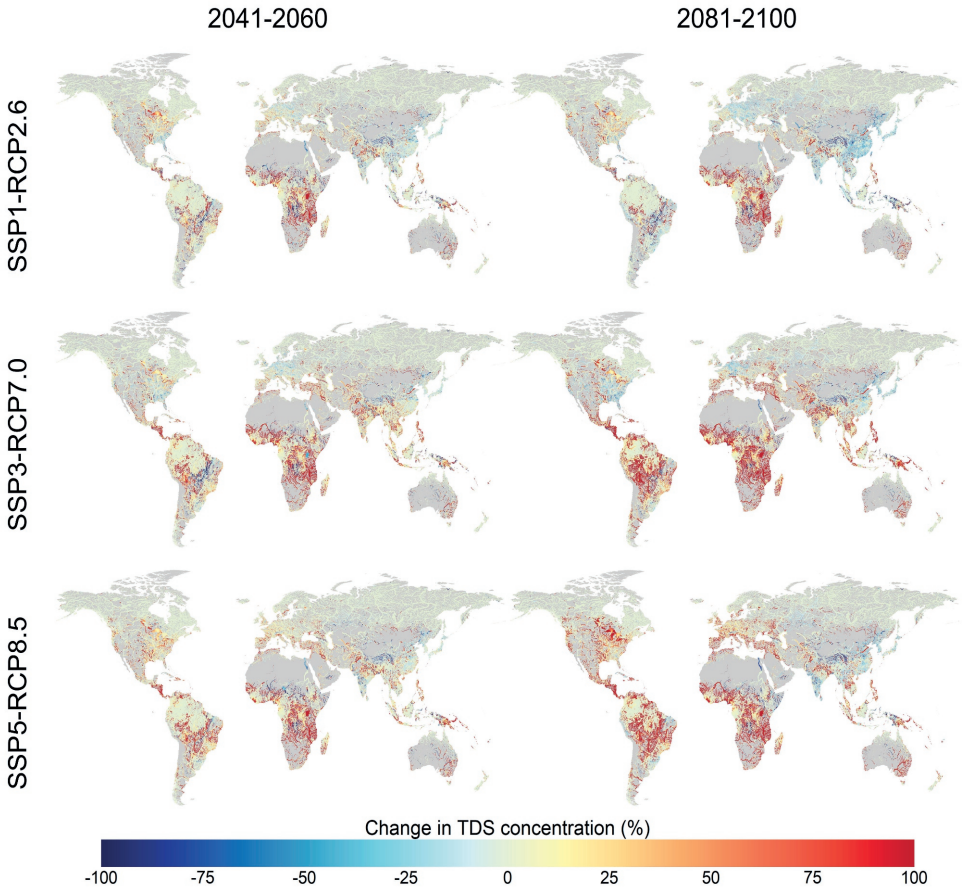

Figure C.7 Percentage changes in total dissolved solids (TDS) concentrations in the time periods 2041–2060 and 2081–2100 under three combined climate and socioeconomic scenarios, relative to a historical reference period (2005–2020).

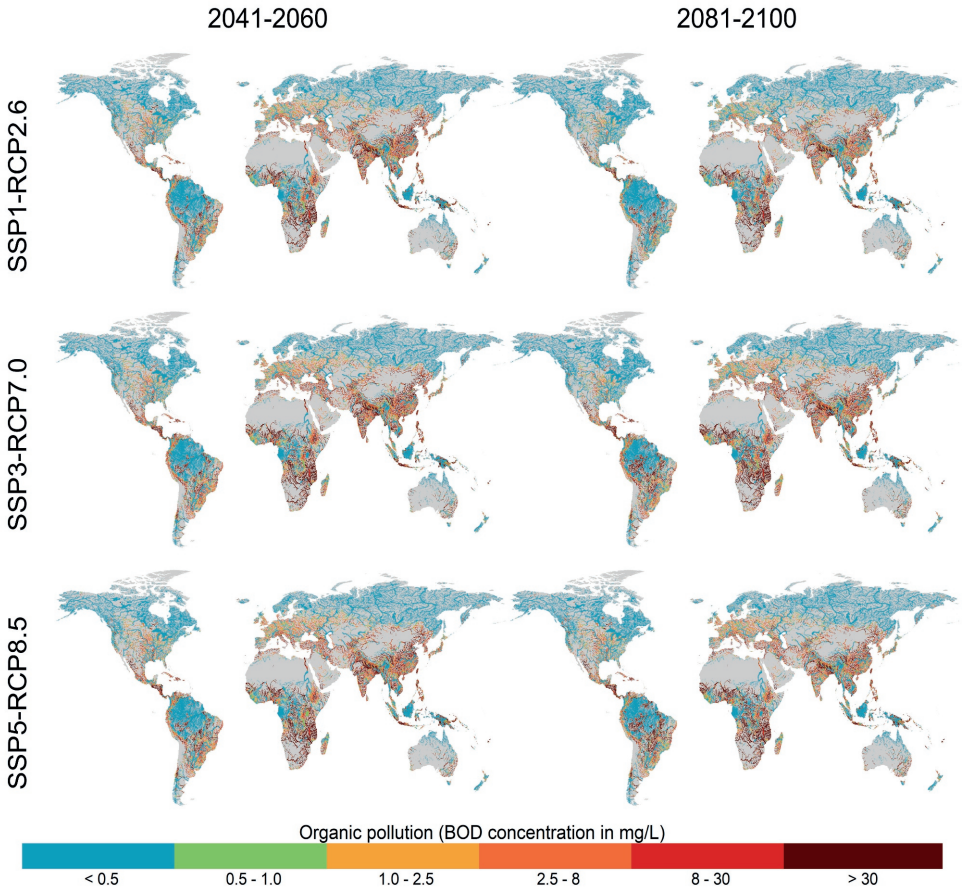

Figure C.8 Average annual biological oxygen demand (BOD) concentrations (mg l^{-1}) in the time periods 2041–2060 and 2081–2100 under three combined climate and socioeconomic scenarios.

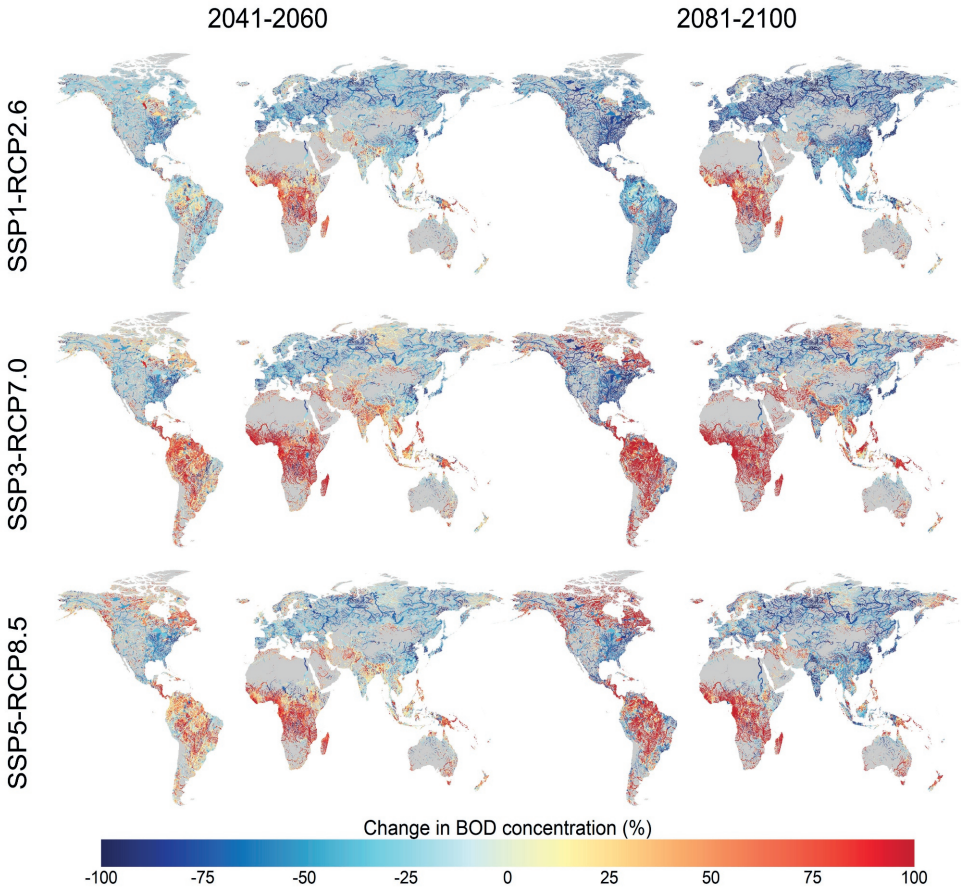

Figure C.9 Percentage changes in biological oxygen demand (BOD) concentrations in the time periods 2041–2060 and 2081–2100 under three combined climate and socioeconomic scenarios, relative to a historical reference period (2005–2020).

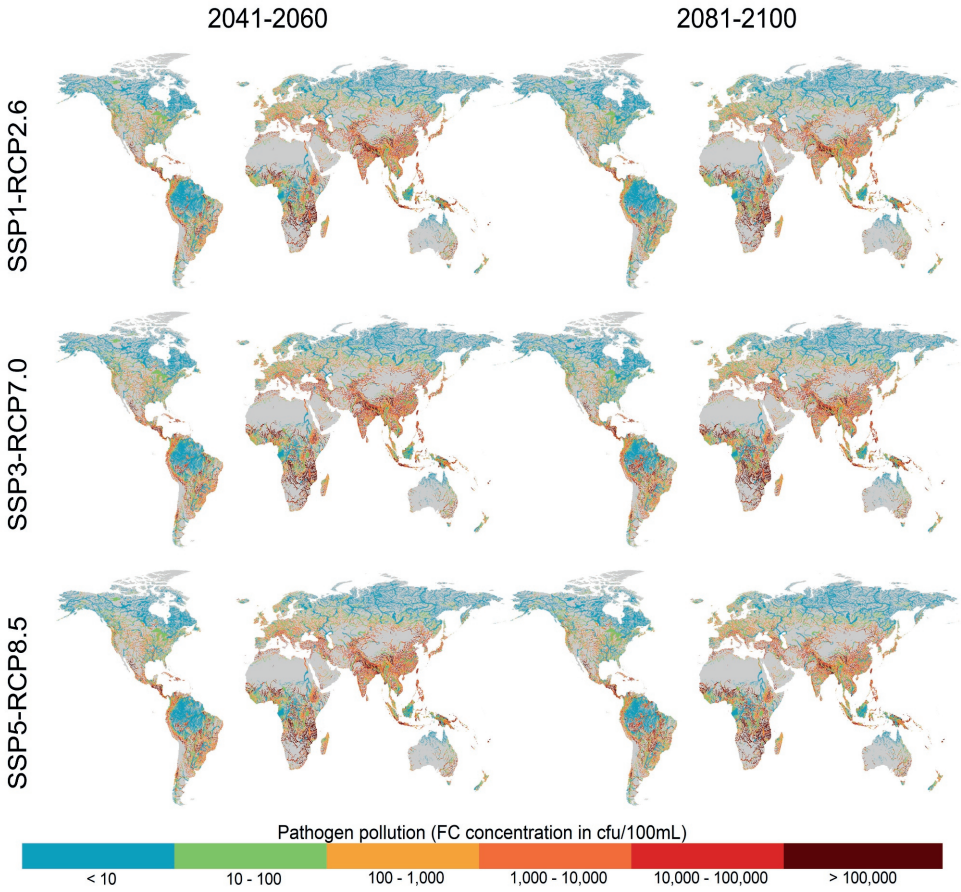

Figure C.10 Average annual fecal coliform (FC) concentrations (cfu $100ml^{-1}$) in the time periods 2041–2060 and 2081–2100 under three combined climate and socioeconomic scenarios.

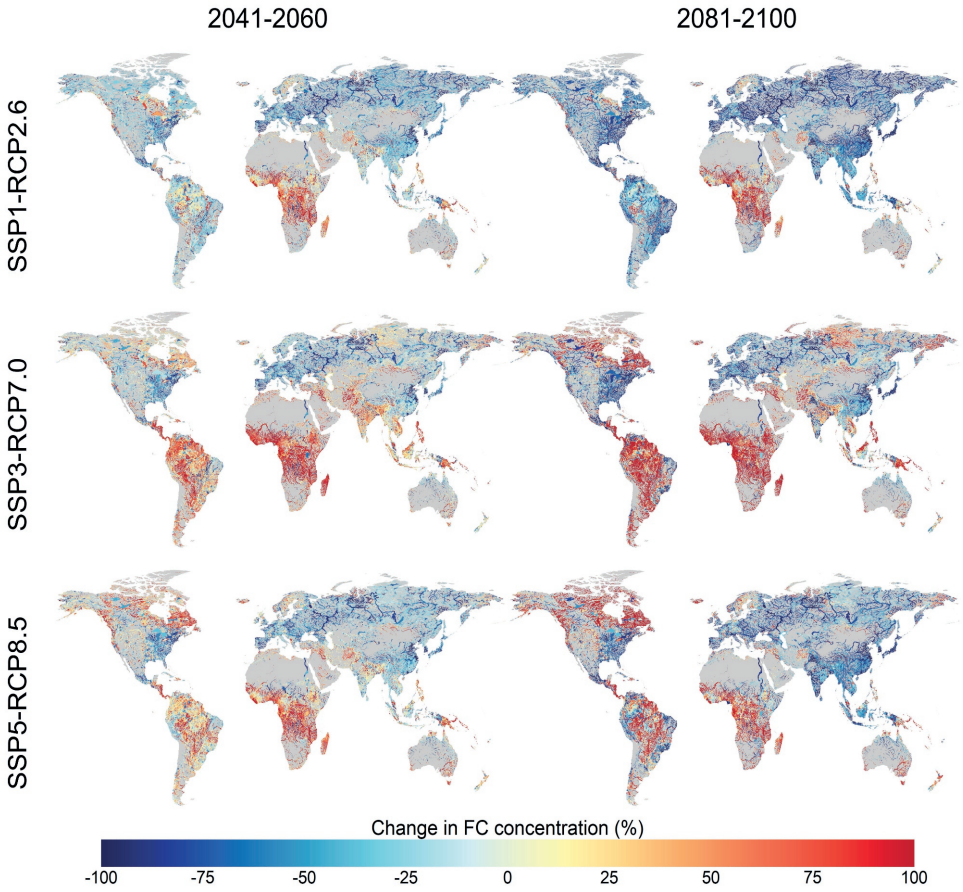

Figure C.11 Percentage changes in fecal coliform (FC) concentrations in the time periods 2041–2060 and 2081–2100 under three combined climate and socioeconomic scenarios, relative to a historical reference period (2005–2020).

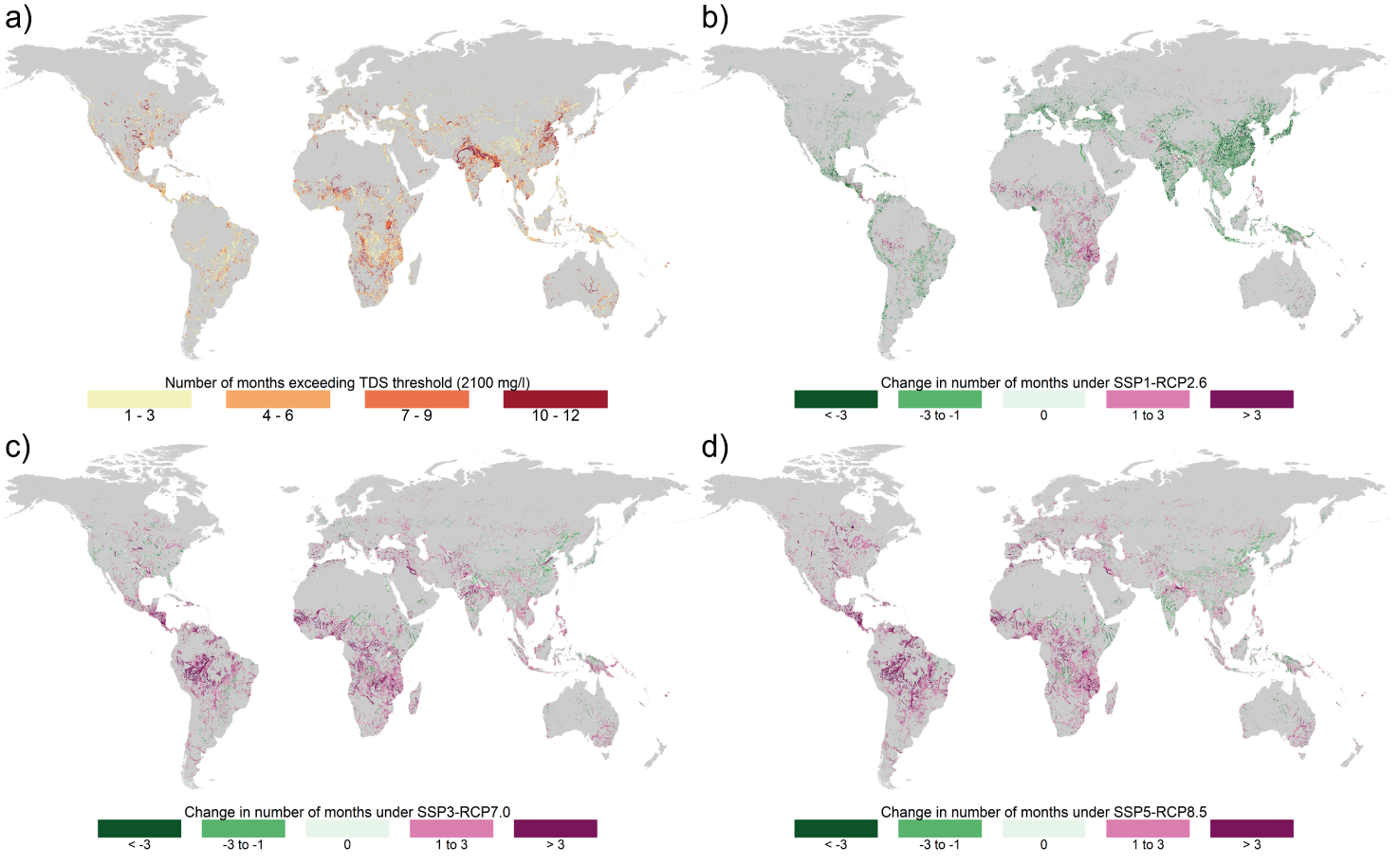

Figure C.12 a) Number of months per year that surface waters exceed a total dissolved solids (TDS) threshold of 2,100 mg l^{-1} in a historical reference period (2005–2020). Panels b), c) and d) display the change in number of months that TDS thresholds are exceeded in a future time period (2081–2100) under three combined climate and socioeconomic scenarios, relative to historical exceedances (i.e. panel a).

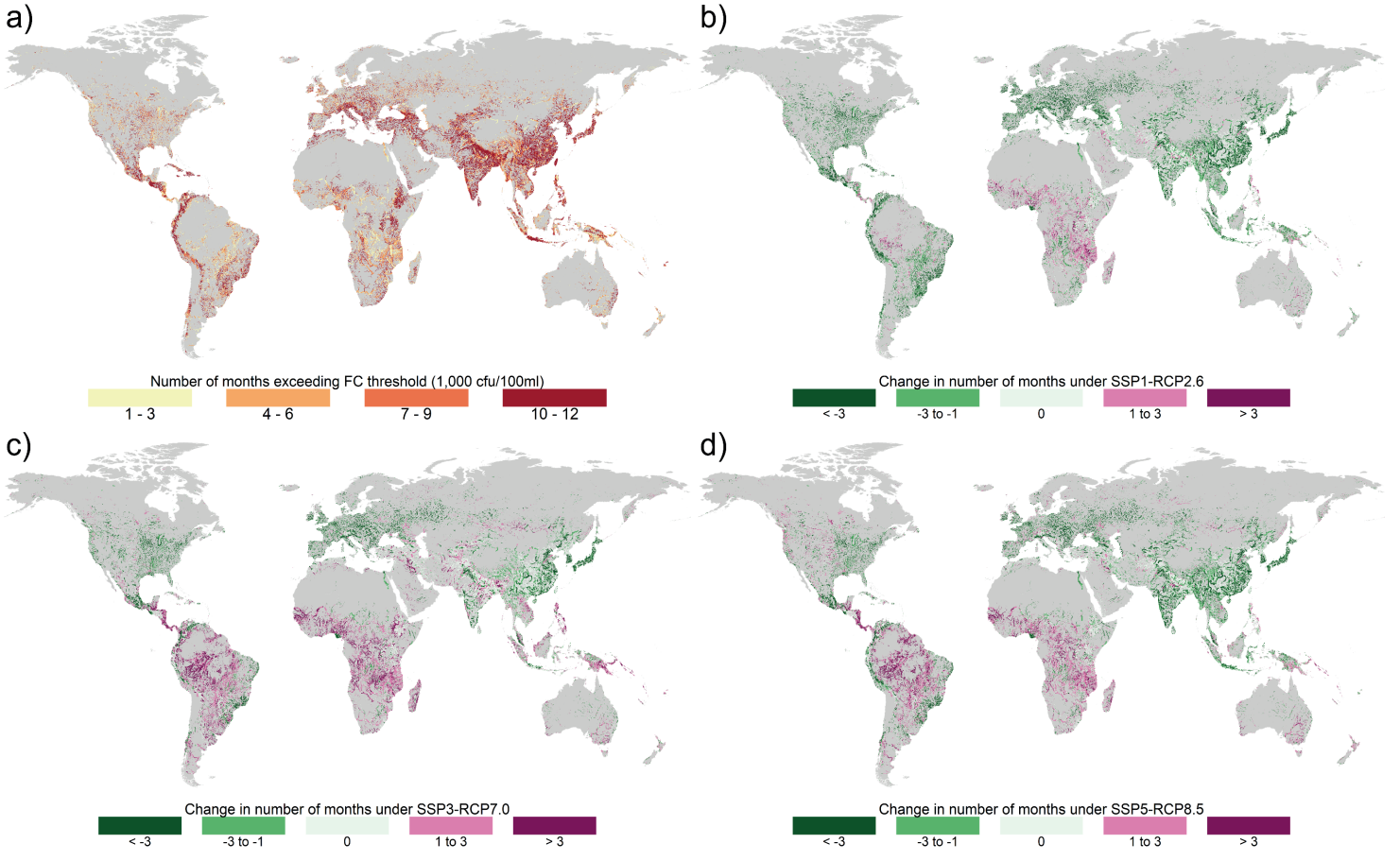

Figure C.13 a) Number of months per year that surface waters exceed a fecal coliform (FC) threshold of 1,000 cfu $100ml^{-1}$ in a historical reference period (2005–2020). Panels b), c) and d) display the change in number of months that FC thresholds are exceeded in a future time period (2081–2100) under three combined climate and socioeconomic scenarios, relative to historical exceedances (i.e. panel a).

C.3 Population exposed to polluted surface water

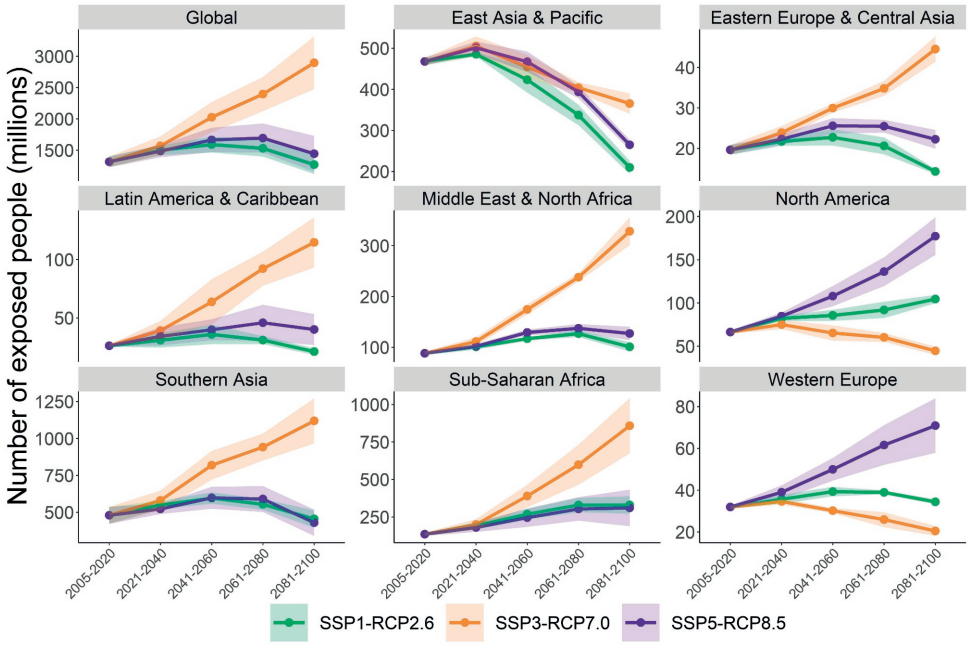

Figure C.14 Number of people exposed to surface water quality that exceed a total dissolved solids (TDS) concentration of 2,100 mg l^{-1} under the different combined climate and socioeconomic scenarios, disaggregated by geographic region. Lines display the mean average over the 5 general circulation models (GCMs) considered, while shaded areas represent the uncertainty arising from variations in GCM simulations as ±1 standard deviation.

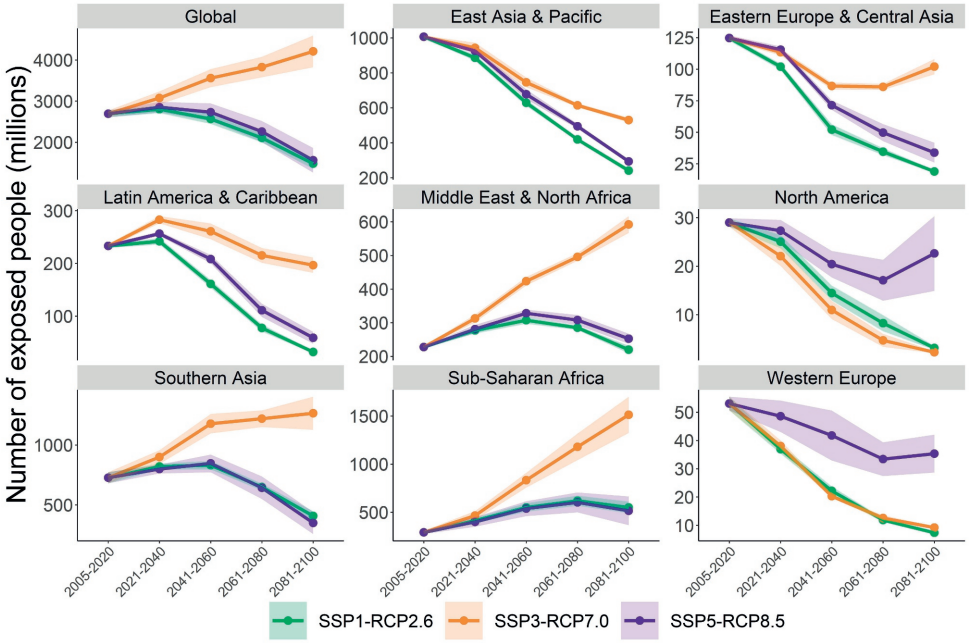

Figure C.15 Number of people exposed to surface water quality that exceed a biological oxygen demand (BOD) concentration of 8 mg l^{-1} under the different combined climate and socioeconomic scenarios, disaggregated by geographic region. Lines display the mean average over the 5 general circulation models (GCMs) considered, while shaded areas represent the uncertainty arising from variations in GCM simulations as ±1 standard deviation.

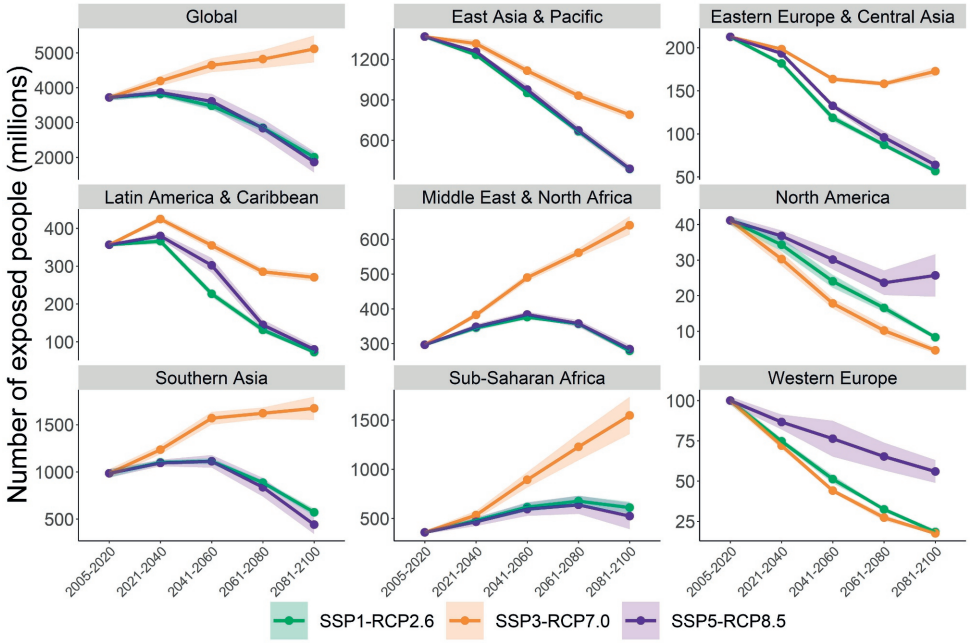

Figure C.16 Number of people exposed to surface water quality that exceed a fecal coliform (FC) concentration of 1,000 cfu 100ml^{-1} under the different combined climate and socioeconomic scenarios, disaggregated by geographic region. Lines display the mean average over the 5 general circulation models (GCMs) considered, while shaded areas represent the uncertainty arising from variations in GCM simulations as ±1 standard deviation.

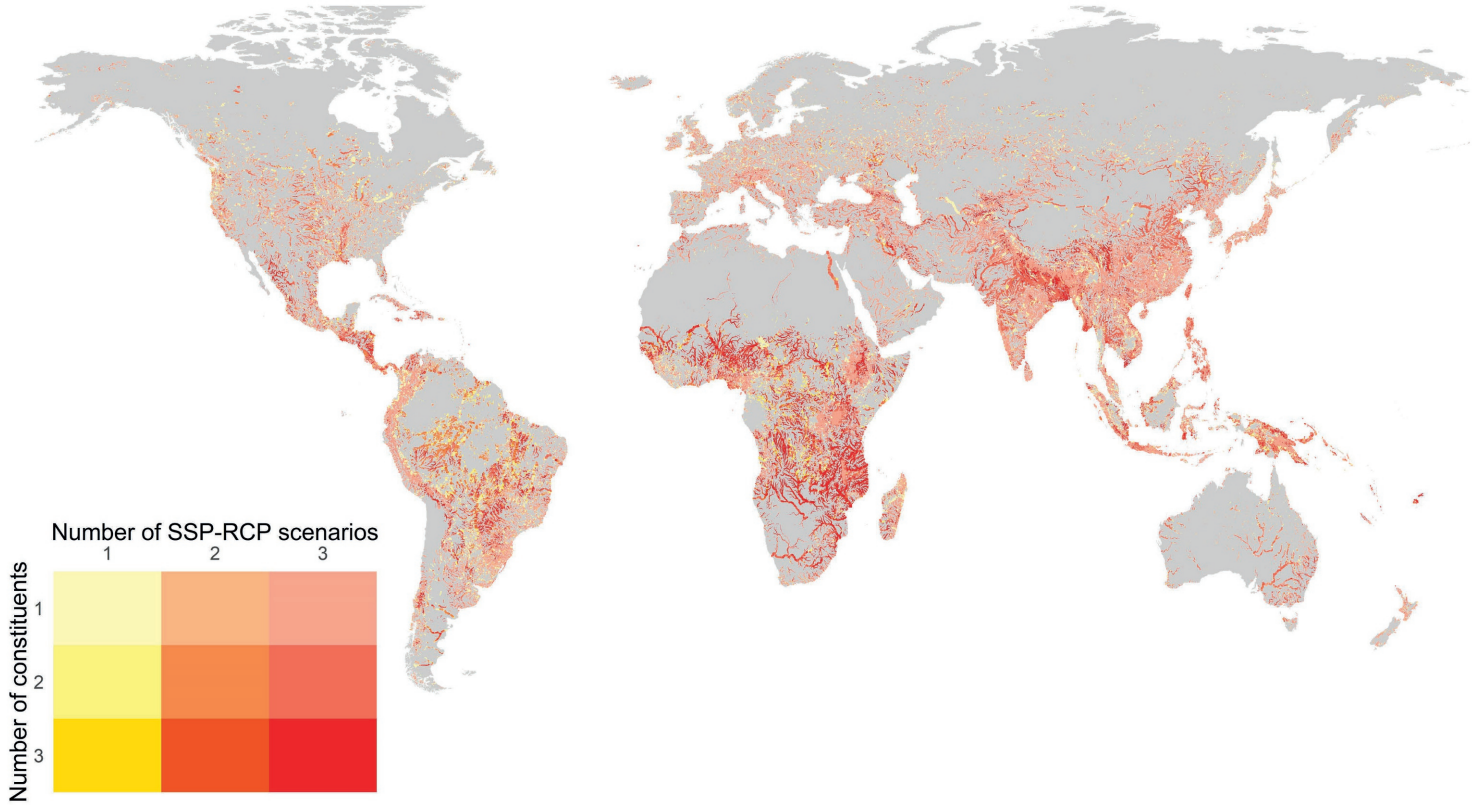

Figure C.17 Combined number of constituents that exceed water quality thresholds, and under how many scenarios, averaged over 2081–2100. Water quality thresholds considered are 2,100 mg l^{-1}, 8 mg l^{-1} and 1,000 cfu $100ml^{-1}$ for total dissolved solids (TDS), biological oxygen demand (BOD) and fecal coliform (FC), respectively.

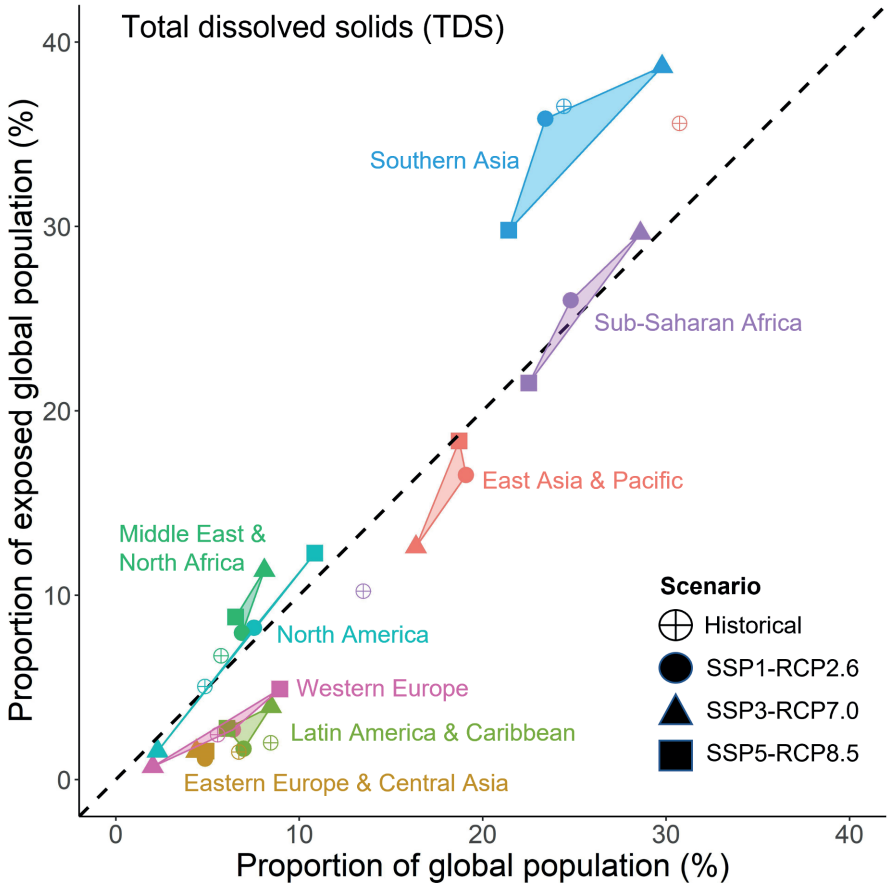

Figure C.18 Percentage of the global population residing in different world regions compared to the percentage of the global population that is exposed to surface waters that exceed a total dissolved solids (TDS) concentration of 2,100 mg l^{-1} in each world region. Results are for averaged over multi-year periods for both a historical reference period (2005–2020) and for the time period 2081–2100 under the three different combined climate and socioeconomic scenarios.

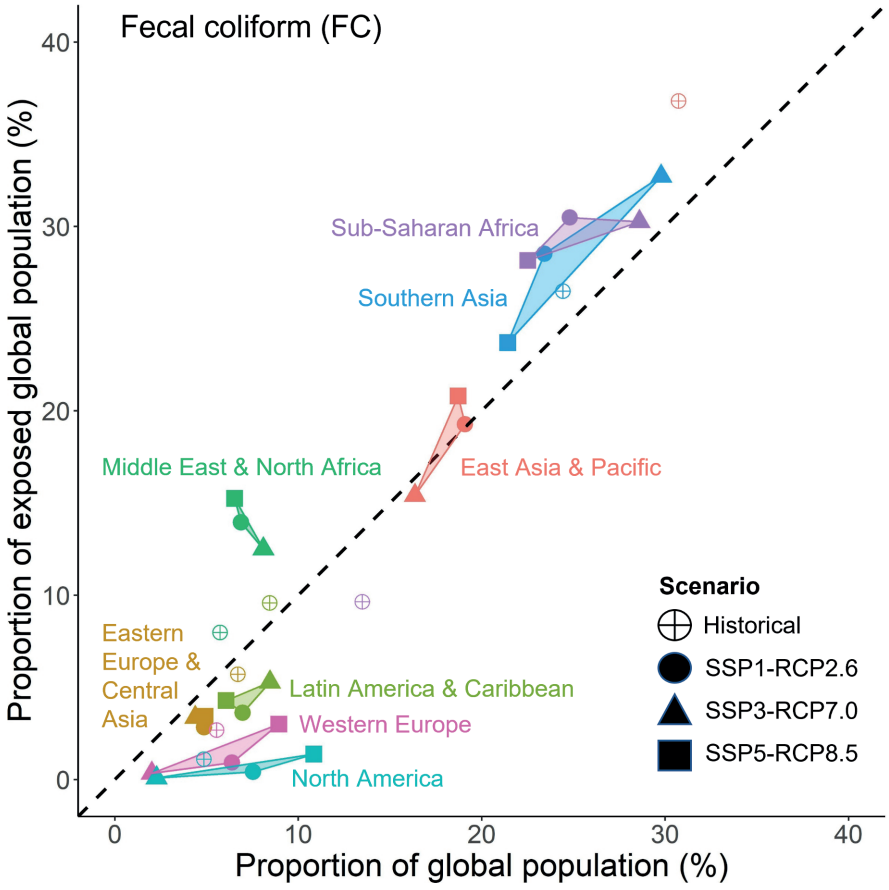

Figure C.19 Percentage of the global population residing in different world regions compared to the percentage of the global population that is exposed to surface waters that exceed a fecal coliform (FC) concentration of 1,000 cfu $100ml^{-1}$ in each world region. Results are for averaged over multi-year periods for both a historical reference period (2005–2020) and for the time period 2081–2100 under the three different combined climate and socioeconomic scenarios.

Appendix D | Supplementary information to Chapter 6

Supplementary to: Synthesis

D.1 Water scarcity indicators

Methods building on the grey water footprint concept have been used to evaluate quality-induced water scarcity (Liu et al., 2016; Wan et al., 2016; Zhao et al., 2016; van Vliet et al., 2017; van Vliet et al., 2021). The grey water footprint represents the volume of water required to assimilate pollution to meet ambient water quality standards via dilution (Hoekstra and Mekonnen, 2012). While the dilution does not necessarily happen in reality, the purpose of this approach is to estimate a fresh water equivalent to facilitate a comparable measure of quantity and quality aspects for water scarcity assessment (Wan et al., 2016).

Further building on the method developed by van Vliet et al. (2017) and van Vliet et al. (2021), indicators of water scarcity accounting for: 1) water quantity aspects only (*WS*) (Eq. D.1); and 2) water quantity and quality aspects (*WSq*) (Eq. D.2) are developed.

$$\mathrm{W}S = \frac{D_{nonIrr} + D_{irr} - GWA}{Q - EFR} \tag{D.1}$$

Where: *WS* represents water scarcity based on water quantity only (-); D_{nonIrr} and D_{Irr} represent the monthly average water demands for the non-irrigation (domestic, industrial) and irrigation sectors (m^3 $month^{-1}$), respectively; GWA is the groundwater abstractions for fulfilling sectoral demands (m^3 $month^{-1}$); Q is discharge (m^3 $month^{-1}$); and EFR is the environmental flow requirement (m^3 $month^{-1}$), estimated using the monthly variable flow methods (Pastor et al., 2014).

$$\begin{gathered} WSq = \frac{D_{nonIrr} + D_{irr} - GWA + dq_{max}}{Q - EFR} \\ dq_{max} = max(dq_{TDS}, dq_{BOD}, dq_{FC}) \\ dq_p = \begin{cases} 0, & C_p \leqslant C_{max} \\ \frac{(D_{nonIrr}+D_{irr}-GWA)\cdot C_p}{C_{max}} - (D_{nonIrr} + D_{irr} - GWA), & C_p > C_{max} \end{cases} \end{gathered} \tag{D.2}$$

Where: *WSq* represents water scarcity including both water quantity and water quality [-]; dq_p is the extra water demands for dilution to obtain acceptable quality for water constituent p (m^3 $month^{-1}$); C_p is the surface water concentration of water quality constituent p (TDS and BOD in mg l^{-1}; FC in cfu $100ml^{-1}$); and C_{max_p} is the critical threshold concentration of water quality constituent p considered (TDS: 2,100 mg l^{-1}; BOD: 8 mg l^{-1}; FC: 1,000 $100ml^{-1}$). Other terms are as per Eq. D.1.

WS and WSq values exceeding 1 are used to indicate water scarcity – i.e. the demands for water resources (less those met by groundwater pumping) exceed the renewable water avaliability (less the water required to maintain environmental flows).

References

Alcamo, J., Flörke, M. & Märker, M. (2010). Future long-term changes in global water resources driven by socio-economic and climatic changes. *https://doi.org/10.1623/hysj.52.2.247*, 52 (2), pp. 247–275. DOI:10.1623/HYSJ.52.2.247.

Arnell, N.W. (1999). Climate change and global water resources. *Global Environmental Change*, 9 (SUPPL.), S31–S49. DOI:10.1016/S0959-3780(99)00017-5.

Ashbolt, N.J. (2004). Microbial contamination of drinking water and disease outcomes in developing regions. *Toxicology*, 198 (1-3), pp. 229–238. DOI:10.1016/J.TOX.2004.01.030.

Ayers, R.S. & Westcot, D.W. (1985). *Water quality for agriculture*. Rome : Food and Agriculture Organization of the United Nations.

Barbarossa, V., Bosmans, J., Wanders, N., King, H., Bierkens, M.F.P., Huijbregts, M.A.J. & Schipper, A.M. (2021). Threats of global warming to the world' s freshwater fishes. *Nature Communications*, 12 (1), p. 1701. DOI:10.1038/S41467-021-21655-W.

Bartram, J. & Rees, G. (1999). Monitoring Bathing Waters : A Practical Guide to the Design and Implementation of Assessments and Monitoring Programmes. *Monitoring Bathing Waters*. DOI:10.4324/9780203478264.

Batjes, N.H. (2005). ISRIC-WISE global data set of derived soil properties on a 0.5 by 0.5 degree grid (Version 3.0).

Bauer, N. et al. (2017). Shared Socio-Economic Pathways of the Energy Sector - Quantifying the Narratives. *Global Environmental Change*, 42, pp. 316–330. DOI:10.1016/J.GLOENVCHA.2016.07.006.

Beard, J.E., Bierkens, M.F. & Bartholomeus, R.P. (2019). Following the water: Characterising de facto wastewater reuse in agriculture in the Netherlands. *Sustainability (Switzerland)*, 11 (21). DOI:10.3390/SU11215936.

Beusen, A.H., Beek, L.P.V., Bouwman, A.F., Mogollón, J.M. & Middelburg, J.J. (2015). Coupling global models for hydrology and nutrient loading to simulate nitrogen and phosphorus retention in surface water - Description of IMAGE-GNM and analysis of performance. *Geoscientific Model Development*, 8 (12), pp. 4045–4067. DOI:10.5194/GMD-8-4045-2015.

Beusen, A.H., Dekkers, A.L., Bouwman, A.F., Ludwig, W. & Harrison, J. (2005). Estimation of global river transport of sediments and associated particulate C, N, and P. *Global Biogeochemical Cycles*, 19 (4). DOI:10.1029/2005GB002453.

Beusen, A.H., Doelman, J.C., Beek, L.P.V., Puijenbroek, P.J.V., Mogollón, J.M., Grinsven, H.J.V., Stehfest, E., Vuuren, D.P.V. & Bouwman, A.F. (2022). Exploring river nitrogen and phosphorus loading and export to global coastal waters in the Shared Socio-economic pathways. *Global Environmental Change*, 72, p. 102426. DOI:10.1016/J.GLOENVCHA.2021.102426.

Bierkens, M.F. (2015). Global hydrology 2015: State, trends, and directions. *Water Resources Research*, 51 (7), pp. 4923–4947. DOI:10.1002/2015WR017173.

Bierkens, M.F. & Wada, Y. (2019). Non-renewable groundwater use and groundwater depletion: A review. *Environmental Research Letters*, 14 (6). DOI:10.1088/1748-9326/AB1A5F.

Binzer, A., Guill, C., Rall, B.C. & Brose, U. (2016). Interactive effects of warming, eutrophication and size structure: impacts on biodiversity and food-web structure. *Global change biology*, 22 (1), pp. 220–227. DOI:10.1111/GCB.13086.

Bosmans, J., Wanders, N., Bierkens, M.F., Huijbregts, M.A., Schipper, A.M. & Barbarossa, V. (2022). FutureStreams, a global dataset of future streamflow and water temperature. *Scientific Data 2022 9:1*, 9 (1), pp. 1–10. DOI:10.1038/S41597-022-01410-6.

Bruinsma, J. (2003). World agriculture : towards 2015/2030 : an FAO perspective, p. 432.

Caretta, M.A. et al. (2022). *Water*. DOI:10.1017/9781009325844.006.

Chapra, S. & Pelletier, G. (2004). QUAL2K: A Modeling Framework for Simulating River and Stream Water Quality.

Chhipi-Shrestha, G., Hewage, K. & Sadiq, R. (2017). Fit-for-purpose wastewater treatment: Conceptualization to development of decision support tool (I). *Science of the Total Environment*, 607-608, pp. 600–612. DOI:10.1016/J.SCITOTENV.2017.06.269.

Chowdhury, S., Mazumder, M.A., Al-Attas, O. & Husain, T. (2016). Heavy metals in drinking water: Occurrences, implications, and future needs in developing countries. *The Science of the total environment*, 569-570, pp. 476–488. DOI:10.1016/J.SCITOTENV.2016.06.166.

Cucchi, M., Weedon, G.P., Amici, A., Bellouin, N., Lange, S., Schmied, H.M., Hersbach, H. & Buontempo, C. (2020). WFDE5: Bias-adjusted ERA5 reanalysis data for impact studies. *Earth System Science Data*, 12 (3), pp. 2097–2120. DOI:10.5194/ESSD-12-2097-2020.

Damania, R.R., Desbureaux, S., Rodella, A.-S., Russ, J. & Zaveri, E. (2019). *Quality Unknown : The Invisible Water Crisis*. World Bank.

Deblonde, T., Cossu-Leguille, C. & Hartemann, P. (2011). Emerging pollutants in wastewater: A review of the literature. *International Journal of Hygiene and Environmental Health*, 214 (6), pp. 442–448. DOI:10.1016/J.IJHEH.2011.08.002.

Desbureaux, S., Mortier, F., Zaveri, E., van Vliet, M.T.H., Russ, J., Rodella, A.S. & Damania, R. (2022). Mapping global hotspots and trends of water quality (1992-2010): a data driven approach. *Environmental Research Letters*, 17 (11), p. 114048. DOI:10.1088/1748-9326/AC9CF6.

Drechsel, P., Qadir, M. & Wichelns, D. (2015). *Wastewater: Economic asset in an urbanizing world*. Springer Netherlands, pp. 1–282. DOI:10.1007/978-94-017-9545-6.

Dumont, E., Williams, R., Keller, V., Voß, A. & Tattari, S. (2012). Modelling indicators of water security, water pollution and aquatic biodiversity in Europe. *https://doi.org/10.1080/02626667.2012.715747*, 57 (7), pp. 1378–1403. DOI:10.1080/02626667.2012.715747.

Döll, P., Trautmann, T., Gerten, D., Schmied, H.M., Ostberg, S., Saaed, F. & Schleussner, C.F. (2018). Risks for the global freshwater system at 1.5 °C and 2 °C global warming. *Environmental Research Letters*, 13 (4), p. 044038. DOI:10.1088/1748-9326/AAB792.

EEA (2019). *Waterbase - UWWTD: Urban Waste Water Treatment Directive - reported data*.

Englert, D., Zubrod, J.P., Schulz, R. & Bundschuh, M. (2013). Effects of municipal wastewater on aquatic ecosystem structure and function in the receiving stream. *Science of The Total Environment*, 454-455, pp. 401–410. DOI:10.1016/J.SCITOTENV.2013.03.025.

Ercin, A.E. & Hoekstra, A.Y. (2014). Water footprint scenarios for 2050: A global analysis. *Environment International*, 64, pp. 71–82. DOI:10.1016/J.ENVINT.2013.11.019.

Fick, S.E. & Hijmans, R.J. (2017). WorldClim 2: new 1-km spatial resolution climate surfaces for global land areas. *International Journal of Climatology*, 37 (12), pp. 4302–4315. DOI:HTTPS://DOI.ORG/10.1002/JOC.5086.

Fipps, G. (2003). Irrigation Water Quality Standards and Salinity Management Strategies.

Flörke, M., Kynast, E., Bärlund, I., Eisner, S., Wimmer, F. & Alcamo, J. (2013). Domestic and industrial water uses of the past 60 years as a mirror of socio-economic development: A global simulation study. *Global Environmental Change*, 23 (1), pp. 144–156. DOI:10.1016/J.GLOENVCHA.2012.10.018.

Fujimori, S., Hasegawa, T., Masui, T., Takahashi, K., Herran, D.S., Dai, H., Hijioka, Y. & Kainuma, M. (2017). SSP3: AIM implementation of Shared Socioeconomic Pathways. *Global Environmental Change*, 42, pp. 268–283. DOI:10.1016/J.GLOENVCHA.2016.06.009.

Garcia, X. & Pargament, D. (2015). Reusing wastewater to cope with water scarcity: Economic, social and environmental considerations for decision-making. *Resources, Conservation and Recycling*, 101, pp. 154–166. DOI:10.1016/J.RESCONREC.2015.05.015.

Geissen, V., Mol, H., Klumpp, E., Umlauf, G., Nadal, M., van der Ploeg, M., van de Zee, S.E. & Ritsema, C.J. (2015). Emerging pollutants in the environment: A challenge for water resource management. *International Soil and Water Conservation Research*, 3 (1), pp. 57–65. DOI:10.1016/J.ISWCR.2015.03.002.

Gholizadeh, M.H., Melesse, A.M. & Reddi, L. (2016). A Comprehensive Review on Water Quality Parameters Estimation Using Remote Sensing Techniques. *Sensors 2016, Vol. 16, Page 1298*, 16 (8), p. 1298. DOI:10.3390/S16081298.

Gilbert, M., Nicolas, G., Cinardi, G., Boeckel, T.P.V., Vanwambeke, S.O., Wint, G.R. & Robinson, T.P. (2018). Global distribution data for cattle, buffaloes, horses, sheep, goats, pigs, chickens and ducks in 2010. *Scientific Data 2018 5:1*, 5 (1), pp. 1–11. DOI:10.1038/SDATA.2018.227.

Graaf, I.E.D., van Beek, L.P., Wada, Y. & Bierkens, M.F. (2014). Dynamic attribution of global water demand to surface water and groundwater resources: Effects of abstractions and return flows on river discharges. *Advances in Water Resources*, 64, pp. 21–33. DOI:10.1016/J.ADVWATRES.2013.12.002.

Graham, N.T., Davies, E.G.R., Hejazi, M.I., Calvin, K., Kim, S.H., Helinski, L., Miralles-Wilhelm, F.R., Clarke, L., Kyle, P., Patel, P., Wise, M.A. & Vernon, C.R. (2018). Water Sector Assumptions for the Shared Socioeconomic Pathways in an Integrated Modeling Framework. *Water Resources Research*, 54 (9), pp. 6423–6440. DOI:HTTPS://DOI.ORG/10.1029/2018WR023452.

Greve, P., Kahil, T., Mochizuki, J., Schinko, T., Satoh, Y., Burek, P., Fischer, G., Tramberend, S., Burtscher, R., Langan, S. & Wada, Y. (2018). Global assessment of water challenges under uncertainty in water scarcity projections. *Nature Sustainability 2018 1:9*, 1 (9), pp. 486–494. DOI:10.1038/S41893-018-0134-9.

Gude, V.G. (2017). Desalination and water reuse to address global water scarcity. *Reviews in Environmental Science and Biotechnology*, 16 (4), pp. 591–609. DOI:10.1007/S11157-017-9449-7.

Gudmundsson, L., Boulange, J., Do, H.X., Gosling, S.N., Grillakis, M.G., Koutroulis, A.G., Leonard, M., Liu, J., Schmied, H.M., Papadimitriou, L., Pokhrel, Y., Seneviratne, S.I., Satoh, Y., Thiery, W., Westra, S., Zhang, X. & Zhao, F. (2021). Globally observed trends in mean and extreme river flow attributed to climate change. *Science*,

371 (6534), pp. 1159–1162. DOI:10.1126/SCIENCE.ABA3996/SUPPL_FILE/ABA3996_GUDMUNDSSON_SM.PDF.
Gupta, H.V., Kling, H., Yilmaz, K.K. & Martinez, G.F. (2009). Decomposition of the mean squared error and NSE performance criteria: Implications for improving hydrological modelling. *Journal of Hydrology*, 377 (1-2), pp. 80–91. DOI:10.1016/J.JHYDROL.2009.08.003.
GWI (2015). *Country-specific data on total volume of municipal wastewater produced at the national level*.
Haddeland, I., Heinke, J., Biemans, H., Eisner, S., Flörke, M., Hanasaki, N., Konzmann, M., Ludwig, F., Masaki, Y., Schewe, J., Stacke, T., Tessler, Z.D., Wada, Y. & Wisser, D. (2014). Global water resources affected by human interventions and climate change. *Proceedings of the National Academy of Sciences of the United States of America*, 111 (9), pp. 3251–3256. DOI:10.1073/PNAS.1222475110/SUPPL_FILE/PNAS.201222475SI.PDF.
Hanasaki, N., Fujimori, S., Yamamoto, T., Yoshikawa, S., Masaki, Y., Hijioka, Y., Kainuma, M., Kanamori, Y., Masui, T., Takahashi, K. & Kanae, S. (2013). A global water scarcity assessment under Shared Socio-economic Pathways - Part 2: Water availability and scarcity. *Hydrology and Earth System Sciences*, 17 (7), pp. 2393–2413. DOI:10.5194/HESS-17-2393-2013.
Hanasaki, N., Yoshikawa, S., Pokhrel, Y. & Kanae, S. (2018). A Quantitative Investigation of the Thresholds for Two Conventional Water Scarcity Indicators Using a State-of-the-Art Global Hydrological Model With Human Activities. *Water Resources Research*, 54 (10), pp. 8279–8294. DOI:10.1029/2018WR022931.
Hansen, E., Rodrigues, M.A.S. & de Aquim, P.M. (2016). Wastewater reuse in a cascade based system of a petrochemical industry for the replacement of losses in cooling towers. *Journal of Environmental Management*, 181, pp. 157–162. DOI:10.1016/J.JENVMAN.2016.06.014.
Hartmann, J., Lauerwald, R. & Moosdorf, N. (2014). A Brief Overview of the GLObal RIver Chemistry Database, GLORICH. *Procedia Earth and Planetary Science*, 10, pp. 23–27. DOI:10.1016/J.PROEPS.2014.08.005.
He, C., Liu, Z., Wu, J., Pan, X., Fang, Z., Li, J. & Bryan, B.A. (2021). Future global urban water scarcity and potential solutions. *Nature Communications*, 12 (1), p. 4667. DOI:10.1038/S41467-021-25026-3.
Heal, K.V., Bartosova, A., Hipsey, M.R., Chen, X., Buytaert, W., Li, H.Y., McGrane, S.J., Gupta, A.B. & Cudennec, C. (2021). Water quality: the missing dimension of water in the water-energy-food nexus. *https://doi.org/10.1080/02626667.2020.1859114*, 66 (5), pp. 745–758. DOI:10.1080/02626667.2020.1859114.
Hernandez-Sancho, F., Molinos-Senante, M. & Sala-Garrido, R. (2011). Cost modelling for wastewater treatment processes. *Desalination*, 268 (1-3), pp. 1–5. DOI:10.1016/J.DESAL.2010.09.042.
Hernández-Chover, V., Águeda Bellver-Domingo & Hernández-Sancho, F. (2018). Efficiency of wastewater treatment facilities: The influence of scale economies. *Journal of Environmental Management*, 228, pp. 77–84. DOI:10.1016/J.JENVMAN.2018.09.014.
Hoch, J.M., Sutanudjaja, E.H., Wanders, N., van Beek, R.L.P.H. & Bierkens, M.F.P. (2023). Hyper-resolution PCR-GLOBWB: opportunities and challenges from refining model spatial resolution to 1 km over the European continent. *Hydrology and Earth System Sciences*, 27 (6), pp. 1383–1401. DOI:10.5194/HESS-27-1383-2023.
Hoekstra, A.Y. & Mekonnen, M.M. (2012). The water footprint of humanity. *Proceedings of the National Academy of Sciences of the United States of America*, 109 (9), pp. 3232–3237. DOI:10.1073/PNAS.1109936109/SUPPL_FILE/PNAS.1109936109_SI.PDF.
Hofstra, N., Bouwman, A.F., Beusen, A.H. & Medema, G.J. (2013). Exploring global Cryptosporidium emissions to surface water. *Science of The Total Environment*, 442, pp. 10–19. DOI:10.1016/J.SCITOTENV.2012.10.013.
Hrachowitz, M. et al. (2013). A decade of Predictions in Ungauged Basins (PUB)—a review. *https://doi.org/10.1080/02626667.2013.803183*, 58 (6), pp. 1198–1255. DOI:10.1080/02626667.2013.803183.
Hurtt, G.C. et al. (2020). Harmonization of global land use change and management for the period 850-2100 (LUH2) for CMIP6. *Geoscientific Model Development*, 13 (11), pp. 5425–5464. DOI:10.5194/GMD-13-5425-2020.
IPCC (2022). *Climate Change 2022: Impacts, Adaptation and Vulnerability. Contribution of Working Group II to the Sixth Assessment Report of the Intergovernmental Panel on Climate Change*. Ed. by H.O. Pörtner, D.C. Roberts, M. Tignor, E.S. Poloczanska, K. Mintenbeck, A. Alegría, M. Craig, S. Langsdorf, S. Löschke, V. Möller, A. Okem & B. Rama. Cambridge University Press: Cambridge, UK and New York, NY, USA. DOI:10.1017/9781009325844.
Jarosiewicz, P., Fazi, S. & Zalewski, M. (2022). How to boost Ecohydrological Nature-Based Solutions in water quality management. *Ecohydrology & Hydrobiology*, 22 (2), pp. 226–233. DOI:10.1016/J.ECOHYD.2021.11.005.
Jiménez, B. & Asano, T. (2008). Water Reuse: An International Survey of current practice, issues and needs. *Water Intelligence Online*, 7 (0), pp. 9781780401881–9781780401881. DOI:10.2166/9781780401881.
Jones, B. & O'Neill, B.C. (2016). Spatially explicit global population scenarios consistent with the Shared Socioeconomic Pathways. *Environmental Research Letters*, 11 (8), p. 084003. DOI:10.1088/1748-9326/11/8/084003.
Jones, E.R., Bierkens, M.F.P., Wanders, N., Sutanudjaja, E.H., van Beek, L.P.H. & van Vliet, M.T.H. (2022). Current wastewater treatment targets are insufficient to protect surface water quality. *Communications Earth & Environment*, 3 (1), p. 221. DOI:10.1038/S43247-022-00554-Y.

Jones, E.R., Bierkens, M.F.P., Wanders, N., Sutanudjaja, E.H., van Beek, L.P.H. & van Vliet, M.T.H. (2023). DynQual v1.0: a high-resolution global surface water quality model. *Geoscientific Model Development*, 16 (15), pp. 4481–4500. DOI:10.5194/GMD-16-4481-2023.

Jones, E.R., Qadir, M., van Vliet, M.T., Smakhtin, V. & Kang, S.-M. (2019). The state of desalination and brine production: A global outlook. *Science of the Total Environment*, 657. DOI:10.1016/J.SCITOTENV.2018.12.076.

Jones, E.R., van Vliet, M.T., Qadir, M. & Bierkens, M.F. (2020). *Country-level and gridded wastewater production, collection, treatment and re-use*. DOI:10.1594/PANGAEA.918731.

Jones, E.R., van Vliet, M.T., Qadir, M. & Bierkens, M.F. (2021). Country-level and gridded estimates of wastewater production, collection, treatment and reuse. *Earth System Science Data*, 13 (2), pp. 237–254. DOI:10.5194/ESSD-13-237-2021.

Kantur, Z. & Özcan, G. (2021). What pandemic inflation tells: Old habits die hard. *Economics Letters*, 204, p. 109907. DOI:10.1016/J.ECONLET.2021.109907.

Kaushal, S.S., Groffman, P.M., Band, L.E., Shields, C.A., Morgan, R.P., Palmer, M.A., Belt, K.T., Swan, C.M., Findlay, S.E. & Fisher, G.T. (2008). Interaction between urbanization and climate variability amplifies watershed nitrate export in Maryland. *Environmental Science and Technology*, 42 (16), pp. 5872–5878. DOI:10.1021/ES800264F/SUPPL_FILE/ES800264F-FILE002.PDF.

Kaushal, S.S., Mayer, P.M., Vidon, P.G., Smith, R.M., Pennino, M.J., Newcomer, T.A., Duan, S., Welty, C. & Belt, K.T. (2014). Land Use and Climate Variability Amplify Carbon, Nutrient, and Contaminant Pulses: A Review with Management Implications. *JAWRA Journal of the American Water Resources Association*, 50 (3), pp. 585–614. DOI:10.1111/JAWR.12204.

Khalil, M. & Hussein, H. (2008). Use of waste water for aquaculture: an experimental field study at a sewage-treatment plant, Egypt. *Aquaculture Research*, 28 (11), pp. 859–865. DOI:10.1046/J.1365-2109.1997.00910.X.

Knoben, W.J., Freer, J.E. & Woods, R.A. (2019). Technical note: Inherent benchmark or not? Comparing Nash-Sutcliffe and Kling-Gupta efficiency scores. *Hydrology and Earth System Sciences*, 23 (10), pp. 4323–4331. DOI:10.5194/HESS-23-4323-2019.

Konapala, G., Mishra, A.K., Wada, Y. & Mann, M.E. (2020). Climate change will affect global water availability through compounding changes in seasonal precipitation and evaporation. *Nature Communications 2020 11:1*, 11 (1), pp. 1–10. DOI:10.1038/S41467-020-16757-W.

Kraaijenbrink, P.D.A., Stigter, E.E., Yao, T. & Immerzeel, W.W. (2021). Climate change decisive for Asia' s snow meltwater supply. *Nature Climate Change*, 11 (7), pp. 591–597. DOI:10.1038/S41558-021-01074-X.

Kroeze, C., Gabbert, S., Hofstra, N., Koelmans, A.A., Li, A., Löhr, A., Ludwig, F., Strokal, M., Verburg, C., Vermeulen, L., van Vliet, M.T.H., de Vries, W., Wang, M. & van Wijnen, J. (2016). Global modelling of surface water quality: a multi-pollutant approach. *Current Opinion in Environmental Sustainability*, 23, pp. 35–45. DOI:10.1016/J.COSUST.2016.11.014.

Kummu, M., Guillaume, J.H., Moel, H.D., Eisner, S., Flörke, M., Porkka, M., Siebert, S., Veldkamp, T.I. & Ward, P.J. (2016). The world's road to water scarcity: Shortage and stress in the 20th century and pathways towards sustainability. *Scientific Reports*, 6. DOI:10.1038/SREP38495.

Lange, S & Buchner, M. (2021). *ISIMIP3b bias-adjusted atmospheric climate input data*. DOI:10.48364/ISIMIP.842396.1.

Lange, S, Menz, C, Gleixner, S, Cucchi, M, Weedon, G., Amici, A., Bellouin, N., Schmied, H., Hersbach, H., Buontempo, C. & Cagnazzo, C. (2021). *WFDE5 over land merged with ERA5 over the ocean (W5E5 v2.0)*. DOI:10.48364/ISIMIP.342217.

Lange, S. & Geiger, T. (2020). *ISIMIP3a population input data*. DOI:10.48364/ISIMIP.822480.

Liu, J., Liu, Q. & Yang, H. (2016). Assessing water scarcity by simultaneously considering environmental flow requirements, water quantity, and water quality. *Ecological Indicators*, 60, pp. 434–441. DOI:10.1016/J.ECOLIND.2015.07.019.

Liu, J., Yang, H., Gosling, S.N., Kummu, M., Flörke, M., Pfister, S., Hanasaki, N., Wada, Y., Zhang, X., Zheng, C., Alcamo, J. & Oki, T. (2017). Water scarcity assessments in the past, present, and future. *Earth's Future*, 5 (6), pp. 545–559. DOI:10.1002/2016EF000518.

Lohrmann, A., Farfan, J., Caldera, U., Lohrmann, C. & Breyer, C. (2019). Global scenarios for significant water use reduction in thermal power plants based on cooling water demand estimation using satellite imagery. *Nature Energy 2019 4:12*, 4 (12), pp. 1040–1048. DOI:10.1038/S41560-019-0501-4.

Loucks, D.P. & van Beek, E. (2017). Water Quality Modeling and Prediction. *Water Resource Systems Planning and Management*, pp. 417–467. DOI:10.1007/978-3-319-44234-1_10.

Luthy, R.G., Sedlak, D.L., Plumlee, M.H., Austin, D. & Resh, V.H. (2015). Wastewater-effluent-dominated streams as ecosystem-management tools in a drier climate. *Frontiers in Ecology and the Environment*, 13 (9), pp. 477–485. DOI:10.1890/150038.

Macedo, H.E., Lehner, B., Nicell, J., Grill, G., Li, J., Limtong, A. & Shakya, R. (2022). Distribution and characteristics of wastewater treatment plants within the global river network. *Earth System Science Data*, 14 (2), pp. 559–577. DOI:10.5194/ESSD-14-559-2022.

Madden, N., Lewis, A. & Davis, M. (2013). Thermal effluent from the power sector: an analysis of once-through cooling system impacts on surface water temperature. *Environmental Research Letters*, 8 (3), p. 035006. DOI:10.1088/1748-9326/8/3/035006.

Mateo-Sagasta, J., Raschid-Sally, L. & Thebo, A. (2015). *Global wastewater and sludge production, treatment and use*. Springer Netherlands, pp. 15–38. DOI:10.1007/978-94-017-9545-6_2.

Meinshausen, M. et al. (2020). The shared socio-economic pathway (SSP) greenhouse gas concentrations and their extensions to 2500. *Geoscientific Model Development*, 13 (8), pp. 3571–3605. DOI:10.5194/GMD-13-3571-2020.

Miller, J.D. & Hutchins, M. (2017). The impacts of urbanisation and climate change on urban flooding and urban water quality: A review of the evidence concerning the United Kingdom. *Journal of Hydrology: Regional Studies*, 12, pp. 345–362. DOI:10.1016/J.EJRH.2017.06.006.

Moreno-Rodenas, A.M., Tscheikner-Gratl, F., Langeveld, J.G. & Clemens, F.H. (2019). Uncertainty analysis in a large-scale water quality integrated catchment modelling study. *Water Research*, 158, pp. 46–60. DOI:10.1016/J.WATRES.2019.04.016.

Morote, A., Olcina, J. & Hernández, M. (2019). The use of non-conventional water resources as a means of adaptation to drought and climate change in semi-arid regions: South-eastern Spain. *Water (Switzerland)*, 11 (1). DOI:10.3390/W11010093.

Morée, A.L., Beusen, A.H., Bouwman, A.F. & Willems, W.J. (2013). Exploring global nitrogen and phosphorus flows in urban wastes during the twentieth century. *Global Biogeochemical Cycles*, 27 (3), pp. 836–846. DOI:10.1002/GBC.20072.

Moussaoui, T.E., Wahbi, S., Mandi, L., Masi, S. & Ouazzani, N. (2019). Reuse study of sustainable wastewater in agroforestry domain of Marrakesh city. *Journal of the Saudi Society of Agricultural Sciences*, 18 (3), pp. 288–293. DOI:10.1016/J.JSSAS.2017.08.004.

Murray, A. & Drechsel, P. (2011). Why do some wastewater treatment facilities work when the majority fail? Case study from the sanitation sector in Ghana. *Waterlines*, 30 (2), pp. 135–149. DOI:10.3362/1756-3488.2011.015.

Nahian, M.A., Ahmed, A., Lázár, A.N., Hutton, C.W., Salehin, M. & Streatfield, P.K. (2018). Drinking water salinity associated health crisis in coastal Bangladesh. *Elementa*, 6. DOI:10.1525/ELEMENTA.143/112784.

Olson, J.R. & Hawkins, C.P. (2012). Predicting natural base-flow stream water chemistry in the western United States. *Water Resources Research*, 48 (2). DOI:10.1029/2011WR011088.

O'Neill, B.C., Kriegler, E., Ebi, K.L., Kemp-Benedict, E., Riahi, K., Rothman, D.S., van Ruijven, B.J., van Vuuren, D.P., Birkmann, J., Kok, K., Levy, M. & Solecki, W. (2017). The roads ahead: Narratives for shared socioeconomic pathways describing world futures in the 21st century. *Global Environmental Change*, 42, pp. 169–180. DOI:10.1016/J.GLOENVCHA.2015.01.004.

O'Neill, B.C., Tebaldi, C., Vuuren, D.P.V., Eyring, V., Friedlingstein, P., Hurtt, G., Knutti, R., Kriegler, E., Lamarque, J.F., Lowe, J., Meehl, G.A., Moss, R., Riahi, K. & Sanderson, B.M. (2016). The Scenario Model Intercomparison Project (ScenarioMIP) for CMIP6. *Geoscientific Model Development*, 9 (9), pp. 3461–3482. DOI:10.5194/GMD-9-3461-2016.

Ozaki, N., Fukushima, T., Harasawa, H., Kojiri, T., Kawashima, K. & Ono, M. (2003). Statistical analyses on the effects of air temperature fluctuations on river water qualities. *Hydrological Processes*, 17 (14), pp. 2837–2853. DOI:10.1002/HYP.1437.

Pastor, A.V., Ludwig, F., Biemans, H., Hoff, H. & Kabat, P. (2014). Accounting for environmental flow requirements in global water assessments. *Hydrology and Earth System Sciences*, 18 (12), pp. 5041–5059. DOI:10.5194/HESS-18-5041-2014.

Popp, A. et al. (2017). Land-use futures in the shared socio-economic pathways. *Global Environmental Change*, 42, pp. 331–345. DOI:10.1016/J.GLOENVCHA.2016.10.002.

Prüss-Ustün, A., Wolf, J., Bartram, J., Clasen, T., Cumming, O., Freeman, M.C., Gordon, B., Hunter, P.R., Medlicott, K. & Johnston, R. (2019). Burden of disease from inadequate water, sanitation and hygiene for selected adverse health outcomes: An updated analysis with a focus on low- and middle-income countries. *International journal of hygiene and environmental health*, 222 (5), pp. 765–777. DOI:10.1016/J.IJHEH.2019.05.004.

Qadir, M., Noble, A.D., Karajeh, F. & George, B. (2015). Potential business opportunities from saline water and salt-affected land resources. *Potential business opportunities from saline water and salt-affected land resources*. DOI:10.5337/2015.206.

Qadir, M., Sharma, B.R., Bruggeman, A., Choukr-Allah, R. & Karajeh, F. (2007). Non-conventional water resources and opportunities for water augmentation to achieve food security in water scarce countries. *Agricultural Water Management*, 87 (1), pp. 2–22. DOI:10.1016/J.AGWAT.2006.03.018.

Qadir, M., Wichelns, D., Raschid-Sally, L., McCornick, P.G., Drechsel, P., Bahri, A. & Minhas, P.S. (2010). The challenges of wastewater irrigation in developing countries. *Agricultural Water Management*, 97 (4), pp. 561–568. DOI:10.1016/J.AGWAT.2008.11.004.

Qadir, M., Drechsel, P., Cisneros, B.J., Kim, Y., Pramanik, A., Mehta, P. & Olaniyan, O. (2020). Global and regional potential of wastewater as a water, nutrient and energy source. *Natural Resources Forum*, 44 (1), pp. 40–51. DOI:10.1111/1477-8947.12187.

Qadir, M., Jiménez, G.C., Farnum, R.L., Dodson, L.L. & Smakhtin, V. (2018). Fog water collection: Challenges beyond technology. *Water (Switzerland)*, 10 (4). DOI:10.3390/W10040372.

Raptis, C.E., van Vliet, M.T.H. & Pfister, S (2016). Global thermal pollution of rivers from thermoelectric power plants. *Environmental Research Letters*, 11 (10), p. 104011. DOI:10.1088/1748-9326/11/10/104011.

Raschid-Sally, L & Jayakody, P (2008). *Drivers and Characteristics of Wastewater Agriculture in Developing Countries: Results from a Global Assessment*. International Water Management Institute.

Read, E.K., Carr, L., Cicco, L.D., Dugan, H.A., Hanson, P.C., Hart, J.A., Kreft, J., Read, J.S. & Winslow, L.A. (2017). Water quality data for national-scale aquatic research: The Water Quality Portal. *Water Resources Research*, 53 (2), pp. 1735–1745. DOI:10.1002/2016WR019993.

Reder, K., Flörke, M. & Alcamo, J. (2015). Modeling historical fecal coliform loadings to large European rivers and resulting in-stream concentrations. *Environmental Modelling and Software*, 63, pp. 251–263. DOI:10.1016/J.ENVSOFT.2014.10.001.

Riahi, K. et al. (2017). The Shared Socioeconomic Pathways and their energy, land use, and greenhouse gas emissions implications: An overview. *Global Environmental Change*, 42, pp. 153–168. DOI:10.1016/J.GLOENVCHA.2016.05.009.

Rice, J. & Westerhoff, P. (2017). High levels of endocrine pollutants in US streams during low flow due to insufficient wastewater dilution. *Nature Geoscience 2017 10:8*, 10 (8), pp. 587–591. DOI:10.1038/NGEO2984.

Rice, J., Wutich, A. & Westerhoff, P. (2013). Assessment of de facto wastewater reuse across the U.S.: Trends between 1980 and 2008. *Environmental Science and Technology*, 47 (19), pp. 11099–11105. DOI:10.1021/ES402792S.

Rietz, D.N. & Haynes, R.J. (2003). Effects of irrigation-induced salinity and sodicity on soil microbial activity. *Soil Biology and Biochemistry*, 35 (6), pp. 845–854. DOI:10.1016/S0038-0717(03)00125-1.

Robinson, T.P., Thornton, P.K., Francesconi, G.N., Kruska, R., Chiozza, F., Notenbaert, A.M.O., Cecchi, G., Herrero, M.T., Epprecht, M., Fritz, S., You, L., Conchedda, G. & See, L. (2011). Global livestock production systems. *Physical Review A*, p. 152.

Rode, M., Arhonditsis, G., Balin, D., Kebede, T., Krysanova, V., Griensven, A.V. & Zee, S.E.V.D. (2010). New challenges in integrated water quality modelling. *Hydrological Processes*, 24 (24), pp. 3447–3461. DOI:10.1002/HYP.7766.

Sato, T., Qadir, M., Yamamoto, S., Endo, T. & Zahoor, A. (2013). Global, regional, and country level need for data on wastewater generation, treatment, and use. *Agricultural Water Management*, 130, pp. 1–13. DOI:10.1016/J.AGWAT.2013.08.007.

Schewe, J. et al. (2014). Multimodel assessment of water scarcity under climate change. *Proceedings of the National Academy of Sciences of the United States of America*, 111 (9), pp. 3245–3250. DOI:10.1073/PNAS.1222460110.

Scott, C.A., Raschid-Sally, L., Bahri, A., Mara, D., Redwood, M. & Jiménez, B. (2010). *Wastewater Irrigation and Health: Challenges and Outlook for Mitigating Risks in Low-Income Countries*.

Sirota, J., Baiser, B., Gotelli, N.J. & Ellison, A.M. (2013). Organic-matter loading determines regime shifts and alternative states in an aquatic ecosystem. *Proceedings of the National Academy of Sciences of the United States of America*, 110 (19), pp. 7742–7747. DOI:10.1073/PNAS.1221037110/SUPPL_FILE/SAPP.PDF.

Smol, M., Adam, C. & Preisner, M. (2020). Circular economy model framework in the European water and wastewater sector. *Journal of Material Cycles and Waste Management*, 22 (3), pp. 682–697. DOI:10.1007/S10163-019-00960-Z.

Smucker, N.J., Beaulieu, J.J., Nietch, C.T. & Young, J.L. (2021). Increasingly severe cyanobacterial blooms and deep water hypoxia coincide with warming water temperatures in reservoirs. *Global Change Biology*, 27 (11), pp. 2507–2519. DOI:10.1111/GCB.15618.

Sood, A. & Smakhtin, V. (2015). Global hydrological models: a review. *https://doi.org/10.1080/02626667.2014.950580*, 60 (4), pp. 549–565. DOI:10.1080/02626667.2014.950580.

Staudinger, M., Stahl, K., Seibert, J., Clark, M.P. & Tallaksen, L.M. (2011). Comparison of hydrological model structures based on recession and low flow simulations. *Hydrology and Earth System Sciences*, 15 (11), pp. 3447–3459. DOI:10.5194/HESS-15-3447-2011.

Sullivan, C.A. et al. (2003). The Water Poverty Index: Development and application at the community scale. *Natural Resources Forum*, 27 (3), pp. 189–199. DOI:10.1111/1477-8947.00054.

Sutanudjaja, E.H., Beek, R.V., Wanders, N., Wada, Y., Bosmans, J.H., Drost, N., Ent, R.J.V.D., Graaf, I.E.D., Hoch, J.M., Jong, K.D., Karssenberg, D., López, P.L., Peßenteiner, S., Schmitz, O., Straatsma, M.W., Vannametee, E.,

Wisser, D. & Bierkens, M.F. (2018). PCR-GLOBWB 2: A 5 arcmin global hydrological and water resources model. *Geoscientific Model Development*, 11 (6), pp. 2429–2453. DOI:10.5194/GMD-11-2429-2018.

Tang, T., Strokal, M., van Vliet, M.T., Seuntjens, P., Burek, P., Kroeze, C., Langan, S. & Wada, Y. (2019). Bridging global, basin and local-scale water quality modeling towards enhancing water quality management worldwide. *Current Opinion in Environmental Sustainability*, 36, pp. 39–48. DOI:10.1016/J.COSUST.2018.10.004.

Thebo, A.L., Drechsel, P. & Lambin, E.F. (2014). Global assessment of urban and peri-urban agriculture: Irrigated and rainfed croplands. *Environmental Research Letters*, 9 (11). DOI:10.1088/1748-9326/9/11/114002.

Thebo, A.L., Drechsel, P., Lambin, E.F. & Nelson, K.L. (2017). A global, spatially-explicit assessment of irrigated croplands influenced by urban wastewater flows. *Environmental Research Letters*, 12 (7). DOI:10.1088/1748-9326/AA75D1.

Thomann, R.V. & Mueller, J.A. (1987). Principles of surface water quality modeling and control, p. 644.

Thomson, K.J. (2003). World agriculture: towards 2015/2030: an FAO perspective: Jelle Briunsma (Ed.), FAO/Earthscan, 2003. 432 pp. ISBNs: 92 5 104835 5 (FAO paperback), 1 84407 007 7 (Earthscan paperback) and 1 84407 008 57 (Earthscan hardback). *Land Use Policy*, 20 (4), p. 375. DOI:HTTPS://DOI.ORG/10.1016/S0264-8377(03)00047-4.

Thorslund, J., Bierkens, M.F., Scaini, A., Sutanudjaja, E.H. & van Vliet, M.T.H. (2022). Salinity impacts on irrigation water-scarcity in food bowl regions of the US and Australia. *Environmental Research Letters*, 17 (8), p. 084002. DOI:10.1088/1748-9326/AC7DF4.

Thorslund, J. & van Vliet, M.T.H. (2020). A global dataset of surface water and groundwater salinity measurements from 1980-2019. *Scientific Data 2020 7:1*, 7 (1), pp. 1–11. DOI:10.1038/S41597-020-0562-Z.

Trenberth, K.E., Dai, A., van der Schrier, G., Jones, P.D., Barichivich, J., Briffa, K.R. & Sheffield, J. (2014). Global warming and changes in drought. *Nature Climate Change*, 4 (1), pp. 17–22. DOI:10.1038/NCLIMATE2067.

UN (2015). *Transforming our World: The 2030 Agenda for Sustainable Development*. United Nations Development Programme.

UNEP (2016). *A Snapshot of the World's Water Quality: Towards a global assessment*. United Nations Environment Programme, pp. 1–266.

UNEP (2019). *GEMStat Database of the Global Environment Monitoring System for Freshwater (GEMS/Water) Programme*.

US-EPA (2020). *EPA Facility Registry Service (FRS): Wastewater Treatment Plants*.

van Beek, L.P., Eikelboom, T., van Vliet, M.T.H. & Bierkens, M.F. (2012). A physically based model of global freshwater surface temperature. *Water Resources Research*, 48 (9), p. 9530. DOI:10.1029/2012WR011819.

van der Wiel, K., Wanders, N., Selten, F.M. & Bierkens, M.F. (2019). Added Value of Large Ensemble Simulations for Assessing Extreme River Discharge in a 2 °C Warmer World. *Geophysical Research Letters*, 46 (4), pp. 2093–2102. DOI:10.1029/2019GL081967.

van Drecht, G., Bouwman, A.F., Harrison, J. & Knoop, J.M. (2009). Global nitrogen and phosphate in urban wastewater for the period 1970 to 2050. *Global Biogeochemical Cycles*, 23 (4). DOI:10.1029/2009GB003458.

van Griensven, A. & Meixner, T. (2006). Methods to quantify and identify the sources of uncertainty for river basin water quality models. *Water science and technology : a journal of the International Association on Water Pollution Research*, 53 (1), pp. 51–59. DOI:10.2166/WST.2006.007.

van Puijenbroek, P.J., Beusen, A.H. & Bouwman, A.F. (2019). Global nitrogen and phosphorus in urban waste water based on the Shared Socio-economic pathways. *Journal of Environmental Management*, 231, pp. 446–456. DOI:10.1016/J.JENVMAN.2018.10.048.

van Vliet, M.T.H., Florke, M. & Wada, Y. (2017). Quality matters for water scarcity. *Nature Geoscience*, 10 (11), pp. 800–802. DOI:10.1038/NGEO3047.

van Vliet, M.T.H., Flörke, M., Harrison, J.A., Hofstra, N., Keller, V., Ludwig, F., Spanier, J.E., Strokal, M., Wada, Y., Wen, Y. & Williams, R.J. (2019). Model inter-comparison design for large-scale water quality models. *Current Opinion in Environmental Sustainability*, 36, pp. 59–67. DOI:10.1016/J.COSUST.2018.10.013.

van Vliet, M.T.H., Franssen, W.H., Yearsley, J.R., Ludwig, F., Haddeland, I., Lettenmaier, D.P. & Kabat, P. (2013). Global river discharge and water temperature under climate change. *Global Environmental Change*, 23 (2), pp. 450–464. DOI:10.1016/J.GLOENVCHA.2012.11.002.

van Vliet, M.T.H., Jones, E.R., Flörke, M., Franssen, W.H., Hanasaki, N., Wada, Y. & Yearsley, J.R. (2021). Global water scarcity including surface water quality and expansions of clean water technologies. *Environmental Research Letters*, 16 (2), p. 024020. DOI:10.1088/1748-9326/ABBFC3.

van Vliet, M.T.H., Sheffield, J., Wiberg, D. & Wood, E.F. (2016). Impacts of recent drought and warm years on water resources and electricity supply worldwide. *Environmental Research Letters*, 11 (12), p. 124021. DOI:10.1088/1748-9326/11/12/124021.

van Vliet, M.T.H., Thorslund, J., Strokal, M., Hofstra, N., Flörke, M., Macedo, H.E., Nkwasa, A., Tang, T., Kaushal, S.S., Kumar, R., van Griensven, A., Bouwman, L. & Mosley, L.M. (2023). Global river water quality under climate

change and hydroclimatic extremes. *Nature Reviews Earth and Environment*, p. 024020. DOI:10.1038/s43017-023-00472-3.

van Vliet, M.T.H., Yearsley, J.R., Franssen, W.H., Ludwig, F., Haddeland, I., Lettenmaier, D.P. & Kabat, P. (2012a). Coupled daily streamflow and water temperature modelling in large river basins. *Hydrology and Earth System Sciences*, 16 (11), pp. 4303–4321. DOI:10.5194/HESS-16-4303-2012.

van Vliet, M.T.H., Yearsley, J.R., Ludwig, F., Vögele, S., Lettenmaier, D.P. & Kabat, P. (2012b). Vulnerability of US and European electricity supply to climate change. *Nature Climate Change 2012 2:9*, 2 (9), pp. 676–681. DOI:10.1038/NCLIMATE1546.

van Vuuren, D.P., Kriegler, E., O'Neill, B.C., Ebi, K.L., Riahi, K., Carter, T.R., Edmonds, J., Hallegatte, S., Kram, T., Mathur, R. & Winkler, H. (2014). A new scenario framework for Climate Change Research: Scenario matrix architecture. *Climatic Change*, 122 (3), pp. 373–386. DOI:10.1007/S10584-013-0906-1/FIGURES/6.

van Wijnen, J., Ragas, A.M. & Kroeze, C. (2019). Modelling global river export of microplastics to the marine environment: Sources and future trends. *The Science of the Total Environment*, 673, pp. 392–401. DOI:10.1016/J.SCITOTENV.2019.04.078.

Vanham, D., Hoekstra, A.Y., Wada, Y., Bouraoui, F., de Roo, A., Mekonnen, M.M., van de Bund, W.J., Batelaan, O., Pavelic, P., Bastiaanssen, W.G., Kummu, M., Rockström, J., Liu, J., Bisselink, B., Ronco, P., Pistocchi, A. & Bidoglio, G. (2018). Physical water scarcity metrics for monitoring progress towards SDG target 6.4: An evaluation of indicator 6.4.2 "Level of water stress". *Science of the Total Environment*, 613-614, pp. 218–232. DOI:10.1016/J.SCITOTENV.2017.09.056.

Velasco, J., Gutiérrez-Cánovas, C., Botella-Cruz, M., Sánchez-Fernández, D., Arribas, P., Carbonell, J.A., Millán, A. & Pallarés, S. (2019). Effects of salinity changes on aquatic organisms in a multiple stressor context. *Philosophical Transactions of the Royal Society B*, 374 (1764). DOI:10.1098/RSTB.2018.0011.

Vermeulen, L.C., van Hengel, M., Kroeze, C., Medema, G., Spanier, J.E., van Vliet, M.T.H. & Hofstra, N. (2019). Cryptosporidium concentrations in rivers worldwide. *Water Research*, 149, pp. 202–214. DOI:10.1016/J.WATRES.2018.10.069.

Vigiak, O., Grizzetti, B., Udias-Moinelo, A., Zanni, M., Dorati, C., Bouraoui, F. & Pistocchi, A. (2019). Predicting biochemical oxygen demand in European freshwater bodies. *Science of The Total Environment*, 666, pp. 1089–1105. DOI:10.1016/J.SCITOTENV.2019.02.252.

Virro, H., Amatulli, G., Kmoch, A., Shen, L. & Uuemaa, E. (2021). GRQA: Global River Water Quality Archive. *Earth System Science Data*, 13 (12), pp. 5483–5507. DOI:10.5194/ESSD-13-5483-2021.

Voulvoulis, N. (2018). Water reuse from a circular economy perspective and potential risks from an unregulated approach. *Current Opinion in Environmental Science and Health*, 2, pp. 32–45. DOI:10.1016/J.COESH.2018.01.005.

Voß, A., Alcamo, J., Bärlund, I., Voß, F., Kynast, E., Williams, R. & Malve, O. (2012). Continental scale modelling of in-stream river water quality: a report on methodology, test runs, and scenario application. *Hydrological Processes*, 26 (16), pp. 2370–2384. DOI:HTTPS://DOI.ORG/10.1002/HYP.9445.

Vörösmarty, C.J., McIntyre, P.B., Gessner, M.O., Dudgeon, D., Prusevich, A., Green, P., Glidden, S., Bunn, S.E., Sullivan, C.A., Liermann, C.R. & Davies, P.M. (2010). Global threats to human water security and river biodiversity. *Nature 2010 467:7315*, 467 (7315), pp. 555–561. DOI:10.1038/NATURE09440.

Wada, Y., Flörke, M., Hanasaki, N., Eisner, S., Fischer, G., Tramberend, S., Satoh, Y., van Vliet, M.T.H., Yillia, P., Ringler, C., Burek, P. & Wiberg, D. (2016). Modeling global water use for the 21st century: The Water Futures and Solutions (WFaS) initiative and its approaches. *Geoscientific Model Development*, 9 (1), pp. 175–222. DOI:10.5194/GMD-9-175-2016.

Wada, Y., Wisser, D. & Bierkens, M.F. (2014). Global modeling of withdrawal, allocation and consumptive use of surface water and groundwater resources. *Earth System Dynamics*, 5 (1), pp. 15–40. DOI:10.5194/ESD-5-15-2014.

Wada, Y., Beek, L.P.V., Viviroli, D., Drr, H.H., Weingartner, R. & Bierkens, M.F. (2011). Global monthly water stress: 2. Water demand and severity of water stress. *Water Resources Research*, 47 (7). DOI:10.1029/2010WR009792.

Wada, Y., Wisser, D., Eisner, S., Flörke, M., Gerten, D., Haddeland, I., Hanasaki, N., Masaki, Y., Portmann, F.T., Stacke, T., Tessler, Z. & Schewe, J. (2013). Multimodel projections and uncertainties of irrigation water demand under climate change. *Geophysical Research Letters*, 40 (17), pp. 4626–4632. DOI:10.1002/GRL.50686.

Walton, N.R.G. (1989). Electrical Conductivity and Total Dissolved Solids-What is Their Precise Relationship? *Desalination*, 12, pp. 275–292.

Wan, L., Cai, W., Jiang, Y. & Wang, C. (2016). Impacts on quality-induced water scarcity: drivers of nitrogen-related water pollution transfer under globalization from 1995 to 2009. *Environmental Research Letters*, 11 (7), p. 074017. DOI:10.1088/1748-9326/11/7/074017.

Wanders, N & Wada, Y (2015). Human and climate impacts on the 21st century hydrological drought. *Journal of Hydrology*, 526. Drought processes, modeling, and mitigation, pp. 208–220. DOI:HTTPS://DOI.ORG/10.1016/J.JHYDROL.2014.10.047.

Wanders, N., van Vliet, M.T.H., Wada, Y., Bierkens, M.F. & van Beek, L.P. (2019). High-Resolution Global Water Temperature Modeling. *Water Resources Research*, 55 (4), pp. 2760–2778. DOI:10.1029/2018WR023250.

Wang, M., Janssen, A.B., Bazin, J., Strokal, M., Ma, L. & Kroeze, C. (2022). Accounting for interactions between Sustainable Development Goals is essential for water pollution control in China. *Nature Communications 2022 13:1*, 13 (1), pp. 1–13. DOI:10.1038/s41467-022-28351-3.

Weaver, A.J. & Zwiers, F.W. (2000). Uncertainty in climate change. *Nature 2000 407:6804*, 407 (6804), pp. 571–572. DOI:10.1038/35036659.

Wen, Y., Schoups, G. & Giesen, N.V.D. (2017). Organic pollution of rivers: Combined threats of urbanization, livestock farming and global climate change. *Scientific Reports 2017 7:1*, 7 (1), pp. 1–9. DOI:10.1038/SREP43289.

Whitehead, P.G., Wilby, R.L., Battarbee, R.W., Kernan, M. & Wade, A.J. (2009). A review of the potential impacts of climate change on surface water quality. *https://doi.org/10.1623/hysj.54.1.101*, 54 (1), pp. 101–123. DOI:10.1623/HYSJ.54.1.101.

Williams, R., Keller, V., Voß, A., Bärlund, I., Malve, O., Riihimäki, J., Tattari, S. & Alcamo, J. (2012). Assessment of current water pollution loads in Europe: estimation of gridded loads for use in global water quality models. *Hydrological Processes*, 26 (16), pp. 2395–2410. DOI:10.1002/HYP.9427.

Wright, B., Stanford, B.D., Reinert, A., Routt, J.C., Khan, S.J. & Debroux, J.F. (2014). Managing water quality impacts from drought on drinking water supplies. *Journal of Water Supply: Research and Technology-Aqua*, 63 (3), pp. 179–188. DOI:10.2166/AQUA.2013.123.

Wurtsbaugh, W.A., Paerl, H.W. & Dodds, W.K. (2019). Nutrients, eutrophication and harmful algal blooms along the freshwater to marine continuum. *Wiley Interdisciplinary Reviews: Water*, 6 (5), e1373. DOI:10.1002/WAT2.1373.

WWAP (2017). *The United Nations World Water Development Report 2017. Wastewater: The Untapped Resource*. UNESCO, p. 180.

WWQA (2021). *First Global Display of a Water Quality Baseline. A consortium effort by the World Water Quality Alliance - towards a full global assessment. Information Document Annex for display at the 5th Session of the United Nations Environment Assembly*. World Water Quality Alliance.

Xie, H. & Ringler, C. (2017). Agricultural nutrient loadings to the freshwater environment: the role of climate change and socioeconomic change. *Environmental Research Letters*, 12 (10), p. 104008. DOI:10.1088/1748-9326/AA8148.

Zaman, M., Shahid, S.A. & Heng, L. (2018). Guideline for Salinity Assessment, Mitigation and Adaptation Using Nuclear and Related Techniques. *Guideline for Salinity Assessment, Mitigation and Adaptation Using Nuclear and Related Techniques*. DOI:10.1007/978-3-319-96190-3.

Zhang, Y. & Shen, Y. (2019). Wastewater irrigation: past, present, and future. *Wiley Interdisciplinary Reviews: Water*, 6 (3). DOI:10.1002/WAT2.1234.

Zhao, X., Liu, J., Yang, H., Duarte, R., Tillotson, M.R. & Hubacek, K. (2016). Burden shifting of water quantity and quality stress from megacity Shanghai. *Water Resources Research*, 52 (9), pp. 6916–6927. DOI:10.1002/2016WR018595.

Summary

Clean water is essential for supporting human livelihoods and maintaining ecosystem health. However, our knowledge of water quality is severely impaired by a lack of quantitative information. Observations from water quality monitoring stations – the fundamental basis of water quality assessment – are expensive and time-consuming, and therefore are highly limited in space and fragmented across time. Being under-monitored and often imperceptible to the human eye, water pollution has been branded an 'invisible crisis'.

Global surface water quality data is required to assess the key regions where pollution poses risks to safe water use. Similarly, protecting and improving the quality of surface waters globally is contingent upon an improved understanding of the problem and its drivers. Process-based models are tools that can supplement our knowledge of water quality beyond what is possible using in situ measurements alone. Surface water quality models simulate the emission and transport of pollution along the river network directly, based on input data representing climatic, hydrological and socioeconomic drivers. The philosophy of global surface water quality modelling is to apply an approach that is consistent across all world regions in order to facilitate meaningful comparisons at large scales. While the field of global water quality modelling is still in its infancy, there are increasing efforts to simulate a diverse range of water quality constituents. Representing one of these efforts, this thesis introduces and applies the **Dyn**amical Surface Water **Qual**ity (*DynQual*) model in order to address the research objective:

To assess the past and current status of surface water quality globally, and to evaluate the impact of (uncertain) global change on future surface water quality.

Anthropogenic activities are key drivers of water quality deterioration. Water that is extracted for sectoral purposes, but which is not consumed, is often discharged to surface waters. The quality of this wastewater will be reflective of the human use activity and the pathway by which it re-enters the environment. Realistic representation of the existence of and degree to which treatment practices reduce contaminant levels before environmental discharge is therefore important for surface water quality models. However, the availability of wastewater data at large-scales is sparse, often outdated and pertains to inconsistent reporting years. This thesis provides a comprehensive and consistent global assessment of wastewater production, collection, treatment and reuse, both at country-level and gridded (5 arc-min resolution) level (**Chapter 2**). Results show that approximately half (52%) of global wastewater is treated, opposed to previous estimates of ~20%. However, wastewater treatment plants are unevenly distributed across the world, with just 4.2% of wastewater treated in 'low-income' countries compared to 74% in 'high-income' countries. Country-level results provide quantitative information for understanding the global wastewater status, while, as leveraged in this thesis, spatially explicit (gridded) results can be used as input for large-scale water resource assessments.

In this thesis, *DynQual* was applied to provide a global assessment of past and current surface water quality (1980–2019) using state-of-the-art climate and socioeconomic input data (**Chapter 3**). The model was used to simulate water temperature (Tw) and indicators of salinity (total dissolved solids; TDS), organic (biological oxygen demand; BOD) and pathogen (fecal coliform; FC) pollution. Modelled results demonstrate that surface water quality issues are globally relevant, with exceedances of key concentration thresholds for TDS, BOD and FC pollution occurring across all world regions albeit with different frequencies and magnitudes. Current year-round and multi-pollutant hotspots of poor surface water quality are located across northern India and eastern China, whereas trends towards surface water quality deterioration in the last ~40 years are most profound in Sub-Saharan Africa and southern Asia.

Both the availability and quality of water resources will change in the future. Process-based models provide unique opportunities to quantitatively assess the impact of future change on in-stream pollutant concentrations. This includes exploring hypothetical 'what-if' questions, such as the effectiveness of management and intervention strategies for improving water quality. In this thesis, *DynQual* was applied to assess the effectiveness of halving the proportion of untreated wastewater entering the environment by 2030 (i.e. achieving SDG 6.3) for improving ambient surface water quality (**Chapter 4**). While substantial reductions in organic (BOD) and pathogen (FC) pollution are achieved, changes to the frequency and magnitude of water quality threshold exceedances drastically vary across world regions. Particularly in the developing world, reductions in pollutant loadings are locally effective but the transmission of pollution from upstream areas still leads to water quality issues downstream. The results therefore highlight the need to go beyond the SDG-target for wastewater in order to achieve the overarching goal of 'clean water for all'.

Lastly, this thesis presents the first assessment of the impact of global change on long-term water quality (**Chapter 5**). To this end, *DynQual* was forced with state-of-the-art projections of societal change and trajectories of climate change. Three diverging scenarios are considered, ranging from a world characterised by sustainability and equality (SSP1-RCP2.6), to resurging nationalism and widening inequality (SSP3-RCP7.0), to strong but fossil-fueled economic development (SSP5-RCP8.5). Results indicate that the proportion of the global population exposed to salinity, organic and pathogen pollution by the end of the century ranges from 17–27%, 20–37% and 22–44%, respectively, with poor surface water quality disproportionately affecting people living in developing countries. Exhibiting the largest increases in both the absolute and relative number of people exposed to polluted surface water, irrespective of climate change and socioeconomic development scenario, this thesis concludes that Sub-Saharan Africa will increasingly become the key hotspot of surface water pollution. Preliminary results suggest that this surface water quality deterioration, in combination with the increased prevalence of water gaps (i.e. instances where human water demands exceed the renewable water supply), will establish Sub-Saharan Africa as a key hotspot of (year-round) water scarcity in the future (**Chapter 6**).

Inability to meet our clean water demands is considered one of the major risks to humankind both in terms of likelihood and potential impacts, and water scarcity issues will further intensify into the future. This thesis highlights the need to better understand and account for water quality aspects, in addition to water availability aspects, in order to achieve sustainable management of water resources globally.

Samenvatting

Schoon water is essentieel voor het levensonderhoud van de mens en voor gezonde ecosystemen. Onze kennis van waterkwaliteit wordt echter beperkt door de beperkte beschikbaarheid aan data. Het monitoren van waterkwaliteit met behulp van meetstations is kostbaar en tijdrovend. Als gevolg hiervan zijn metingen van de waterkwaliteit beperkt in wereldwijde geografische spreiding en gefragmenteerd over tijd. Vanwege beperkte monitoring in verschillende werelddelen (bijvoorbeeld Afrika) en het gebrek aan direct zichtbare gevolgen wordt waterverontreiniging bestempeld als een 'onzichtbare crisis'.

Wereldwijde gegevens over de kwaliteit van het oppervlaktewater zijn nodig om te beoordelen in welke regio's watervervuiling risico's vormen voor veilig watergebruik. Daarnaast is het beschermen en het verbeteren van de kwaliteit van het oppervlaktewater afhankelijk van een beter begrip van het probleem en de oorzaken. Om de beperkte kennis over de mondiale waterkwaliteit aan te vullen kunnen we gebruik maken van computermodellen die de belangrijkste processen van waterkwaliteit representeren. Op basis van klimatologische, hydrologische en socio-economische ontwikkelingen kunnen deze proces-gebaseerde modellen de belasting en het transport van vervuilende stoffen in rivieren simuleren. Het idee achter mondiale waterkwaliteitsmodellering is dat het wereldwijd toepassen van één methode zinvolle vergelijkingen van de waterkwaliteit tussen verschillende regio's mogelijk maakt. Hoewel de modellering van de wereldwijde waterkwaliteit nog in de kinderschoenen staat, ziet men recentelijk een sterke groei in studies waarin verschillende aspecten van grootschalige waterkwaliteit worden gemodelleerd. Dit proefschrift is één van deze studies. In dit proefschrift wordt het **Dyn**amical Surface Water **Qual**ity (*DynQual*) model, of in het kort *DynQual*, geïntroduceerd en gebruikt om het volgende onderzoeksdoel te behalen:

Het bepalen van de status van wereldwijde oppervlaktewaterkwaliteit in het heden en het verleden en het evalueren van de invloed van (onzekere) wereldwijde veranderingen op de toekomstige kwaliteit van het oppervlaktewater.

Menselijke activiteiten zijn de belangrijkste oorzaak van de achteruitgang van de waterkwaliteit. Water dat wordt onttrokken maar niet geheel wordt verbruikt, wordt vaak geloosd in het oppervlaktewater. De kwaliteit van dit afvalwater weerspiegelt het eerdere gebruik en de route dat het heeft afgelegd voordat het weer in het milieu terecht kwam. De juiste representatie van afvalwaterzuivering en de effectiviteit waarmee verontreinigingen verwijderd worden, is daarom van groot belang voor modellering van oppervlaktewaterkwaliteit. De beschikbaarheid van data van afvalwater op grote schaal is echter schaars, vaak verouderd en inconsistent over tijd. Dit proefschrift biedt een uitgebreid en consistent overzicht van de productie, opvang, zuivering en hergebruik van afvalwater, zowel op landenniveau als ruimtelijk expliciet niveau- (5 arc-min grid resolutie) wereldwijd (**Hoofdstuk 2**). Resultaten tonen dat ongeveer de helft (52%) van het mondiaal afvalwater gezuiverd wordt, terwijl eerdere studies aantoonden dat dit ongeveer ∼20% was. De verdeling van afvalwaterzuiveringsinstallaties wereldwijd is echter onevenredig, met slechts 4.2% van het afvalwater dat in lage inkomens-landen gezuiverd wordt, ten opzichte van 74% in hoge inkomens-landen. Resultaten op landniveau zorgen voor kwantitatieve informatie die gebruikt kunnen worden voor een beter begrip van de status van het afvalwater wereldwijd. De ruimtelijk expliciete resultaten met een resolutie van 5 arc-min kunnen worden gebruikt als input voor grootschalige waterkwaliteit(model)studies.

In dit proefschrift is het *DynQual* model ontwikkeld en gebruikt om op mondiale schaal een overzicht te geven van de kwaliteit van het oppervlaktewater in het heden en het verleden (1980–2019) op basis van de nieuwste klimaat en socio-economische data (**Hoofdstuk 3**). Dit model

simuleert de oppervlakte watertemperatuur (Tw), saliniteit (total dissolved solids; TDS), organische verontreiniging (biochemical oxygen demand; BOD) en pathogenen verontreiniging (fecal coliform; FC). De modelresultaten laten zien dat problemen met de waterkwaliteit van wereldwijd belang zijn. Belangrijke drempelwaarden voor de waterkwaliteit, zoals voor TDS, BOD en FC vervuiling, worden in alle regio's in de wereld overschreden, zij het in verschillende mate en frequenties. Huidige hotspots, waar de waterkwaliteit het hele jaar slecht is door meerdere vervuilingsbronnen, zijn vooral te vinden in Noord-India en Oost-China. De regio's waarbij de waterkwaliteit het meest verslechterd is in de aflopen ∼40 jaar zijn Sub-Saharaans-Afrika en Zuid-Azië.

Zowel de beschikbaarheid als de kwaliteit van water zal in de komende decennia veranderen. Proces-gebaseerde modellen bieden een unieke mogelijkheid om de effecten van toekomstige veranderingen in klimaat en socio-economische veranderingen op oppervlaktewaterkwaliteit te evalueren. Deze modellen bieden ook de mogelijkheid om 'wat-als' vragen te stellen en op te lossen zoals; wat is de effectiviteit van bepaalde beleidsmaatregelen en interventiestrategieën? In dit proefschrift is het *DynQual* model toegepast om te evalueren wat het effect is van het halveren van het aandeel ongezuiverd afvalwater dat in het milieu terechtkomt tegen 2030 (d.w.z. het bereiken van SDG 6.3) op het verbeteren van de oppervlaktewaterkwaliteit (**Hoofdstuk 4**). Hoewel een halvering van het ongezuiverde afvalwater zorgt voor een substantiële vermindering van organische (BOD) en pathogene (FC) vervuiling op mondiale niveau, verschillen de vervuilingsniveaus sterk per regio en worden de kritische drempelwaardes voor waterkwaliteit in veel regio's in de wereld nog steeds overschreden. Met name in ontwikkelende landen is de vermindering in verontreinigende stoffen effectief op lokale schaal, maar het transport van verontreiniging vanuit stroomopwaarts gelegen gebieden zorgt nog steeds voor problemen voor de waterkwaliteit stroomafwaarts. Deze resultaten benadrukken daarom dat het noodzakelijk is om verder te gaan dan de SDG-doelstelling voor afvalwater om het algehele doel van 'schoon water voor iedereen' te kunnen bereiken.

Ten slotte presenteert dit proefschrift de eerste analyse van de impact van mondiale veranderingen op de oppervlaktewaterkwaliteit in de toekomst (**Hoofdstuk 5**). Hiervoor werd het *DynQual* model aangedreven door de nieuwste socio-economische en klimaat-scenario's voor de 21ste eeuw. Verschillende combinaties van socio-economische en klimaat-scenario's werden gebruikt op basis van zogenaamde Shared Socioeconomic Pathway (SSPs) en Representative Concentration Pathways (RCPs). In totaal, zijn drie uiteenlopende scenario's getest. Deze variëren van een wereld die wordt gekenmerkt door duurzaamheid en gelijkheid (SSP1-RCP2.6), tot heroplevend nationalisme en toenemende ongelijkheid (SSP3-RCP7.0), tot sterke maar door fossiele brandstoffen aangedreven economische ontwikkeling (SSP5-RCP8.5). De resultaten van deze scenario's laten zien dat tegen het einde van de eeuw het deel van de bevolking dat is blootgesteld aan een te hoog zoutgehalte, en organische en pathogene vervuiling varieert tussen respectievelijk 17–27%, 20–37% en 22–44%. Hierbij geldt dat met name mensen in ontwikkelingslanden te maken zullen krijgen met verslechtering van oppervlaktewaterkwaliteit. Dit proefschrift laat zien dat, ongeacht welk klimaat of socio-economisch scenario, Sub-Saharaans Afrika de toekomstige mondiale kritische regio (hotspot) zal zijn voor oppervlaktewatervervuiling. Eerste resultaten laten zien dat deze regio in de toekomst ook meer waterschaarste zal ondervinden door verslechtering in oppervlaktewaterkwaliteit in combinatie met een toenemende disbalans tussen de beschikbaarheid versus vraag naar water voor menselijke gebruiken (**Hoofdstuk 6**).

Het onvermogen om aan onze huidige vraag naar schoon water te voldoen wordt nu al beschouwd als één van de grootste risico's voor de mensheid, zowel in termen als waarschijnlijkheid als de potentiële gevolgen Dit onvermogen zal leiden tot een sterke toename van waterschaarste, niet alleen door geringe waterbeschikbaarheid, maar ook in grote mate door slechte waterkwaliteit. Dit proefschrift laat zien dat voor duurzaam waterbeheer het voor de meeste gebieden in de wereld essentieel is om rekening te houden met de kwaliteit van water.

List of publications

Articles

Jones, E.R. and van Vliet, M.T.H. (2018). Drought impacts on river salinity in the southern US: Implications for water scarcity, *Science of The Total Environment 644*, pp. 844-853, DOI:10.1016/j.scitotenv.2018.06.373

Jones, E.R., Qadir, M., van Vliet, M.T.H., Smakhtin, V., and Kang, S.M. (2019). The state of desalination and brine production: A global outlook. *Science of the Total Environment, 657*, pp. 1343-1356, DOI:10.1016/j.scitotenv.2018.12.076

Kalanaki, M., Ritzema, H., Bamshad, R., **Jones, E.R.**, and Fazilatnia, M. (2020). Application of bio-desalinization for reclamation of salt-affected soil under composted cow manure and deficit irrigation with saline water, *Paddy and Water Environment, 18*, pp. 469-479, DOI:10.1007/s10333-020-00795-7

van Vliet, M.T.H., **Jones, E.R.**, Flörke, M., Franssen, W.H.P., Hanasaki, N., Wada, Y., and Yearsley, J.R. (2021). Global water scarcity including surface water quality and expansions of clean water technologies, *Environmental Research Letters, 16*, 024020, DOI:10.1088/1748-9326/abbfc3

Jones, E.R. and Qadir, M. (2021). The State of Desalination and Brine Production *in* Solar Co-Generation of Electricity and Water - Large Scale Photovoltaic Systems, *Encyclopedia of Life Support Systems (EOLSS)*, Developed under the Auspices of the UNESCO, EOLSS Publishers, Paris, France [https://www.eolss.net]

Jones, E.R., van Vliet, M.T.H., Qadir, M., and Bierkens, M.F.P. (2021). Country-level and gridded estimates of wastewater production, collection, treatment and reuse. *Earth System Science Data, 13(2)*, pp. 237-254, DOI:10.5194/essd-13-237-2021

Jones, E.R., Bierkens, M.F.P., Wanders, N., Sutanudjaja, E.H., van Beek, L.P.H., and van Vliet, M.T.H. (2022). Current wastewater treatment targets are insufficient to protect surface water quality. *Communications Earth & Environment, 3(1)*, pp. 1-8, DOI: 10.1038/s43247-022-00554-y

Jia,Y., Hahn, J., Quack, B., **Jones, E.R.**, and Tegtmeier, S. (2023). Anthropogenic Bromoform at the Extratropical Tropopause. *Geophysical Research Letters, 50(9)*, e2023GL102894, DOI: 10.1029/2023GL102894

Jones, E.R., Bierkens, M.F.P., Wanders, N., Sutanudjaja, E.H., van Beek, L.P.H., and van Vliet, M.T.H. (2023) DynQual v1.0: a high-resolution global surface water quality model. *Geoscientific Model Development, 16*, pp. 4481–4500, DOI: 10.5194/gmd-16-4481-2023

Jones, E.R., Bierkens, M.F.P., van Puijenbroek, P.J.T.M., van Beek, L.P.H., Wanders, N., Sutanudjaja, E.H., and van Vliet, M.T.H. (2023) Sub-Saharan Africa will increasingly become the dominant hotspot of surface water pollution. *Nature Water, 1*, pp. 602-613, DOI: 10.1038/s44221-023-00105-5

United Nations Environment Programme and GRID-Arendal (2023) Wastewater – Turning Problem to Solution. *A UNEP Rapid Response Assessment*, DOI: 10.59117/20.500.11822/43142

Conference abstracts (selected)

van Vliet, M.T.H., Franssen, W., Jones E.R., Behrens, P., Droppers, B., Wada, Y., Flörke, M. (2018) Water quality-driven water scarcity for energy and food production under climate variability and change, *American Geophysical Union Conference 2018*, Washington D.C., USA

van Vliet, M.T.H., Jones, E.R., Flörke, M., Franssen, W.H.P., Hanasaki, N., Wada, Y., Yearsley, J.R. (2020) Global water scarcity reduction requires water quality solutions, *European Geosciences Union Conference 2020*, Vienna, Austria, DOI: 10.5194/egusphere-egu2020-2718

Jones, E.R., Bierkens, M.F.P., Wanders, N., Sutanudjaja, E.H., van Beek, L.P.H., and van Vliet, M.T.H (2022) Surface water quality under the Sustainable Development Agenda - the role of improved wastewater treatment, *European Geosciences Union Conference 2022*, Vienna, Austria, DOI: 10.5194/egusphere-egu22-3599

Jones, E.R., Bierkens, M.F.P., Wanders, N., Sutanudjaja, E.H., van Beek, L.P.H., and van Vliet, M.T.H (2022) *DynQual*: A High-Resolution Global Surface Water Quality Model, *American Geophysical Union Conference 2022*, Chicago, USA

van Vliet, M.T.H., Thorslund, J., **Jones, E.R.**, Bierkens, M.F.P., Interplay of water quality and sectoral water use at regional to global scales. *American Geophysical Union Conference 2022*, Chicago, USA

Jones, E.R., Bierkens, M.F.P., van Puijenbroek, P.J.T.M, and van Vliet, M.T.H (2023) Global surface water quality under uncertain climate and socio-economic change, *European Geosciences Union Conference 2023*, Vienna, Austria, DOI: 10.5194/egusphere-egu23-1161

Open-access model code and data

Jones, E.R., van Vliet, M.T.H., Qadir, M., and Bierkens, M.F.P. (2020). Country-level and gridded wastewater production, collection, treatment and re-use [Data set], *PANGAEA*, DOI: 10.1594/PANGAEA.918731

DynQual GitHub repository (including model code, manual and README) at: https://github.com/UU-Hydro/DYNQUAL

Jones, E.R. and Sutanudjaja, E.H. (2022) *DynQual v1.0* stable release. *Zenodo*. DOI: 10.5281/zenodo.7398411

Jones, E.R., Bierkens, M.F.P., Wanders, N., Sutanudjaja, E.H., van Beek, L.P.H., and van Vliet, M.T.H. (2022) Global monthly TDS, BOD and FC concentrations from 1980 to 2015 at 10km spatial resolution [Data set], *figshare*, DOI: 10.6084/m9.figshare.20486277.v1

Jones, E.R., Bierkens, M.F.P., Wanders, N., Sutanudjaja, E.H., van Beek, L.P.H., and van Vliet, M.T.H. (2022) Global monthly averaged TDS, BOD and FC concentrations from 2021 to 2030 at 10km spatial resolution for 5 GCMs under two wastewater treatment scenarios [Data set], *figshare*, DOI: 10.6084/m9.figshare.20486310.v1

Jones, E.R. (2022) *DynQual* input example: Rhine basin [Data set], *Zenodo*, DOI: 10.5281/zenodo.7027242

Jones, E.R., Bierkens, M.F.P., Wanders, N., Sutanudjaja, E.H., van Beek, L.P.H., and van Vliet, M.T.H. (2022) Global monthly hydrology and water quality datasets, derived from the dynamical surface water quality model (*DynQual*) at 10km spatial resolution [Data set], *Zenodo*, DOI: 10.5281/zenodo.7139222

Jones, E.R., Bierkens, M.F.P., van Puijenbroek, J.T.M., van Beek, L.P.H., Wanders, N., Sutanudjaja, E.H., and van Vliet, M.T.H. (2023) Global hydrology and water quality datasets under uncertain climate and socio-economic change, derived from the dynamical surface water quality model (*DynQual*) at 10 km spatial resolution [Data set], *Zenodo*, DOI: 10.5281/zenodo.7811612

Media outreach (selected)

Fountain, H. (2019) The World Can Make More Water From the Sea, but at What Cost? (*The New York Times*): https://www.nytimes.com/2019/10/22/climate/desalination-water-climate-change.html

McGrath, M. (2019) Concerns over increase in toxic brine from desalination plants (*BBC News*: https://www.bbc.com/news/science-environment-46863146

Root, T. (2019) Desalination plants produce more waste brine than thought (*National Geographic*): https://www.nationalgeographic.com/environment/article/desalination-plants-produce-twice-as-much-waste-brine-as-thought

Deutsche Welle (2021) Can desalination solve the global water crisis? (*D*eutsche Welle Planet A): https://www.youtube.com/watch?v=XPCaM9Rzzbs

Jones, E.R. (2021) We now treat half the world's wastewater - and we can make inroads into the other half (*The Conversation*): https://theconversation.com/we-now-treat-half-the-worlds-wastewater-and-we-can-make-inroads-into-the-other-half-154715

AQUATECH (2021) 50% Global Wastewater Treatment Still Not Enough (*AQUATECH*: https://www.aquatechtrade.com/news/wastewater/50-per-cent-of-wastewater-now-treated-worldwide/

Jones, E.R. (2022) Current wastewater treatment targets are insufficient to protect surface water quality (*Nature Portfolio: Behind the paper*): https://earthenvironmentcommunity.nature.com/posts/current-wastewater-treatment-targets-are-insufficient-to-protect-surface-water-quality

Tozer, L. (2023) Water pollution 'timebomb' threatens global health (*Nature*): https://www.nature.com/articles/d41586-023-02337-7

Bhandari, S. (2023) 5.5 billion people could be affected by surface water pollution by 2100 (*Radio Free Asia*): https://www.rfa.org/english/news/environment/water-pollution-07172023224901.html

Jones, E.R. (2023) Sub-Saharan Africa will increasingly become the dominant hotspot of surface water pollution (*Nature Portfolio: Behind the paper*): https://earthenvironmentcommunity.nature.com/posts/sub-saharan-africa-will-increasingly-become-the-dominant-hotspot-of-surface-water-pollution?channel_id=behind-the-paper

About the author

Edward Jones was born in London, United Kingdom on the 2nd April 1995. He completed his primary and secondary education at St. Dunstan's College (1999–2013), before attending Lancaster University to study for a bachelor's degree in Geography (2013–2016). Inspired by talented lecturers in the fields of hydrology, water resources management and climate change adaptation at the Lancaster Environment Centre, combined with a desire to move abroad, Edward decided to continue his studies by pursuing a Master's degree in Environmental Science at Wageningen University & Research (WUR) (2016–2018).

In Wageningen, Edward continued to develop his interest in water resources, especially considering future (uncertain) global change. His thesis focused on the impact of drought on river water salinity in the southern USA, along with a provisional assessment of the potential implications for water use. As part of the degree programme, Edward undertook an internship at the United Nations University – Institute for Water, Environment and Health (UNU-INWEH) in Canada, where he focused on the advantages and trade-offs associated with unconventional water resources (e.g. desalination, wastewater reuse). Moving back to Europe, Edward returned to WUR to start a role as a research assistant, also assisting in the development of new course material for various Master's courses.

In Autumn 2019, Edward started his PhD at Utrecht University under the supervision of dr. Michelle van Vliet and prof. dr. ir. Marc Bierkens. His research primarily focused on the development and application of a surface water quality model, coupled to the global hydrological model *PCR-GLOBWB2*, to analyse large-scale spatial patterns and temporal trends in surface water pollution for past, present and future conditions. In addition to water quality modelling, Edward is interested in the relationship between sectoral water demands and clean water availability in the context of water scarcity assessments, and for the potential of unconventional water resources to mitigate water scarcity issues in the future.

Utrecht University
Faculty of Geosciences
Department of Physical Geography

ISSN 2211-4335